Prohlášení:

Prohlašuji, že jsem závěrečnou práci zpracoval samostatně a že jsem řádně uvedl a citoval všechny použité prameny a literaturu. Současně prohlašuji, že práce nebyla využita k získání jiného nebo stejného titulu.

Souhlasím s trvalým uložením elektronické verze mé práce v databázi systému meziuniverzitního projektu Theses.cz za účelem soustavné kontroly podobnosti kvalifikačních prací.

V Praze 31.1.2015

Pavel Honsa

CHARLES UNIVERSITY IN PRAGUE

2ND FACULTY OF MEDICINE

and

ACADEMY OF SCIENCES OF THE CZECH REPUBLIC

INSTITUTE OF EXPERIMENTAL MEDICINE

Mgr. Pavel Honsa

Adult neurogenesis and gliogenesis after ischemic brain injury

PhD thesis

Supervisor: Ing. Miroslava Anděrová, CSc.

Prague 2015

ACKNOWLEDGEMENTS

I would like to express my gratitude to my supervisor, Dr. Miroslava Anderova, for her advice and patient guidance from the very early beginning of my research experience. I would also like to thank my colleagues and the technicians in the laboratory who participated in these experiments.

AUTHOR`S PUBLICATIONS:

Publications related to the thesis and contributions of individual co-authors:

1) **Pavel Honsa**, Helena Pivonkova, David Dzamba, Marcela Filipova, Miroslava Anderova (2012), Polydendrocytes display large lineage plasticity following focal cerebral ischemia, PloS One 7(5), IF 3.730

CONTRIBUTIONS:
Animal surgery: Honsa P.
Generation of double transgenic mice: Honsa P., Dzamba D., Filipova M.
Patch-clamp recording *in situ*: Honsa P., Pivonkova H.
Immunohistochemical analysis: Honsa P.
Data analysis: Honsa P., Anderova M.

2) Vendula Rusnakova, **Pavel Honsa**, David Dzamba, Anders Ståhlberg, Mikael Kubista, Miroslava Anderova (2013), Heterogeneity of Astrocytes: From Development to Injury–Single Cell Gene Expression, PloS one 8 (8), IF 3.730

CONTRIBUTIONS:
Animal surgery: Honsa P.
Cell isolation: Honsa P., Dzamba D.
RT-qPCR: Rusnakova V.,
Data analysis: Stahlberg A., Kubista M., Anderova M.

3) **Pavel Honsa**, Helena Pivonkova, Miroslava Anderova (2013), Focal cerebral ischemia induces the neurogenic potential of mouse *Dach1* expressing cells in the dorsal part of the lateral ventricles; Neuroscience, 2013/3/1, IF 3.122

CONTRIBUTIONS:
Animal surgery: Honsa P.
Patch-clamp recording *in vitro* and *in situ*: Honsa P., Pivonkova H.

Immunohistochemical analysis: Honsa P.
Data analysis: Honsa P., Anderova M.

Other author`s publications:

4) **Pavel Honsa**, Helena Pivonkova, Lenka Harantova, Olena Butenko, Jan Kriska, David Dzamba, Vendula Rusnakova, Lukas Valihrach, Mikael Kubista, Miroslava Anderova (2014) Increased expression of hyperpolarization-activated cyclic nucleotide-gated (HCN) channels in reactive astrocytes following ischemia. Glia. 2014 Jul 14. doi: 10.1002/glia.22721, IF 5.466

5) Iva Prajerova**, Pavel Honsa,** Alexandr Chvatal, Miroslava Anderova (2010) Neural stem/progenitor cells derived from the embryonic dorsal telencephalon of D6/GFP mice differentiate primarily into neurons after transplantation into a cortical lesion, Cellular and Molecular Neurobiology. *30(2),* IF 2.423

6) Olena Butenko, David Dzamba, Jana Benesova, **Pavel Honsa**, Valentina Benfenati, Vendula Rusnakova, Stefano Ferroni, Miroslava Anderova (2012); The increased activity of TRPV4 channel in the astrocytes of the adult rat hippocampus after cerebral hypoxia/ischemia; PloS One 7 (6), IF 3.730

7) Jana Benesova, Vendula Rusnakova, **Pavel Honsa**, Helena Pivonkova, David Dzamba, Mikael Kubista, Miroslava Anderova (2012); Distinct expression/function of potassium and chloride channels contributes to the diverse volume regulation in cortical astrocytes of GFAP/EGFP mice; PloS One 7(1), IF 3.730

8) Iva Prajerova, **Pavel Honsa**, Alexander Chvatal, Miroslava Anderova (2010); Distinct effects of Sonic hedgehog and Wnt-7a on differentiation of neonatal neural stem/progenitor cells *in vitro,* Neuroscience 171(3), IF 3.215

9) David Dzamba, **Pavel Honsa**, Miroslava Anderova (2013); NMDA Receptors in Glial Cells: Pending Questions; Current Neuropharmacology 11(3), IF 2.031

Book chapter:

10) Miroslava Anderova, **Pavel Honsa** (2012); Neural Stem/Progenitor Cell Proliferation and Differentiation: Role of Sonic Hedgehog and Wingless/Int-1 Proteins; Stem Cells and Cancer Stem Cells, Volume 4, pp 3-18; Editor: Hayat M.A. Publisher: Springer

TABLE OF CONTENTS

LIST OF ABBREVIATIONS

4-AP	4-aminopyridine
aCSF	artificial cerebrospinal fluid
Aldh1l1/ALDH1L1	aldehyde dehydrogenase 1 family gene/protein
aNSC	adult neural stem cell
AMPA	α-Amino-3-hydroxy-5-methyl-4-isoxazolepropionic acid
APC	Adenomatous polyposis coli
Aqp1/AQP1	aquaporin 1 gene/protein
Aqp4/AQP4	aquaporin 4 gene/protein
Aqp9/AQP9	aquaporin 9 gene/protein
bFGF	basic fibroblast growth factor
BL	basal lamina
BLBP	brain lipid-binding protein
BV	blood vessel
CD	current density
CD11b	Integrin alpha
Clcn2/CLCN2	chloride channel protein 2 gene/protein
C_m	membrane capacitance
CNS	central nervous system
Cspg4/CSPG4	chondroitin sulphate proteoglycan gene/protein
CXCL 10	interferon gamma-induced protein
DAPI	4',6-diamidino-2-phenylindole
DCX	doublecortin
DG	gyrus dentatus
Eaat1/EAAT1	excitatory amino acid transporter gene/protein
EGFP	enhanced green fluorescent protein
FCI	focal cerebral ischemia
GAM	goat anti-mouse antibody

GAR	goat anti-rabbit antibody
GCI	global cerebral ischemia
GCL	granular cell layer
Gfap/GFAP	glial fibrillary acidic protein gene/protein
GFP	green fluorescent protein
GL	glomerular layer
GLAST	glutamate/aspartate transporter
Glul	glutamine synthetase
GM	gray matter
Gria1	glutamate receptor, ionotropic, AMPA 1
Gria2	glutamate receptor, ionotropic, AMPA 2
Gria3	glutamate receptor, ionotropic, AMPA 3
Gria4	glutamate receptor, ionotropic, AMPA 4
Grik1	glutamate receptor, ionotropic, kainate 1
Grik2	glutamate receptor, ionotropic, kainate 2
Grik3	glutamate receptor, ionotropic, kainate 3
Grik4	glutamate receptor, ionotropic, kainate 4
Grik5	glutamate receptor, ionotropic, kainate 5
Grin1	glutamate receptor, ionotropic, N-methyl D-aspartate 1
Grin2a	glutamate receptor, ionotropic, N-methyl D-aspartate 2a
Grin2b	glutamate receptor, ionotropic, N-methyl D-aspartate 2b
Grin2c	glutamate receptor, ionotropic, N-methyl D-aspartate 2c
Grin2d	glutamate receptor, ionotropic, N-methyl D-aspartate 2d
Grin3a	glutamate receptor, ionotropic, N-methyl D-aspartate 3a
Grm1	metabotropic glutamate receptor 1
Grm3	metabotropic glutamate receptor 3
Grm5	metabotropic glutamate receptor 5
Hcn1/HCN1	hyperpolarization-activated cyclic nucleotide-gated channel 1 gene/protein

Hcn2/HCN2	hyperpolarization-activated cyclic nucleotide-gated channel 2 gene/protein
Hcn3/HCN3	hyperpolarization-activated cyclic nucleotide-gated channel 3 gene/protein
Hcn4/HCN4	hyperpolarization-activated cyclic nucleotide-gated channel 4 gene/protein
HEPES	4-(2-hydroxyethyl)-1-piperazineethanesulfonic acid
HP	hippocampus
HyTh	hypothalamus
Iba-1	calcium-binding adapter molecule 1
IFNy	Interferon gamma
Il-1b	Interleukin-1 beta
IL-6	Interleukin 6
I_{Na}	sodium current
iPSC	induced pluripotent stem cells
K_A	A-type potassium channel
Kcna3	potassium voltage-gated channel, shaker-related subfamily, member 3
Kcna4	potassium voltage-gated channel, shaker-related subfamily, member 4
Kcna5	potassium voltage-gated channel, shaker-related subfamily, member 5
Kcnj10	ATP-sensitive inward rectifier potassium channel 10
Kcnj16	potassium inwardly- rectifying channel, subfamily J, member 16
Kcnj2	potassium inwardly- rectifying channel, subfamily J, member 2
Kcnk1	potassium channel, subfamily K, member 1
Kcnk10	potassium channel, subfamily K, member 10
Kcnk2	potassium channel subfamily K member 2
K_{DR}	delayed outwardly rectifying potassium channels
Ki-67	nuclear cellular marker of proliferation
K_{IR}	inward-rectifier potassium ion channel
LV	lateral ventricle

LY	Lucifer Yellow
MAP-2	microtubule associated protein 2
MCA	middle cerebral artery
MCAo	middle cerebral artery occlusion
MOhms	megaohms
MOSP	myelin/oligodendrocyte specific protein
mV	milivolts
NeuN	neuronal nuclei
NG2	neuron glia specific protein
NMDA	N-methyl-D-aspartate
NO	nitric oxid
OB	olfactory bulb
OPC	oligodendrocyte precursor cell
PCR	polymerase chain reaction
pA	picoamperes
Pax-6	aniridia type II protein
PB	phosphate buffer
PBS	phosphate buffer saline
PCA	principal component analysis
PCNA	proliferation cell nuclear antigen
Pdgfra/PDGFαR	platelet-derived growth factor receptor alpha gene/protein
Pdgfrb/PDGFβR	platelet-derived growth factor receptor beta gene/protein
pF	picofarad
PFA	paraformaldehyde
PLL	polylysine
PTB	pentobarbital
qPCR	quantitative polymerase chain reaction
R_m	membrane resistance
RMS	rostral migratory stream

RT-PCR	real time polymerase chain reaction
S100b/S100β	β-subunit of S-100 calcium-binding gene/protein
SGZ	subgranular zone
Slc1a3	solute carrier family 1
Snap25 /SNAP25	synaptosomal-associated protein 25 gene/protein
SOM	Kohonen self-organizing maps
SVZ	subventricular zone
TEA	tetraethylamonium
TH	tyrosine hydroxylase
TNFa	tumor necrosis factor alfa
tPA	tissue plasminogen activator
Trpv4/TRPV4 protein	transient receptor potential cationic channel V member 4 gene/
TTC	2,3,5-triphenyltetrazolium chloride
TTX	tetrodotoxin
V_{rest}	resting membrane potential
WM	white matter

INTRODUCTION

Focal cerebral ischemia or its synonym stroke is the third most common cause of death in the industrialized countries with an estimated global mortality of 4.7 million people per year. It is the major cause of serious, long-term disability, with more than 18 million adults reporting functional limitations resulting from stroke. Moreover, recent evidence suggests that the presence of small strokes or of local chronic ischemia may be much more common in aging populations than previously thought. Simultaneously, recent studies indicate that the brain ischemia occurs more frequently in middle age population, which is alarming situation that increase the demand for effective prevention and treatment of this disease (Béjot et al., 2014).

However, after several years of studying and preclinical testing of more than 1000 possible drugs on animal models there is currently only one treatment that is somewhat successful in a subpopulation of stroke victims. The thrombolytic, tissue plasminogen activator (tPA) has been proven effective in treating stroke in the humans when given within 3 hours after the onset of neurological symptoms (Bramlett and Dietrich, 2004).

Great expectations were seen in the stroke treatment employing neural stem cells obtained from several sources – cell based therapy. The most used and promising source was from human embryos. The embryonic neural stem cells could be implanted into ischemic regions and differentiated into neurons, nevertheless only small number of them survived and integrated into neuronal circuits, so the favorable outcome was negligible and ethical issues were enormous (Muir and Kalladka, 2014). To overcome the ethical issues several investigators tried to generate induced pluripotent stem cells (iPSC) from patient cells and differentiated them *in vitro* into neuroblasts, which could be implanted into ischemic regions. Nevertheless, this approach is complicated due to low numbers of neuroblasts generated from iPSC and potential teratogenicity of these cell types (Kwon et al., 2012).

Simultaneously with the above-mentioned methods a number of researches started to study the naturally ongoing endogenous processes after ischemia – the neurogenesis and gliogenesis in order to understand these processes and eventually increase their rate and significance in the post-ischemic regeneration. This approach

should eliminate ethical issues and there should be no problems with patient's immune system after implantation of donor's cells. Therefore, this thesis is focused on the processes of adult neurogenesis and gliogenesis predominantly after ischemia.

Adult neurogenesis

Neurogenesis (birth of neurons) is the process by which neurons are generated from neural stem- and progenitor cells. This phenomenon is mainly active during mammalian pre-natal development; neurogenesis is responsible for populating the growing brain with neurons (Zhao et al., 2008). This process is in ongoing development immediately followed by gliogenesis, where non-neuronal glia cell populations are derived from multipotent neural stem cells. Since the adult central nervous system (CNS) of mammals possesses a limited capacity for regeneration after injury (Gage and Temple, 2013) it was though for a long time that these cell-generating processes take place mainly in prenatal or neonatal brains. However, within last 20 years, numerous studies confirmed generation of new neural cells also in the fully matured mammalian CNS under physiological as well as pathological conditions. Currently, it is generally accepted that neurogenesis and gliogenesis occurs in adult mammalian brain.

In adult brain, two specific regions with the highest production of new neural cells were discovered: the subventricular zone (SVZ) of the lateral ventricles (LV, Figure 1), where new neurons are generated and then migrate through the rostral migratory stream (RMS) to the olfactory bulb to become interneurons (Song et al., 2002) and the subgranular zone (SGZ) in the dentate gyrus of the hippocampus, where new dentate granule cells are generated (Figure 2). In both of these regions the process of adult neurogenesis is, on the cellular level, based on three main cell types.

The first comprises the adult neural stem cells that exhibit properties almost identical as astrocytes, but additionally, they have the ability to divide asymmetrically. In the SVZ neurogenic region they are known as B cells and as type 1 cells in the SGZ. Their typical markers are glial fibrillary acidic protein (GFAP), nestin, vimentin or Musashi (Strojnik et al., 2007). They renew themselves and also give rise to so-called transit-amplifying cells (C cells in the SVZ region and type 2 cells in the SGZ

region). These cells proliferate fast and give rise to neuroblasts (A cells) in the SVZ and to new granule cells in the SGZ.

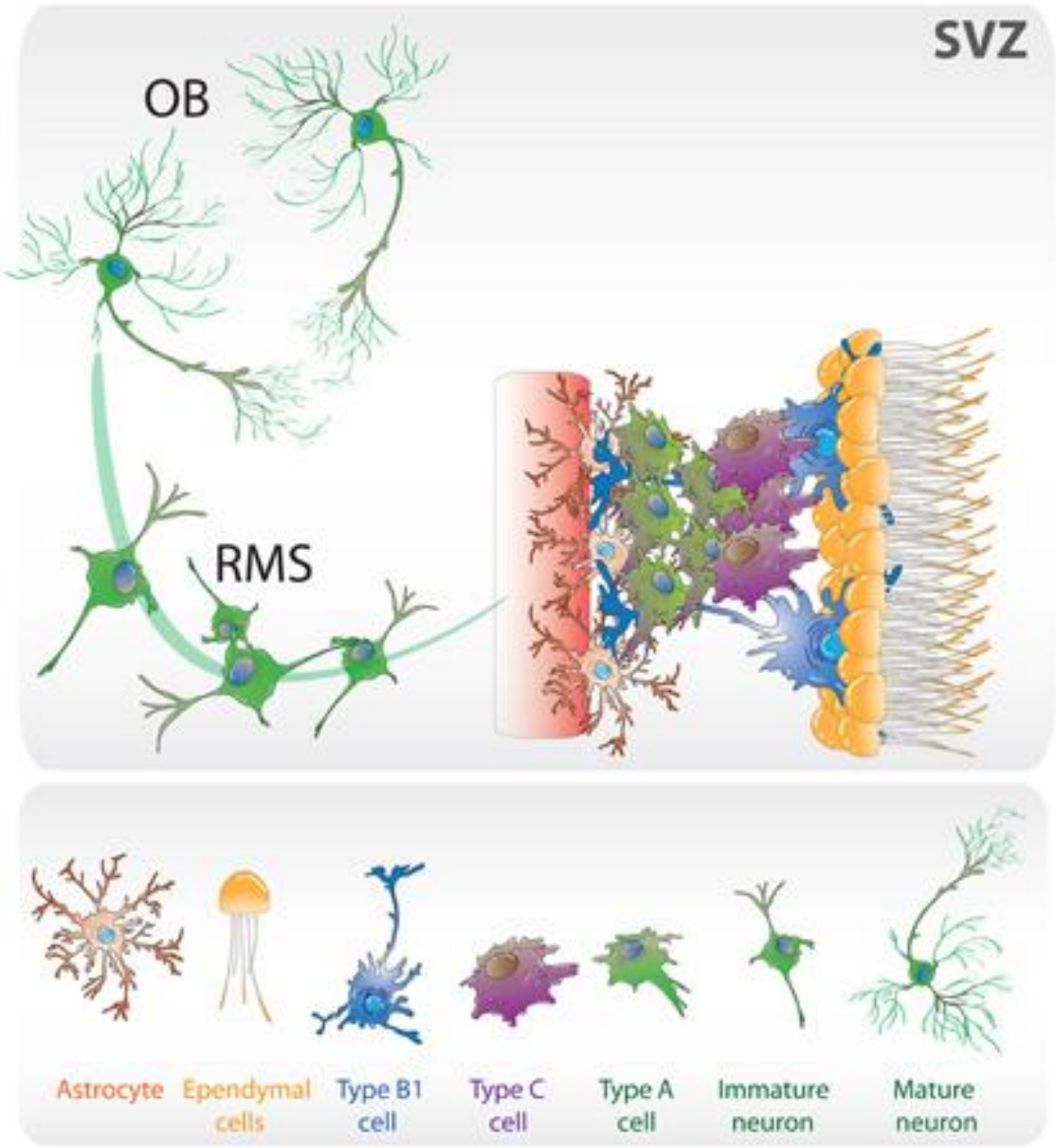

Figure 1. Adult neurogenesis in the subventricular zone (SVZ). Neurogenic niche composed of type B1 cells that correspond to neural stem cells, type C cells that rapidly proliferate and type A neuroblasts, which migrate through the rostral migratory stream (RMS) to the olfactory bulb (OB) where they mature into interneurons (Varela-Nallar and Inestrosa, 2013).

Neuroblasts express some immunohistochemical markers of immature neurons (e.g. doublecortin, beta III-tubulin) and they are able to migrate to different regions in the brain. In the case of SVZ, neuroblasts use RMS as a long migration pathway to get into olfactory bulb and differentiate into interneurons, but in SGZ new granule cells

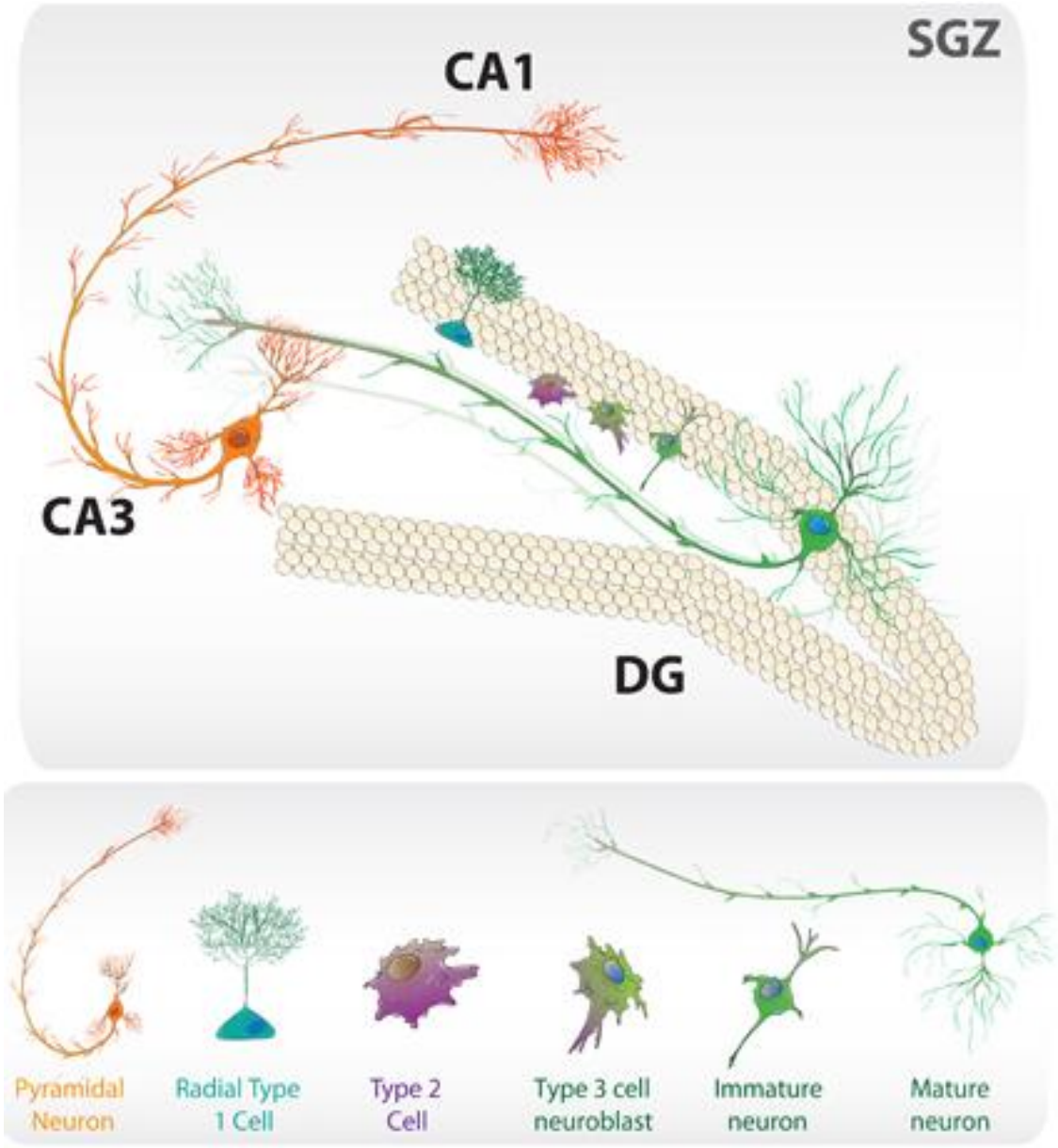

Figure 2. Adult neurogenesis in the subgranular zone (SGZ), (Radial type 1 cells give rise to type 2 cells that differentiate into type 3 neuroblasts that become immature neurons, which then mature into granule neurons after their migration into the granule cell layer (Varela-Nallar and Inestrosa, 2013).

have only short migration pathway into granular zone, where they undergo the process of differentiation into mature neurons (Varela-Nallar and Inestrosa, 2013). Currently, with discovering new, more sensitive methods, the process of neurogenesis was also identified in many other brain regions under physiological conditions, but in significantly lower extent when compared to SGZ or SVZ regions. To such regions in adult mammals belong, for example, hypothalamus (Cheng, 2013), striatum (Gould, 2007), cortex (Tan and Shi, 2012) or cerebellum (Carletti and Rossi, 2008).

Adult gliogenesis

A different situation is in the case of gliogenesis. There exist four main types of glial cells in the adult mammalian CNS with different functions and properties: astrocytes, oligodendrocytes, microglia and polydendrocytes.

Astrocytes are the main glial cells that maintain the ionic and neurotransmitter homeostasis, participate in maintaining the blood brain barrier, stabilize and modify synapses, regulate immune response, remodel the extracellular space and connect blood vessel with neurons thus supplying the neurons with energy (Allaman et al., 2011). Some authors also claim that adult neural stem cells in the adult CNS belong to a subpopulation of astrocytes (Doetsch, 2003). Oligodendrocytes are the main myelinating cells in the CNS thereby accelerate transmission of action potentials and are numerous predominantly in the white matter (Brophy, 1991). Microglia cells are the main immune cells in the CNS with massive phagocytic activity and are the only glial cells that are not derived from ectoderm, but mesoderm, invading developing neural tissue before closing the blood brain barrier (Zabel and Kirsch, 2013). Polydendrocytes (also known as NG2 cells, synantocytes, interglia or oligodendrocyte precursor cells) represent a fourth glial population in the mammalian brain, distinct from mature oligodendrocytes, astrocytes or microglia. Until recently they have been assumed to give rise only to oligodendrocytes in the intact adult CNS, but recently, it was demostrated that they express larger differentiation potential and are able to form synapses with neurons, which implies their more important functions

(Yang et al., 2013). Some of these glial cell types were shown to be generated continuously during entire lifetime in many brain regions under physiological conditions. A large number of widespread, actively proliferating glial progenitors have been detected throughout the brain (Figure 3). In the healthy brain, these progenitors generate glial cells almost exclusively of the oligodendrocyte lineage. In the cerebral cortex, virtually all cycling cells express the proteoglycan NG2 (Simon et al., 2011) the transcription factor Olig2 (Buffo et al., 2008) and the platelet-derived growth factor receptor alpha (PDGFαR), (Rivers et al., 2008). Consistent with the molecular

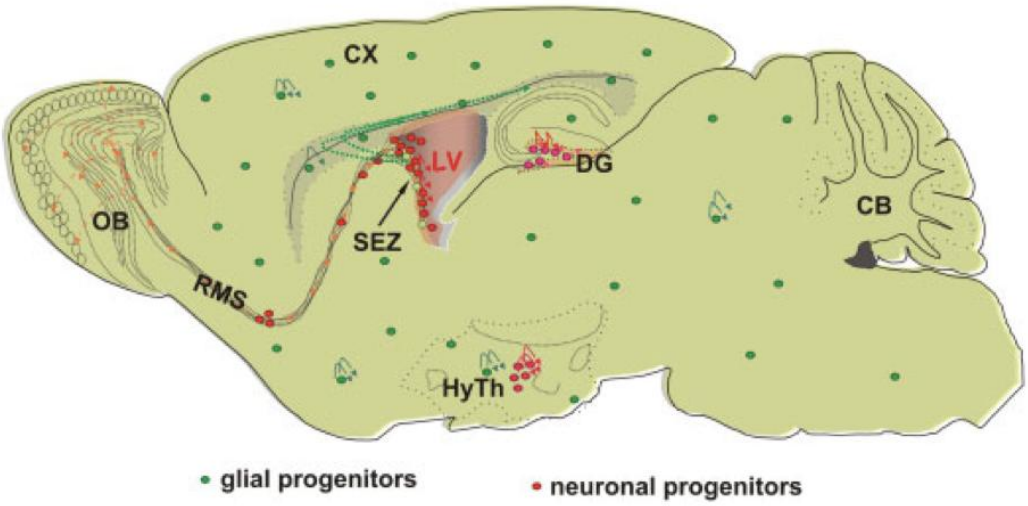

Figure 3. Neurogenesis, but not gliogenesis, is spatially restricted in the adult mouse brain. Scheme depicting the neurogenic (red) and gliogenic zones (green) in the adult mouse brain. Note that neuronal progenitors (red) are restricted to three regions of the mouse brain: subependymal zone (SEZ) of the lateral ventricles, subgranular zone in the dentate gyrus (DG) and hypothalamus (HyTh), while gliogenic progenitors (green) are spread throughout the brain parenchyma. Abbreviations: OB, olfactory bulb; CX, cortex; RMS, rostral migratory stream; CB, cerebellum; LV, lateral ventricle (Ninkovic and Götz, 2014).

similarity of these adult progenitors to oligodendrocyte progenitor cells (OPCs) during development, tamoxifen-inducible genetic labelling of these progenitors demonstrated that Olig2- or PDGFαR progenitors largely generate cells of the oligodendroglial lineage in the adult brain (Dimou et al., 2008). Interestingly, the progeny of adult Olig2 progenitors differs between white matter (WM) regions of the

adult cerebral cortex, where mostly myelinating oligodendrocytes are generated, and grey matter (GM) regions, where more polydendrocytes persist (Dimou et al., 2008). Notably, evidence for ongoing gliogenesis and NG2/Olig2 dividing cells have also been observed in the human brain (Hampton et al., 2004) suggesting active and widespread gliogenesis in the adult mammalian brain. However, in contrast to neurogenesis, the function of gliogenesis in the healthy adult brain has so far not been addressed, but is probably related to plasticity of neuronal connections (Bohlen und Halbach, 2011). Under the physiological conditions no proliferation and generation of other glial cells types was detected; however, massive neurogenesis as well as gliogenesis were observed after different types of CNS injuries headed by the most common type of injury – brain ischemia.

Ischemic brain injury

Ischemia is a typical and the most common type of injury in the CNS. There are two main types of ischemia – global cerebral ischemia (GCI) often a phenomenon after cardiac arrest and focal cerebral ischemia (FCI), which is caused either by a blood clot of some main brain arteries (typically middle cerebral artery [MCA]) or by subarachnoidal/intracerebral hemorrhage.

Ischemic brain injury is a very complex process and this complexity significantly slows and limits the possible treatment therapy. Immediately after blood flow reduction, a variety of ionic imbalances and glutamate release occur, resulting in neuronal cell death. Propagated or non-propagated depressions of electrical activity commonly called cortical spreading depression have been described in number of experimental models of focal cerebral ischemia (Hansen and Lauritzen, 1984; Back et al., 1994; Koroleva and Bures, 1996; Zhang et al., 2002). Importantly, these ionic events contribute to additional neuronal damage in the ischemic penumbra (Mies et al., 1993; Back et al., 1996). Both necrotic and apoptotic cell death mechanisms have been implicated in the pathogenesis of ischemia (Liu and Zhu, 1999; Snider et al., 1999; Martin, 2000; Graham and Chen, 2001). The brain is vulnerable to oxidative stress due to its high rate of oxidative metabolic activity (Maier and Chan, 2002) and such oxidative stress ultimately leads to calcium accumulation, mitochondrial

dysfunction and the production of reactive oxygen radicals, which are important triggers of cell death following ischemic insults (Globus et al., 1995). Importantly, while necrotic neuronal damage is commonly observed early after severe ischemic insults, apoptotic cell death may also occur following rather mild insults. Several studies on cerebral ischemia have also implicated calcium-induced calpain-mediated proteolysis in the pathogenesis (Hong et al., 1994; Bartus et al., 1995; Saatman et al., 1996; Posmantur et al., 1997; Büki et al., 1999) of ischemic injury. Uncontrolled calpain proteolysis of multiple substrates has serious consequences, in terms of cell survival and death. In the CNS an inflammatory response to ischemic injury may have various consequences on the outcome following ischemia, depending upon the degree of inflammatory response. Both acute and chronic inflammatory processes have been shown to influence processes after ischemia. While acute inflammatory events may contribute to secondary injury processes, more delayed inflammatory events may be reparative (Kerschensteiner et al., 1999; Bethea and Dietrich, 2002). Severe ischemia results in metabolic stress and very fast depletion of essential energy metabolites (Back, 1998; Dirnagl et al., 1999). Simultaneously, ischemic injury can result in K^+-induced release of excitatory amino acids, due to low activity of Na^+/K^+ ATPase (Figure 4). This high concentration of neurotransmitters (including glutamate, glycine, GABA, and dopamine) causes predominantly opening of glutamate receptor associated ion channels and the influx of Ca^{2+} (Choi et al., 1987; Siesjö et al., 1989). An important role in the pathophysiology of cerebral ischemia plays also nitric oxide (NO), of which high concentrations were documented (Dalkara and Moskowitz, 1994; Iadecola, 1997; Stagliano et al., 1997; Ashwal et al., 1998). However, when studied in ischemic models, abnormal NO production was shown to be both beneficial and detrimental, depending upon when and where this diffusible neurotransmitter is released (Iadecola, 1997).

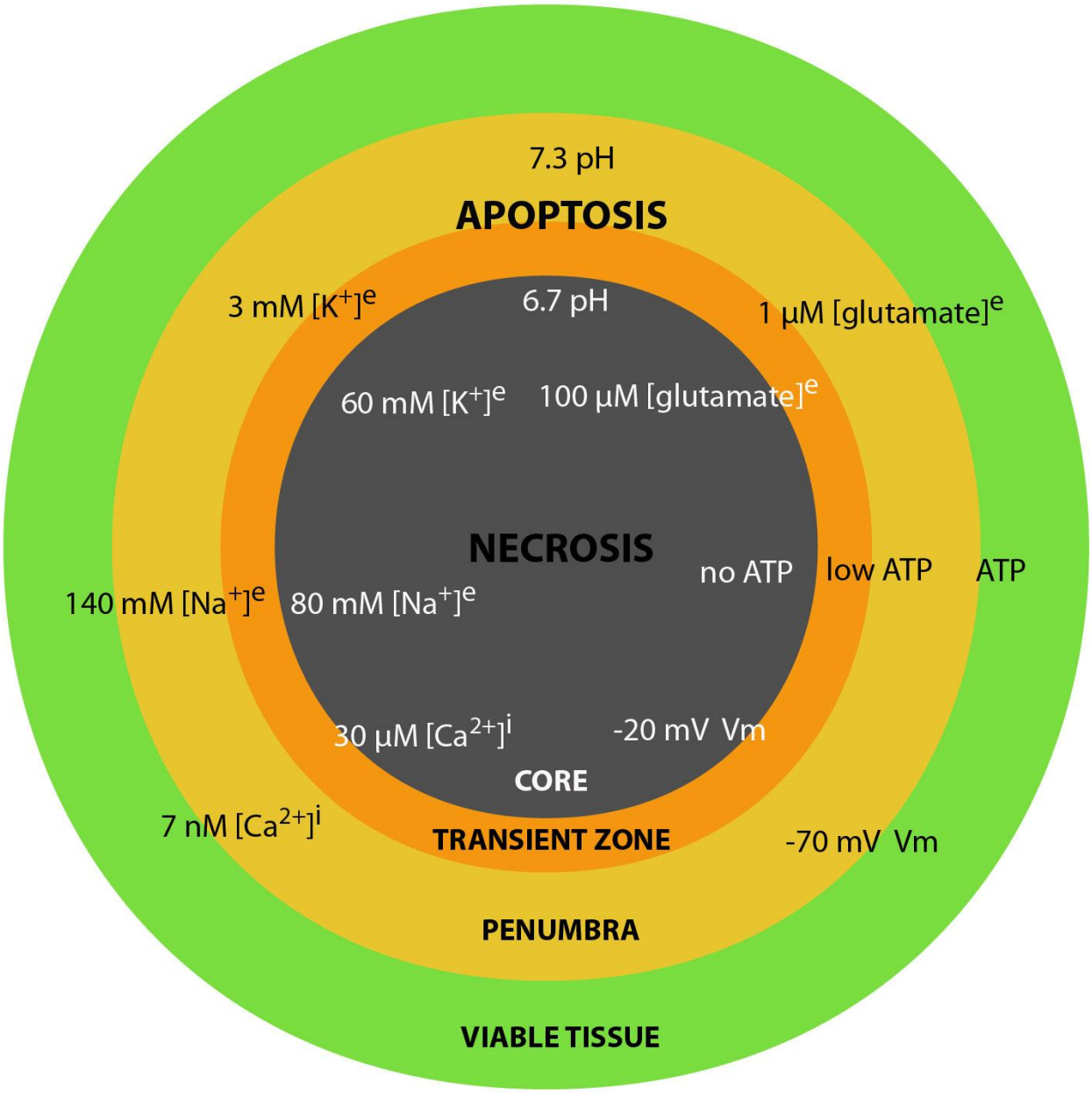

Figure 4. Schema depicting the main physiological changes in the ischemic core and penumbra. Due to lack of oxygen and glucose, there is low concentration of ATP in the ischemic core, which leads to low efficiency of Na^+/K^+ ATPase, and high extracellular concentration of K^+ and glutamate. Simultaneously, the cells in the ischemic core have depolarized membrane potential and there is also significant acidification. All these factors result in necrotic death of cells in the ischemic core and to massive apoptotic death in the surrounding penumbra. Abbreviations: e, extracellular concentration; i, intracellular concentration.

Animal models of focal cerebral ischemia

Several animals' models were developed enabling to study the ischemic injury in the CNS. Initially, larger rodents, such as rats, gerbils or rabbits were used as model organism and almost all pathological processed were described on them. The simplest model of ischemia is animal decapitation, suitable for analyzing processes occurring immediately after blood absence (Gerasimov et al., 2004). Moreover, a cortical stab wound was used to simulate traumatic brain injury together with ischemia (Anderova et al., 2004). Another model closely simulating local brain ischemia is photochemical lesion, in which photosensitive substance is injected into animals and the illuminated part of brain cortex is damaged (Watson et al., 1985; Prajerova et al., 2010); however, in this model of ischemic injury the penumbra is missing. Recently, several models more accurately simulating local brain ischemia were developed. Intraluminal MCA occlusion was the most common model used in rats, in which a long filament with defined diameter is inserted through common carotid artery to block blood flow to the MCA territory. This method yielded constant extent of injury when compared to other often-used method as photochemical lesion. Alternatively, FCI could be induced by application of endothelin-1, which results in contraction of MCA and reduced blood flow. Recently, also embolic models were introduced, where blood cloth or numerous compounds are injected into internal carotid artery and produce artificial emboli; however, with enormous variability (Sicard and Fisher, 2009).

Nowadays, the most researchers study ischemia in mice, because the availability of numerous transgenic mouse strains significantly accelerates the research. Since mice are smaller and more sensitive to ischemia, such switch in experimental animals brings several complications, which results in higher mortality rate and more demanding surgical procedures. From this reason a transcranial model of MCAo, where MCA is electro-coagulated directly on the brain surface, was introduced. This model has low variability and high survival rate, because the ischemia is localized only in a small cortical region. Therefore, this model was also used in this study.

Impact of ischemic injury on gliogenesis

It is well known that CNS injuries, such as traumatic brain injury or ischemia, trigger neurogenesis and gliogenesis in the adult mammalian brain. Almost every type of injury, which occurs in the CNS, evokes complex reaction of the neural tissue, which is accompanied by the formation of reactive astrogliosis (Figure 5). This process is vital for isolating necrotic tissue from its uninjured surroundings, it decreases the spreading of pathogens, immune cells as well as ionic- and neurotransmitter misbalance to the uninjured healthy neural tissue. On the other hand, the astrogliosis markedly impedes regenerative processes, since this dense structure is impenetrable barrier for cells migration or axonal re-growth, predominantly in the case of spinal cord injury (Pekny et al., 2014). The gliotic scar is composed mainly from astrocytes that are in reactive state, which is characterized by upregulated transcription of dozens of genes and increased expression of many proteins, especially cytoskeletal proteins (GFAP, nestin, vimentin, synuclein), (Fellner et al., 2011). These newly expressed proteins help to increase the mechanical strength at the site of the scar and some of them are necessary for cell proliferation. The reactive astrocytes are hypertrophied, because of enlargement of their cell bodies as well as cellular processes, and such changes in astrocyte morphology significantly decrease extracellular space at the site of injury (Roitbak and Syková, 1999). Reactive astrocytes can also produce pro-inflammatory cytokines that exacerbate the CNS regeneration. Many recent studies showed that adult reactive astrocytes posses the ability to proliferate and thereby also increase their number and cell density at the site of injury (Bardehle et al., 2013). Moreover, recent studies revealed that these proliferating astrocytes posses many properties of neural stem cells and may differentiate into other neural cell types under proper conditions (Sirko et al., 2013).

Nevertheless, the origin of reactive astrocytes in the glial scar is still a matter of debate. Some authors claim that these newly derived astrocytes are generated from original astrocytic population (Komitova et al., 2011), but on the other hand, relative low proliferative capacity of astrocytes precludes this hypothesis (Anderova et al., 2010). Recently, attention has turned to polydendrocytes and their possible role in the regeneration following ischemia.

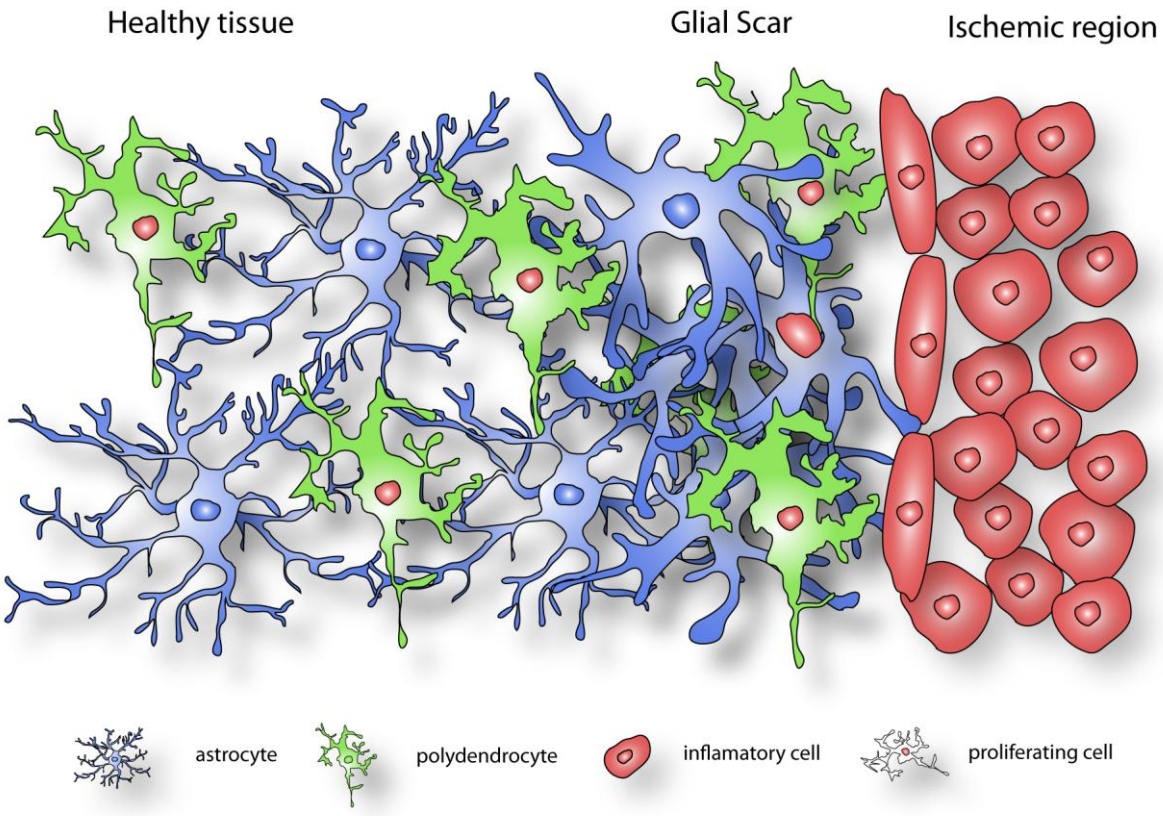

Figure 5. Scheme of cell types in the post-ischemic cortex. Formation of compact glial scar occurs along borders to areas of overt tissue damage and inflammation, and includes newly generated astrocytes (blue cells) and other cell types such as polydendrocytes (green cells), as well as deposition of dense collagenous extracellular matrix. In the compact glial scar, astrocytes have densely overlapping processes. Mature glial scars tend to persist for long periods and act as barriers not only to axon regeneration, but also to inflammatory cells (red cells), infectious agents, and non-neural cells in such a manner that protect healthy tissue from nearby areas of intense inflammation. Red nuclei indicate proliferating cells.

Polydendrocytes in the adult brain can be identified by their highly branched morphology and their expression of NG2 proteoglycan (NG2) together with PDGFαR (Nishiyama, 2007) as was mentioned above. Until recently they have been assumed to give rise only to oligodendrocytes in the intact adult CNS, although polydendrocytes are known to be capable of generating neurons and astrocytes *in vitro* in the presence of specific morphogens (Belachew, 2003) and *in vivo* after transplantation into the hippocampus (Aguirre, 2004). Additionally, shortly after

ischemia in the surrounding tissue the polydendrocytes are the most proliferating cells and they are able to migrate to the site of injury. Therefore, a hypothesis exists that some reactive astrocytes in the glial scar could differentiate from polydendrocytes. Nevertheless, recent studies using lineage-specific Cre-recombinase transgenes for genetic fate-mapping studies in the intact CNS have revealed inconsistent findings. The capability of polydendrocytes to differentiate into oligodendrocytes *in vivo* was clearly confirmed by Guo and colleagues (Guo et al., 2010); however, Rivers and co-authors (Rivers et al., 2008) also demonstrated the differentiation of polydendrocytes into grey matter astrocytes. Additionally, several recent studies have described the generation of new neurons in the piriform cortex from polydendrocytes in PDGFαR- or Plp-promoter-driven Cre-recombinase transgenic mice (Rivers et al., 2008; Guo et al., 2010). On the other hand, in NG2- or Olig2- promoter-driven Cre-recombinase transgenic animals, such neuronal differentiation was not observed (Dimou et al., 2008; Zhu et al., 2008).

Interestingly, polydendrocytic differentiation into oligodendrocytes is under ischemic conditions almost completely blocked (Sozmen et al., 2009). And moreover, the oligodendrocytes in the proximity of the ischemic lesion represent, beside neurons, one of the most sensitive cells to pathological conditions induced by ischemic injury and massively die. The main cause of this high sensitivity to ischemia is an increased expression of calcium permeable N-methyl-D-aspartate (NMDA) receptors on oligodendrocytic membranes. Under physiological conditions these NMDA receptors are important for regulation of myelin formation in response to neuronal activity (De Biase et al., 2011), but during ischemia they conduct calcium entry, which activates apoptotic mechanisms.

Besides astrocytes and polydendrocytes, brain immune cells, microglia, play an important role in the processes around ischemic region. After stroke they rapidly change their status from resting microglia into activated microglia. During this transformation microglia start to migrate, express specific surface proteins and pro-inflammatory mediators, such as IFNγ, Il-1β, TNFα, Il-6, CXCL10, etc. The ability of microglia to fast migrate into ischemic regions through detection of chemoattractant gradients is mainly neuroprotective, because they rapidly phagocytize debris in damaged tissue, neutrophils, and apoptotic cells that have the potential to release damaging molecules. Simultaneously with migration and activation, microglia also massively proliferate and thereby increase the immune response. However, the

presence of high numbers of active microglia results in release of high concentrations of neurotoxic substance like TNF-α, NO and matrix metalloproteinases, which significantly damage neuronal cells in the ischemic penumbra and deteriorate the ischemic impact (Platel et al., 2010).

THE AIMS OF PHD THESIS

Hypothesis 1.: Polydendrocytes were shown to have multipotent differentiation potential after their isolation from adult mouse brain under *in vitro* conditions as well as *in vivo* during embryonic brain development (Belachew, 2003; Zhu et al., 2007). During development multipotency of polydendrocytes is probably caused by their exposure to various growth factors that are also released in post-ischemic tissue (Krüger et al., 2006), therefore we hypothesized that polydendrocytes under ischemic conditions might display an extended differentiation potential as well. For that reason, we used genetic fate-mapping technique to confirm or exclude their multipotency.

Aim 1.: To determine the differentiation potential of polydendrocytes in the gliotic scar around the focal ischemic injury in the primary somatosensory cortex – focus on their neurogenic or gliogenic potential.

Hypothesis 2: The glial scar is a structure, which develops after ischemia and comprises several cell types, predominantly reactive astrocytes. Despite the fact that astrocytes after ischemia posses only limited proliferative potential, their number following ischemic injury increases. Such finding indicates that other cell types, such as polydendrocytes, might participate in generating reactive astrocytes. Therefore, a question arose whether all reactive astrocytes in the glial scar represent a uniform cell population or distinct subpopulations of reactive glial cells co-exist in the vicinity of ischemic lesion. Using gene expression profiling on single-cell level could reveal the heterogeneity or homogeneity of reactive cells population.

Aim 2.: To define changes in gene expression profile of glial cell during ischemia-induced gliogenesis.

Hypothesis 3.: Adult SVZ comprises neural stem cells that originated from different regions of embryonic brain. The lateral wall of the LV contains adult neural stem cells of striatal origin and their properties and role in neurogenesis are already well described. On the other hand, the stem cell potential of cells from the dorsal part of the LV, which are predominatly of the cortical origin, was not elucidated yet. Using transgenic mouse strain that enabled visualization of cells with cortical origin, we examined whether these cells posses neural stem cell properties and contribute to post-ischemic neurogenesis.

Aim 3.: To clarify the role of adult neural stem cells localized in the dorsal part of the LV in the process of adult neurogenesis and gliogenesis during physiological as well as post-ischemic conditions.

MATERIALS AND METHODS

Transgenic mice

All procedures involving the use of laboratory animals were performed in accordance with the European Communities Council Directive 24 November 1986 (86/609/EEC) and animal care guidelines approved by the Institute of Experimental Medicine ASCR Animal Care Committee on April 17, 2009.

To study differentiation potential of polydendrocytes we used, NG2creBAC transgenic mice, which express constitutively active Cre-recombinase in polydendrocytes (Zhu et al., 2008). NG2creBAC mice were crossed with the reporter mouse strain Z/EG to generate NG2creBAC:ZEG double transgenic mice. The mice carrying both modifications were selected by polymerase chain reaction (PCR). These double transgenic mice express Cre-recombinase under the control of the mouse NG2 (*Cspg4*) promoter/enhancer. In the Cre-recombinase-expressing cells, lacZ expression is replaced with enhanced green fluorescent protein (EGFP) expression, and these cells can be easily visualized and tracked (Figure 6). All mouse strains were obtained from The Jackson Laboratory, Bar Harbor, USA.

To define changes in gene expression profile of astrocytic/glial subpopulations during post-ischemic gliogenesis GFAP/EGFP mice were used. In these genetically modified mice the promoter of human GFAP controls the expression of EGFP. In this mouse strain a subpopulation of astrocytes and polydendrocytes express EGFP (Nolte et al., 2001), (Figure 6).

The transgenic mice, in which expression of green fluorescent protein (GFP) is driven by the promoter of mouse *Dach1* gene (D6/GFP mice) were used for elucidating the role of adult neural stem cells localized in the dorsal part of the LV in the process of adult neurogenesis and gliogenesis. This mouse strain was kindly provided by Dr. Machon and Dr. Kozmik (Machon et al., 2002), (Figure 6).

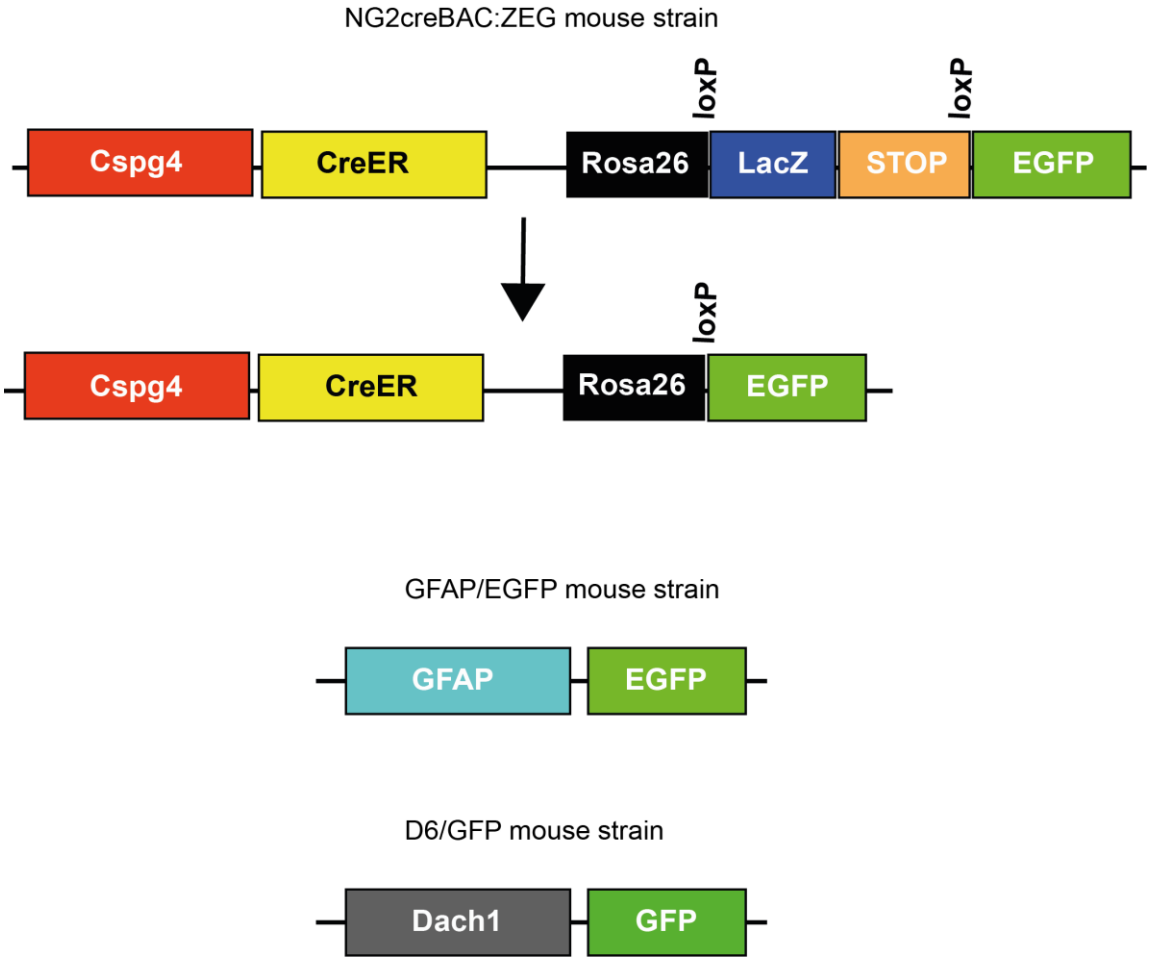

Figure 6. Schema summarizing all genetically modified mouse strains used in this work. For experiments studying differentiation of polydendrocytes double trangenic mouse strain NG2creBAC:ZEG was used, in which the stop sequence and LacZ gene in the EGFP promoter are cut out concomitantly with *Cspg4* expression and the CSPG4-positive cells (polydendrocytes, pericytes) start to express EGFP. To study predominantly astrocytes GFAP/EGFP mouse strain was used. D6/GFP mouse strain was employed in the study describing adult neurogenesis of dorsal lateral ventricle.

Induction of distal middle cerebral artery occlusion (MCAo) in adult mice

To induce FCI a transcranial MCA occlusion (MCAo) was employed. This approach has significantly lower mortality rate, is highly reproducible and less time-consuming than filament method (Rosell et al., 2013).

Mice (60-90 days old) were anaesthetized for MCAo induction with 1.5% Isoflurane and maintained in 1% Isoflurane using a vaporizer (Tec-3, Cyprane Ltd., Keighley, UK). A skin incision was made between the orbit and the external auditory meatus, and a 1-2 mm hole was drilled through the frontal bone 1 mm rostral to the fusion of the zygoma and the squamosal bone and ~3.5 mm ventral to the dorsal surface of the brain. The middle cerebral artery (MCA) was exposed after the dura was opened and removed. The MCA was occluded by short coagulation with bipolar tweezers at a proximal location, followed by transection of the vessel to ensure permanent disruption. The mice received 0.5 ml saline subcutaneously, and their body temperature during the surgery was maintained at 37 ± 1°C using a heating pad. Sham operated animals (controls) were subjected to the same surgical procedure, without dura opening and vessel occlusion. To visualize the ischemic region unfixed brain slices were stained with 2% 2.3.5-triphenyltetrazolium chloride (TTC) at 37°C for 20 minutes. This MCAo model yielded smaller infarcts localized only in the cortical region (Figure 7).

Figure 7. Triphenyltetrazolium staining of coronal slices of the uninjured mouse brain (left) and the brain 24 hours after ischemia (right). White area represents cortical structures damaged by ischemia. MCAo, middle cerebral artery occlusion.

Preparation of acute brain slices

Control animals or mice 3, 4, 7 or 14 days after MCAo (D3, D7, D14) were deeply anaesthetized with pentobarbital (PTB), (100 mg/kg, i.p.) and perfused transcardially with cold (4-8°C) isolation solution containing (in mM): 110 NMDG-Cl, 2.5 KCl, 24.5 $NaHCO_3$, 1.25 Na_2HPO_4, 0.5 $CaCl_2$, 7 $MgCl_2$, 20 glucose, osmolality 290 mOsm/kg. The mice were decapitated, the brains were quickly dissected out and transversal 200 µm thick slices were cut using a vibration microtome (HM 650 V, Thermo Scientific Microm, Walldorf, Germany). The slices were incubated for 30 minutes at 34°C in the isolation solution and then held at room temperature in artificial cerebrospinal fluid solution (aCSF) containing (in mM): 122 NaCl, 3 KCl, 28 $NaHCO_3$, 1.25 Na_2HPO_4, 1.5 $CaCl_2$, 1.3 $MgCl_2$, 10 glucose, osmolality 305 mOsm/kg. Solutions were equilibrated with gas mixture containing 95% O_2/ 5% CO_2 in order to reach a final pH of 7.4 and sufficient saturation with O2 for keeping brain slices. Osmolality was measured using a vapor pressure osmometer (Vapro 5520, Wescor, Logan, UT, USA).

Patch-clamp recordings

Cell membrane currents were recorded with the patch-clamp technique in the whole-cell configuration (Hamill et al., 1981). Recording pipettes with a tip resistance of 6–8 Mohms were made from borosilicate capillaries (0.86 ID, Sutter Instruments Company, Novato, CA, USA) using a Brown-Flaming micropipette puller (P-97, Sutter Instruments Company, Novato, CA, USA). Electrodes were filled with a solution containing (in mM): 130.0 KCl, 0.5 $CaCl_2$, 2.0 $MgCl_2$, 5.0 EGTA, 10.0 HEPES. The pH was adjusted with KOH to 7.2; or 130 K-gluconate, 0.5 $CaCl_2$, 5 EGTA, 10 HEPES, 3 Mg-ATP and 0.3 Na-GTP; the final pH was adjusted to 7.2 with KOH.To visualize the recorded cells within the GFP^+ or $EGFP^+$ cell population, the cells were filled with Lucifer Yellow (LY, Sigma–Aldrich, Germany) or Alexa Fluor 594 hydrazide (Invitrogen, CA, USA) by dialyzing the cytoplasm with the patch pipette solution. The morphology of cells imaged by intracellular dye was used for subsequent immunocytochemical identification using a confocal microscope. The recordings were

made either in slices or cover slips perfused with aCSF at a temperature of 22–25°C. The slices (or cover slips) were placed into a chamber mounted on the stage of a fluorescence microscope (Axioskop2 FS plus, Zeiss, Oberkochen, Germany). Slices were fixed using a U-shaped platinum wire with a grid of nylon threads. The cells were approached by the patch electrode using an INFRAPATCH system (Luigs & Neumann, Ratingen, Germany). The cells and the recording electrodes were imaged with a digital camera (Axiocam HRc, Zeiss, Oberkochen, Germany). Current signals were amplified with an EPC-10 amplifier (HEKA Elektronik, Lambrecht/Pfalz, Germany), lowpass filtered at 3 kHz and sampled at 5 kHz. Data acquisition and storage were performed with PATCHMASTER and analysis was performed with FITMASTER (HEKA Elektronik, Lambrecht/Pfalz, Germany).

Electrophysiological measurements and protocols

Resting membrane potential (V_{rest}) was measured by switching the EPC-10 amplifier to the current-clamp mode. Membrane capacitance (C_m) was determined automatically during acquisition by PATCHMASTER using ‘‘lock in’’ mode. Membrane resistance (R_m) was determined from the currents elicited by a 10-mV test pulse depolarizing the cell membrane from a holding potential of -70 to -60 mV, 40 ms after the onset of the depolarizing pulse. Current patterns were obtained by clamping the cell membrane from a holding potential of either -70 or -50 mV to values ranging from -160 to +40 mV, respectively, at intervals of 10 mV. Pulse duration was 50 ms. In order to isolate the voltage-gated delayed outwardly rectifying K^+ (K_{DR}) current component; a voltage step from -70 to -60 mV was used to subtract time- and voltage-independent currents. To activate K_{DR} current only, the cells were held at -50 mV, and the amplitude of the K_{DR} current was measured at +40 mV at the end of the pulse. The fast activating and fast inactivating outwardly rectifying K^+ (K_A) current component was isolated by subtracting the current traces clamped at -110 mV from those clamped at -50 mV, and its amplitude was measured at the peak value. Tetraethyl-ammonium chloride (TEA, 10 mM) and 4-aminopyridine (4-AP; 5 mM) were used to identify the K_A and K_{DR} current components. The inwardly rectifying K^+ (K_{IR}) current component was isolated by subtracting the current traces recorded in 1 mM CsCl-containing solution from those recorded under control conditions. K_{IR}

current amplitudes were measured at the end of the pulse. Tetrodotoxin- (TTX, Alomone Labs, Jerusalem, Israel) sensitive Na^+ (I_{Na}) currents were isolated by subtracting the current traces recorded in 1 µM TTX-containing solution from those recorded under control conditions. Na^+ current amplitudes were measured at the peak value. Current densities (CD) were calculated by dividing the maximum current amplitudes by the corresponding C_m for each individual cell.

All ion channel blockers/activators were diluted in aCSF and applied on cells using a pressurized 8-channel perfusion system (AutoMate Scientific, Inc. Berkeley, CA, USA). All chemicals were purchased from Sigma–Aldrich. The solution was continuously gassed with a mixture of 95% O_2 and 5% CO_2 to maintain a final pH of 7.4.

Immunohistochemistry and cell identification

Cell culture and neurospheres: neurospheres or cells attached to PLL-coated cover slips were fixed in 4% paraformaldehyde solution (in 0.2 M phosphate buffer—PB, pH 7.4) for 15 min, washed twice and kept in 0.01 M PBS at 4°C for further processing.
Brains: The mice were deeply anaesthetized 3, 4, 7, or 14 days after MCAo with PTB (100 mg/kg, i.p.) and perfused transcardially with 20 ml of saline followed by 20 ml of cooled 4% paraformaldehyde (PFA) in 0.1 M phosphate buffer (PB). Brains were dissected out, post-fixed for 2 hours and placed stepwise in solutions with gradually increasing sucrose concentrations (10%, 20%, 30%) for cryoprotection. Coronal, 30 µm thick slices were prepared using a microtome (HM550, Microm International, Walldorf, Germany). For cell identification after patch-clamp recording, the measured cells were filled with Alexa Fluor 594 hydrazide (0.1 mM; Molecular Probes, Invitrogen, CA, USA) by dialyzing the cytoplasm with the patch pipette solution. Post-recording, the slices were fixed with 4% PFA in 0.1 M PB for 25 minutes and then kept at 4-8°C in phosphate-buffered saline (PBS). The slices/coverslips were incubated with 5% Chemiblocker (Millipore, MA, USA) and 0.2% Triton in PBS. This blocking solution was also used as the diluent for the antisera. The slices/coverslips were incubated with the primary antibodies at 4-8°C overnight, and the secondary antibodies were applied for 2 hours. The neurospheres were stained in suspension, and the staining solutions were changed after centrifugation and the supernatant was

removed. The list of primary and secondary antibodies is summarized in Table 1. To visualize the cell nuclei, the slices were incubated with 300 nM 4, 6-diamidino-2-phenylindole (DAPI) in PBS for 5 minutes at room temperature and mounted using Aqua Poly/Mount (Polysciences Inc., Eppelheim, Germany). All chemicals were purchased from Sigma–Aldrich (St. Louis, MO, USA), unless otherwise stated.

A Zeiss 510DUO LSM confocal microscope equipped with Arg/HeNe lasers and 40x or 63x oil objectives was used for immunohistochemical analysis. Stacks of consecutive confocal images taken at intervals of 3 µm were acquired sequentially with two lasers to avoid cross-talk between fluorescent labels. The background noise of each confocal image was reduced by averaging four image inputs. For each image stack the gain and detector offset were adjusted to minimize saturated pixels, yet still permit the detection of weakly stained cell processes. Colocalization of images and their maximum *z* projections were made using a Zeiss LSM Image Browser.

Table 1. List of antibodies used for immunohisto/cytochemistry.

Antigen	Dilution	Isotype	Manufacturer	Secondary antibody
ALDH1L1	1:100	Mouse IgG	NeuroMab	GAM 594/660
APC	1:200	Mouse IgG	Calbiochem	GAM 594/660
BLBP	1:200	Rabbit IgG	Abcam	GAM 594
Calbindin	1:200	Mouse IgG	Millipore	GAR 594
Calretinin	1:400	Mouse IgG	Millipore	GAM 594
Caspase-3	1:300	Mouse IgG	Alexis Biochem.	GAM 660
CD11b	1:200	Mouse IgG	Millipore	GAR 594
DCX	1:1000	Rabbit IgG	Abcam	GAR 594/660
GFAP	1:800	Mouse IgG	Sigma-Aldrich	Cy3 conjugated
GFP	1:800	Goat IgG	Abcam	FITC conjugate
GLAST	1:500	Rabbit IgG	Abcam	GAR 594/660
Iba-1	1:300	Mouse IgG	Millipore	GAM 594

Ki-67	1:1000	Rabbit IgG	Abcam	GAR 594/660
MAP-2	1:800	Mouse IgG	Millipore	GAM 594/660
MOSP	1:1000	Mouse IgG	Millipore	IgM Cy3
Nestin	1:800	Mouse IgG	Millipore	GAM 594/660
Neun	1:100	Mouse IgG	Millipore	GAM 594
NG2	1:400	Rabbit IgG	Millipore	GAR 594/660
Olig-2	1:1000	Rabbit IgG	Millipore	GAR 660
Parvalbumin	1:200	Mouse IgG	Millipore	GAM 594
Pax-6	1:300	Rabbit IgG	Covance	GAR 594
PCNA	1:500	Mouse IgG	Abcam	GAM 594
PDGFαR	1:200	Rabbit IgG	Santa Cruz	GAR 594/660
PDGFβR	1:200	Rabbit IgG	Santa Cruz	GAR 594/660
S100β	1:150	Mouse IgG	Sigma-Aldrich	GAM 660
TH	1:400	Mouse IgG	Millipore	GAM 594
Vimentin	1:1000	Mouse IgG	Abcam	GAM 594
β III tubulin	1:800	Mouse IgG	Sigma-Aldrich	GAM 594/660

ALDH1L1, aldehyde dehydrogenase; APC, Adenomatous polyposis coli; CD11b, Integrin alpha; DCX, doublecortin; GFP, green fluorescent protein; GLAST, glutamate/ aspartate transporter; Iba-1, ionized calcium-binding adapter molecule 1; Ki-67, nuclear cellular marker of proliferation; Neun, neuronal nuclei; NG2, neuron glia specific protein; Pax-6, aniridia type II protein; PCNA, proliferating cell nuclear antigen; PDGFαR, platelet-derived growth factor receptor alpha; PDGFβR, platelet-derived growth factor receptor beta; S100β, β-subunit of S-100 calcium-binding protein; BLBP, brain lipid-binding protein; GFAP, glial fibrillary acidic protein; TH, tyrosine hydroxylase; MAP-2, microtubule associated protein 2; MOSP, myelin/oligodendrocyte specific protein, GAR 594/660, goat anti-rabbit IgG conjugated with Alexa Fluor 594 or 660; GAM594/660, goat anti-mouse IgG conjugated with Alexa Fluor 594 or 660; DAG 594/660, donkey anti-goat IgG conjugated with Alexa Fluor 594 or 660 (all from Invitrogen); IgM Cy3, goat anti-mouse IgM conjugated with Cy3 (Millipore)

Cell isolations

Isolation of adult neural stem cells from the dorsal part of the LV

Control animals or mice 4 days after MCAo were deeply anaesthetized with PTB (100 mg/kg, i.p.), and perfused transcardially with cold (4–8°C) isolation solution. The forebrain was isolated by the removal of the olfactory lobes, cerebellum, and midbrain/hindbrain structures by dissection. To isolate the dorsal part of the LV, the brain was sliced in 450 µm coronal sections using a vibrating microtome HM650V (MICROM International GmbH, Walldorf, Germany), and the dorsal part of the LV was carefully dissected away from the dorsal white matter tracks and from the lateral walls of the ventricular zone. The tissue was incubated with continuous shaking at 37°C for 60 minutes in 5 ml of a papain solution (20 U/ml) and 0.2 ml DNAase (both from Worthington, Lakewood, NJ, USA). After papain treatment the tissue was mechanically dissociated by gentle trituration using a 1 ml pipette. Dissociated cells were layered on top of 5 ml of Ovomucoid inhibitor solution (Worthington, Lakewood, NJ, USA) and harvested by centrifugation (140 x g for 6 minutes). The resulting single-cell suspension was cultured as floating neurospheres in a humidified atmosphere with 5% CO_2 at 37°C and maintained in Neurobasal-A medium supplemented with B27-supplement, penicillin/streptomycin (all from Invitrogen, Carlsbad, CA, USA), 4 mM glutamine (Sigma–Aldrich, St. Louis, MO, USA; further referred to as basal medium), 10 ng/ml bFGF and 30 ng/ml EGF (both from Peprotech, USA). Several isolations were used for single cell assays; the cells were diluted and cultivated in 96-well plates. After one week the formed neurospheres were analyzed or used for further analyses of their differentiation potential. They were transfered onto poly-L-lysine-coated cover slips (PLL, Sigma–Aldrich) and cultivated in basal medium supplemented with 20 ng/ml bFGF, then analyzed after 4 days of differentiation.

Isolation of EGFP$^+$ cell from the cortex of GFAP/EGFP mice

GFAP/EGFP transgenic mice 50 days old (P50) or 3, 7, and 14 days after MCAo (D3, D7, D14) were deeply anaesthetized with sodium pentobarbital (PTB, 100 mg/kg,

i.p.), and perfused transcardially with cold (4–8°C) isolation buffer containing (in mM): 136.0 NaCl, 5.4 KCl, 10.0 HEPES, 5.5 glucose, osmolarity 290 ± 3 mOsmol/kg. The forebrain was isolated by the removal of the olfactory lobes, cerebellum, and midbrain/hindbrain structures by dissection. To isolate the cerebral cortex the part of brain (+2 mm to -2 mm from bregma) was sliced into 400 µm coronal sections using a vibrating microtome HM650V (MICROM International GmbH), and the dorsal cerebral cortex was carefully dissected out from the corpus calosum white matter tracks. The tissue was incubated with continuous shaking at 37°C for 90 minutes in 5 ml of a papain solution (20 U/ml) and 0.2 ml DNase (both from Worthington, Lakewood, NJ, USA) prepared in isolation buffer. After papain treatment the tissue was mechanically dissociated by gentle trituration using a 1 ml pipette. Dissociated cells were layered on the top of 5 ml of Ovomucoid inhibitor solution (Worthington, Lakewood, NJ, USA) and harvested by centrifugation (140 x g for 6 minutes). This method routinely yielded ~2 x 10^6 cells per mouse forebrain. Cell aggregates were removed by filtering with 30 nm cell strainer (Becton Dickinson, CA, USA) and cells were kept on ice until sorting using flow cytometry.

Cell differentiation *in vitro*

D6/GFP cells grown as neurospheres were trypsinised and plated on poly-L-lysine-coated cover slips (PLL, Sigma–Aldrich) at a cell density of 6 x 10^4/cm^2 and cultured in basal medium supplemented with 20 ng/ml bFGF. One week after the onset of differentiation, the cells were analyzed for the expression of K^+ and Na^+ currents using the patch-clamp technique; after fixation, the cells were analyzed for the expression of glial and neuron-specific markers.

Collection of single $EGFP^+$ cells for RT-qPCR

$EGFP^+$ single cells were sorted using flow cytometry (BD Influx, USA). The flow cytometer was manually calibrated to deposit a single cell in the centre of each collection tube. Hoechst 33258 (Life Technologies, CA, USA) was added to the

suspension of cells to check viability. Single cells were collected into 96-well plate (Life Technologies, CA, USA) containing 5 µl nuclease free water with bovine serum albumin (1 mg/µl, Fermentas) and RNaseOut 20 U (Life Technologies, CA, USA). Plates were placed on a pre-cooled rack. The glial cells collected were positive for EGFP and viable based on propidium iodide staining. Collected cells in 96-well plates were immediately placed at -80°C.

cDNA synthesis

cDNA synthesis was performed with SuperScript III RT (Life Technologies, CA, USA). Lysed single cells in 5 µl water containing 0.5 µM dNTP (Promega, CA, USA), 1.0 µM oligo (dT15), (Invitrogen) and 1.0 µM random hexamers (Eastport, Prague, Czech Republic) were incubated at 70°C for 5 min. 50 mM Tris–HCl, 75 mM KCl, 3 mM $MgCl_2$, 5 mM dithiothreitol, 20U RNaseOut and 100U SuperScript III (all Life Technologies, CA, USA) were added to a final volume of 10 µl. Reverse transcription was performed at 25°C for 5 min, then at 50°C for 60 min, followed by 55°C for 15 min and finally terminated by heating at 70°C for 15 min. 4 µl from each sample was diluted 4 times and used for pre-testing. 5 µl of cDNA was used for preamplification.

Quantitative PCR

Primers were design with BeaconDesigner (version 7.91, Premier Biosoft International) as previously described (Benesova et al., 2012), (Table 2.). All single cells were tested for the expression of glutamate transporter (*Slc1a3*), glutamine synthase (*Glul*), which are markers for astrocytes, chondroitin sulphate proteoglycan (*Cspg4*), platelet-derived growth factor α receptor (*Pdgfra*), which are markers for polydendrocytes in order to select samples for further gene expression profiling using assays for 47 genes. A CFX384 (BioRad, Hercules, CA, USA) was used for all qPCR measurements. To each reaction (10 µl) containing iQ SYBR Green Supermix (BioRad, Hercules, CA, USA) and 400 nM of each primer (EastPort, Prague, Czech Republic), 3 µl of diluted cDNA was added. The temperature profile was 95° C for 3 min followed by 50 cycles of amplification (95°C for 15 s, 60°C for 15 s and 72°C for

20 s). All samples were subjected to melting curve analysis. The same experimental set-up was used to test preamplification.

Table 2. List of primers used for qPCR

Gene	PubMed ID	Forward primer	Reverse primer
Aldh1l1	NM_027406.1	CTGGAAGATGGCAAGATGATG	TTCTACCTCTGGGACATTGG
Aqp1	NM_007472.2	CTGGCTGCGGTATCAACC	GGATGAAGTCATAGATGAGCACTG
Aqp4	NM_009700.2	CGGCATCCTCTACCTGGTCACA	GCCAGCGGTGAGGTTTCCAT
Aqp9	NM_022026.2	GAAGGATGGAGTGGTTCAAGTTC	TGGCACGGATACAAATGGTTT
Clcn2	NM_009900.2	TGCCAATGTCTTCCTTACTCTG	ATTCGGTAGGTGCTGCTATC
Cspg4	NM_139001.2	TGATGGAAGTGAGACACAGACAGA	GGAAGGATGGTGATCGTGAAGG
Gfap	NM_001131020.1	GAACAACCTGGCTGCGTATAG	GCGATTCAACCTTTCTCTCCAA
Gfapd	NM_001131019.1	ATGTGTCTCAGTTGTGAAGGTCTA	TGGAAGGATGGTTGTGGATTCT
Glul	NM_008131.3	CGCAAAGACCCCAACAAG	ATTCCTGCTCCATTCCAAAC
Gria1	NM_001113325.1	ACTCAAGCGTCCAGAATAGAAC	AATCTCAAGTCGGTAGGAATAGC
Gria2	NM_001039195.1	CAGATTGTAGACTACGACGACTC	TCATCACTTGGACAGCATCATAA
Gria3	NM_016886.3	GGTCATTCTCACGGAGGATTC	GGTGTTCTGGTTGGTGTTGTA
Gria4	NM_001113180.1	CCAGTAGAGGACAACGCAATT	TGACAGAGTGAAGGTTACAGGAA
Grik1	NM_146072.4	CACGAGACGGCTGCTGAA	ACCACTGTACCTGTAGAGTTCCA
Grik2	NM_001111268.1	ACAATCAACAGGAACAGGACTCT	TGCTGATGAACTGTGTGAAGGA
Grik3	NM_001081097.2	GCTCAGAGGTGGTGGAGAATA	GCCGTGTAGGAGGAGATGAT
Grik4	NM_175481.5	CGCATGGTAGAATTGGAAGGT	AAGAGACTGTCAGAGATGTTGGA
Grik5	NM_008168.2	CCACCTTGTCCTCCGTAA	CTCCACGATACCATCCAGAT
Grin1	NM_001177656.1	AGATAGTGACAATCCACCAAGAAC	ACCATTGACTGTGAACTCCTC
Grin2a	NM_008170.2	GACCAGATGCTTCAGGAGACAG	CTTGAGGCTTATGCTACGAGAGG
Grin2b	NM_008171.3	GGTGTTTAACAACTCCGTACCT	GAAACCTGGTCCACATACTCCTC

Grin2c	NM_010350.2	CGTGTGGTTAGTACCTAATCTG	TTCTGGCGTAGGCTAAGG
Grin2d	NM_008172.2	AACCGAGACTACTCCTTCAATGA	GCCATAGCGGGACCATAGA
Grin3a	NM_001033351.1	GACAAAGCCCTTCTGGATTATGA	ATGTTAGAGGTCAACGGAGAGT
Grm1	NM_001114333.2	CGAGTGGAGTGACATAGAATC	TACCAGCCAGAATGATATAGCA
Grm3	NM_181850.2	CGACCACATATTCTCAGTCCTCT	AGCACTTCGTCTAACAGCCTATA
Grm5	NM_001081414.2	CAGCTTAGATCGCAGCCACT	CAAGAATTTGGGTAAAATCACCA
Hcn1	NM_010408.3	CTCAGTCTCTTGCGGTTATTACG	TGGCGAGGTCATAGGTCAT
Hcn2	NM_008226.2	ATCGCATAGGCAAGAAGAACTC	CAATCTCCTGGATGATGGCATT
Hcn3	NM_008227.1	GATGTTTGATGAAGAGAGCATCC	CCCGGCAGGTGAAGTTAATA
Hcn4	NM_001081192.1	GCATGATGCTTCTGCTGTGT	GCTTCCCCCAGGAGTTATTC
Kcna3	NM_008418.2	GTAAGTCGGAGTATATGGTGAT	CAGTGAATATCTTCTTGATGTTGA
Kcna4	NM_021275.4	CTGAATGACACCTCGGCAC	AGCATCGAACCACAAACTCA
Kcna5	NM_145983.2	CGTGTCGGTCTTGGTCATTC	CGTAACAGCTCCCGTTCATC
Kcnj10	NM_001039484.1	AACTTGGGAGATTGAGATATGATATA	AAGTCTGAATACTTCCTTCTGTAC
Kcnj16	NM_010604.3	CCTGTGTCTCCTCTTGAAGG	TGTGCTTAGGTGATACAATACGG
Kcnj2	NM_008425.4	TCCCTCCCTTTCCCAAACAC	GAGGCTTGATTTTGAGACGC
Kcnk1	NM_008430.2	GGGAAATTGGAATTGGGACTTCA	TGCCGATGACAGAGTAGATGAT
Kcnk10	NM_029911.4	CACTGTGGCTATCTCCTTAACC	GGCTGAGGCGGTGTAATC
Kcnk2	NM_010607.2	ATTCGTATCATCTCCACCATCATC	CACACCACAGGCTTGTAGAA
Nestin	NM_016701.3	AGCAACTGGCACACCTCAA	GGTATTAGGCAAGGGGGAAG
Pdgfra	NM_001083316.1	AAGAGACCCTCCTTCTACCAC	TATCAGAGTCCACCCGCAT
S100b	NM_009115.3	TCTAACTCAGGACCGAGAATCA	GGAGCAAGGAAGATACAACTAACT
Slc1a3	NM_148938.3	ATCGTCCTGCCTCTCCTCTAC	GTCCACACCATTGTTCTCTTCCA
Snap	NM_011428.3	TCATCTGGTGGCTCTAATTCCTAA	AACAGCACATTGAGCATTCCTAA
Trpv4	NM_022017.3	AGAGACAAGTGGCGTAAGTT	GCTGATAGTAGGCGGTGAG
Vim	NM_011701.4	TGCCAACCTTTTCTTCCCTG	TCTCTGGTCTCAACCGTCTT

Preamplification and qPCR

The applied preamplification protocol was verified on samples from three animals. The RNA was extracted and cDNA was prepared to test the preamplification protocol. Each reaction contained 25 µl iQ Supermix (BioRad, Hercules, CA, USA), 5 µl of a mix of all primers (final concentration 25 nM each), 5 µl non-diluted cDNA, and water added to a final volume of 50 µl. The temperature profile was 95°C for 3 min followed by 18 cycles of amplification (95°C for 20 s, 57°C for 4 min and 72°C for 20 s on BioRad CFX96). The sample was diluted 5 times in water.

High throughput qPCR

The sample reaction mixture had a volume of 5 µl and contained 2.4 µl of diluted preamplified cDNA, 0.25 µl of DNA Binding Dye Sample Loading Reagent (Fluidigm, San Francisco, CA, USA), 2.5 µl SsoFast EvaGreen Supermix (Biorad, Herculers, CA, USA), and 0.01 µl ROX (Invitrogen, CA, USA). The primer reaction mixture had a final volume of 5 µl and contained 2.5 µl Assay Loading Reagent (Fluidigm, San Francisco, CA, USA) and 2.5 µl of a mix of reverse and forward primers corresponding to a final concentration of 4 µM. The chip was first primed with an oil solution in the NanoFlex™ 4-IFC Controller (Fluidigm, San Francisco, CA, USA) to fill control wells of the dynamic array. Reaction mixture (5 µl) was loaded into each sample well and 5 µl of the primer reaction mixtures was loaded into each assay well of the 48x48 dynamic array. The dynamic array was then placed in the NanoFlex™ 4-IFC Controller for automatic loading and mixing. After 55 min the dynamic array was transformed to the BioMark qPCR platform (Fluidigm, San Francisco, CA, USA). The cycling program was 3 min at 95 °C for activation, followed by 40 cycles of denaturation at 95°C for 5 s, annealing at 60°C for 15 s, and elongation at 72°C for 20 s. After the PCR melting curves were collected between 60°C and 95°C with 0.5°C increments.

Data pre-processing

qPCR data were pre-processed for expression analysis using GenEx (MultiD, version 5.3) as follows. Cq values registered from amplifications that generated melt curves with aberrant Tm were removed, Cq values larger than 26 were replaced with 26, and Cq values with products giving rise to a double peak in melt curves (corresponding to a mixture of expected and aberrant PCR products) were also replaced with 26. All missing data, for each gene separately, were then replaced with the highest Cq+2, effectively assigning a concentration of 25% of the lowest measured concentration to the off scale values. The Cq data were, for each gene separately, converted into relative quantities expressed relative to the sample with lowest expression (maximum Cq) and finally converted to logarithmic scale with base 2. The data were not normalized to any reference genes, because of the large variation of all transcript levels among individual cells (Stahlberg et al., 2011); with this pre-processing levels are expressed per cell.

Analysis of RT-qPCR data

The non-parametric Mann-Whitney test was used to compare expression of individual genes between groups of cells. Kohonen self-organizing maps (SOM) of size 3x1, forcing dividing of the samples into three groups, were trained using GenEx with the following parameters: 0.10 learning rate, 3 neighbours and 5000 iterations. The SOM analysis was repeated eight times with identical classification of the samples in six of those. This stable classification of samples into three groups was accepted and verified with principal component analysis (PCA). For Kohonen SOMs and PCA gene expression data were mean-centred to reduce the effect of variation in the overall expression levels of the different genes. The Spearman correlation coefficients between genes were calculated for each group separately (SAS vers. 9.2) using all data, including the managed off-scale data, and then also for the truly positive expression values only. Only correlation coefficients for genes expressed in at least 50% of cells and had a p-value <0.05 were considered for further analysis. Indirect correlations between genes were established by calculating partial Spearman correlation coefficients (only genes expressed in at least 80% of the cells were

considered). An interaction was classified indirect when the correlation coefficient lost significance (at 95% confidence) or was reduced to below 0.4 (Stahlberg et al., 2011).

Cell counts

To determine the fate of polydendrocytes in the post-ischemic cortex, confocal images (315 µm x 315 µm x 20 µm) covering the borders of the ischemic core were taken from brain coronal slices from control mice and from mice 3, 7 and 14 days after MCAo (5 - 7 animals from each group, 5 slices, 5 regions from one slice, bregma -1.2 mm) and stained for NG2, nestin, GFAP, Ki-67 and DCX. The total number of EGFP positive ($EGFP^+$) cells and the number of cells that were double positive for EGFP and NG2, nestin, Ki-67, GFAP or DCX were counted in the cortex within the astrogliotic region. Between 1000 and 1500 $EGFP^+$ cells were scored.

To determine the number of GFP^+/DCX^+ cells in the dorsal part of the LV or the number of GFP^+ neurons in the glomerular or granular cell layer in the OB, confocal images (315 µm x 315 µm x 20 µm) covering the studied regions were taken of brain coronal slices from controls and from mice 4 days or 4 weeks after MCAo (5 - 9 animals from each group, 3 regions from one slice, bregma -0.5 mm). Between 1000 and 1500 GFP^+ cells were scored. The number of cells was estimated from superimposed images using a GSA Image Analyzer v3.7.7 (Bansemer & Scheel GbR, Rostock, Germany) and expressed as the percentage of DCX^+ cells from the total number of GFP^+ cells; as the number of GFP^+ cells per mm^3 or as the percentage of double-positive cells from the total number of $EGFP^+$ cells.

Statistics

The results are expressed as the mean ± SEM. Statistical analyses of the differences between groups were performed using one-way ANOVA for multiple comparisons with Dunnett's post-hoc test or using an unpaired *t* test. Values of $p < 0.05$ were considered significant (*), $p < 0.01$ very significant (**) and $p < 0.001$ extremely significant (***).

RESULTS

The differentiation potential of polydendrocytes after ischemia

To unravel the origin of reactive astrocytes and the differentiation potential of polydendrocytes after focal cerebral ischemia a transgenic mouse strain that expresses Cre-recombinase under the control of the NG2 promoter was used. After cross-breeding with reporter mouse strain Z/EG the cells with ongoing NG2 proteoglycan expression started to express EGFP and this expression persisted also after the cell phenotype change. This approach enabled us to follow the fate and differentiation of polydendrocytes for a long time period after ischemia, even when they differentiated into another phenotype. To determine the differentiation potential of polydendrocytes we performed a complex immunohistochemical and electrophysiological analyses of the newly derived cells after ischemia in adult mice.

Under physiological conditions polydendrocytes in the somatosensory cortex either self-renew or give rise to oligodendrocytes

The NG2creBAC:ZEG mice exhibited widespread EGFP expression in a large population of cells in the brain and spinal cord. Polydendrocytes express NG2 and PDGFαR (Trotter et al., 2010); however, both proteins are down-regulated immediately upon differentiation. Therefore, this approach enables to follow the fate of differentiating polydendrocytes based on their EGFP labeling.

To determine the phenotype of $EGFP^+$ cells in the adult brain, a complex immunohistochemical analysis of brain coronal sections was performed; initially, the total number of $EGFP^+$ cells in the dorsal part of the cortex of the control animals was estimated. It was found 9892 ± 783 $EGFP^+$ cells per mm^3, which represented 4.1% ± 0.3% of all $DAPI^+$ cells. $EGFP^+$ cells could be divided into several morphological types. The first, most common morphological phenotype comprised cells with several highly branched processes, characteristics typical of polydendrocytes. These cells were predominantly positive for the polydendrocytic markers NG2 and PDGFαR (Figure 8A, B) and 55.4% ± 1.2% of $EGFP^+$ cells expressed NG2 in the cortex of control mice. $NG2^+$ cells are known to possess the highest proliferation rate in the

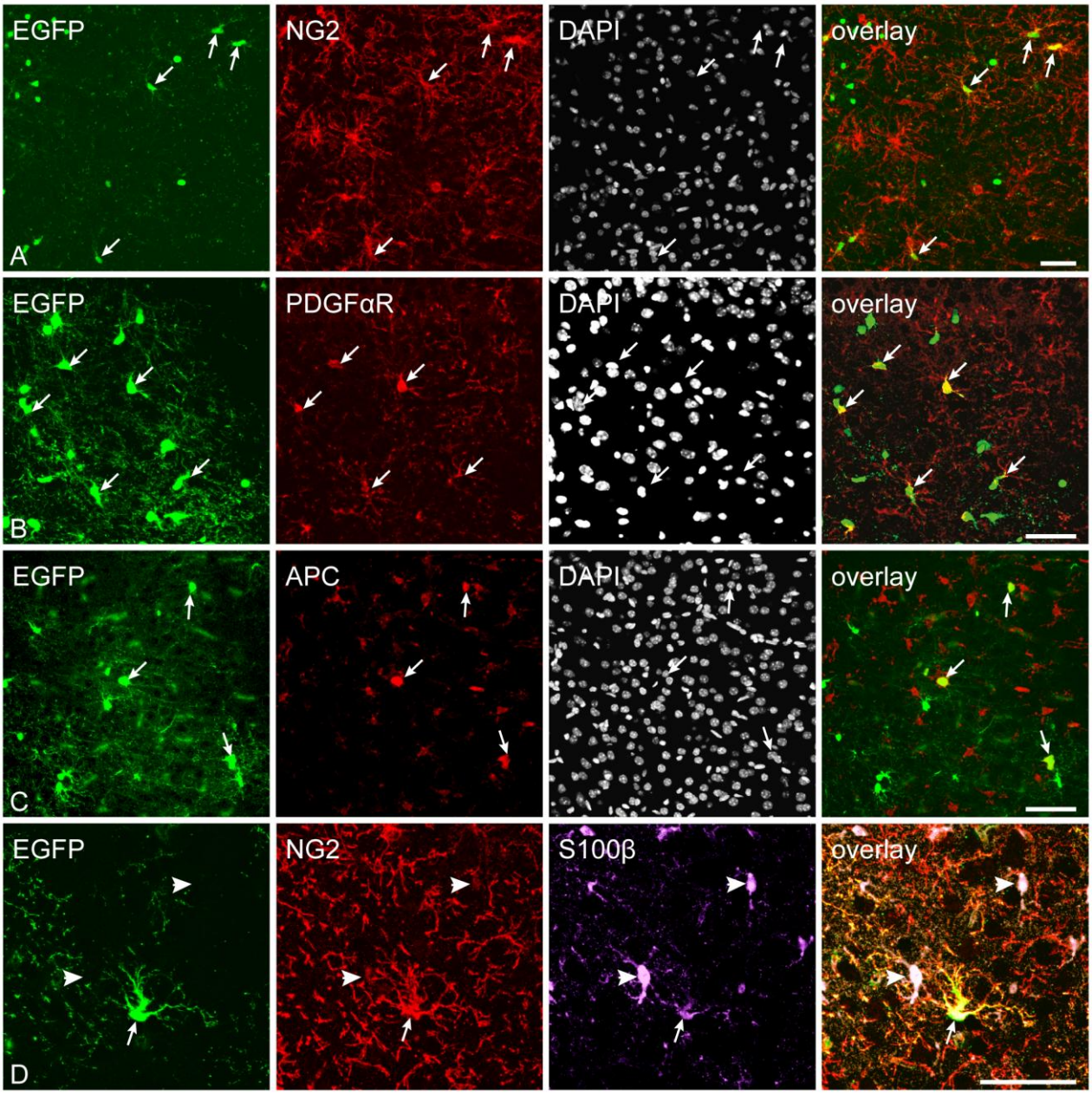

Figure 8. Enhanced green fluorescent protein (EGFP) expression is restricted to polydendrocytes and oligodendrocytes in the control somatosensory cortex of NG2creBAC:ZEG mice. A, Immunostaining for NG2 proteoglycan in the cortex illustrating the high number of $EGFP^+/NG2^+$ cells. White arrows highlight several examples. **B,** The same population of $EGFP^+$ cells expressed platelet-derived growth factor alpha receptor (PDGFαR) in a typical polarized pattern only in part of the processes. **C,** A subpopulation of $EGFP^+$ cells in the somatosensory cortex expressed the oligodendrocytic lineage marker Adenomatous polyposis coli (APC). **D,** Double immunohistochemistry revealed the co-expression of β-subunit of S-100 calcium-binding protein (S100β) with NG2 in $EGFP^+$ cells, which excludes S100β as a specific marker of astrocytes. The $EGFP^-/NG2^-$ cells are astrocytes (indicated by arrowheads). Scale bars, 50 µm.

adult mammalian brain, which was confirmed by immunostaining for Ki-67 (a nuclear cellular marker of proliferation). In the somatosensory cortex 3.7% ± 1.3% $EGFP^+$ cells expressed Ki-67 and 20.6% ± 2.3% $EGFP^+$ cells expressed proliferation cell nuclear antigen (PCNA). The second group of $EGFP^+$ cells displayed a typical oligodendrocytic morphology, with large, round cell bodies; they expressed the oligodendrocytic marker Adenomatous polyposis coli (APC, Figure 8C) and represented 27.6 ± 3.5% of the total number of $EGFP^+$ cells. The third group of $EGFP^+$ cells in the somatosensory cortex had a morphology resembling that of pericytes and, accordingly, they expressed the marker of pericytes – platelet-derived growth factor beta receptor (PDGFβR, Figure 9A). Moreover, some studies described expression of NG2 in the microglial cells, therefore we labeled $EGFP^+$ cells with antibody against microglia marker Iba-1 and found no co-expression of this microglial marker with $EGFP^+$(Figure 9B).

Since it has been shown that in some Cre-recombinase transgenic mouse strains a certain subpopulation of astrocytes can be $EGFP^+$ (Muskhelishvili et al., 2003; Dimou et al., 2008), the somatosensory cortex was analyzed for the expression of several astrocytic markers, however no $EGFP^+$ cells expressing astrocytic markers were detected. Based on our extensive immunohistochemical analyses of the uninjured adult somatosensory cortex, we may conclude that the expression of EGFP is restricted only to polydendrocytes, oligodendrocytes and pericytes in adult NG2creBAC:ZEG double transgenic mice.

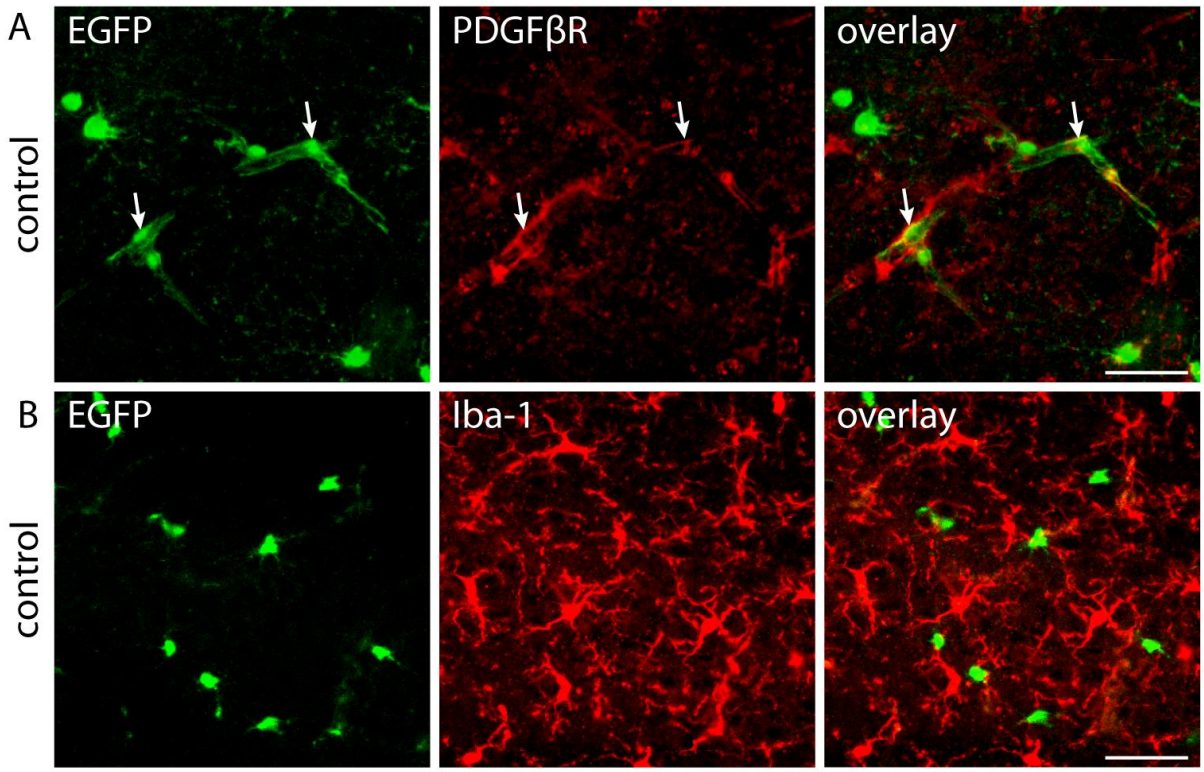

Figure 9. Enhanced green fluorescent protein (EGFP) is expressed also in pericytes, but not in microglia in the control somatosensory cortex of NG2creBAC:ZEG mice.

A, Immunostaining for platelet-derived growth factor beta receptor (PDGFβR) in the cortex showing several $EGFP^+/PDGF\beta R^+$ cells with morphology of pericytes. White arrows highlight several examples. **B,** Image showing immunostaining for microglial marker ionized calcium-binding adapter molecule 1 (Iba-1); however, $EGFP^+$ cells never express this marker. Scale bars, 50 µm.

Polydendrocytes respond to focal cerebral ischemia by increased proliferation

To determine whether polydendrocytes in the somatosensory cortex of adult mice display marked proliferation and an extended differentiation potential in response to ischemic injury, we induced MCAo in NG2creBAC:ZEG double transgenic mice and analyzed their brains 3 days after ischemia. Three days after MCAo the ischemic lesion developed in the dorsal brain and occupied approximately one-third of the cortex in the left hemisphere (Figure 10A). The necrotic tissue was surrounded by

massive astrogliosis starting 3 days after MCAo with a maximal intensity of GFAP staining 7 days after MCAo (Figure 10B).

Three days after MCAo the number, distribution and morphology of $EGFP^+$ cells were significantly changed at the lesion border (Figure 11D-F) when compared to controls (Figure 11A-C). $EGFP^+$ cells had larger cell bodies with a smaller number of processes, and their numbers significantly increased (24798 ± 1937 $EGFP^+$

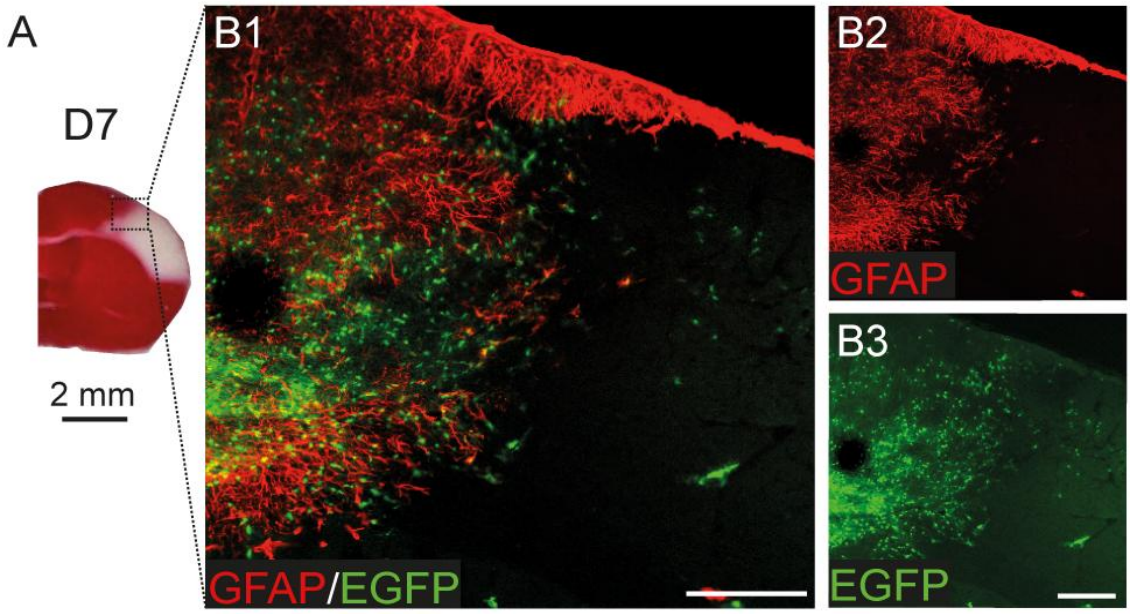

Figure 10. Focal cerebral ischemia leads to a marked increase in the number of enhanced green fluorescent protein-positive $(EGFP)^+$ cells around the ischemic lesion. **A,** A coronal brain section stained with triphenyltetrazolium indicates the volume of ischemic tissue (white color) 7 days after MCAo. The boxed area in **A** is shown in higher magnification in **B**. **B1–B2,** An overview image showing glial fibrillary acidic protein (GFAP) overexpression around the ischemic region. **B3,** Typical localization and a high number of $EGFP^+$ cells around the ischemic core 7 days after ischemia. Note that few $EGFP^+$ cells were found directly in the ischemic tissue. Scale bars, 50 µm. MCAo, middle cerebral artery occlusion.

$p < 0.001$). The estimated number represented 9.8% ± 0.6% of all $DAPI^+$ cells and was approximately 2.5-fold higher than that found in controls (Figure 12A2, C). At this time point only 36.0% ± 2.9% of $EGFP^+$ cells expressed NG2 (Figure 11D, 10D), while in 19.6% ± 1.5% of $EGFP^+$ cells the expression of nestin was detected, which is

an intermediate filament up-regulated in immature proliferating glia (Carmichael, 2005), (Figure 11E). The number of $EGFP^+$/$nestin^+$ cells was significantly increased when compared to controls (Figure 12D; $p < 0.001$), and furthermore, the number of proliferating cells, which were positive for Ki-67, increased 3 days after MCAo (Figure 11F), reaching 11.5% ± 2.7% of all $EGFP^+$ cells (Figure 12D; $p < 0.05$). Another marker of proliferating cell – PCNA was also massively expressed 3 days after MCAo (Figure 13).

Collectively, 3 days after MCAo a large number of polydendrocytes expressed proliferative markers, which accords well with the higher number of $EGFP^+$ cells at the lesion borders. In addition, a large number of $EGFP^+$ cells did not express polydendrocytic markers, which might already indicate changes in their phenotype in response to ischemia.

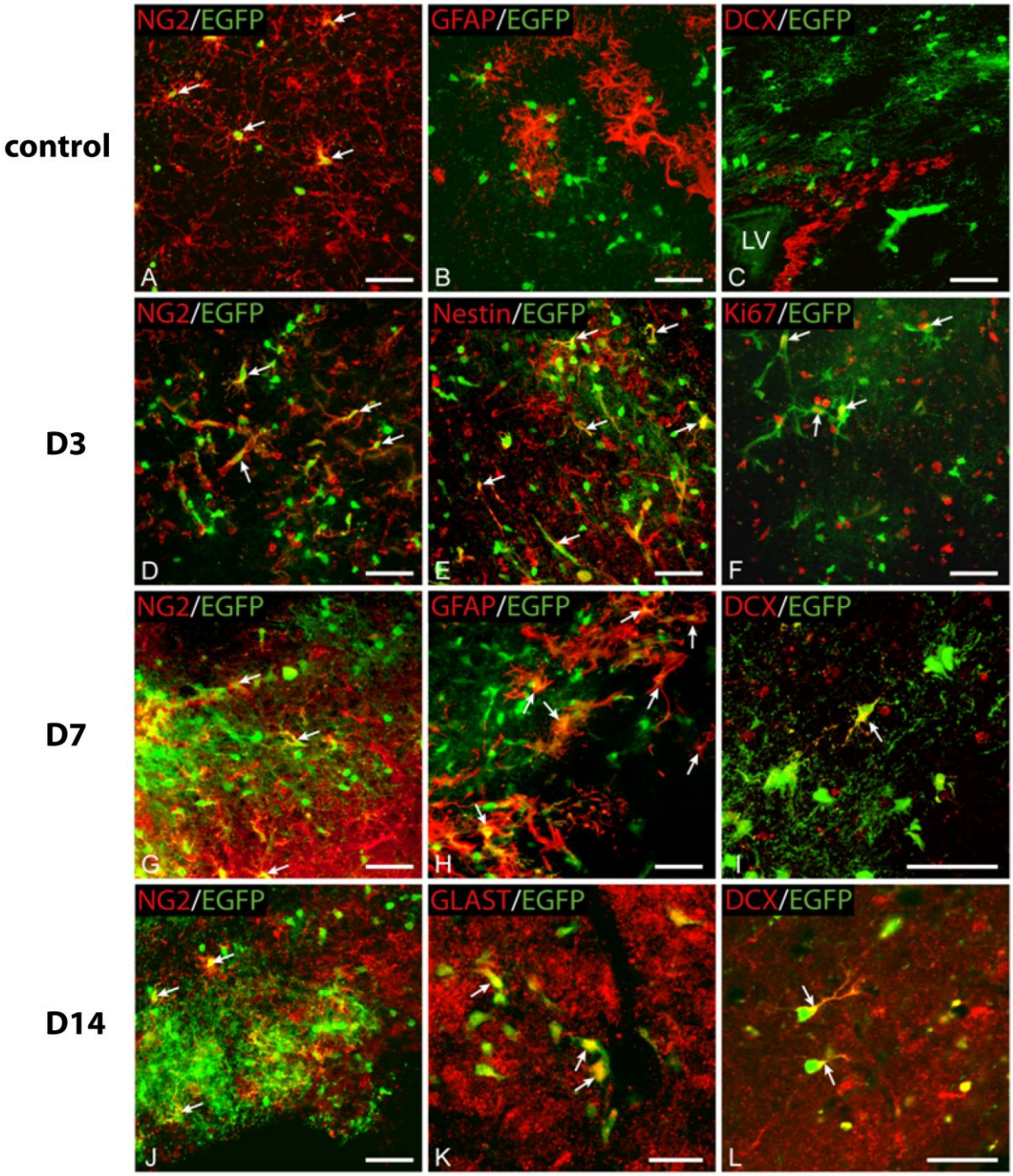

Figure 11. Enhanced green fluorescent protein-positive (EGFP)$^+$ cells express markers of astrocytes and neuronal precursor cells in the somatosensory cortex after ischemia. **A,** EGFP$^+$ cells in sham-operated mice (control) expressed a high level of NG2 proteoglycan in the majority of processes. White arrows highlight several examples. **B,** Virtually no EGFP$^+$ cells in the dorsal control cortex were positive for glial fibrillary acidic protein (GFAP). **C,** Low density of EGFP$^+$ cells in the subventricular zone (SVZ). EGFP$^+$ cells were never co-labeled with doublecortin (DCX) in the SVZ of control brains or those after ischemia, which indicates no contribution of polydendrocytes to the process of adult neurogenesis in SVZ; (LV, lateral ventricle). **D,** Three days after MCAo the number of EGFP$^+$

cells is significantly increased when compared to controls. Moreover, a large number of $EGFP^+$ cells expressed markers of proliferating cells – nestin (**E**) and Ki-67 (**F**). **G,** $EGFP^+$ cells were present at high density seven days after MCAo; however, only a small subpopulation of them expressed NG2 proteoglycan. **H,** Some $EGFP^+$ cells were positive for the astrocytic marker GFAP. **I,** Starting 7 days after MCAo some scattered cells expressed DCX in their cell bodies and processes. **J,** Fourteen days after MCAo only a small subpopulation of $EGFP^+$ cells expressed NG2 proteoglycan. **K,** $EGFP^+$ cells expressing glutamate/aspartate transporter (GLAST), a marker of mature astrocytes. **L,** A subpopulation of $EGFP^+$ cells displaying polarized and highly developed processes, which were positive for DCX. Scale bars, 50 µm. MCAo, middle cerebral artery occlusion.

Polydendrocytes differentiate into reactive astrocytes and neuronal precursor cells in the later stages following ischemia

To elucidate the fate of polydendrocytes and their progeny during the later stages of astrogliosis, brains were analyzed 7 days after MCAo. At this time point the number of $EGFP^+$ cells significantly increased when compared to controls. These $EGFP^+$ cells had a more complex morphology with multiple processes, and there was a sharp interface between the ischemic/necrotic and astrogliotic tissue. There we counted 30555 ± 1355 $EGFP^+$ cells/mm^3, which represented 12.5% ± 0.4% of all $DAPI^+$ cells ($p < 0.001$). This number was 3-fold higher than that obtained in controls (Figure 12A3, C). However, only 25.4% ± 1.2% of these $EGFP^+$ cells expressed NG2 (Figure 11G, 10D). Moreover, a large number of newly derived cells started to express proteins that are typical for other cell types than polydendrocytes or oligodendrocytes. Almost 17% (16.8% ± 1.6%) of $EGFP^+$ cells expressed high levels of GFAP in their processes (Figure 11H), and these $EGFP^+/GFAP^+$ cells were localized in regions very close to the ischemic tissue. These cells lacked the typical bushy protoplasmic morphology, but resembled the morphology of reactive astrocytes, and some of them were positive for a marker of reactive astrocytes, such as vimentin.

Since it has been demonstrated previously that polydendrocytes can give rise to neurons *in vitro* and after their transplantation into the hippocampus (Aguirre, 2004; Michalczyk and Ziman, 2005), $EGFP^+$ cells were examined for the expression

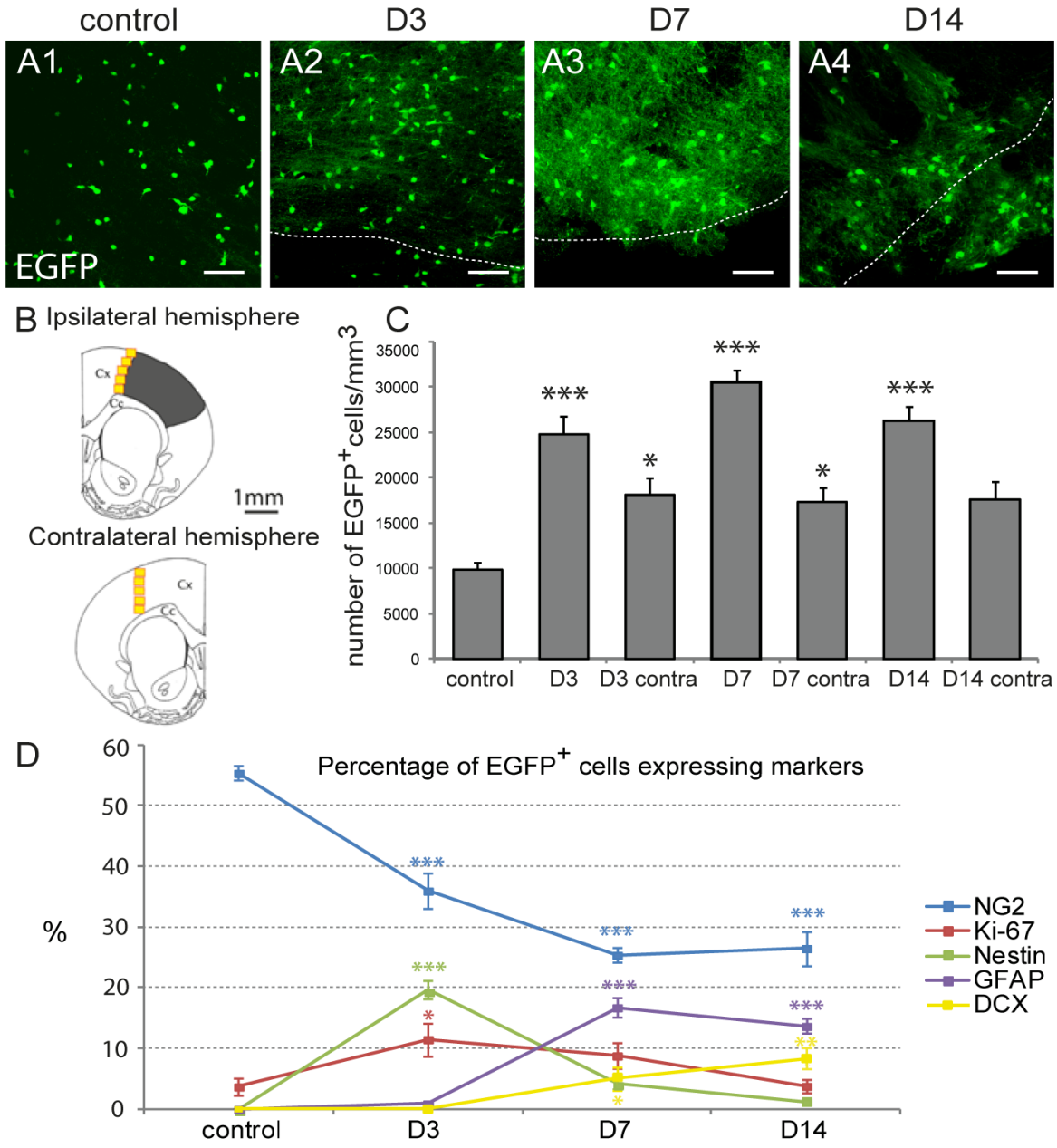

Figure 12. Quantification of the changes in the number of enhanced green fluorescent protein-positive (EGFP)$^+$ cells and in the expression of markers typical for glia, neurons and proliferating cells evoked by ischemia. **A,** Brain sections showing the increasing number and different distribution of EGFP$^+$ cells 3, 7 and 14 days after MCAo (**A2, A3, A4**) when compared to controls (**A1**). Borders of the ischemic tissue are highlighted with the dashed lines. Scale bars, 50 µm. **B,** Schematic figure of coronal slices of the ipsilateral and contralateral hemispheres depicting the size and localization of tissue injury 7 days after ischemia (grey region), together with the highlighted regions used for immunohistochemical quantification (yellow squares) in both hemispheres; Cx, cortex; Cc, corpus callosum. **C,** Bar graph showing quantification of EGFP$^+$ cell numbers per 1 mm^3 in the ipsilateral and contralateral hemispheres in control mice and those after ischemia. **D,** Graph showing the

percentage of EGFP$^+$ cells expressing markers of polydendrocytes (NG2), proliferating cells (Ki-67, nestin), astrocytes (glial fibrillary acidic protein, GFAP) and neuronal precursor cells (doublecortin, DCX) in controls and after MCAo. Asterisks indicate significant differences between control cortex and post-ischemic cortex; *,p<0.05; ***, p<0.001. MCAo, middle cerebral artery occlusion.

of DCX, a marker of newly derived neurons and neuroblasts. We detected almost 5.0% ± 1.9% of EGFP$^+$ cells (Figure 12D), which expressed DCX 7 days after MCAo. The expression of DCX was localized in the cell bodies as well as in the short processes (Figure 11I).

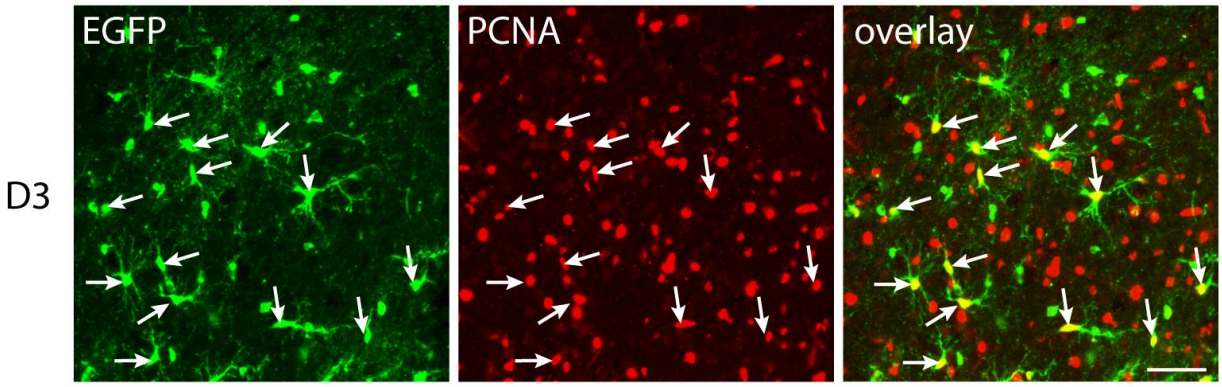

Figure 13. Proliferation of enhanced green fluorescent protein-positive (EGFP)$^+$ cells after ischemia. Immunostaining for proliferating cell nuclear antigen (PCNA) in the cortex showing almost all EGFP$^+$ cells expressing this proliferation marker 3 days after ischemia. White arrows highlight several examples. Scale bars, 50 µm. MCAo, middle cerebral artery occlusion.

Additional analyses of ischemic brains 14 days after MCAo revealed that the number of EGFP$^+$ cells was still significantly enhanced when compared to controls (26199 ± 1763 cells/mm^3) and that they represented 9.3% ± 0.4% of all DAPI$^+$ cells (Figure 12A4, C; p < 0.001). Immunohistochemical staining for NG2 revealed its high expression at the lesion border, but only 26.5% ± 2.8% of EGFP$^+$ cells expressed this proteoglycan (Figure 11J). The number of EGFP$^+$/GFAP$^+$ cells was slightly decreased compared to 7 days after MCAo, but still 13.7% ± 1.2% of EGFP$^+$ cells expressed GFAP (Figure 12D). The number of proliferating EGFP$^+$ cells declined and

reached the proliferation rate observed in the controls, and only 1.2% ± 0.4% of $EGFP^+$ cells expressed nestin (Figure 12D). On the other hand, a large number of $EGFP^+/DCX^+$ cells were detected, comprising 8.9% ± 1.6% of all $EGFP^+$ cells (Figure 12D).

In summary, detailed analyses of the ischemic border after MCAo revealed that polydendrocytes contribute to the generation of reactive astrocytes and, moreover, they also differentiate into a population of neuronal precursor cells, of which survival is quite low, probably due to the influence of growth factors near the ischemic tissue.

Polydendrocytes respond to ischemia with significant changes in their electrophysiological properties

Based on immunohistochemical staining, we found that polydendrocytes, besides their self-renewal, give rise to a large population of astrocytes, but also to neuronal precursor cells. Next, we aimed to characterize the electrophysiological properties of polydendrocytes and their progeny following MCAo using the patch-clamp technique in the whole-cell configuration.

Initially, the electrophysiological phenotype of polydendrocytes in control brains was determined. As expected, electrophysiological recordings revealed a complex current pattern typical of a polydendrocytic population, i.e., they displayed time- and voltage-independent K^+ conductance together with K_{DR}, K_A and K_{IR} currents (Komitova et al., 2009)(Figure 14A). Their average membrane properties are summarized in Table 3. Cells displaying a complex current pattern represented 81.5% ± 9.9% of all measured $EGFP^+$ cells in the control cortex (Figure 15).

After MCAo we found polydendrocytes with a complex current pattern at all studied time points; however, their number, passive membrane properties and current densities were markedly changed when compared to polydendrocytes in controls (Table 3). These changes in the membrane properties have been shown to reflect the high proliferative activity of polydendrocytes soon after ischemia (Nishiyama et al., 2009; Pivonkova et al., 2010), which is also in good correlation with the increased expression of Ki-67 and nestin in $EGFP^+$ cells 3 days after ischemia. Our post-recording immunohistochemical identification revealed polydendrocytes positive for NG2 and nestin 3 days after MCAo (Figure 16a1). Seven days after MCAo the percentage of polydendrocytes with a complex current pattern had significantly decreased to 23.4% ± 6.9% ($p < 0.001$), (Figure 15). Fourteen days after MCAo there was a further significant decrease in the quantity of polydendrocytes with a complex current pattern when compared to controls. Only 20.9% ± 6.1% ($p < 0.001$) of all measured $EGFP^+$ cells revealed a complex current pattern (Figure 15). These cells always expressed only polydendrocytic markers, such as NG2 and PDGFαR, 7 and 14 days after MCAo.

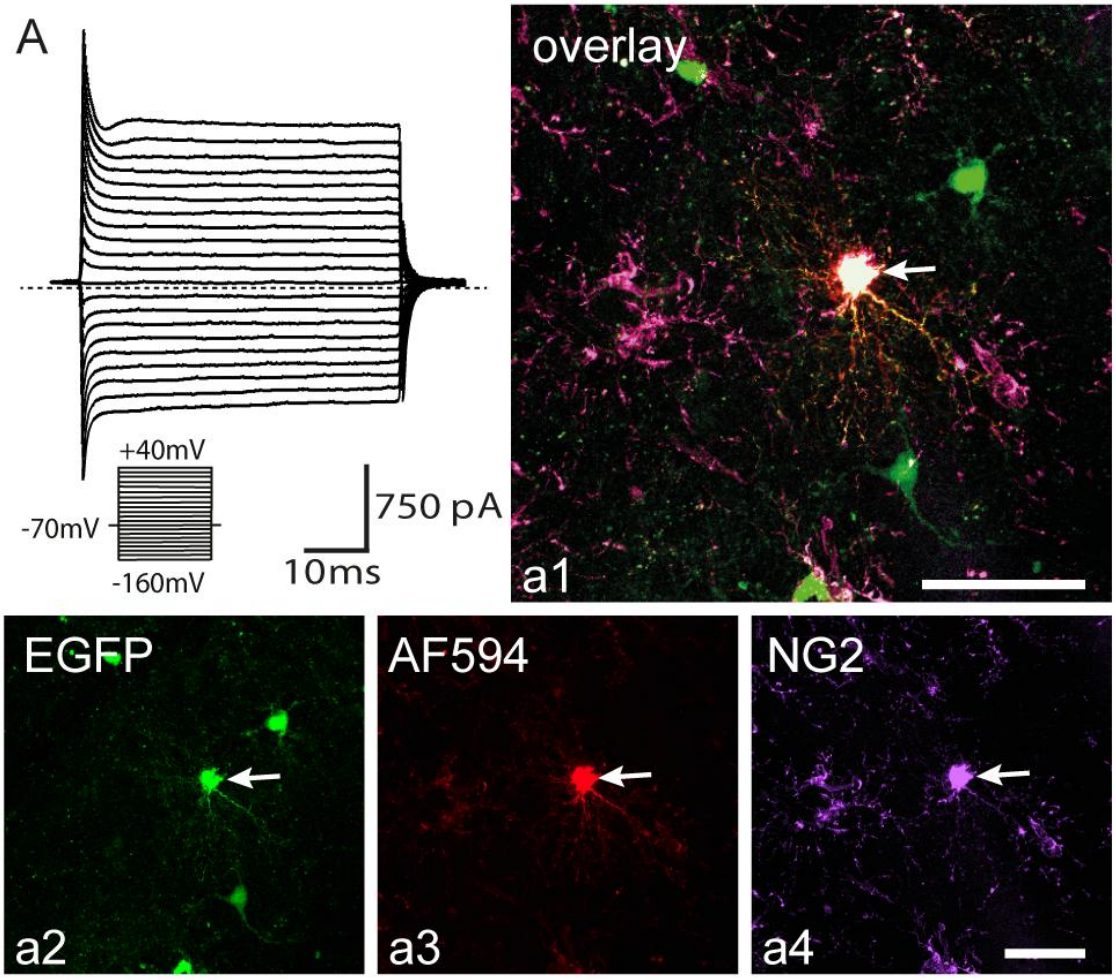

Figure 14. Enhanced green fluorescent protein (EGFP)$^+$ cells in the cortex of sham-operated mice (control) are NG2$^+$ polydendrocytes displaying a complex current pattern. **A,** Polydendrocytic current pattern in controls obtained after depolarizing the cell membrane from a holding potential of -70 mV to +40 mV and hyperpolarizing to -160 mV (see the inset, bottom). Polydendrocytes showed a complex current pattern, i.e., time- and voltage-independent K^+ currents, K_{DR}, K_A and K_{IR} currents. The dashed line marks zero current. An overlayed image of polydendrocyte (**a1**) expressing EGFP in control cortex (**a2**), loaded with Alexa Fluor 594 hydrazide (AF594) during patch-clamp measurement (**a3**), subsequently stained with an antibody directed against NG2 proteoglycan (**a4**). Scale bars, 50 µm. MCAo, middle cerebral artery occlusion.

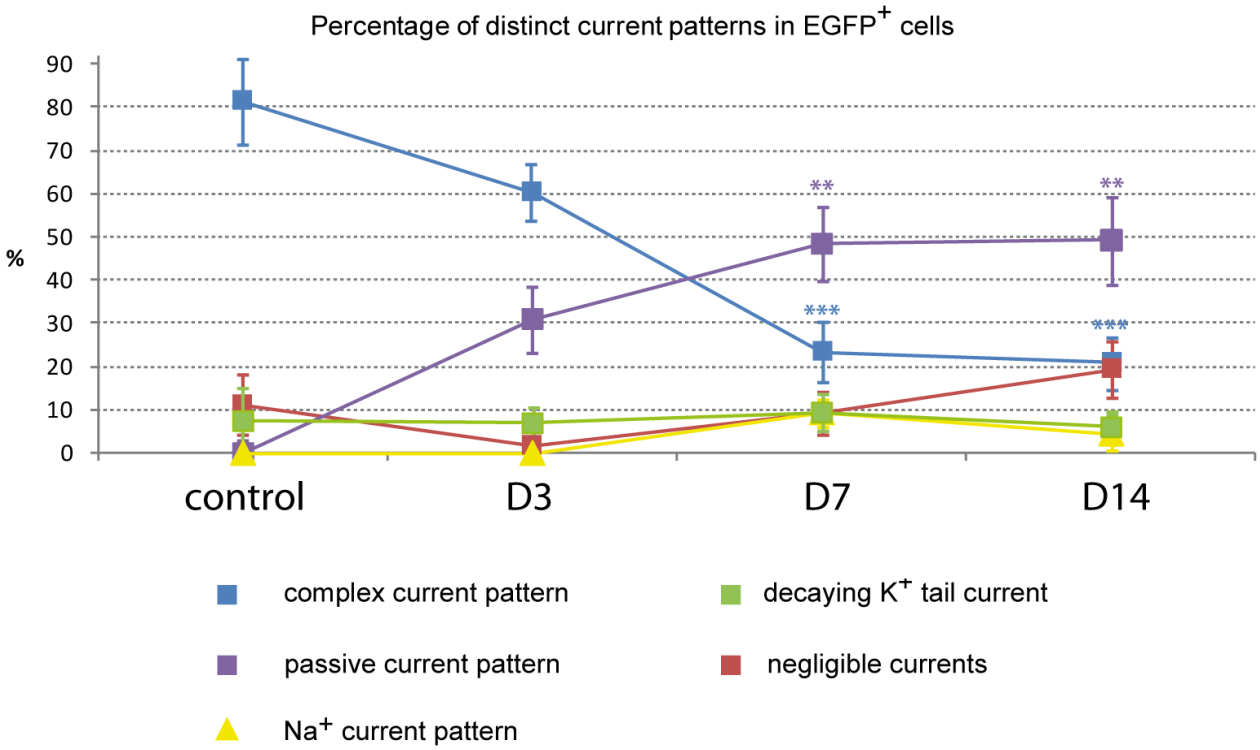

Figure 15. Ischemia-induced changes in the percentage of enhanced green fluorescent protein (EGFP)$^+$ cell displaying distinct current patterns. Asterisks indicate significant differences between control cortex and post-ischemic cortex; **, $p<0.01$; ***, $p<0,001$.

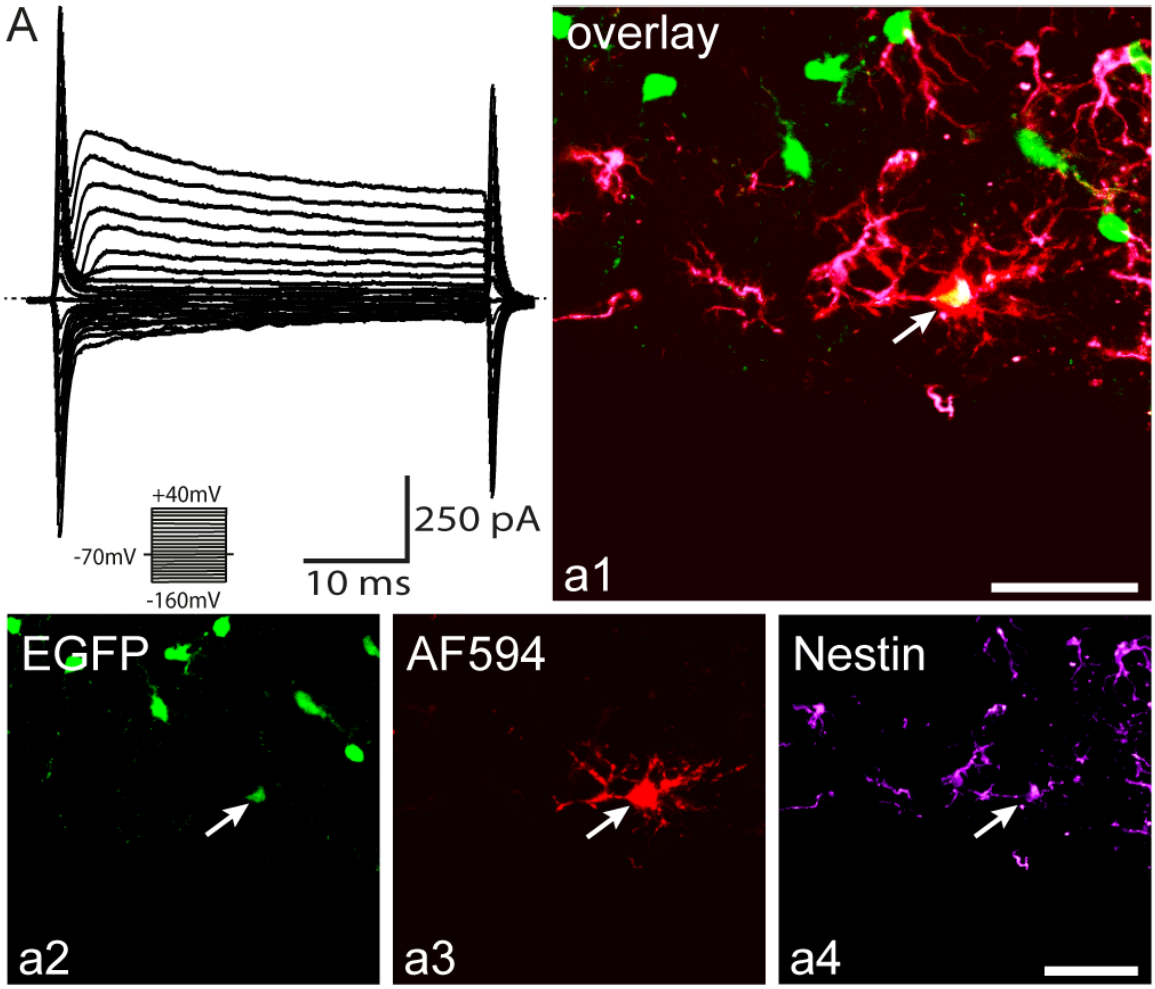

Figure 16. Polydendrocytes proliferate and change their current pattern after ischemia. **A,** A typical current pattern of polydendrocytes measured 3 days after MCAo obtained after depolarizing the cell membrane from a holding potential of -70 mV to +40 mV and hyperpolarizing to -160 mV (see the inset, bottom). Polydendrocytes showed a current pattern with K_{DR}, K_A, small K_{IR} currents and fast activating Na^+ inward currents in a few cells 3 days after MCAo. Zero current is marked by the dashed line. An overlayed image of polydendrocyte (**a1**) expressing enhanced green fluorescent protein (EGFP) 3 days after MCAo (**a2**) loaded with Alexa Fluor 594 hydrazide (AF594) during patch-clamp measurement (**a3**) subsequently stained with an antibody directed against nestin (**a4**). White arrow indicates the recorded cell. Scale bars, 50 µm. MCAo, middle cerebral artery occlusion.

Taken together, our electrophysiological analyses of polydendrocytes during the post-ischemic period revealed significant changes in their membrane properties 3 days after MCAo that coincided with their increased proliferation and alteration in their differentiation potential toward other cellular types 7 and 14 days after MCAo.

Table 3. Electrophysiological properties of EGFP$^+$ cells with a complex current pattern.

	Control	D3	D7	D14
V_{rest} (mV)	-77.5 ± 1.3	-69.5 ± 2.1(*)	-59.5 ± 5.2(***)	-65.2 ± 3.1(*)
R_m (Mohms)	121.1 ± 10.7	525.3 ± 88.4(**)	372.7 ± 42.5	309.3 ± 39.7
C_m (pF)	9.5 ± 0.8	8.9 ± 0.8	7.2 ± 0.9	8.8 ± 1.3
CDK_{IR} (pA/pF)	17.5 ± 6.5	3.3 ± 0.8(**)	9.6 ± 1.3	7.0 ± 1.3
CDK_{DR} (pA/pF)	8.1 ± 2.3	29.6 ± 3.4(***)	31.2 ± 3.6(***)	8.3 ± 1.9
CDK_A (pA/pF)	12.4 ± 3.0	14.7 ± 2.1	11.7 ± 3.0	14.6 ± 3.4
CDNa (pA/pF)	0.0 ± 0.0	3.5 ± 1.3(*)	0.0 ± 0.0	0.0 ± 0.0
n	22	35	15	14
%	81.0 ± 9.9	60.0 ± 6.6	23.4 ± 6.9(***)	20.9 ± 6.1(***)

V_{rest}, resting membrane potential; R_m, membrane resistance; C_m, membrane capacitance; CDK_{IR}, current density of inwardly-rectifying K^+ currents; CDK_{DR}, current density of voltage-gated delayed outwardly-rectifying K^+ currents; CDK_A, current density of the fast activating and inactivating outwardly-rectifying K^+ currents; CDNa, current density of Na^+ currents; n, number of measured cells; %, percentage of the cell type; *, $p < 0.05$; **, $p < 0.01$;***, $p < 0.001$.

Polydendrocytes differentiate into cells with the functional properties of astrocytes after ischemia

During the post-ischemic period a subpopulation of EGFP$^+$ cells displayed a current profile with predominant time- and voltage-independent non-decaying K^+ conductance, a so-called passive current pattern (Figure 17A). These cells were detected in all post-ischemic periods, and their passive membrane properties as well as their current densities did not significantly differ in all studied post-ischemic time points (Table 4). Significant differences were found in their appearance in the post-ischemic periods. EGFP$^+$ cells with a passive current pattern were never detected in

controls, and their incidence increased with time after ischemia. Their number was significantly increased 7 and 14 days after MCAo when compared to controls; from all measured cells they represented 48.4% ± 8.5% ($p < 0.01$) and 49.3% ± 10.2% ($p < 0.01$), respectively (Figure 15). Some of them expressed nestin, Ki-67 or GFAP 3 days after MCAo. In conclusion we demonstrated that a certain subpopulation of newly derived cells of polydendrocytic origin expresses astrocytic markers and these cells also display membrane properties typical of astrocytes.

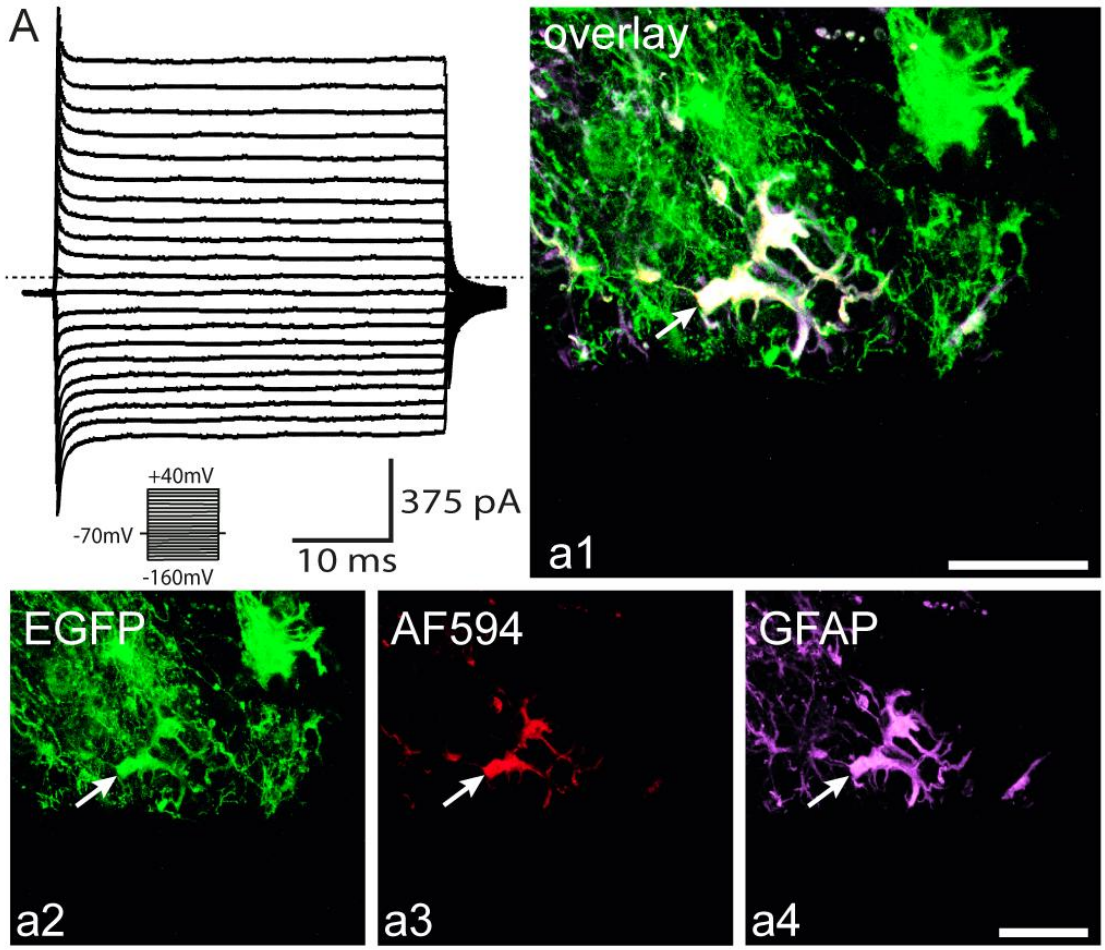

Figure 17. Polydendrocytes differentiate into reactive astrocytes after ischemia.

A, Current pattern of enhanced green fluorescent protein-positive $(EGFP)^+$ astrocytes 7 days after MCAo obtained after depolarizing the cell membrane from a holding potential of -70 mV to +40 mV and hyperpolarizing to -160 mV (see the inset, bottom). $EGFP^+$ astrocytes showed a passive current pattern, i.e., time- and voltage-independent non-decaying K^+ currents, with only small voltage activated K^+ currents. An overlayed image of astrocytes (**a1**) expressing EGFP 7 days after MCAo (**a2**) loaded with Alexa Fluor 594 (AF594) hydrazide during patch-clamp measurement (**a3**), stained with an antibody directed against glial fibrillary acidic protein (GFAP, **a4**), a marker of astrocytes. Note dye coupling (a3) between $EGFP^+$ cells with a passive current pattern. Scale bars, 50 µm. MCAo, middle cerebral artery occlusion.

Table 4. Electrophysiological properties of EGFP$^+$ cells with a passive current pattern.

	D3	D7	D14
V_{rest} (mV)	-56.0 ± 4.4	-52.8 ± 2.7	-47.5 ± 1.0
R_m (Mohms)	165.0 ± 13.0	168.4 ± 8.3	135.3 ± 8.0
C_m (pF)	8.4 ± 0.9	9.7 ± 1.6	7.5 ± 0.6
CDK_{IR} (pA/pF)	2.7 ± 1.3	2.8 ± 1.1	0.5 ± 0.3
CDK_{DR} (pA/pF)	10.5 ± 3.0	9.0 ± 1.9	8.0 ± 3.3
CDK_A (pA/pF)	0.0 ± 0.0	0.0 ± 0.0	0.0 ± 0.0
CDNa (pA/pF)	0.0 ± 0.0	0.0 ± 0.0	0.0 ± 0.0
n	18	31	33
%	31.0 ± 7.6	48.4 ± 8.5	49.3 ± 10.2

V_{rest}, resting membrane potential; R_m, membrane resistance; C_m, membrane capacitance; CDK_{IR}, current density of inwardly-rectifying K^+ currents; CDK_{DR}, current density of voltage-gated delayed outwardly-rectifying K^+ currents; CDK_A, current density of the fast activating and inactivating outwardly-rectifying K^+ currents; CDNa, current density of Na^+ currents; n, number of measured cells; %, percentage of the cell type.

Polydendrocytes also differentiate into cells with the functional properties of neuronal precursor cells after ischemia

In agreement with our immunohistochemical analysis, a subpopulation of EGFP$^+$ cells expressed a current profile that resembled that of neuronal precursor cells (Figure 18A). These cells appeared 7 and 14 days after MCAo, and their passive membrane properties as well as the current densities of their voltage activated channels did not significantly differ between these two time points (Table 5). The percentage of neuronal precursor cells reached 9.4% ± 3.1% of all recorded cells 7 days after MCAo and 4.5% ± 4.0% 14 days after MCAo (Figure 15). Post-recording immunohistochemical identification confirmed DCX expression in EGFP$^+$ neuronal precursor cells (Figure 18).

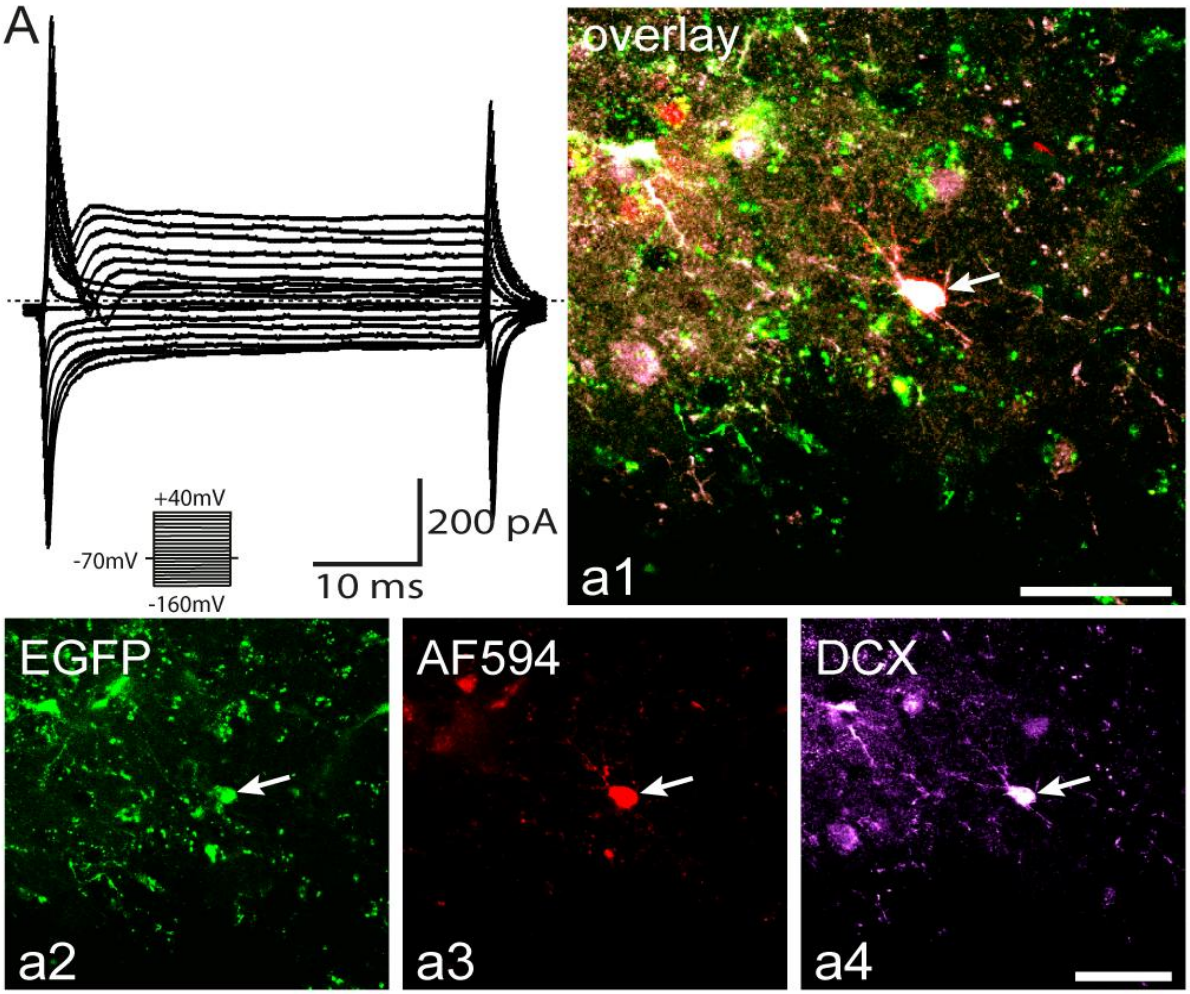

Figure 18. Polydendrocytes also differentiate into immature neurons after ischemia.

A, Current pattern of enhanced green fluorescent protein-positive ($EGFP^+$) neuronal precursor cells 7 days after MCAo obtained after depolarizing the cell membrane from a holding potential of -70 mV to +40 mV and hyperpolarizing to -160 mV (see the inset, bottom). $EGFP^+$ neuronal precursor cells displayed outwardly rectifying K^+ currents (K_{DR}, K_A currents) together with increased amplitudes of Na^+ currents when compared to polydendrocytes. An overlayed image of neuronal precursor cells (**a1**) expressing EGFP 7 days after MCAo (**a2**), loaded with Alexa Fluor 594 hydrazide (AF594) during patch-clamp recording (**a3**), subsequently stained with an antibody directed against doublecortin (DCX, **a4**), a marker of newly-derived neuronal precursor cells. Scale bars, 50 µm. MCAo, middle cerebral artery occlusion.

Table 5. Electrophysiological properties of EGFP$^+$ neuronal precursor cells.

	D7 MCAo	D14 MCAo
V_{rest} (mV)	-58.2 ± 5.0	-62.7 ± 9.3
R_m (Mohms)	840.4 ± 144.9	1189.7 ± 631.9
C_m (pF)	5.2 ± 0.9	6.9 ± 0.9
CDK_{IR} (pA/pF)	1.3 ± 1.3	0.0 ± 0.0
CDK_{DR} (pA/pF)	34.70 ± 6.0	46.1 ± 5.8
CDK_A (pA/pF)	17.9 ± 2.0	15.7 ± 2.5
CDNa (pA/pF)	39.5 ± 10.2	21.5 ± 12.0
n	6	3
%	9.4 ± 3.1	4.5 ± 4.1

V_{rest}, resting membrane potential; R_m, membrane resistance; C_m, membrane capacitance; CDK_{IR}, current density of inwardly-rectifying K^+ currents; CDK_{DR}, current density of voltage-gated delayed outwardly-rectifying K^+ currents; CDK_A, current density of the fast activating and inactivating outwardly-rectifying K^+ currents; CDNa, current density of Na^+ currents; n, number of measured cells; %, percentage of the cell type.

After ischemia only a small population of oligodendrocytes in the cortex arises from polydendrocytes

Furthermore, in some EGFP$^+$ cells time- and voltage-independent decaying K^+ currents, a typical current pattern of oligodendrocytes were recorded (Xie et al., 2007), (Figure 19A). These cells were present at all analyzed time points, and their electrophysiological properties and quantity did not significantly change after MCAo when compared to controls (Figure 15).

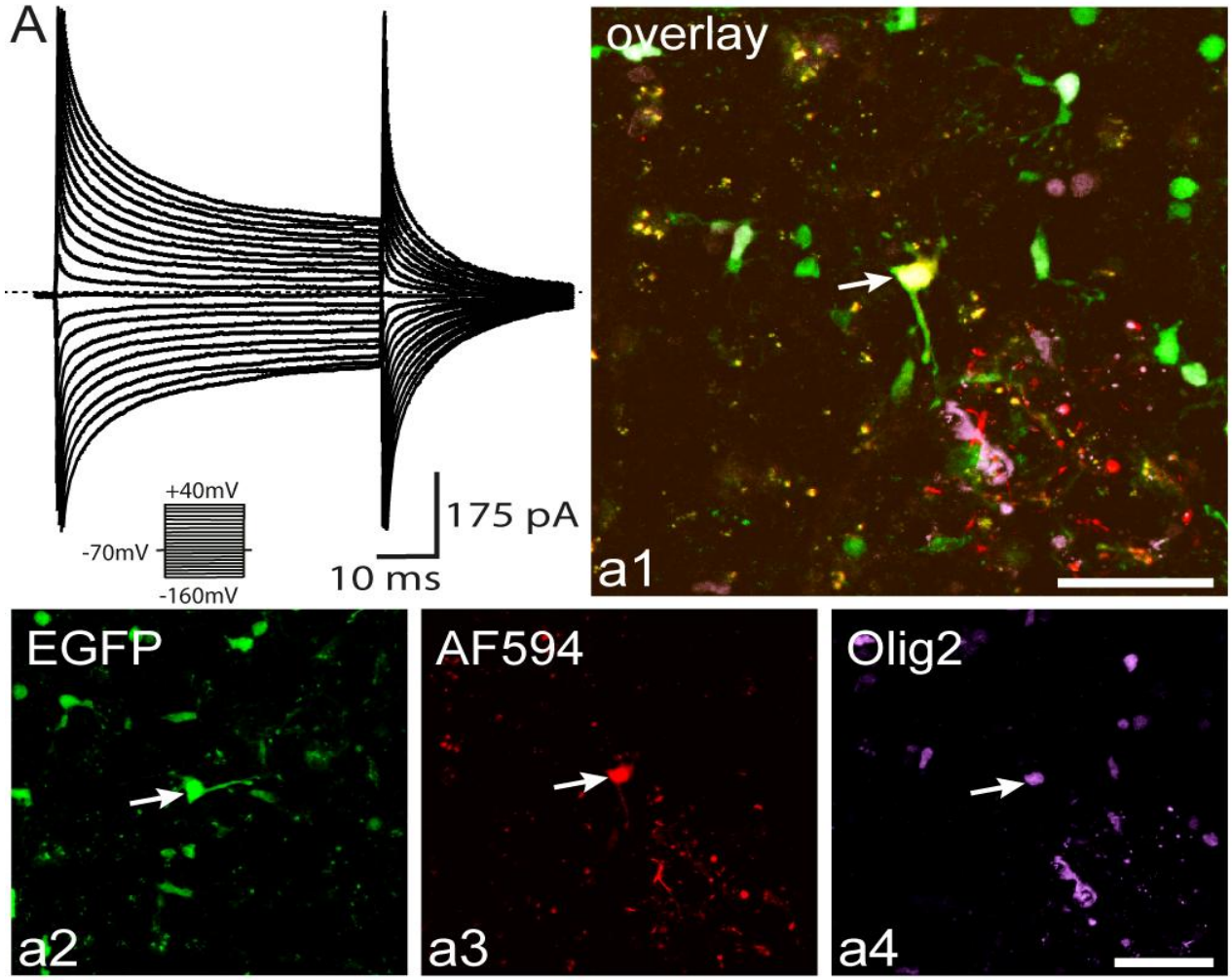

Figure 19. Polydendrocytes differentiate into oligodendrocytes after ischemia.

A, Current pattern of enhanced green fluorescent protein-positive $(EGFP)^+$ oligodendrocytes 7 days after ischemia obtained after depolarizing the cell membrane from a holding potential of -70 mV to +40 mV and hyperpolarizing to -160 mV (see the inset, bottom). $EGFP^+$ oligodendrocytes displayed time- and voltage-independent K^+ currents decaying during the duration of the voltage pulse. An overlayed image of oligodendrocytes (**a1**) expressing EGFP 7 days after MCAo (**a2**) loaded with Alexa Fluor 594 hydrazide (AF594) during patch-clamp measurement (**a3**), subsequently stained with an antibody directed against Olig2 (**a4**). Scale bars, 50 µm. MCAo, middle cerebral artery occlusion.

Changes in gene expression profile of glial cell subpopulations during post-ischemic gliogenesis

Gene expression profiling of glial cell subpopulations is another approach that may unravel and help to understand the process of adult gliogenesis following ischemic injury. For identification of glial cell subpopulations we used GFAP/EGFP mouse strain. Because of the possible heterogeneity of glia cells, it was necessary to collect dissociated single cells by flow cytometry and analyze them individually by RT-qPCR. For pre-amplification and further analysis $EGFP^+$ cells were selected that expressed the astrocytic markers *Glul* and/or *Slc1a3* and $EGFP^+$ cells that were also positive for *Cspg4* and/or *Pdgfra*, which are markers of polydendrocytes. In these cells the gene expression of the following markers was measured: glial cell markers (*Slc1a3, Gfap, Gfapd, Glul, S100b, Pdgfra, Cspg4)*, developmental markers nestin and vimentin (*Nes* and *Vim*), aquaporins (*Aqp1, Aqp4, Aqp9*), subunits of glutamate ionotropic AMPA receptors (*Gria1, Gria2, Gria3, Gria4*), glutamate ionotropic NMDA receptors (*Grin1, Grin2a, Grin2b, Grin2c, Grin2d, Grin3a*), glutamate ionotropic kainate receptors (*Grik1, Grik2, Grik3, Grik4, Grik5*), glutamate metabotropic receptors (*Grm1, Grm3, Grm5*), outwardly rectifying K^+ channels (*Kcna3, Kcna4, Kcna5*), inwardly rectifying K^+ channels (*Kcnj2, Kcnj10, Kcnj16*), two pore domain K^+ channels (*Kcnk1, Kcnk2, Kcnk10*) and hyperpolarization-activated cyclic nucleotide-gated channels (*Hcn1, Hcn2, Hcn3, Hcn4*), voltage-gated chloride channels (*Clcn2*), transient receptor potential channels (*Trpv4*), and *Snap25* encoding synaptosomal-associated protein SNAP-25 (Table 2). The markers were selected based on previous work (Benesova et al., 2012), which revealed significant differences between astrocytic subpopulations in the expression of genes that code glial membrane proteins participating in K^+/glutamate homeostasis maintenance.

All cells collected from the cortex were analyzed for the expression of *Slc1a3, Glul, Cspg4* and *Pdgfra* to estimate the ratio between cells that express only astrocytic markers (*Slc1a3* and *Glul*) and cells that also express at least one of the polydendrocytic markers (Figure 20). After ischemic injury there was a distinct increase in the number of cells expressing polydendrocytic markers 3 days after MCAO, but their number decreased again at later post-ischemic stages. For single

cell qPCR expression profiling 50 cells were collected from P50, 90 cells from D3, 74 cells from D7, and 78 cells from D14. The cDNA produced from these cells was preamplified and measured on the Biomark platform.

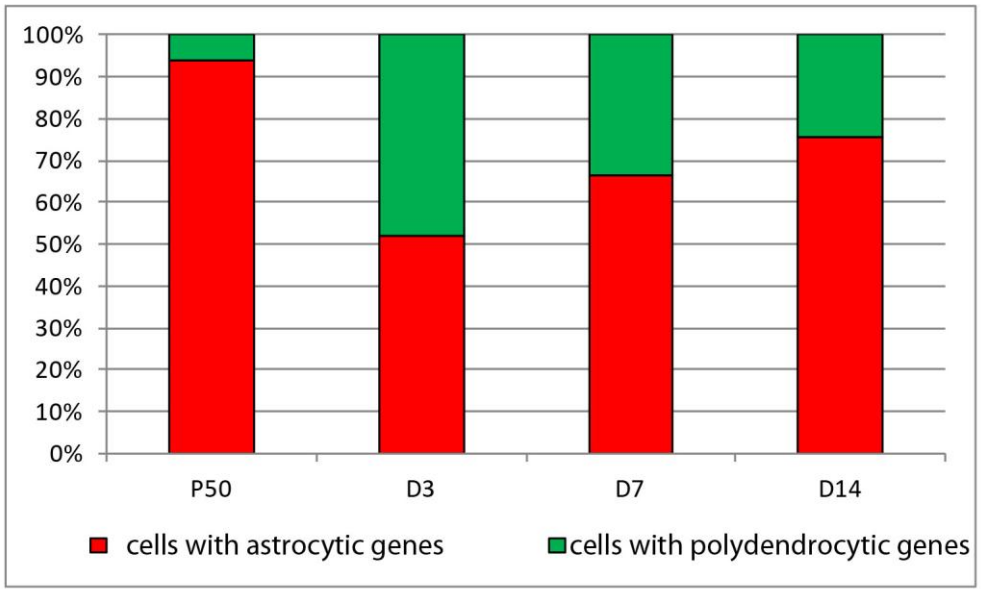

	P50	D3	D7	D14
Cells with only markers of astrocytes	107	77	64	103
Cells with markers of polydendrocytes	7	71	32	33
All cells	114	148	96	136

Figure 20. Characteristics of enhanced green fluorescent protein (EGFP)$^+$ cells in the cortex of GFAP/EGFP mice. Percentage of EGFP$^+$ cells expressing either predominantly astrocytic or polydendrocytic markers at 3, 7 and 14 days (D3, D7 and D14) following focal cerebral ischemia. Cells expressing *Cspg4* and/or *Pdgfra* are shown in green, while cells expressing only *Slc1a3* and/or *Glul* are shown in red. The total numbers of the investigated cells were 114 for P50, 148 for D3, 96 for D7 and 136 for D14.

Expression profiles of reactive glia following focal cerebral ischemia

Three days after ischemia the expression profiles of EGFP$^+$ cells was already changed. Approximately 50% of all EGFP$^+$ cells began to express *Pdgfra*, *Vim*, and *Grik5*, while *Aqp4, Glul* and *Slc1a3* expression was decreased. Seven days after ischemia the cells were transcriptionally more active with particularly high expression of *Pdgfra, Vim, S100b, Slc1a3, Glul*. Furthermore, the cells also began to express

Gfap and *Gfapd*. At this time, the expression of *Glul* returned to the basal level (P50, Figure 21A). Fourteen days after ischemia, the difference in expression compared to control (P50) was the largest. The expression of *Vim, Gfap, Gfapd, Aqp4, S100b* and *Grm3* was dramatically decreased, while the expression of *Hcn1, Hcn2, Hcn3, Aqp1, Aqp9, Grm5, Gria3, Grin2a, Grin2d* and *Kcna3* was markedly increased. At all post-ischemic stages cells expressing *Cspg4* and *Pdgfra* were found as well.

All cells (P50, D3, D7 and D14) were divided by SOM into 3 subpopulations and confirmed by PCA to have different expression profiles (Figure 21B). These subpopulations are further termed B1, B2 and B3. To characterize these subpopulations, the expressions of the genes were compared individually in histograms and by conventional univariate statistics. B1 subpopulation comprised cells mainly from P50 (35%), (Figure 21C) and from D3 (47%), however cells from D7 (15%) and D14 (3%) were also present. The B1 subpopulation displayed the lowest overall transcriptional activity; high expression was observed only for *Slc1a3, Glul, Aqp4* and *Gria2*. Subpopulation B2 was more transcriptionally active with the high expression of genes encoding glutamate ionotropic receptors, K^+ channels, *Grm3, Aqp4, Hcn2, Gfap, Gfapd, Glul, Slc1a3, S100b, Vim, Cspg4* and *Pdgfra*. Most B2 cells were from D7 (66%), 31% were from D3 and only 2 cells were from P50. Notably, the two P50 cells also expressed *Pdgfra* and *Cspg4*. Subpopulation B3 was composed of only D14 cells. The very high expression of many genes makes this group unique, and there is no overlap in the PCA between B3 and the other subpopulations.

Generally, reactive astrocytes isolated from post-ischemic stages (D3, D7 and D14) showed much higher gene expression than those collected from the postnatal developmental stages (Rusnakova et al., 2013). Within each subpopulation B1-B3 many significant correlations were found.

The expressions of *Slc1a3* and *Glul* in B1 and B3 were correlated (r = 0.66 and 0.79), and a correlation of *Slc1a3* and *Aqp4* was found in B1, B2 and B3 (r = 0.43, 0.69, 0.81). A strong correlation was also found between the expressions of *Gfap* and *Gfapd* in B1 and B2 (r = 0.76 and 0.87). The expressions of the latter two genes also correlated with those of *Hcn1, Hcn2, Hcn3, Hcn4, Grin2a, Grin2d, Gria3, Grm5, Kcna3,* and *Kcnk2*. In fact, the expressions of almost all of these genes were strongly correlated on the single cell level in B3 (r close to or larger than 0.7).

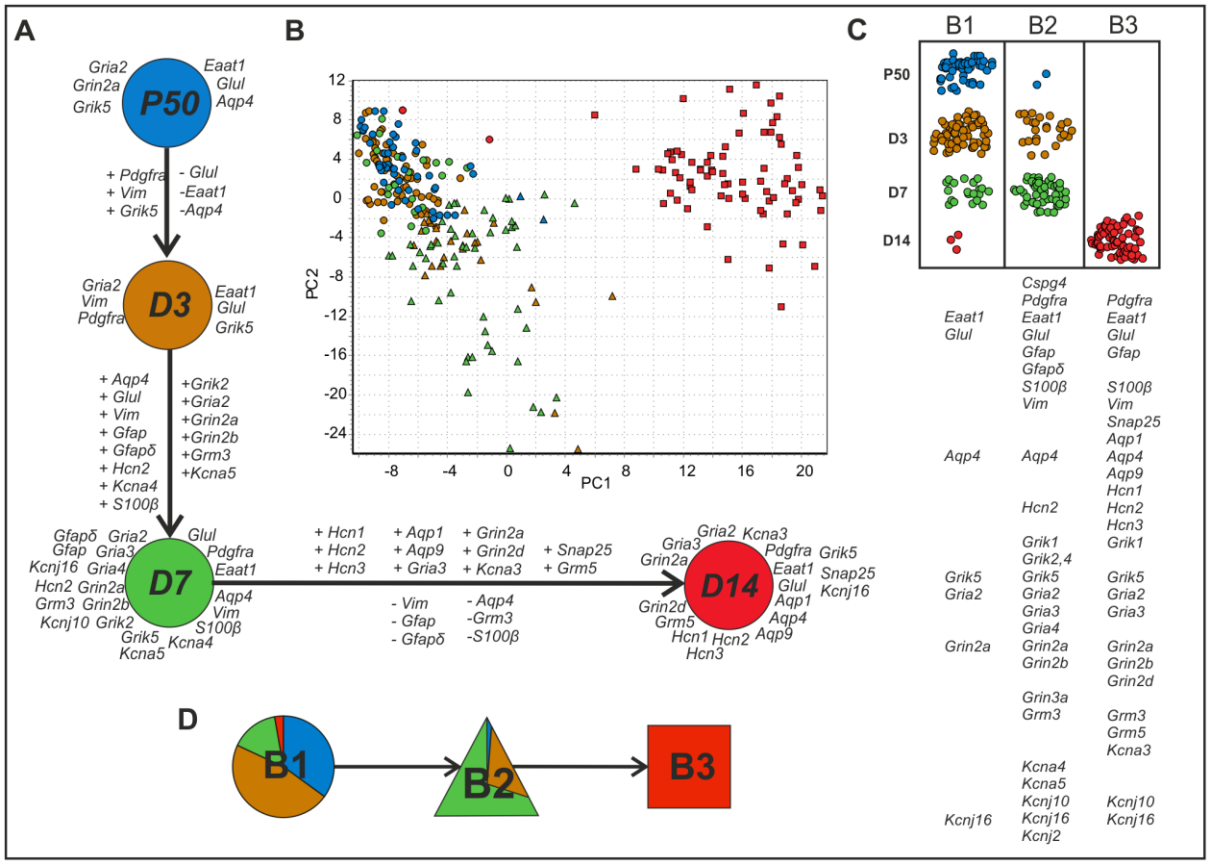

Figure 21. Changes in the gene expression of enhanced green fluorescent protein (EGFP)$^+$ cells after ischemia. A, Changes in the gene expression of highly expressed astrocytic/polydendrocytic markers and membrane proteins at P50 (blue, control), D3 (orange, 3 days after ischemia), D7 (green, 7 days after ischemia), and D14 (red, 14 days after ischemia). The listed genes show at least 2-fold up (+) or 2-fold downregulation (-) between sequential stages. **B,** PCA clustering of cells from all post-ischemic stages and P50 (data mean-centered along genes). The stages are indicated in color (P50 blue, D3 orange, D7 green, and D14 red), and the three groups identified by SOM are indicated by symbols (squares for B3; circles for B1 and triangles for B2). **C,** The incidence of cells from the three subpopulations at post-ischemic stages and P50. The genes under the table indicate highly expressed genes in particular subpopulations. **D,** The distribution of control and post-ischemic stages in individual subpopulations

Such a strong correlation between the above-listed genes suggests significant alterations in the membrane properties of reactive astrocytes at D14, namely the appearance of *Hcn1-4*, which so far have been described only in neurons (Wahl-Schott and Biel, 2008). On the other hand, a significant negative correlation was

found between the expressions of *Cspg4* or *Pdgfra* and *Glul, Aqp9, Hcn1, Grin2a* and *Gria3* (r,-0.55). This clearly demonstrates that polydendrocytes from D14 (B3 subpopulation) lose the expression of *Cspg4* and *Pdgfra* while they change into reactive astrocytes comprising a permanent glial scar.

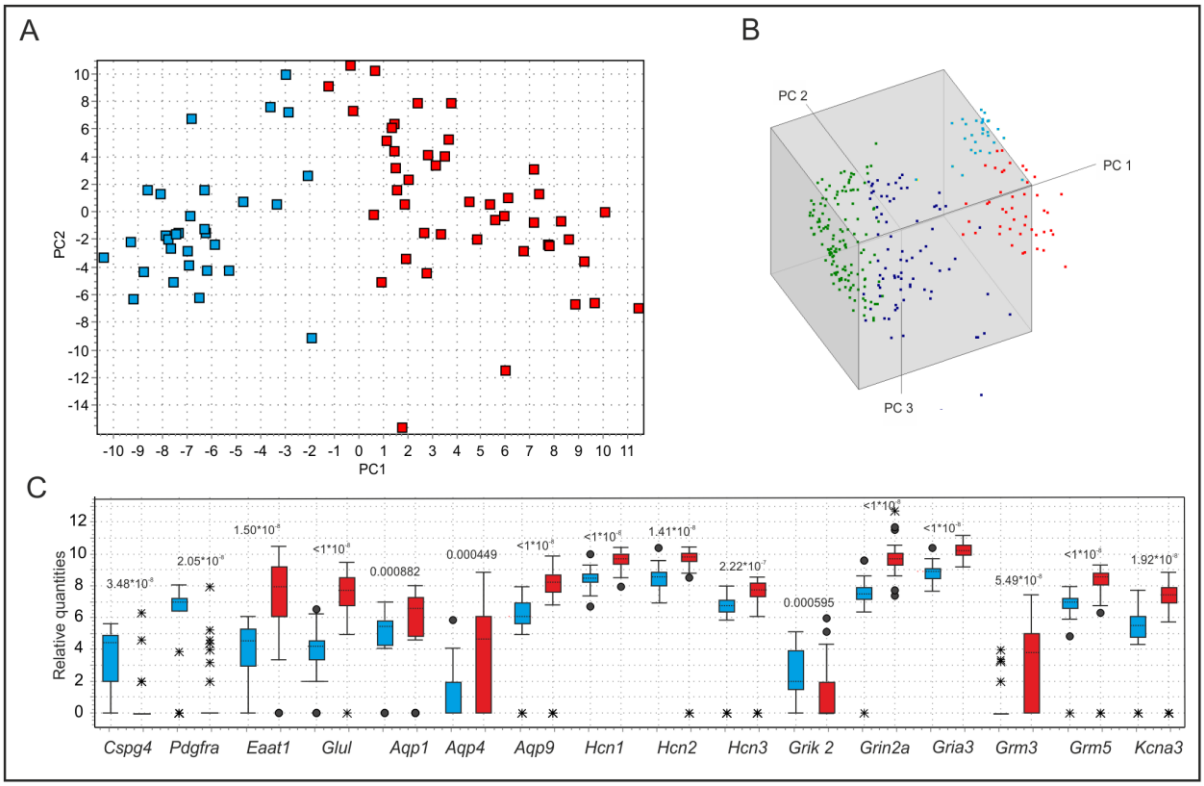

Figure 22. Classification of reactive glia subpopulations (B3) into two subgroups. A, PCA scatter plot of the cells in subpopulation B3 (reactive glia). Colors indicate the two groups (B3A red and B3B blue) obtained by decomposing the data by SOM analysis (data are mean-centered). **B,** Three-dimensional PCA scatter plot of all post-ischemic cells and P50 reflecting the normal state for comparison - B1 (green), B2 (dark blue), B3A (red) and B3B (light blue). PC3 separates B3A from B3B. The first PC accounts for 32%, the second 14% and the third 8%, of the total variance in the data. **C,** Box plots showing genes differentially expressed in B3A (red) and B3B (blue). The box indicates the median value and the 25th and 75th percentiles, the whiskers are 1.56 the distance of the 25th and 75th percentiles, the circles indicate outliers and the crosses extreme outliers. p-values (Mann-Whitney) are indicated for each gene.

Further classification of the reactive glial cells in subpopulation B3 using SOM

revealed that it is not a homogenous group; rather there are two subgroups, which were referred to as B3A and B3B and their existence was clearly confirmed by PCA (Figure 22A). Viewing the data in a 3-dimensional PC1 vs. PC2 vs. PC3 space shows that the B3A/B3B subpopulations separate along PC3 (Figure 22B). Hence, the genes distinguishing B3A from B3B are those with high weights in PC3, thus being different from the genes distinguishing B3 from B1/B2, which are those with high weights in PC1 and PC2. The expression of genes in the B3A and B3B subgroups were compared using the non-parametric Mann-Whitney test, and those with significant p-values after Bonferroni correction for multiple testing ($p = 0.00109$) are shown in Figure 22C. The most important differences between the B3A and B3B subgroups are the down-regulation of *Pdgfra*, *Cspg4* and *Grik2* and the up-regulation of *Slc1a3*, *Glul, Aqp1, Aqp4, Aqp9, Hcn1, Hcn2, Hcn3, Grin2a, Gria3, Grm3, Grm5 and Kcna3* (Figure 22C).

The result from single cell qPCR clearly showed striking heterogeneity of glial cells after ischemia. A large number of glial cells after ischemia expressed markers of polydendrocytes, which clearly demonstrates important role of polydendrocytes in formation of glial scar after ischemia and nervous tissue regeneration. Classifying the reactive glial cells phenotype on mRNA levels also suggests differentiation of polydendrocytes into certain subpopulation of reactive astrocytes in later phases after ischemia.

Characterization of the neurogenic zone in the dorsal part of the LV

The subventricular zone of the lateral ventricles is one of the most important regions of adult neurogenesis in the mammalian brain as was pointed out in introduction. Neurogenesis predominantly occurs in the lateral wall of the LV; however, several studies have described the existence of cell populations with neurosphere-forming ability also in the dorsal part of the LV (Willaime-Morawek et al., 2006; Young et al., 2007). The D6/GFP mice were developed primarily for studying the role of the mouse

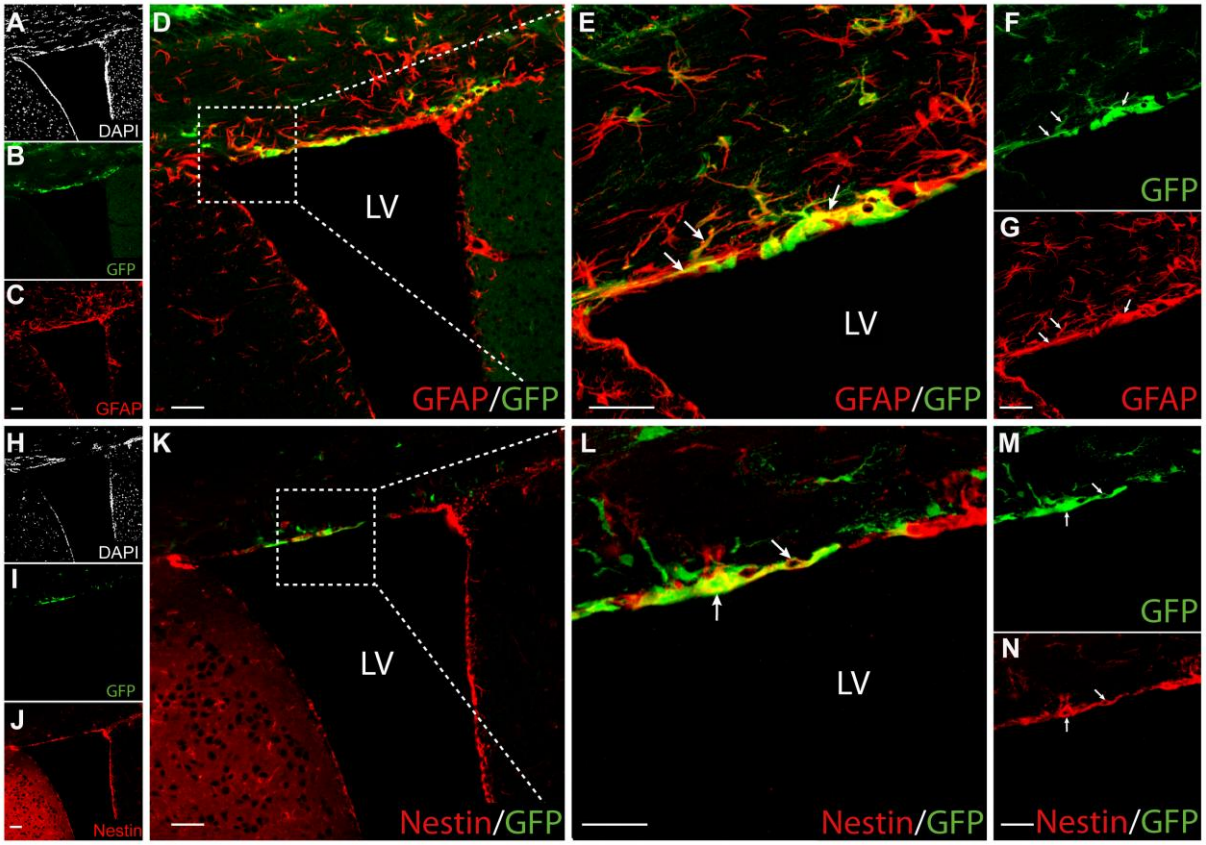

Figure 23. Characterization of green fluorescent protein (GFP)$^+$ cells in the dorsal part of the lateral ventricles (LV) in uninjured brain. **A–D,** Images illustrating the dorsal localization of GFP$^+$ **(B)** and glial fibrillary acidic protein (GFAP)$^+$ cells **(C)** around the LV. **E–G,** A detailed image of GFP$^+$ cells in the dorsal part of the LV shows the expression of GFAP in many GFP$^+$ cells. **H–K,** An overview of the LV showing the dorsal localization of GFP$^+$ **(I)** and nestin-positive cells **(J)** around the LV. **L–N,** A detailed image of GFP$^+$ cells in the dorsal part of the LV shows the expression of nestin in many GFP$^+$ cells. White arrows indicate GFP$^+$/GFAP$^+$ or GFP$^+$/nestin$^+$ cells. DAPI was used to visualize the cell nuclei and the borders of the LV. Scale bars, 50 µm.

Dach1 gene in the embryonic development of the neocortex; however, persisting activity of this gene was also detected in the adult mouse brain. Besides subpopulations of neurons and astrocytes in the somatosensory cortex and CA1 area in the hippocampus, the mouse *Dach1* gene is also active in a narrow region in the dorsal part of the LV (Machon et al., 2002), (Figure 23). Using D6/GFP mouse strain we aimed to elucidate the neurogenic or gliogenic differentiation potential of GFP^+ cell subpopulation that persists in the adult dorsal part of the LV and displays a sustained *Dach1* gene expression under physiological conditions. In this genetically modified mouse strain cells expressing mouse *Dach1* gene express concomitantly GFP, which makes the identification of these cells very easy. *Dach1* gene expression is first detected at embryonic day 10.5 in scattered cells of the arising cortical vesicles, while by embryonic day 12.5; *Dach1* gene activity expands throughout the developing neocortex and the hippocampus (Machon et al., 2002).

Collectively, here we aimed to demonstrate the existence of a subpopulation of neural stem cells in the dorsal wall of the LV and to clarify their role in the process of endogenous post-ischemic neurogenesis/gliogenesis in the adult cortex.

Initially, immunohistochemical analyses were performed to identify the phenotype of GFP^+ cells in this region. GFP^+ cells were found along the entire area of the dorsal part, and they formed several rows of cells in the subependymal zone. The majority of GFP^+ cells expressed GFAP, a marker of astrocytes (Figure 23, A-G), but also markers of adult neural stem cells (aNSCs), such as nestin or vimentin. The assumption that GFP^+ cells in this region expressed the phenotype of aNSCs was confirmed by the immunohistochemical detection of nestin (Figure 23, H-N). Both markers were expressed mainly by GFP^+ cells with many well-developed processes; however, there were also GFP^+ cells without or with a few short processes, scattered throughout the entire dorsal area. Nevertheless, their density was higher in the proximity of the lateral RMS, and they predominantly expressed DCX, a marker of migrating neuroblasts (Figure 24, A-G).

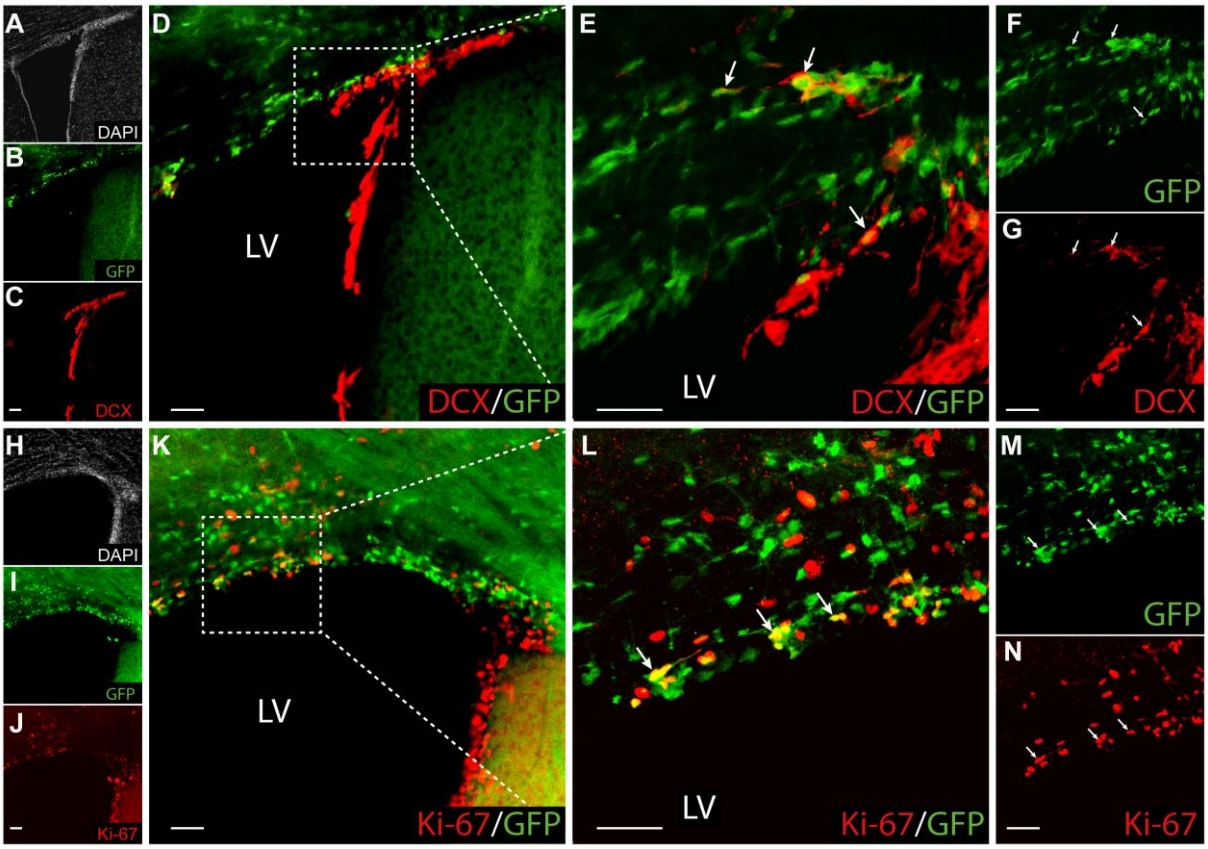

Figure 24. Characterization of green fluorescent protein (GFP)$^+$ cells in the dorsal part of the lateral ventricles (LV) in uninjured brain. **A–D,** An overview of the LV showing the dorsal localization of GFP$^+$ cells **(B)** and doublecortin (DCX) immunoreactivity (**C**) in several GFP$^+$ cells **(E-G)**. **H–K,** An overview of the LV showing the dorsal localization of GFP$^+$ **(I)** and Ki-67$^+$ cells **(J)** around the LV. **L–N,** A detailed image of GFP$^+$ cells in the dorsal part of the LV shows the expression of the proliferation marker Ki-67 in several GFP$^+$ cells. White arrows indicate GFP$^+$/Ki-67$^+$ or GFP$^+$/DCX$^+$ cells. DAPI was used to visualize the cell nuclei and the borders of the LV. Scale bars, 50 µm.

To determine whether the GFP$^+$ cells in dorsal part of LV of adult brain possess the properties of neural stem/progenitor cells, a single cell neurosphere-forming assay was carried out. The dorsal wall of the LV from the brain of controls was carefully dissected and prepared a single cell suspension that was diluted and cultured under proliferating conditions in 96-well plates. After one week these cells formed neurospheres, and 26.1 ± 2.5% (n = 5 animals; Figure 25, A-I) of them expressed GFP and were GFAP- or nestin-positive. The same neurosphere-forming assay was performed with GFP$^+$ cells isolated from mice 4 days after MCAo. These cells also

formed GFP^+ neurospheres, and their number was significantly ($p < 0.01$) increased to 43.2 ± 4.3% (n = 5 animals) when compared to controls; some of them comprised, besides $GFAP^+$ or $nestin^+$, also GFP^+/DCX^+ cells. The neurospheres were further cultured under differentiating conditions. The cells attached to the PLL-coated cover slips and expressed predominantly glial markers, such as nestin, brain lipid-binding protein (BLBP) or GFAP; however, the expression of the neuronal progenitor marker DCX was found only in cells originating from the ischemic brains and never from the control brains (Figure 25).

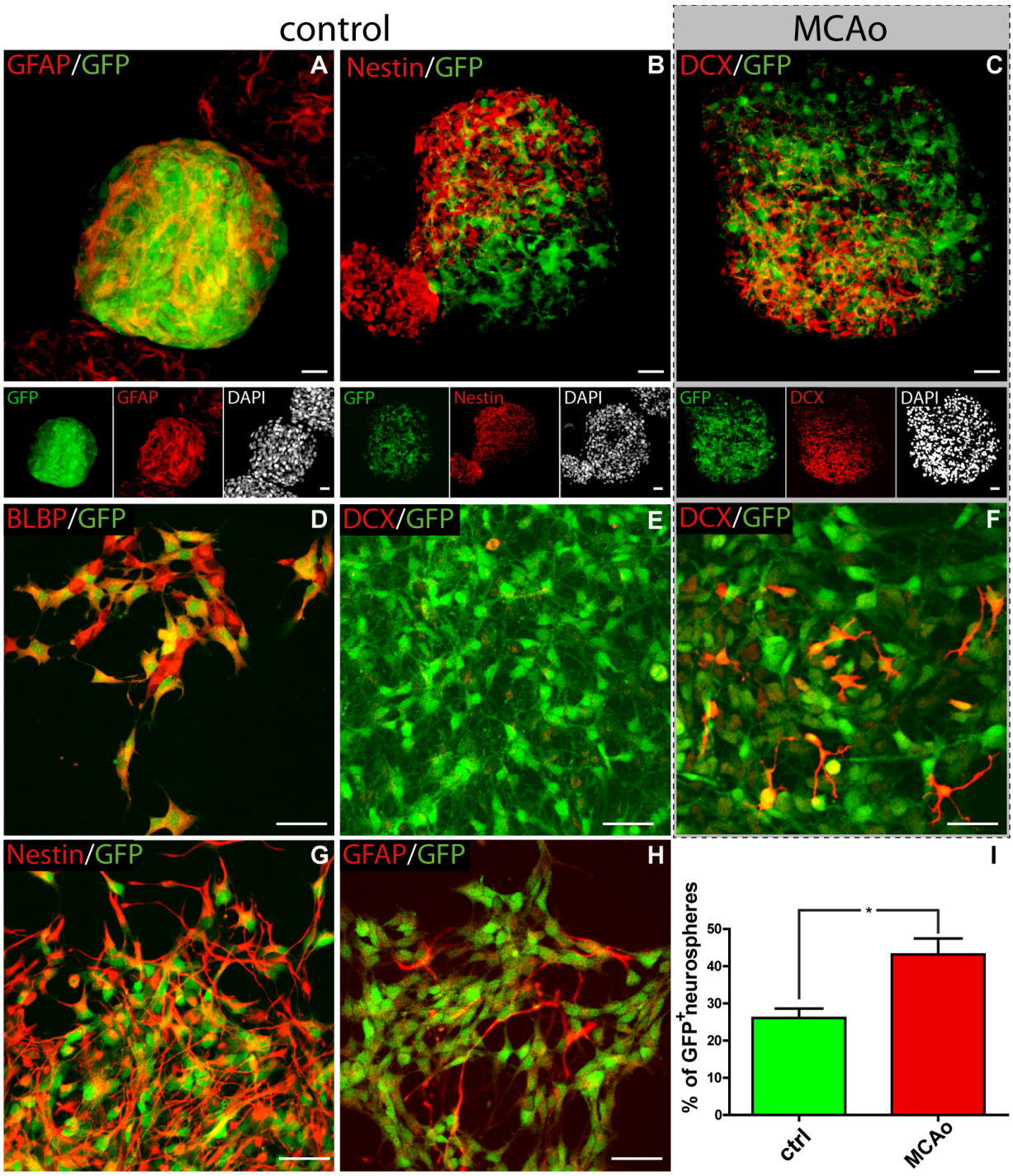

Figure 25. Green fluorescent protein (GFP)$^+$ cells form neurospheres *in vitro.* A, An image showing neurospheres formed from GFP$^+$ cells isolated from the dorsal part of the lateral ventricles (LV) in uninjured mouse brain (controls). Many GFP$^+$ cells expressed glial fibrillary acidic protein (GFAP). **B,** An image showing neurospheres formed by GFP$^+$ cells isolated from the dorsal part of the LV of controls. Many GFP$^+$ cells expressed nestin. **C,** An image showing neurospheres formed by GFP$^+$ cells isolated from the dorsal part of the LV of mice 4 days after MCAo. Several neurospheres consisted of GFP$^+$/DCX$^+$ cells. **E,** Four days after differentiation, almost all GFP$^+$ cells from control neurospheres express brain lipid-

binding protein (BLBP). **F,** Four days after differentiation, virtually no GFP^+ cells from control neurospheres express doublecortin (DCX), which is in contrast to the frequent expression of DCX in GFP^+ cells derived from neurospheres isolated from dorsal LV of ischemic brains. Figures **G** and **H** depict the strong expression of neural stem cell markers (nestin and GFAP) in differentiated GFP^+ cells. **I**, Bar graphs show the increased number of neurospheres formed from GFP^+ cells isolated from the dorsal part of the LV of ischemic brains. Scale bars, 50 µm. MCAo, middle cerebral artery occlusion.

Differentiated GFP^+ cells from the dorsal part of the LV display a passive or neuronal current pattern

To determine the electrophysiological properties of differentiated GFP^+ cells isolated from control brains or those 4 days after MCAo, patch-clamp recordings was performed in the whole-cell configuration. Two cell populations with distinct passive membrane properties and current patterns were detected, correlating with the morphological and immunohistochemical features described above. GFP^+ cells isolated from control brains had only a large flat morphology and expressed time- and voltage-independent non-decaying K^+ currents. Such current pattern was previously termed as a passive current pattern (Zhou, 2005). On the other hand, in the cell culture obtained from ischemic brains two electrophysiological phenotypes were found in GFP^+ cells. A subpopulation of GFP^+ cells with a passive current pattern was detected and moreover, some cells displayed electrophysiological properties resembling those of neuronal precursors (a neuronal-like current pattern (Bellardita et al., 2011). GFP^+ cells with a neuronal current pattern comprised 27.0 ± 10.2% of all measured GFP^+ cells isolated from ischemic brains (Figure 26A-I). The membrane properties are summarized in Table 6. Post-recording identification revealed the predominant expression of DCX in these GFP^+ cells.

In summary, these data indicate that GFP^+ cells isolated from the dorsal part of the LV of control brains have the ability to form neurospheres *in vitro* and their differentiation potential is mainly gliogenic. On the other hand, GFP^+ cells isolated from the dorsal part of the LV of ischemic brains also form neurospheres; however, their potential is also neurogenic.

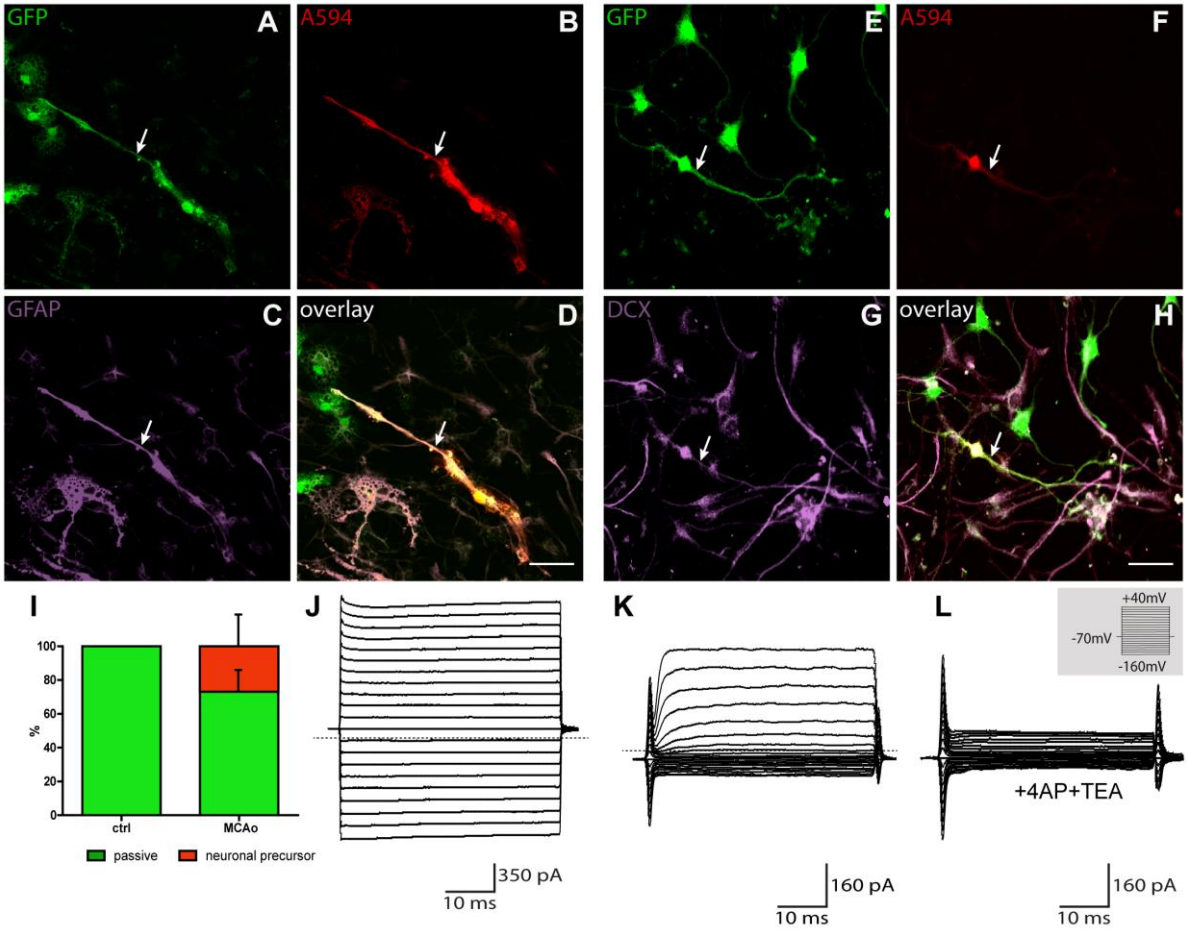

Figure 26. The *in vitro* differentiation potential of green fluorescent protein (GFP)$^+$ cells is altered following ischemia. A, GFP$^+$ cell isolated from a uninjured brain (control) and differentiated for 4 days, then loaded with Alexa Fluor 594 hydrazide (A594) during patch-clamp measurement **(B)** and subsequently stained with an antibody directed against glial fibrillary acidic protein (GFAP), (**C**). An overlay image is shown in (**D**). **E,** GFP$^+$ cell isolated from an ischemic brain loaded with Alexa Fluor 594 hydrazide during patch-clamp measurement **(F)**, subsequently stained with an antibody directed against doublecortin (DCX), (**G**). An overlay image is shown in **(H)**. The white arrows indicate the recorded cells. **I,** Graph demonstrating the differences in the incidence of passive and neuronal precursor cells between GFP$^+$ cells isolated from controls and brains 4 days after MCAo. **J**, All GFP$^+$ cells isolated from controls differentiated into cells with a passive current pattern, i.e., time- and voltage-independent non-decaying K^+ current. Zero current is marked by the dashed line. The current pattern was measured after depolarizing/hyperpolarizing the cell membrane from a holding potential of -70 mV; for the voltage protocol see the inset in **(L)**. **K**, A subpopulation of GFP$^+$ cells isolated from ischemic brains differentiated into cells with a neuronal current pattern, i.e., outwardly rectifying K^+ currents (K_{DR}, K_A currents). Zero current is marked by the dashed line. The current pattern was measured with the same protocol as in (**J).** **L**,Outwardly-rectifying K^+ currents were almost completely blocked by 4-aminopyridine (4AP) and tetraethylamonium (TEA). Scale bars, 50 µm. MCAo, middle cerebral artery occlusion.

Table 6. Electrophysiological properties of GFP$^+$ cells *in vitro.*

	Control	MCAo	
	passive	passive	neuronal
V_{rest} (mV)	-78.1 ± 2.0	-60.7 ± 3.5 (***)	-43.6 ± 3.8
R_m (MOhms)	63.8 ± 8.5	137.2 ± 21.3 (***)	716.5 ± 160.2
C_m (pF)	65.0 ± 9.7	20.7 ± 3.1 (***)	8.4 ± 0.5
CDK_{IR} (pA/pF)	0.5 ± 0.2	2.6 ± 0.7 (***)	0.3 ± 0.2
CDK_{DR} (pA/pF)	4.2 ± 0.9	5.2 ± 1.6	24.6 ± 9.3
CDK_A (pA/pF)	0.6 ± 0.4	1.5 ± 0.6	9.8 ± 6.1
CDNa (pA/pF)	0.0 ± 0.0	0.0 ± 0.0	0.0 ± 0.0
n	43	24	9
%	100.0 ± 0.0	73.0 ± 10.2	27.0 ± 10.2

V_{rest}, resting membrane potential; R_m, membrane resistance; C_m, membrane capacitance; CDK_{IR}, current density of inwardly-**r**ectifying K^+ currents; CDK_{DR}, current density of voltage-gated delayed outwardly-rectifying K^+ currents; CDK_A, current density of the fast activating and inactivating outwardly-rectifying K^+ currents; CDNa, current density of Na^+ currents; n, number of measured cells; %, percentage of the cell type; *, $p < 0.05$; **, $p < 0.01$;***, $p < 0.001$. MCAo, middle cerebral artery occlusion.

GFP$^+$ cells in the dorsal part of the LV express two distinct electrophysiological phenotypes in situ

We also performed *in situ* patch-clamp recordings to determine the phenotype of GFP$^+$ cells in the dorsal part of the LV in control brains and those 4 days after MCAo. Similarly to *in vitro* study the GFP$^+$ cells were divided into two distinct electrophysiological phenotypes. The first group displayed passive current pattern (Figure 27A). Post-recording identification revealed the predominant expression of GFAP (Figure 27B-E), nestin or Olig2 in these cells. Their membrane properties were similar to those described previously in aNSCs in the SVZ (Liu et al., 2006; Lacar, 2010) and thus, they were classified as aNSCs. They were found in control brains as

well as in brains 4 days after MCAo. Their membrane properties are summarized in Table 7.

The second group displayed significantly different membrane properties when compared to cells with a passive current pattern; these cells expressed large amplitudes of K_{DR} currents (Figure 27F). Post-recording identification revealed the predominant expression of DCX in these GFP^+ cells (Figure 27G-J). Their membrane properties were similar to those described previously in neuroblasts in the SVZ (Lacar, 2010), thus they were classified as neuroblasts. Their membrane properties are summarized in Table 7.

Taken together, our patch-clamp analyses of GFP^+ cells *in situ* revealed that the mouse *Dach1* gene is active in a certain subpopulations of cells with electrophysiological properties similar to aNSCs or neuroblasts, and focal cerebral ischemia has an important impact on the membrane properties of these cells.

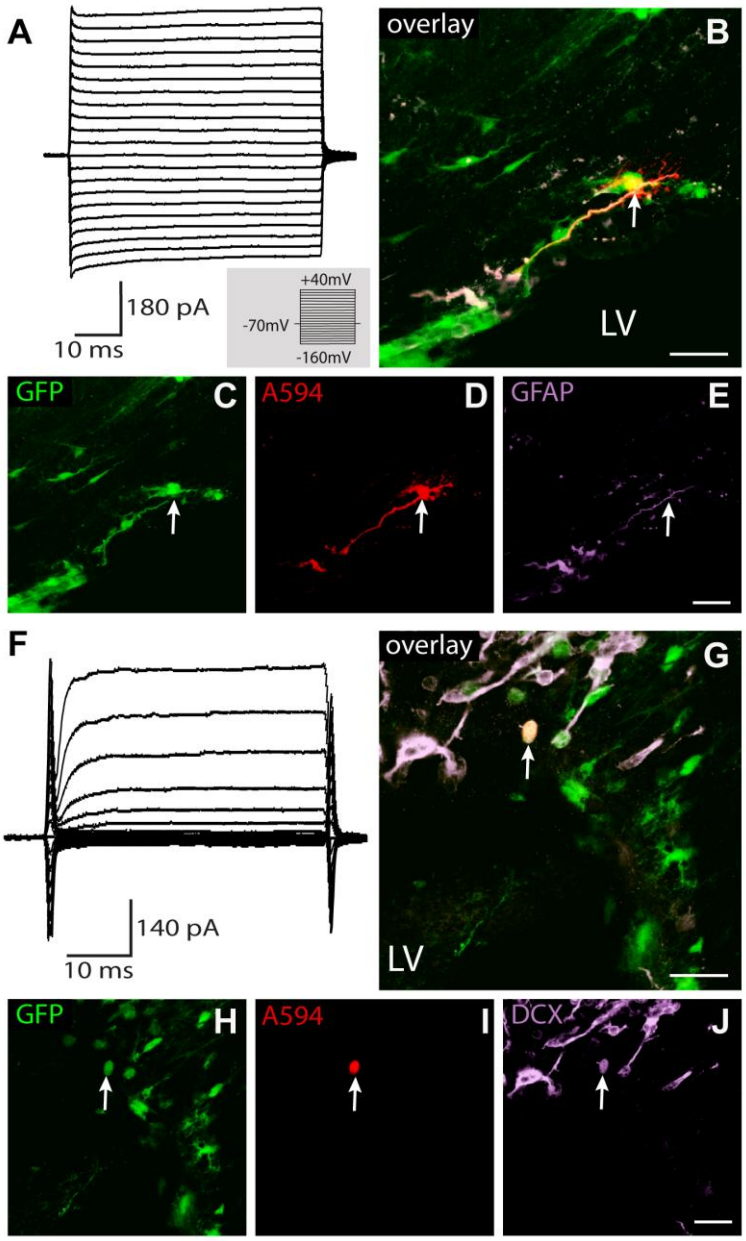

Figure 27. Green fluorescent protein (GFP)$^+$ cells *in situ* displayed two electrophysiologically and immunohistochemically distinct phenotypes. A, A portion of GFP$^+$ cells expressed a passive current pattern, i.e., time- and voltage-independent non-decaying K^+ currents. The current pattern was measured after depolarizing/hyperpolarizing the cell membrane from a holding potential of -70 mV, for the voltage protocol see the inset. Zero current is marked by the dashed line. **B-E,** GFP$^+$ cell with a passive current pattern (**C**), labeled with Alexa Fluor 594 hydrazide (A594) during patch-clamp measurement (**D**), subsequently stained with an antibody directed against glial fibrillary acidic protein (GFAP, **E**), a marker of astrocytes. An overlay image is shown in (**B**). **F**, Many GFP$^+$ cells expressed a neuronal current, i.e., outwardly rectifying K^+ currents (K_{DR}, K_A currents) together with higher Na^+ currents. The current pattern was measured with the same protocol as in (**A)**. Zero current is marked by the dashed line. **G-J,** GFP$^+$ cell with a neuronal current pattern (**H**), labeled with Alexa Fluor 594 hydrazide during patch-clamp measurement (**I**), subsequently stained with an antibody directed against doublecortin (DCX, **J**), a marker of neuronal precursors. An overlay image is shown in (**G**). Scale bars, 50 µm. LV, lateral ventricle.

Table 7. Electrophysiological properties of GFP$^+$ cells *in situ*

	Control		MCAo	
	passive	**neuronal**	**passive**	**neuronal**
V_{rest} (mV)	-56.2 ± 1.6	-39.0 ± 4.4	-50.2 ± 1.9 (*)	-46.6 ± 4.1
R_m (MOhms)	213.0 ± 21.7	3193.3 ± 407.6	320.4 ± 40.9 (*)	2690.1 ± 374.2
C_m (pF)	6.3 ± 1.0	3.8 ± 0.2	6.2 ± 1.5	4.2 ± 0.9
CDK_{IR} (pA/pF)	0.5 ± 0.5	0.4 ± 0.4	3.7 ± 2.2	0.5 ± 0.4
CDK_{DR} (pA/pF)	16.6 ± 3.6	49.2 ± 5.2	17.3 ± 4.6	38.9 ± 4.6
CDK_A (pA/pF)	0.0 ± 0.0	0.4 ± 0.4	0.0 ± 0.0	4.8 ± 2.2 (*****)
CDNa (pA/pF)	0.0 ± 0.0	5.2 ± 2.4	0.0 ± 0.0	1.5 ± 1.0
n	26	22	28	14
%	54.1 ± 9.9	45.9 ± 6.6	66.6 ± 6.9	33.3 ± 6.1

V_{rest}, resting membrane potential; R_m, membrane resistance; C_m, membrane capacitance; CDK_{IR}, current density of inwardly-rectifying K^+ currents; CDK_{DR}, current density of voltage-gated delayed outwardly-rectifying K^+ currents; CDK_A, current density of the fast activating and inactivating outwardly-rectifying K^+ currents; CDNa, current density of Na^+ currents; n, number of measured cells; %, percentage of the cell type; *, $p < 0.05$; **, $p < 0.01$;***, $p < 0.001$. MCAo, middle cerebral artery occlusion.

MCAo induces an increase in generation of GFP$^+$/DCX$^+$ neuroblasts in the dorsal part of the LV

To determine the influence of focal cerebral ischemia on adult neurogenesis in the dorsal part of the LV, the number of GFP$^+$/DCX$^+$ neuroblasts was estimated in control brains and brains 4 days after MCAo. In controls 9.4 ± 1.0% (n = 6 animals) of all GFP$^+$ cells in the dorsal part of the LV expressed DCX (Figure 28A, B).

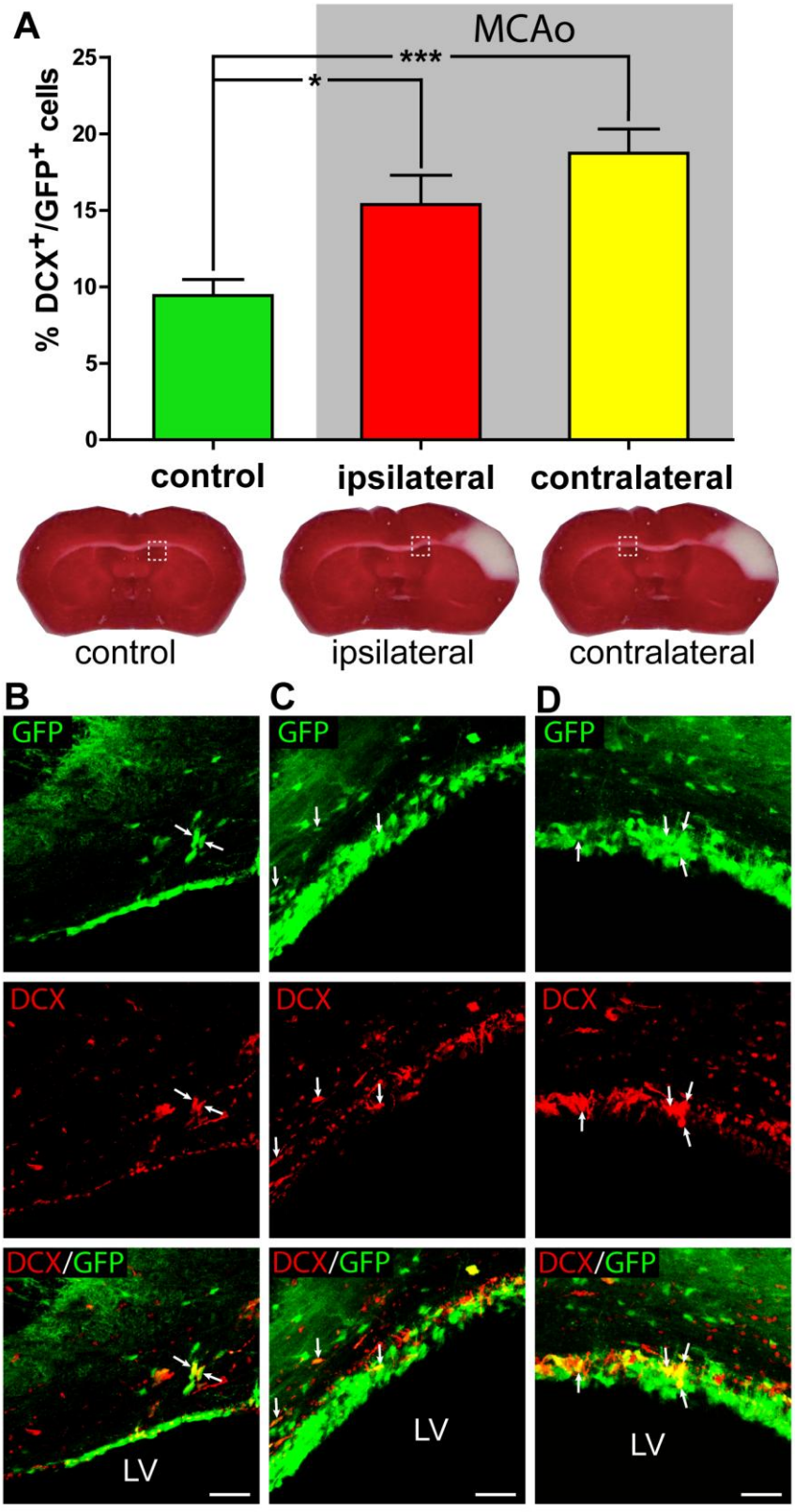

Figure 28. Increased percentage of green fluorescent protein (GFP)$^+$ neuroblasts in the dorsal part of the lateral ventricles (LV) 4 days after ischemia, A, Graph showing the percentage of doublecortin (DCX)$^+$ cells from all GFP$^+$ cells in the dorsal part of the LV. Asterisks indicate significant differences between uninjured (control; n = 7 animals) and post-ischemic (ipsilateral: n = 7 animals; contralateral: n = 7 animals) dorsal parts of the LV (tetrazolium chloride staining in the lower part of the image); *, $p < 0.05$; ***, $p < 0{,}001$. **B**, An image showing DCX$^+$ and GFP$^+$ cells in the dorsal part of the

LV in a control brain. Note the localization of GFP^+ cells only in a narrow region in the dorsal part of the LV. **C**, Image showing DCX^+ and GFP^+ cells in the dorsal part of the LV on the ipsilateral side of an ischemic brain. Note the increased number of GFP^+ cells in the dorsal part of the LV and the greater incidence of DCX^+ cells around the ipsilateral LV. **D**, Image showing DCX^+ and GFP^+ cells in the dorsal part of the LV on the contralateral side of an ischemic brain. Note the significantly increased number of GFP^+ cells in the dorsal part of the LV and the greater incidence of DCX^+ cells around the contralateral LV. Arrows indicate GFP^+/DCX^+ cells. Scale bars, 50 μm. MCAo, middle cerebral artery occlusion.

In the brains 4 days after MCAo the number of GFP^+/DCX^+ cells was estimated in the dorsal part of the ipsilateral as well as contralateral LV to reveal the impact of ischemic injury on neurogenesis in the dorsal part of the LV of both hemispheres. We found that MCAo resulted in an increased number of GFP^+ cells ipsilaterally (Figure 28C), and also the number of GFP^+/DCX^+ cells significantly increased to 15.4 ± 1.9% of all GFP^+ cells ($p<0.05$, n = 6 animals, Figure 28A, C) when compared to control brains. Moreover, the number of GFP^+/DCX^+ in the dorsal part of the contralateral LV was also significantly increased and reached 18.7 ± 1.6% ($p<0.001$, n = 6 animals, Figure 28A, D) when compared to control brains.

These results indicate that GFP^+ cells with an active *mouse Dach1* gene in the dorsal part of the LV play an important role in the increased production of neuroblasts after injury and that this process is also enhanced in the contralateral hemisphere.

GFP^+ cells in other brain regions

Additionally, the localization and properties of GFP^+ cells were analyzed in other brain regions with respect to SVZ neurogenesis and GFP^+ cell migration. The first region, in which GFP^+ cells were found, was the RMS. As shown in a sagital section from adult D6/GFP mouse (Figure 29 B-E), the GFP^+ cells were detected within and around the stream of migrating neuroblasts and based on the expression of GFAP in their processes, these GFP^+ cells probably participate in the formation of the glial tunnel. The RMS navigates neuroblasts into the OB, where they differentiate into olfactory neurons and interneurons (Singer et al., 2009). Therefore, the coronal sections of OB were analyzed and GFP^+ cells were found scattered in the granular cell layer (GCL), (15711 ± 3243 GFP^+cell / mm^3, n = 6 animals) and glomerular layer (GL), (13261 ± 3433 GFP^+cell / mm^3, n = 6 animals). These cells had large round cell

bodies and mostly one long process; immunohistochemistry revealed the expression of a marker of mature neurons – NeuN (Figure 29F-I). Detailed immunohistochemical analyses revealed the expression of the inter-neuronal marker calretinin in GFP^+ cells in the GL and GCL (Figure 29O-R), and some GFP^+ cells in the GL also expressed tyrosine hydroxylase (TH), (Figure 29S-V).

Furthermore, we also analyzed the distribution and phenotype of GFP^+ cells in the RMS and the OB after MCAo. As mentioned before, the number of GFP^+/DCX^+ cells was significantly increased in the dorsal part of the LV 4 days after MCAo, while 1 week after MCAo GFP^+/DCX^+ cells were also present inside the RMS between the migrating neuroblasts (Figure 29B-E). Additional experiments were performed to reveal whether GFP^+/DCX^+ cells leave the RMS and migrate into the site of the ischemic lesion. However, there were no GFP^+ cells around the cortical ischemic lesion expressing DCX or other neuronal markers at any studied point after MCAo. On the other hand, 4 weeks after MCAo a significantly increased number of GFP^+ neurons in the ipsilateral GCL (35637 ± 6801 GFP^+ cell/mm^3, n = 8 animals, $p < 0.05$) as well as in the ipsilateral GL (26486 ± 2827) GFP^+ cell/mm^3, n = 8 animals, $p < 0.05$) was found; (Figure 29J-N) when compared to controls.

In summary, ischemic injury significantly increases number of GFP^+ neurons in OB probably due to enhanced adult neurogenesis following ischemia and these newly derived neurons in OB express calretinin and TH. On the other hand, there were no signs of GFP^+ cells contributing to tissue repair at the site of the ischemic lesion.

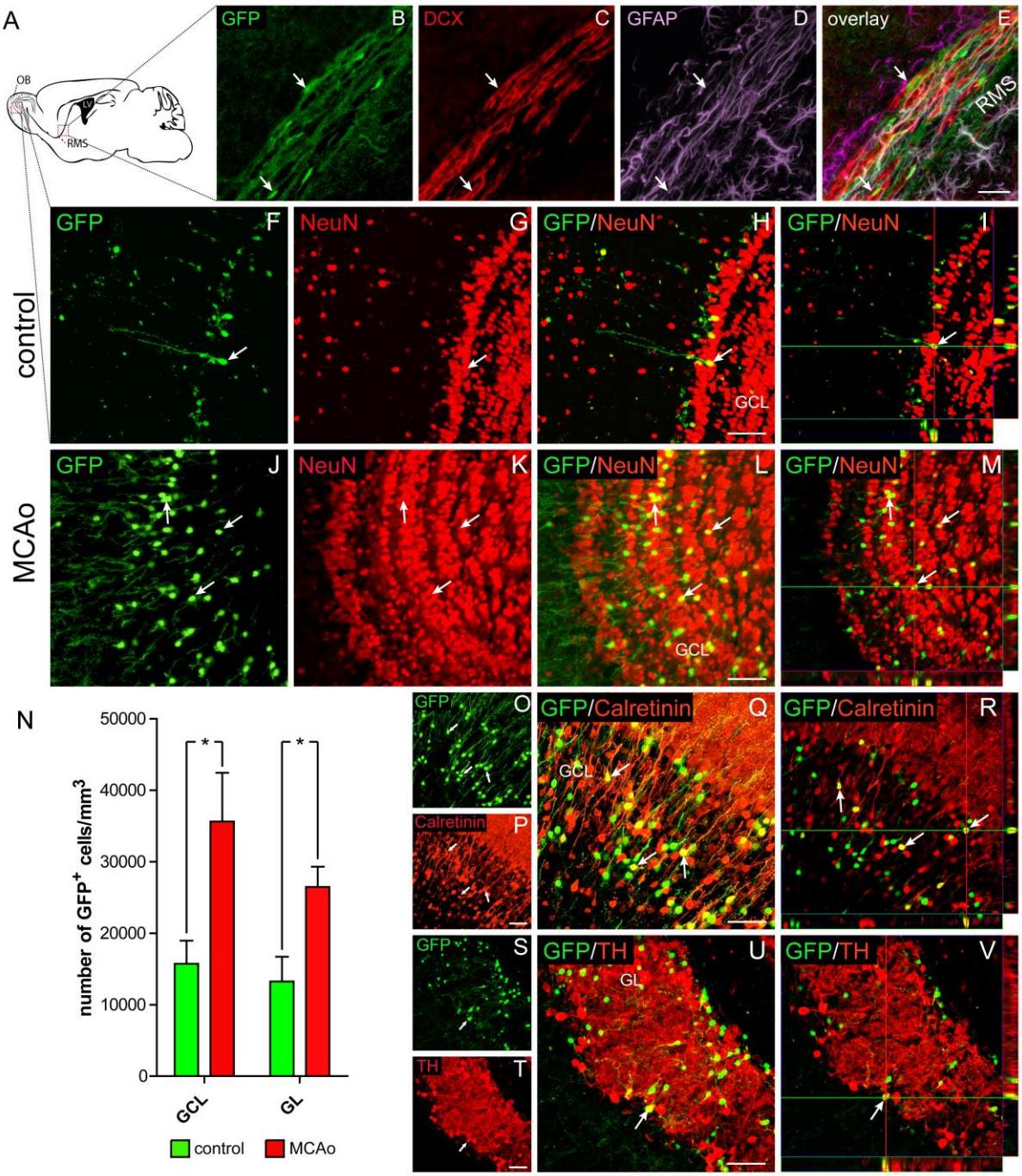

Figure 29. Green fluorescent protein (GFP)$^+$ cells from the dorsal part of the lateral ventricles (LV) give rise to olfactory bulb interneurons. A, Schematic figure of a sagittal section through an adult mouse brain indicating the regions (red squares), where the number of GFP$^+$ cells and their phenotype was analyzed. **B-E**, A detailed image of the rostral migratory stream (RMS) after MCAo showing GFP$^+$/DCX$^+$ cells in the RMS, which is delimited by GFAP$^+$ fibers. The white arrows highlight several GFP$^+$/DCX$^+$ cells. **F-I**, Several GFP$^+$ cells were scattered in the granular cell layer (GCL) and expressed a marker of adult neurons (NeuN, **G**). A orthogonal image confirmed the expression of neuronal nuclei (NeuN) in GFP$^+$cells (**I**). **J-M**, The number of GFP$^+$/NeuN$^+$ cells was increased in the olfactory bulb (OB) 4 weeks after MCAo. **N**, Graph showing the number of GFP$^+$ cells in the GCL and granular layer (GL) before and 4 weeks after MCAo. **O-R**, Images demonstrating the expression of calretinin in the GFP$^+$ cells in the GCL. **S-V**, Images depicting the expression of tyrosine hydroxylase (TH) in the GFP$^+$ cells in the GL. Scale bars, 50 µm. MCAo, middle cerebral artery occlusion.

DISCUSSION

Polydendrocytes are bipotent cells in the healthy adult brain

A number of recent studies have shown the importance of selecting an appropriate polydendrocytic marker as a Cre-recombinase promoter. In our study we used NG2, as a generally accepted marker of polydendrocytes and, moreover, this proteoglycan is not down-regulated after injury as in the case of PDGFαR (Hampton et al., 2004). Although NG2 and PDGFαR are strongly co-expressed in cells in the uninjured brain, more distinct polydendrocytic subpopulations can arise following ischemia.

We used the NG2creBAC mice strain with constitutive Cre-expression and a high recombination rate, in which a large polydendrocyte population and their progeny express EGFP. This approach enabled us to analyze a larger sample of $EGFP^+$ cells before and after ischemia than in mice with an inducible form of Cre-recombinase with low recombination efficiency. Although inducible Cre-recombinase brings the advantage of labeling a cohort of cells with a currently expressed marker, our analysis proved that in the uninjured adult cortex we have a well characterized cell population clearly restricted to only polydendrocytes, oligodendrocytes and pericytes. Polydendrocytes expressing NG2 and EGFP displayed immunocytochemical and electrophysiological properties that suggested the absence of any additional subpopulations of $EGFP^+$ cells expressing NG2 in the adult cortex. This finding is in agreement with study (Zhu et al., 2008), where a uniform population of polydendrocytes was detected in the adult hippocampus.

Polydendrocytes respond to ischemia by increased proliferation

After ischemia we detected a significantly increased number of $EGFP^+$ cells on the lesion edge at all studied time points, a phenomenon already described after stab wound (Dimou et al., 2008; Komitova et al., 2011) cryo-injury model (Tatsumi et al., 2008), experimental autoimmune encephalomyelitis (Tripathi et al., 2010), focal

demyelination (Zawadzka et al., 2010) or following global cerebral ischemia (Pivonkova et al., 2010). In our model of FCI the number of Ki-67$^+$/EGFP$^+$ cells or PCNA$^+$/EGFP$^+$ cells almost tripled and such extensive proliferation of polydendrocytes in early stages after injury led us to assumption that such increase in number of EGFP$^+$ cells is caused by the generation of new EGFP$^+$ cells from existing polydendrocytes. However, we cannot entirely exclude polydendrocyte migration from the surrounding tissue to the site of injury. Another eventuality is that other cell types began to transiently express NG2, as was shown, for example, in the case of microglia cells. Although several recent studies reported the low expression of NG2 in resting microglia, we never detected EGFP in these CD11b$^+$/Iba-1$^+$ cells in the control brain (Wohl et al., 2011). Moreover, the transiently increased expression of NG2 has been shown in activated microglia cells after several types of injury; on the other hand other studies exclude the possibility of NG2 expression in these cells (Bulloch et al., 2008; Karram et al., 2008). In our study we never detected EGFP$^+$ cells that displayed any microglial immunohistochemical or electrophysiological properties at any studied time point after MCAo. This indicates that microglia cells in our model of FCI do not activate NG2 promoter or that a weak or only a short, transient activation of the CSPG4 promotor in the adult brain is not sufficient to trigger the expression of EGFP in other cells types, thus confirming that newly-derived EGFP$^+$ cells originate from pre-ischemic EGFP$^+$ cells.

Immunohistochemical analysis showed an increased amount of NG2 at the lesion site in the later phases after ischemia, which accords well with previously published results (Tripathi et al., 2010); however, the total number of EGFP$^+$ cells with detectable NG2 expression decreased. This phenomenon can be explained by the increased release of soluble NG2 form from many cell types into the extracellular space (Tripathi et al., 2010) and, concurrently, by differentiating of NG2$^+$ polydendrocytes into another cell type.

Genetic fate mapping enabled us to determine the functional properties of polydendrocytes even in the later phases after ischemia, when it is extremely difficult to perform patch-clamp measurements of newly-derived cells in the gliotic scar full of reactive astrocytes and microglia. We found that polydendrocytes responded to ischemia with marked changes in their electrophysiological properties, especially in the early phases after ischemia, which has been already shown previously (Pivonkova et al., 2010). However, in the late phases after ischemia their membrane

properties were comparable to those of controls, indicating the rapid recovery of polydendrocytic electrophysiological properties to the pre-ischemic state.

Polydendrocytes display multipotent differentiation potential after ischemia

Our immunohistochemical analyses of post-ischemic cortex revealed that large population of $EGFP^+$ cells (~75%) does not express NG2 14 days after MCAo and additional electrophysiological analyses disclosed that majority of $EGFP^+$ cells (~80%) displays a current pattern distinct from that observed in polydendrocytes. The expression of GFAP, GLAST or vimentin together with a passive current pattern and dye-coupling in a large subpopulation of $EGFP^+$ cells represent strong evidence that polydendrocytes can give rise to reactive astrocytes after ischemia. The generation of a reactive astrocyte subpopulation from polydendrocytes was already shown in models of cryoinjury (Tatsumi et al., 2008), stab wound (Dimou et al., 2008; Komitova et al., 2011), experimental autoimmune encephalomyelitis (Tripathi et al., 2010) or focal demyelination (Zawadzka et al., 2010). However, in the majority of these injuries the generation of new astrocytes was limited and represented ~8% of $EGFP^+$ cells (Komitova et al., 2011), and their number declined in the later phases after injury. In our study we detected ~17% of $EGFP^+$ cells with an astrocytic phenotype 7 days after ischemia, and their number only slightly decreased in the later phases following ischemia. Such discrepancy is probably caused by using different injury models. In contrast to the majority of studies, which employed rather mild types of cortical injuries or models of demyelination in the spinal cord, we used a model of severe ischemic brain injury, in which the stronger involvement of repair processes and higher levels of growth factors might play an important role, resulting in greater differentiation of polydendrocytes into astrocytes. Moreover, we analyzed in detail the electrophysiological properties of newly-derived astrocytes. These cells displayed a passive current profile with 4-AP sensitive K_{DR} currents, of which amplitude decreased towards the later phases after ischemia. Our results are in good agreement with previously published electrophysiological analyses of reactive astrocytes after ischemia in the hippocampus (Pivonkova et al., 2010) and following

cortical stab wound (Anderova et al., 2004), and show that these newly-derived astrocytes are comparable with reactive astrocyte populations in the later phases after ischemia.

Importantly, we also identified cells of polydendrocyte origin that displayed the immunohistochemical and electrophysiological properties of neuronal precursor cells and comprised ~ 9% of $EGFP^+$ cells 7 days after ischemia. Although recent studies described DCX expression and the differentiation of $PDGF\alpha R^+$ or PLP^+ cells into neurons in the healthy adult brain, this phenomenon was always strictly localized only in the piriform cortex (Rivers et al., 2008; Guo et al., 2010). Nevertheless, in our study we did not detect any $EGFP^{+/}DCX^+$ cells in any brain regions including the SVZ of sham-operated mice. After ischemia, some $EGFP^+/DCX^+$ cells displayed Na^+ currents with a significantly higher CD and markedly different kinetics when compared to polydendrocytes, which is together with high membrane resistance, a typical feature of neuroblasts (Lacar, 2010). Since it is relatively easy to force polydendrocytes *in vitro* to differentiate into neurons (Belachew, 2003; Aguirre, 2004), a suitable mixture of growth factors and morphogens released at the lesion site may also promote this phenomenon *in vivo*. However, detailed analysis of $EGFP^+$ cells in the later phases after ischemia revealed that $EGFP^+/DCX^+$ cells detected at early post-ischemic stages were probably incapable of surviving and maturing into cells with a more developed neuronal phenotype. This assumption is based on observation of strong expression of caspases-3 in several $EGFP^+/DCX^+$ cells and their inability to survive in damaged ischemic region was also described previously in newly-derived SVZ neuroblasts migrating into the site of injury after stroke (Carlén et al., 2009). We described the generation of neuronal precursor cells in mature, but still very young mice; however, we presume that multipotency and ability to differentiate into different cell types is strongly age-dependent. Many studies describing multipotency of polydendrocytes were done on postnatal or very young animals (Kondo and Raff, 2000; Belachew, 2003), thus the ability to produce cells of neuronal lineage could be strongly suppressed in older mice. The same scenario probably applies to ability of polydendrocytes to give rise to astrocytes in the healthy brain. As was shown recently polydendrocytes in embryonic brain differentiate into astrocytes, but this capability is not maintained into adulthood (Zhu et al., 2011).

In our study we also detected $EGFP^+$ oligodendrocytes before and after ischemia; however, in comparison to the large number of other newly-derived cell

types, newly generated oligodendrocytes did not comprise the major cell population that originated from polydendrocytes after ischemia. The low number of $EGFP^+$ oligodendrocytes in the gray matter of the healthy brain is in agreement with previous studies describing the generation of oligodendrocytes predominantly in the white matter (Rivers et al., 2008; Kang et al., 2010). Nonetheless, we also detected a low number of oligodendrocytes after ischemia, which accords well with recent findings (Anderova et al., 2010), but contrasting to other recently published studies (Rivers et al., 2008; Komitova et al., 2011). Importantly, we employed a more severe model of injury, in which high levels of glutamate are released and this might be an adverse environment for oligodendrocyte survival, which are strongly susceptible to excitotoxic death (Matute et al., 2007).

The last type of $EGFP^+$/ $NG2^+$ cells found in uninjured and ischemic brains are quite often overlooked pericytes. Since these cells express both NG2 and PDGFαR (Goritz et al., 2011), they are probably involved in every fate mapping study that uses these proteins as markers of polydendrocytes. In our study pericytes were identified based on PDGFβR expression and the absence of any voltage activated currents; their number almost doubled 14 days after ischemia when compared to control. Although we did not performed a detailed immunohistochemical analysis there was evident increase in the number of $EGFP^+$ cells with pericytic morphology, which lined vessels in the vicinity of the ischemic lesion. Nevertheless, a recent study described a massive proliferation of pericytes and their participation in scar formation after spinal cord injury (Goritz et al., 2011). We did not detect any $EGFP^+$ pericytes inside ischemic core, which could be caused by employing different model of injury in a different CNS region. Moreover, there are probably several types of pericytes and $NG2^+$ pericytes labeled in our study might have different role after injury. Recently published data described wide differentiation potential of pericytes *in vitro*, so we cannot exclude their contribution to the generation of different cell phenotypes after ischemia (Montiel-Eulefi et al., 2011).

It is probable that polydendrocytes close to the ischemic region are exposed to a variety of factors and signals as a result of tissue homeostasis disruption and the lost of the blood–brain barrier integrity. Which components present in the serum, or which signals released from neural and non-neural elements are responsible for their increased proliferation and/or fate decision, remains to be determined. Nevertheless, these factors are likely to activate the Notch-1 pathway, as suggested by its up-

regulation in reactive glial cells after injury (Wang et al., 1998; Yamamoto et al., 2001; Grandbarbe, 2003). A similar up-regulation was described for bone morphogenetic factor in the post-injury niche, and this factor was shown to drive the differentiation of polydendrocytes into astrocytes, while simultaneously its antagonist Noggin reverses this process (Sellers et al., 2009). A very important role in controlling the proliferation and differentiation of polydendrocytes is also played by the β-catenin signaling pathway, which is strongly activated after cortical injury (White et al., 2010). It seems that information about massive ischemic injury is delivered to polydendrocytes in a large part of the CNS; however, only the directly exposed subpopulation of polydendrocytes responds to this pathology not only by proliferation, but also by differentiation into another cell type.

Gene expression in post-ischemic astrocytes

After CNS injury, such as trauma or ischemia, or in neurodegenerative disorders, the glial cells become reactive changing their morphology as well as functional properties (Pekny and Nilsson, 2005; Zamanian et al., 2012). This is in line with our finding that the gene expression profile of astrocytes alters following focal ischemia. Particularly affected is the expression of *Gfap, Gfapd, S100b and Vim*, which is in agreement with previous findings (Robel et al., 2011; Zamanian et al., 2012). Fourteen days after ischemia, *Aqp1* and *Aqp9* were up-regulated as described earlier (Hwang et al., 2007; Zelenina, 2010), and similarly to previous reports, we found up-regulated *Grm5* (Ulas et al., 2000; Ferraguti et al., 2001). Generally, *Aqp1* and/or *Aqp9* are elevated in hypertrophied, GFAP over-expressing astrocytes in a number of pathological states, such as ischemic or traumatic brain injury, Alzheimer's or Creutzfeldt-Jakob diseases (Rodríguez et al., 2006; Mccoy and Sontheimer, 2010; Hoshi et al., 2012). In the present study, we detected their increased expression only in the B3 subpopulation, which comprises mostly $EGFP^+$ cells 14 days after MCAo. Such a delayed increase in *Aqp1* and *Aqp9* expression suggests that they are probably not implicated in water movements during edema formation, but they might play a role as metabolite channels facilitating the diffusion of glycerol and lactate, as suggested previously (Badaut and Regli, 2004; Badaut et al., 2004). Moreover, the ischemic

brain undergoes marked remodeling, which involves the migration of neighboring cells to the injury site, thus the increased *Aqp1* expression may reflect a migratory phenotype of reactive astrocytes as AQP1 was shown to promote cell migration in epithelial cells (Hara-Chikuma, 2005) and glial tumors (Mccoy and Sontheimer, 2007; Papadopoulos and Verkman, 2008). The B2 and B3 subpopulations also highly express AMPA receptor subunits, especially *Gria3*, which suggests that AMPA receptors may significantly contribute to Na^+/Ca^{2+} influx into the reactive astrocytes, and together with the strong expression of metabotropic glutamate receptors (*Grm1, Grm5*) they might mediate Ca^{2+} oscillations and glutamate release as suggested previously (Bezzi et al., 1998). Furthermore, an increase in *Grm5* expression in reactive astrocytes might lead to the increased activity of mGluR5 and thus contribute to astrocytic apoptosis, as described recently (Paquet et al., 2013). On the other hand, an anti-apoptotic effect mediated by mGluR3 activation that leads to reduced intracellular levels of cAMP was described in cultured astrocytes after their exposure to nitric oxide (Durand et al., 2011). In addition, Aguado and colleagues (Aguado et al., 2002) demonstrated that the activation of ionotropic glutamate receptors is required for the generation of correlated astrocytic network activity essential for neuronal development and synaptic plasticity. In mature astrocytes under physiological conditions (P50), the Ca^{2+} permeability of AMPA receptors is diminished compared to immature stages due to the predominant expression of *Gria2*. Interestingly, mRNAs encoding kainate receptor subunits (*Grik1,2,3,5*) are also significantly increased in the B2 and B3 subpopulations; however, their function in reactive astrocytes and those from immature animals has not yet been elucidated.

Marked changes were also observed in the expression of different types of ion channels, such as outwardly and inwardly rectifying K^+ channels and chloride channels (ClCN2), and moreover, *Trpv4* expression almost doubled after ischemia, when comparing the B2 and B3 subpopulations to B1. The expression of *Kcna3-5*, encoding the outwardly rectifying K^+ channels Kv1.3, Kv1.4 and Kv1.5, markedly increased in the post-ischemic B2 and B3 subpopulations. Such an increase might point to the fact that astrocytes enter the cell cycle and proliferate following ischemic injury, as shown previously (Anderova et al., 2004; 2010). In addition, an increase in *Clcn2* expression could suggest the participation of astrocytes in delivering Cl^- to the site of intensive GABAergic transmission (Sík et al., 2000), or Cl^- efflux can play a role in astrocyte proliferation/migration as suggested for gliomas (Ransom et al.,

2002). Furthermore, enhanced *Trpv4* expression following MCAo was detected in both the B2 and B3 subpopulations, which is in agreement with our recent data demonstrating an increased expression/function of TRPV4 following hypoxic/ischemic injury of the rat hippocampus (Butenko et al., 2012). TRPV4 up-regulation might originate from its role as an osmosensor as shown in astrocytes (Benfenati et al., 2007) or from a possible role of this channel in Ca^{2+} signaling in post-ischemic astrocytes, which may lead to enhanced glutamate release via Ca^{2+}-dependent exocytosis (Malarkey et al., 2008) or even result in astrocytic cell death (Pamenter et al., 2012). A transient increase in *Nes* observed in cells 3 and 7 days after MCAo might support the hypothesis that these subpopulations comprise proliferative/newly derived cells. A striking finding is the high expression of Hcn1-4, which encodes hyperpolarization–activated non-specific cationic channels permeable for K^+/Na^+, so far described only in neurons. Despite the fact that their role in astrocytes is unknown, we hypothesize that they might have a role in determining the astrocyte resting membrane potential or they might interact with the glutamate release machinery as described recently for presynaptic terminals (Neitz et al., 2011). A question that still remains incompletely elucidated is the origin of reactive glia. Certain subpopulations of reactive astrocytes have been shown to arise from polydendrocytes (Zhao et al., 2009) or from proliferating astrocytes (Komitova et al., 2011). Based on our findings, we propose that the B2 subpopulation, which is characterized by an increase in the expression of several astrocytic markers including *Gfap, S100b, Gfapd* and *Vim*, but also by a marked increase in *Nes, Pdgfra* and *Cspg4*, represents astrocytes in an ‘‘intermediate stage’’ that increase in number as astrogliosis develops. We hypothesize that polydendrocytes give rise to the B2 subpopulation, which develops into fully reactive astrocytes with a distinct expression profile as in subpopulation B3. Using partial Spearman correlation calculations, we did not identify any master gene in B3 that would account for all of the changes observed upon astrocyte reactivity that follows ischemic injury; however, it is clear that *Gria3* and *Hcn2* are of high importance. In subpopulation B3 we identified several, previously not recognized highly expressed genes: *Hcn1-3, Grin2a*, *Gria2*, *Gria3*, *Grm5* and *Kcna3*. We also found the high expression of *Snap25*, which is expressed only minimally in the other subpopulations and has been suggested to be a marker of cells with exocytotic capabilities under physiological conditions (Cahoy et al., 2008). Similar observations were made in rats (Patanow et al., 1997), where

SNAP25 was found upregulated 3 and 12 days after injury. Despite the fact that synaptosomal-associated protein SNAP-25 has not been detected in astrocytes but SNAP-23 (Hepp et al., 1999), our data revealed mRNA levels coding SNAP-25 were significantly increased in cortical astrocytes 14 days post-ischemia (B3 subpopulation). As astrocytes are known to release glutamate and aspartate in response to elevated intracellular calcium levels via a vesicular release mechanism, in which SNARE proteins are implicated, high levels of *Snap25* might be a sign of a significant glutamate release from reactive astrocytes. We found a positive correlation between the expressions of *Snap25*, *Slc1a3* and *Glul* and the absence of any correlation with *Cspg4* and *Pdgfa* in B3. We also found a strong correlation between *Slc1a3* and *Aqp4* expression, which is in accordance with a recent report suggesting the close relation of excitatory amino acid transporters (EAATs) and AQP4 under pathological conditions with the massive release of glutamate (Zelenina, 2010). Although an association between AQP4 and mGluR5 has been reported (Illarionova et al., 2010), we found no correlation on the gene expression level. On the other hand, we found an extremely strong correlation between *Aqp1*/*Aqp9* and *Grm5* levels in B3 subpopulation.

Heterogeneity of reactive astrocytes in the vicinity of an ischemic lesion has been described previously (Bordey et al., 2001; Anderova et al., 2004). Even within the B3 subpopulation of reactive astroglia, we found evidence for two subgroups using SOM and PCA: B3A and B3B. B3A is positive for traditional astrocytic markers, while B3B has a substantially higher expression of polydendrocytic markers (Figure 8). Even though the entire B3 population has high overall transcriptional activity, much higher than B1 and B2, there is a difference in the expression levels of many genes between the B3A and B3B subgroups. Since we isolated cells from the vicinity of an ischemic lesion, it is possible that B3 comprises cells permanently converted to reactive glia, which are in different states or at different distances from the site of the ischemic lesion.

Adult neurogenesis takes place in dorsal part of the LV

The presence of multipotent Dach1-expressing cells was described previously in the embryonic and early postnatal mouse brain using *in vitro* differentiation (Machon et al., 2002). In our study we turned the attention to adult mouse brains, where *Dach1* expression is localized predominantly in the cortex and the hippocampal CA1 region in differentiated cells (pyramidal neurons and astrocytes), (; however, we also found a narrow region in the dorsal part of the LV, where Dach1-expressing cells showed the properties of aNSCs. Interestingly, these cells displayed an unipotent differentiation potential *in vitro* when isolated from healthy control brains; nevertheless, they revealed an expanded differentiation potential when isolated 4 days after focal cerebral ischemia. In contrast, ischemic injury did not change the differentiation potential of Dach1-expressing cells *in vivo*, which is in agreement with previous findings of Liu and co-authors (Liu et al., 2006; 2009). The discrepancy between the *in vivo* and *in vitro* results may be explained by the different responses of isolated cells to MCAo, due to differences in mRNA expression between cells *in vivo* and *in vitro* following injury. Electrophysiological analysis performed *in vitro* revealed that passive cells originating from ischemic brains expressed significantly altered membrane properties when compared to those from controls. Their membrane potential was significantly depolarized, their membrane resistance was increased and additionally, their membrane capacitance was significantly lower when compared to passive cells isolated from control brains. Such changes in membrane properties are in agreement with previously published results that demonstrated increasing membrane resistance with the progression of *in vitro* differentiation (Jelitai et al., 2007); furthermore, the same study described a decreasing number of gap-junction coupled cells with the progression of *in vitro* differentiation, which clarifies our finding of decreased membrane capacitance. Taken together, based on electrophysiological data, Dach1-expressing cells isolated from ischemic brains exhibit faster and more pronounced *in vitro* differentiation when compared to those isolated from controls.

On the basis of the electrophysiological data and post-recording identification, we can classify the GFP^+ cells in the dorsal part of the LV as aNSCs and neuroblasts. One subpopulation of GFP^+ cells displayed large membrane resistance

reaching several gigaohms, a depolarized membrane potential and small membrane capacitance. These membrane properties together with the presence of outwardly rectifying K^+ currents clearly categorize these cells as neuroblasts (Wang, 2003; Bolteus, 2004; Lacar, 2010). Following ischemic injury their membrane properties were not changed; however, the current densities of the K_A currents were significantly increased. Since the increased activity of outwardly rectifying currents is linked to increased cell proliferation, the enhancement of the K_A currents could be related to this process (Knutson et al., 1997). The second GFP^+ cell subpopulation expressed low membrane resistance; a more hyperpolarized membrane potential and higher cell capacitance. Such membrane properties together with the presence of time- and voltage-independent non-decaying K^+ currents classified these cells as aNSCs (Liu et al., 2006; Lacar, 2010). In response to ischemic injury, GFP^+ aNSCs expressed a significantly depolarized membrane potential and increased membrane resistance. It was previously shown that such changes in membrane properties accompany increased cell proliferation, and therefore, we may conclude that ischemia leads to the enhanced proliferation of GFP^+ aNSCs (Sundelacruz et al., 2009).

Interesting results were obtained by quantifying GFP^+/DCX^+ cell numbers in the dorsal part of the LV in the ipsilateral and contralateral hemispheres. Several previous studies showed that after injury the number of DCX^+ cells is predominantly increased in the SVZ of the ipsilateral hemisphere (Taupin, 2005; Thored et al., 2006; Yamashita, 2006; Liu et al., 2009). However, in our study we also detected an increased number of GFP^+/DCX^+ cells in the dorsal part of the LV in the contralateral hemisphere. These bilateral changes after injury were described previously in the hippocampus (Takasawa et al., 2002), in the cortex (Krüger et al., 2006) and also in the SVZ (Masuda et al., 2007; Li et al., 2010). Here we report that Dach1-expressing cells in the dorsal part of the LV also respond bilaterally to MCAo. Although the exact mechanism underlying this reaction was not clarified, three possibilities were suggested by Masuda and co-authors (Masuda et al., 2007): factors from the lesion site might diffuse and affect a wide area of the brain; commissural fibers and the release of neurotransmitters might participate in this reaction (Platel et al., 2008); and hormonal (Li et al., 2010) or growth factors from other brain regions (Kokaia et al., 1998) as well as cytokines from the immune system might be involved (Ma et al., 2007).

Since the SVZ comprises a heterogeneous collection of NSCs that originate in different parts of the embryonic brain and generate different neuronal progeny, we examined the migration and differentiation of GFP^+ cells in the RMS and OB. Previously, the transcriptional factor Emx-1 was shown to control proliferation, migration and differentiation of embryonic cortical progenitors, and these cells later comprise a population of aNSCs in the dorsolateral wall of the LV (Young et al., 2007). Based on previous reports, the D6/GFP^+ cells in the dorsal part of the LV also originate in the embryonic cortex therefore; the *Dach1* gene might perform a very similar function to Emx-1. GFP^+ cells were found around the RMS as well as in the GCL and GL in the OB. We did not find any differences in the distribution of GFP^+ cells between the GL and GCL as was previously shown for Emx-1-expressing cells (Young et al., 2007). Moreover, the majority of these GFP^+ cells were $NeuN^+$, indicating their neuronal phenotype. Therefore, we used a number of neuronal markers (calretinin, calbindin, TH, parvalbumin) to identify their phenotype. We did not find GFP^+ cells expressing parvalbumin or calbindin in any layer of the OB, which correlates well with previously published results showing that parvalbumin-positive neurons are not generated from aNSCs in adulthood and that calbindin-positive neurons are generated only from aNSCs originating in the lateral wall in the LV and not from aNSCs of cortical origin (Young et al., 2007). Nevertheless, a large population of GFP^+ cells expressed calretinin in the GL as well as in the GCL, which is in agreement with data showing that cortical-derived Emx-1 aNSCs also generate the majority of calretinin-positive neurons (Willaime-Morawek et al., 2006; Young et al., 2007). In addition, several GFP^+ cells expressing TH were found in the GL. The fact that we failed to find any calbindin-positive neurons in the OB confirmed an earlier theory that aNSCs remain functionally distinct throughout life, generating different subsets of olfactory neurons (Lledo et al., 2008). We conclude that GFP^+ neurons in the OB are generated in the SVZ and migrate through the RMS to their final location; however, we cannot exclude the possibility that some GFP^+ cells might also originate in the neurogenic zone in the RMS or directly in the OB. An important finding is that Dach1-expressing cells of cortical origin have the ability to contribute to the process of adult neurogenesis, which is in agreement with several studies (Spadafora et al., 2010). Nevertheless, our findings are in contrast to previous data suggesting only a striatal origin of the aNSCs in the lateral wall of the LV (Wei et al., 2011).

Additionally, we used a model of focal cerebral ischemia to elicit the involvement of Dach1-expressing cells from the dorsal part of the LV in brain regeneration after ischemia. In agreement with several previous studies we did not detect GFP^+ cells participating in glial scar formation or the production of new neurons in the cortex in or around the site of ischemic injury at any analyzed time point after injury (4, 28 or 60 days (Spadafora et al., 2010). On the other hand, some recent reports have described the potential of very similar Emx1-expressing aNSCs to produce new neurons after striatal ischemic injury in neonatal rats (Wei et al., 2011). These contradictory results document the great variability in the responses of SVZ cells to injury, which could depend on the type or severity of injury, the age of the animals or the species used. Immunohistochemical analyses in the OB revealed a significantly higher number of GFP^+ neuronal cells in the GCL as well as in the GL 28 days after ischemia, which is in perfect correlation with the majority of recent studies describing increased SVZ neurogenesis and consequently increased number of newly-derived neurons in the OB in response to ischemic injury (Koketsu et al., 2006; Ohira, 2010; Yoneyama et al., 2010). On the other hand, these data are in contrast to some recently published results showing a negative influence of ischemia on the number of newly-derived cells and their increased apoptotic rate (Spadafora et al., 2010). The use of a slightly different model of MCAo performed in neonatal animals, i.e. during the time period when the formation of the SVZ is still an ongoing process, could explain this discrepancy.

Taken together, our data suggest that the *Dach1* gene does not play an important role only during embryonic or postnatal neural development, but it also acts as an important factor in determining the phenotype of aNSCs and progenitors localized in the dorsal part of the LV in the mature brain. After ischemia, the expansion of SVZ neurogenesis significantly increased the proliferation of Dach-1-expressing cells in the dorsal part of the SVZ; however, this did not change their differentiation or the target of their migration, indicating their low therapeutic potential after cortical injury. In conclusion, Dach1-expressing cells possess the ability to contribute to the process of adult neurogenesis and could therefore be used for genetic labeling of the aNSC subpopulation, genetic fate mapping studies or the manipulation of adult neurogenesis.

CONCLUSIONS

1) To determine the differentiation potential of polydendrocytes in the gliotic scar around the focal ischemic injury in the primary somatosensory cortex – focus on their neurogenic or gliogenic potential.

We used transgenic mice in which the polydendrocytes are EGFP-positive and their fluorescent labeling persists even when they change their phenotype. In accordance with previous studies (Rivers et al., 2008), we detected the generation of oligodendrocytes in the uninjured adult brain; however, in contradiction to some earlier reports (Zhu et al., 2007; 2008) our study did not confirm the generation of astrocytes. Therefore, we conclude that polydendrocytes are bi-potent cells in the cortex of the healthy/uninjured adult brain, where they self-renew and generate oligodendrocytes.

In the mice subjected to focal cerebral ischemia the number of $EGFP^+$ cells after ischemia significantly increased; they displayed heterogeneous morphology and expressed markers of astrocytes and neuronal precursor cells. Polydendrocyte multipotency was confirmed by detailed immunohistochemical and electrophysiological analysis, which proved the generation of astrocytic and neuronal precursor phenotypes from $EGFP^+$ cells after ischemia.

Taken together, polydendrocytes posses the ability to rapidly respond to brain injury by high proliferation rate and differentiation into astrocytes and neuronal precursors, thus becoming very important cellular element during formation of glial scar and nervous tissue regeneration in the adult mammalian brain.

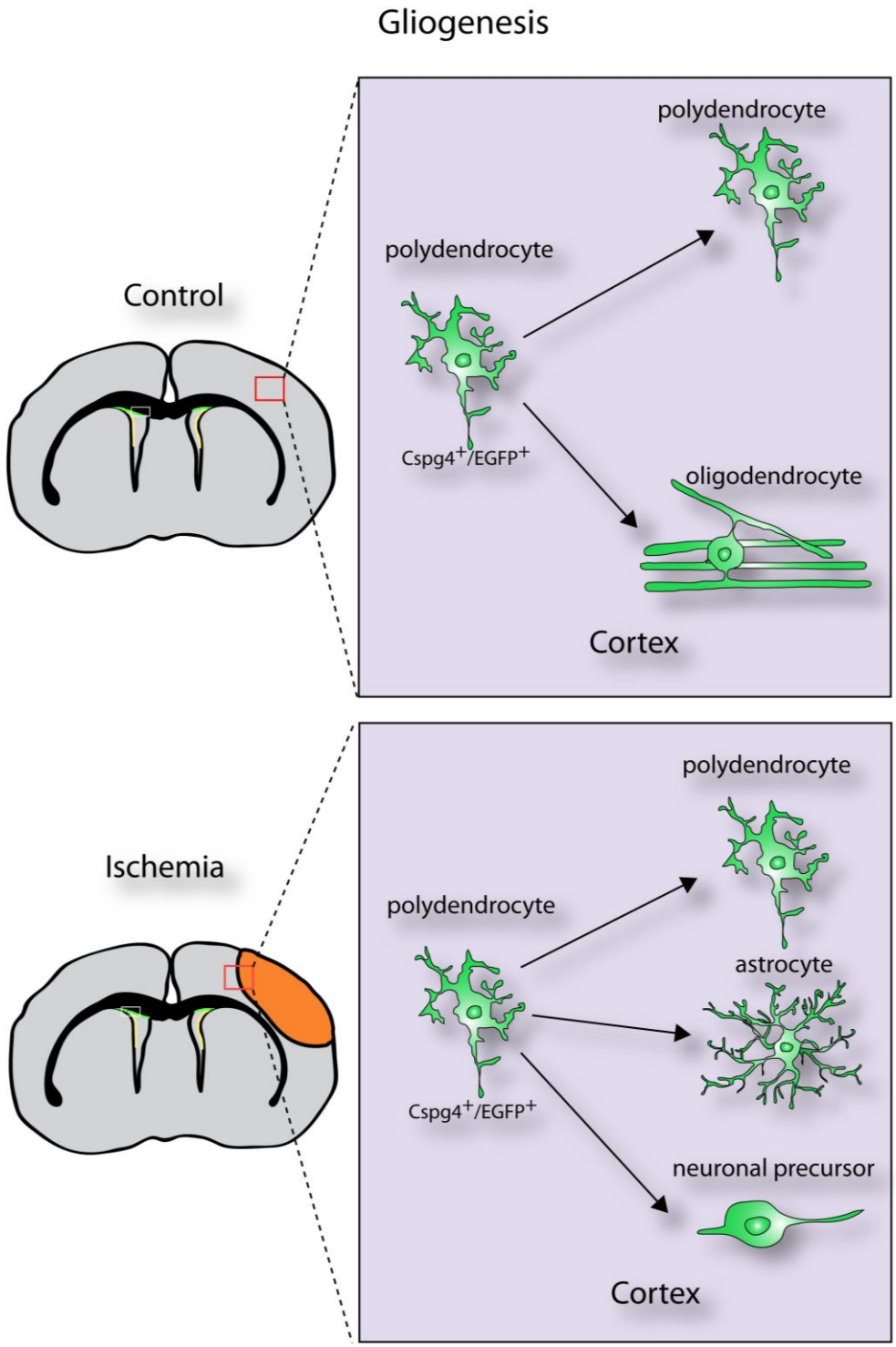

Figure 30. Schema summarizing adult gliogenesis of CSPG4$^+$ polydendrocytes after ischemia.

2) To define changes in gene expression profile of glial cell during gliogenesis following ischemia.

We show that cortical glial cells collected after focal cerebral ischemia are highly heterogeneous with respect to their gene expression profiles. There are several populations of glial cells during post-ischemic period, which probably fulfill different roles in the glial scar formation and maintaining.

Our findings demonstrate that the issue of glial cells heterogeneity is complicated, but can be approached with single cell expression profiling, which reveals and distinguishes cell subpopulations. Using this approach we can identify rare cells types that could be lost using classical bulk experiment, where several thousands of cells are analyzed. More importantly, this approach enabled us to identify new ion channels expressed in reactive glia, such as hyperpolarization activated non-specific cationic ion channels HCN1-4.

Moreover using a different method we also confirmed that reactive astrocytes are derived or differentiated from polydendrocytes during post-ischemic processes.

3) To clarify the role of adult neural stem cells localized the dorsal part of the LV in the process of adult neurogenesis or gliogenesis during physiological as well as post-ischemic conditions.

We used adult transgenic mice with GFP expression driven by the D6 promoter of the *Dach1* gene, which allows visualizing cells with active *Dach1* gene expression in the dorsal part of the LV. We have shown that GFP^+ cells isolated from this region are able to subsequently proliferate and differentiate *in vitro*; GFP^+ cells isolated from uninjured brains display only gliogenic potential; however, GFP^+ cells from post-ischemic brains also possess neurogenic potential, based on immunohistochemical and electrophysiological analyses. Similar analyses carried out *in situ* revealed two populations of GFP^+ cells in the dorsal part of the LV. The first population expressed properties comparable to adult neural stem cells, while the second resembled

neuroblasts. Focal cerebral ischemia influenced the phenotype of these cells and increased the number of GFP^+ neuroblasts in the dorsal part of the LV in both hemispheres. We also detected GFP^+ cells in two brain regions connected with the process of SVZ adult neurogenesis – the rostral migratory stream and the olfactory bulb. In uninjured brains GFP^+ cells expressed predominantly glial markers and possibly participated in forming a glial tunnel in the RMS, while GFP^+ cells in the OB adopted the phenotype of calretinin-positive interneurons in the GCL and GL and also TH-positive interneurons in the GL. Ischemic injury led to occurrence of GFP^+ neuroblasts in the RMS and to a significantly increased number of GFP^+ interneurons in both the GCL and GL in the OB without changes to their phenotype. Taken together the dorsal part of the SVZ in the adult mammalian brain is similarly to the lateral part of the SVZ composed from neural stem cells, which could differentiate into new neurons; but in contrast to the lateral part of the SVZ, these neurons do not participate in the post-ischemic recovery.

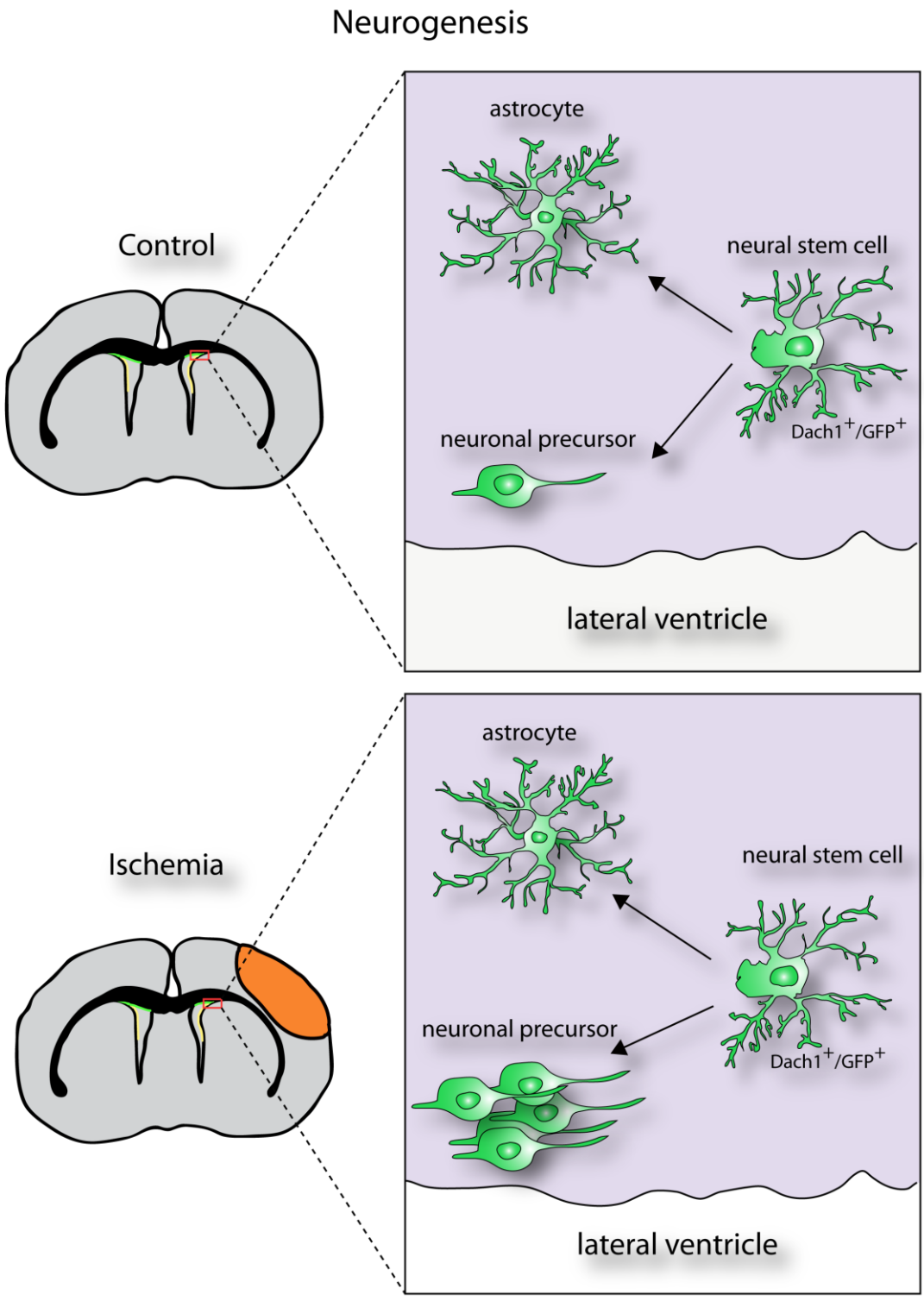

Figure 31. Schema summarizing adult neurogenesis of Dach1$^+$ cells in the dorsal part of the lateral ventricle after ischemia.

In conclusion, this work shed some light on endogenous neurogenic and gliogenic processes occurring in the adult mammalian brain (Figure 30, 31), which is essential for developing future treatment of central nervous system injuries. Supposing the existence of an endogenous potential of neural tissue to recover, discovering mechanisms for strengthening this potential could be very promising treatment of injured tissue in the future.

REFERENCES

Aguado F, Espinosa-Parrilla JF, Carmona MA, Soriano E (2002) Neuronal activity regulates correlated network properties of spontaneous calcium transients in astrocytes in situ. Journal of Neuroscience 22:9430–9444.

Aguirre AA (2004) NG2-expressing cells in the subventricular zone are type C-like cells and contribute to interneuron generation in the postnatal hippocampus. The Journal of Cell Biology 165:575–589.

Allaman I, Bélanger M, Magistretti PJ (2011) Astrocyte-neuron metabolic relationships: for better and for worse. Trends in Neurosciences 34:76–87.

Anderova M, Antonova T, Petrik D, Neprasova H, Chvatal A, Sykova E (2004) Voltage-dependent potassium currents in hypertrophied rat astrocytes after a cortical stab wound. Glia 48:311–326.

Anderova M, Vorisek I, Pivonkova H, Benesova J, Vargova L, Cicanic M, Chvatal A, Sykova E (2010) Cell death/proliferation and alterations in glial morphology contribute to changes in diffusivity in the rat hippocampus after hypoxia–ischemia. Journal of Cerebral Blood Flow & Metabolism 31:894–907.

Ashwal S, Tone B, Tian HR, Cole DJ, Pearce WJ, Faraci FM (1998) Core and penumbral nitric oxide synthase activity during cerebral ischemia and reperfusion. Editorial Comment. Stroke 29:1037–1047.

Back T (1998) Pathophysiology of the ischemic penumbra--revision of a concept. Cell Mol Neurobiol 18:621–638.

Back T, Ginsberg MD, Dietrich WD, Watson BD (1996) Induction of spreading depression in the ischemic hemisphere following experimental middle cerebral artery occlusion: effect on infarct morphology. J Cereb Blood Flow Metab 16:202–213.

Back T, Hoehn-Berlage M, Kohno K, Hossmann KA (1994) Diffusion nuclear magnetic resonance imaging in experimental stroke. Correlation with cerebral

metabolites. Stroke 25:494–500.

Badaut J, Petit JM, Brunet JF, Magistretti PJ, Charriaut-Marlangue C, Regli L (2004) Distribution of Aquaporin 9 in the adult rat brain: Preferential expression in catecholaminergic neurons and in glial cells. Neuroscience 128:27–38.

Badaut J, Regli L (2004) Distribution and possible roles of aquaporin 9 in the brain. Neuroscience 129:969–979.

Bardehle S, Krüger M, Buggenthin F, Schwausch J, Ninkovic J, Clevers H, Snippert HJ, Theis FJ, Meyer-Luehmann M, Bechmann I, Dimou L, Götz M (2013) Live imaging of astrocyte responses to acute injury reveals selective juxtavascular proliferation. Nature Publishing Group 16:580–586.

Bartus RT, Dean RL, Cavanaugh K, Eveleth D, Carriero DL, Lynch G (1995) Time-related neuronal changes following middle cerebral artery occlusion: implications for therapeutic intervention and the role of calpain. J Cereb Blood Flow Metab 15:969–979.

Belachew S (2003) Postnatal NG2 proteoglycan-expressing progenitor cells are intrinsically multipotent and generate functional neurons. The Journal of Cell Biology 161:169–186.

Bellardita C, Bolzoni F, Sorosina M, Marfia G, Carelli S, Gorio A, Formenti A (2011) Voltage-dependent ionic channels in differentiating neural precursor cells collected from adult mouse brains six hours post-mortem. J Neurosci Res 90:751–758.

Benesova J, Rusnakova V, Honsa P, Pivonkova H, Dzamba D, Kubista M, Anderova M (2012) Distinct expression/function of potassium and chloride channels contributes to the diverse volume regulation in cortical astrocytes of GFAP/EGFP mice Hetman M, ed. PLoS ONE 7:e29725.

Benfenati V, Amiry-Moghaddam M, Caprini M, Mylonakou MN, Rapisarda C, Ottersen OP, Ferroni S (2007) Expression and functional characterization of transient receptor potential vanilloid-related channel 4 (TRPV4) in rat cortical astrocytes. Neuroscience 148:876–892.

Bethea JR, Dietrich WD (2002) Targeting the host inflammatory response in traumatic spinal cord injury. Curr Opin Neurol 15:355–360.

Bezzi P, Carmignoto G, Pasti L, Vesce S, Rossi D, Rizzini BL, Pozzan T, Volterra A (1998) Prostaglandins stimulate calcium-dependent glutamate release in astrocytes. Nature 391:281–285.

Béjot Y, Daubail B, Jacquin A, Durier J, Osseby G-V, Rouaud O, Giroud M (2014) Trends in the incidence of ischaemic stroke in young adults between 1985 and 2011: the Dijon Stroke Registry. J Neurol Neurosurg Psychiatr 85:509–513.

Bohlen und Halbach von O (2011) Immunohistological markers for proliferative events, gliogenesis, and neurogenesis within the adult hippocampus. Cell Tissue Res 345:1–19.

Bolteus AJ (2004) GABA Release and uptake regulate neuronal precursor migration in the postnatal subventricular zone. Journal of Neuroscience 24:7623–7631.

Bordey A, Lyons SA, Hablitz JJ, Sontheimer H (2001) Electrophysiological characteristics of reactive astrocytes in experimental cortical dysplasia. Journal of Neurophysiology 85:1719–1731.

Bramlett HM, Dietrich WD (2004) Pathophysiology of cerebral ischemia and brain trauma: Similarities and differences. J Cereb Blood Flow Metab:133–150.

Brophy PJ (1991) Myelin and demyelination. Ann N Y Acad Sci 633:205–208.

Buffo A, Rite I, Tripathi P, Lepier A, Colak D, Horn A-P, Mori T, Götz M (2008) Origin and progeny of reactive gliosis: A source of multipotent cells in the injured brain. Proc Natl Acad Sci USA 105:3581–3586.

Bulloch K, Miller MM, Gal-Toth J, Milner TA, Gottfried-Blackmore A, Waters EM, Kaunzner UW, Liu K, Lindquist R, Nussenzweig MC, Steinman RM, McEwen BS (2008) CD11c/EYFP transgene illuminates a discrete network of dendritic cells within the embryonic, neonatal, adult, and injured mouse brain. J Comp Neurol 508:687–710.

Butenko O, Dzamba D, Benesova J, Honsa P, Benfenati V, Rusnakova V, Ferroni S,

Anderova M (2012) The Increased Activity of TRPV4 Channel in the Astrocytes of the Adult Rat Hippocampus after Cerebral Hypoxia/Ischemia Amédée T, ed. PLoS ONE 7:e39959.

Büki A, Koizumi H, Povlishock JT (1999) Moderate posttraumatic hypothermia decreases early calpain-mediated proteolysis and concomitant cytoskeletal compromise in traumatic axonal injury. Experimental Neurology 159:319–328.

Cahoy JD, Emery B, Kaushal A, Foo LC, Zamanian JL, Christopherson KS, Xing Y, Lubischer JL, Krieg PA, Krupenko SA, Thompson WJ, Barres BA (2008) A transcriptome database for astrocytes, neurons, and oligodendrocytes: A new resource for understanding brain development and function. Journal of Neuroscience 28:264–278.

Carletti B, Rossi F (2008) Neurogenesis in the cerebellum. The Neuroscientist 14:91–100.

Carlén M, Meletis K, Göritz C, Darsalia V, Evergren E, Tanigaki K, Amendola M, Barnabé-Heider F, Yeung MSY, Naldini L, Honjo T, Kokaia Z, Shupliakov O, Cassidy RM, Lindvall O, Frisén J (2009) Forebrain ependymal cells are Notch-dependent and generate neuroblasts and astrocytes after stroke. Nature Neuroscience 12:259–267.

Carmichael ST (2005) Rodent models of focal stroke: size, mechanism, and purpose. NeuroRx 2:396–409.

Cheng M-F (2013) Hypothalamic neurogenesis in the adult brain. Frontiers in Neuroendocrinology 34:167–178.

Choi DW, Peters S, Viseskul V (1987) Dextrorphan and levorphanol selectively block N-methyl-D-aspartate receptor-mediated neurotoxicity on cortical neurons. J Pharmacol Exp Ther 242:713–720.

Dalkara T, Moskowitz MA (1994) The complex role of nitric oxide in the pathophysiology of focal cerebral ischemia. Brain Pathol 4:49–57.

De Biase LM, Kang SH, Baxi EG, Fukaya M, Pucak ML, Mishina M, Calabresi PA,

Bergles DE (2011) NMDA receptor signaling in oligodendrocyte progenitors is not required for oligodendrogenesis and myelination. Journal of Neuroscience 31:12650–12662.

Dimou L, Simon C, Kirchhoff F, Takebayashi H, Gotz M (2008) Progeny of Olig2-expressing progenitors in the gray and white matter of the adult mouse cerebral cortex. Journal of Neuroscience 28:10434–10442.

Dirnagl U, Iadecola C, Moskowitz MA (1999) Pathobiology of ischaemic stroke: an integrated view. Trends in Neurosciences 22:391–397.

Doetsch F (2003) The glial identity of neural stem cells. Nature Neuroscience 6:1127–1134.

Durand D, Carniglia L, Caruso C, Lasaga M (2011) Reduced cAMP, Akt activation and p65-c-Rel dimerization: Mechanisms involved in the protective effects of mGluR3 agonists in cultured astrocytes. Castro MG, ed. PLoS ONE 6:e22235.

Fellner L, Jellinger KA, Wenning GK, Stefanova N (2011) Glial dysfunction in the pathogenesis of α-synucleinopathies: emerging concepts. Acta Neuropathol 121:675–693.

Ferraguti F, Corti C, Valerio E, Mion S, Xuereb J (2001) Activated astrocytes in areas of kainate-induced neuronal injury upregulate the expression of the metabotropic glutamate receptors 2/3 and 5. Exp Brain Res 137:1–11.

Gage FH, Temple S (2013) Perspective. Neuron 80:588–601.

Gerasimov VD, Artemenko DP, Krishtal OA (2004) Therapeutic time window for the neuroprotective action of MK-801 after decapitation ischemia: hippocampal slice data. Brain Research 1017:92–97.

Globus MY, Prado R, Busto R (1995) Ischemia-induced changes in extracellular levels of striatal cyclic GMP: role of nitric oxide. Neuroreport 6:1909–1912.

Goritz C, Dias DO, Tomilin N, Barbacid M, Shupliakov O, Frisen J (2011) A Pericyte origin of spinal cord scar tissue. Science 333:238–242.

Gould E (2007) How widespread is adult neurogenesis in mammals? Nat Rev Neurosci 8:481–488.

Graham SH, Chen J (2001) Programmed cell death in cerebral ischemia. J Cereb Blood Flow Metab 21:99–109.

Grandbarbe L (2003) Delta-Notch signaling controls the generation of neurons/glia from neural stem cells in a stepwise process. Development 130:1391–1402.

Guo F, Maeda Y, Ma J, Xu J, Horiuchi M, Miers L, Vaccarino F, Pleasure D (2010) Pyramidal neurons are generated from oligodendroglial progenitor cells in adult piriform cortex. Journal of Neuroscience 30:12036–12049.

Hamill OP, Marty A, Neher E, Sakmann B, Sigworth FJ (1981) Improved patch-clamp techniques for high-resolution current recording from cells and cell-free membrane patches. Pflugers Arch - Eur J Physiol 391:85–100.

Hampton DW, Rhodes KE, Zhao C, Franklin RJM, Fawcett JW (2004) The responses of oligodendrocyte precursor cells, astrocytes and microglia to a cortical stab injury, in the brain. Neuroscience 127:813–820.

Hansen AJ, Lauritzen M (1984) The role of spreading depression in acute brain disorders. An Acad Bras Cienc 56:457–479.

Hara-Chikuma M (2005) Aquaporin-1 facilitates epithelial cell migration in kidney proximal tubule. Journal of the American Society of Nephrology 17:39–45.

Hepp R, Perraut M, Chasserot-Golaz S, Galli T, Aunis D, Langley K, Grant NJ (1999) Cultured glial cells express the SNAP-25 analogue SNAP-23. Glia 27:181–187.

Hong SC, Lanzino G, Goto Y, Kang SK, Schottler F, Kassell NF, Lee KS (1994) Calcium-activated proteolysis in rat neocortex induced by transient focal ischemia. Brain Research 661:43–50.

Hoshi A, Yamamoto T, Shimizu K, Ugawa Y, Nishizawa M, Takahashi H, Kakita A (2012) Characteristics of aquaporin expression surrounding senile plaques and cerebral amyloid angiopathy in Alzheimer disease. J Neuropathol Exp Neurol 71:750–759.

Hwang IK, Yoo K-Y, Li H, Lee B-H, Suh H-W, Kwon Y-G, Won M-H (2007) Aquaporin 9 changes in pyramidal cells before and is expressed in astrocytes after delayed neuronal death in the ischemic hippocampal CA1 region of the gerbil. J Neurosci Res 85:2470–2479.

Iadecola C (1997) Bright and dark sides of nitric oxide in ischemic brain injury. Trends in Neurosciences 20:132–139.

Illarionova NB, Gunnarson E, Li Y, Brismar H, Bondar A, Zelenin S, Aperia A (2010) Functional and molecular interactions between aquaporins and Na,K-ATPase. Neuroscience 168:915–925.

Jelitai M, Anderova M, Chvatal A, Madarász E (2007) Electrophysiological characterization of neural stem/progenitor cells during in vitro differentiation: Study with an immortalized neuroectodermal cell line. J Neurosci Res 85:1606–1617.

Kang SH, Fukaya M, Yang JK, Rothstein JD, Bergles DE (2010) CNS Glial Progenitors remain committed to the oligodendrocyte lineage in postnatal life and following neurodegeneration. Neuron 68:668–681.

Karram K, Goebbels S, Schwab M, Jennissen K, Seifert G, Steinhäuser C, Nave K-A, Trotter J (2008) NG2-expressing cells in the nervous system revealed by the NG2-EYFP-knockin mouse. Genesis 46:743–757.

Kerschensteiner M, Gallmeier E, Behrens L, Leal VV, Misgeld T, Klinkert WE, Kolbeck R, Hoppe E, Oropeza-Wekerle RL, Bartke I, Stadelmann C, Lassmann H, Wekerle H, Hohlfeld R (1999) Activated human T cells, B cells, and monocytes produce brain-derived neurotrophic factor in vitro and in inflammatory brain lesions: a neuroprotective role of inflammation? J Exp Med 189:865–870.

Knutson P, Ghiani CA, Zhou JM, Gallo V, McBain CJ (1997) K+ channel expression and cell proliferation are regulated by intracellular sodium and membrane depolarization in oligodendrocyte progenitor cells. J Neurosci 17:2669–2682.

Kokaia Z, Andsberg G, Yan Q, Lindvall O (1998) Rapid alterations of BDNF protein levels in the rat brain after focal ischemia: evidence for increased synthesis and

anterograde axonal transport. Experimental Neurology 154:289–301.

Koketsu D, Furuichi Y, Maeda M, Matsuoka N, Miyamoto Y, Hisatsune T (2006) Increased number of new neurons in the olfactory bulb and hippocampus of adult non-human primates after focal ischemia. Experimental Neurology 199:92–102.

Komitova M, Serwanski DR, Richard Lu Q, Nishiyama A (2011) NG2 cells are not a major source of reactive astrocytes after neocortical stab wound injury. Glia 59:800–809.

Komitova M, Zhu X, Serwanski DR, Nishiyama A (2009) NG2 cells are distinct from neurogenic cells in the postnatal mouse subventricular zone. J Comp Neurol 512:702–716.

Kondo T, Raff M (2000) Oligodendrocyte precursor cells reprogrammed to become multipotential CNS stem cells. Science 289:1754–1757.

Koroleva VI, Bures J (1996) The use of spreading depression waves for acute and long-term monitoring of the penumbra zone of focal ischemic damage in rats. Proc Natl Acad Sci USA 93:3710–3714.

Krüger C, Cira D, Sommer C, Fischer A, Schäbitz W-R, Schneider A (2006) Long-term gene expression changes in the cortex following cortical ischemia revealed by transcriptional profiling. Experimental Neurology 200:135–152.

Kwon J, Lee N, Jeon I, Lee HJ, Do JT, Lee DR, Oh S-H, Shin DA, Kim A, Song J (2012) Neuronal differentiation of a human induced pluripotent stem cell line (FS-1) derived from newborn foreskin fibroblasts. Int J Stem Cells 5:140–145.

Lacar (2010) Imaging and recording subventricular zone progenitor cells in live tissue of postnatal mice. Front Neurosci.

Li J, Siegel M, Yuan M, Zeng Z, Finnucan L, Persky R, Hurn PD, McCullough LD (2010) Estrogen enhances neurogenesis and behavioral recovery after stroke. Journal of Cerebral Blood Flow & Metabolism 31:413–425.

Liu F, You Y, Li X, Ma T, Nie Y, Wei B, Li T, Lin H, Yang Z (2009) Brain injury does not alter the intrinsic differentiation potential of adult neuroblasts. Journal of

Neuroscience 29:5075–5087.

Liu X, Bolteus AJ, Balkin DM, Henschel O, Bordey A (2006) GFAP-expressing cells in the postnatal subventricular zone display a unique glial phenotype intermediate between radial glia and astrocytes. Glia 54:394–410.

Liu X, Zhu XZ (1999) Roles of p53, c-Myc, Bcl-2, Bax and caspases in glutamate-induced neuronal apoptosis and the possible neuroprotective mechanism of basic fibroblast growth factor. Brain Res Mol Brain Res 71:210–216.

Lledo P-M, Merkle FT, Alvarez-Buylla A (2008) Origin and function of olfactory bulb interneuron diversity. Trends in Neurosciences 31:392–400.

Ma Y-H, Mentlein R, Knerlich F, Kruse M-L, Mehdorn HM, Held-Feindt J (2007) Expression of stem cell markers in human astrocytomas of different WHO grades. J Neurooncol 86:31–45.

Machon O, van den Bout CJ, Backman M, Røsok Ø, Caubit X, Fromm SH, Geronimo B, Krauss S (2002) Forebrain-specific promoter/enhancer D6 derived from the mouse Dach1 gene controls expression in neural stem cells. NSC 112:951–966.

Maier CM, Chan PH (2002) Role of superoxide dismutases in oxidative damage and neurodegenerative disorders. The Neuroscientist 8:323–334.

Malarkey EB, Ni Y, Parpura V (2008) Ca2+ entry through TRPC1 channels contributes to intracellular Ca2+ dynamics and consequent glutamate release from rat astrocytes. Glia 56:821–835.

Martin L (2000) Neuronal death in newborn striatum after hypoxia-ischemia is necrosis and evolves with oxidative stress. Neurobiology of Disease 7:169–191.

Masuda T, Isobe Y, Aihara N, Furuyama F, Misumi S, Kim T-S, Nishino H, Hida H (2007) Increase in neurogenesis and neuroblast migration after a small intracerebral hemorrhage in rats. Neuroscience Letters 425:114–119.

Matute C, Alberdi E, Domercq M, Sánchez-Gómez M-V, Pérez-Samartín A, Rodríguez-Antigüedad A, Pérez-Cerdá F (2007) Excitotoxic damage to white matter. Journal of Anatomy 210:693–702.

Mccoy E, Sontheimer H (2007) Expression and function of water channels (aquaporins) in migrating malignant astrocytes. Glia 55:1034–1043.

Mccoy E, Sontheimer H (2010) MAPK induces AQP1 expression in astrocytes following injury. Glia 58:209–217.

Michalczyk K, Ziman M (2005) Nestin structure and predicted function in cellular cytoskeletal organisation. Histol Histopathol 20:665–671.

Mies G, Iijima T, Hossmann KA (1993) Correlation between peri-infarct DC shifts and ischaemic neuronal damage in rat. Neuroreport 4:709–711.

Montiel-Eulefi E, Nery AA, Rodrigues LC, Sánchez R, Romero F, Ulrich H (2011) Neural differentiation of rat aorta pericyte cells. Cytometry 81A:65–71.

Muir K, Kalladka D (2014) Brain repair: cell therapy in stroke. SCCAA:31.

Muskhelishvili L, Latendresse JR, Kodell RL, Henderson EB (2003) Evaluation of cell proliferation in rat tissues with BrdU, PCNA, Ki-67(MIB-5) immunohistochemistry and in situ hybridization for histone mRNA. Journal of Histochemistry & Cytochemistry 51:1681–1688.

Neitz A, Mergia E, Eysel UT, Koesling D, Mittmann T (2011) Presynaptic nitric oxide/cGMP facilitates glutamate release via hyperpolarization-activated cyclic nucleotide-gated channels in the hippocampus. European Journal of Neuroscience 33:1611–1621.

Ninkovic J, Götz M (2014) A time and place for understanding neural stem cell specification. Developmental Cell 30:114–115.

Nishiyama A (2007) Polydendrocytes: NG2 cells with many roles in development and repair of the CNS. The Neuroscientist 13:62–76.

Nishiyama A, Komitova M, Suzuki R, Zhu X (2009) Polydendrocytes (NG2 cells): multifunctional cells with lineage plasticity. Nat Rev Neurosci 10:9–22.

Nolte C, Matyash M, Pivneva T, Schipke CG, Ohlemeyer C, Hanisch UK, Kirchhoff F, Kettenmann H (2001) GFAP promoter-controlled EGFP-expressing transgenic

mice: a tool to visualize astrocytes and astrogliosis in living brain tissue. Glia 33:72–86.

Ohira K (2010) Injury-induced neurogenesis in the mammalian forebrain. Cell Mol Life Sci 68:1645–1656.

Pamenter ME, Perkins GA, McGinness AK, Gu XQ, Ellisman MH, Haddad GG (2012) Autophagy and apoptosis are differentially induced in neurons and astrocytes treated with an in vitro mimic of the ischemic penumbra. Arai K, ed. PLoS ONE 7:e51469.

Papadopoulos M, Verkman A (2008) Potential utility of aquaporin modulators for therapy of brain disorders. In: Progress in Brain Research, pp 589–601 Progress in Brain Research. Elsevier.

Paquet M, Ribeiro FM, Guadagno J, Esseltine JL, Ferguson SSG, Cregan SP (2013) Role of metabotropic glutamate receptor 5 signaling and homer in oxygen glucose deprivation-mediated astrocyte apoptosis. Mol Brain 6:9.

Patanow CM, Day JR, Billingsley ML (1997) Alterations in hippocampal expression of SNAP-25, GAP-43, stannin and glial fibrillary acidic protein following mechanical and trimethyltin-induced injury in the rat. NSC 76:187–202.

Pekny M, Nilsson M (2005) Astrocyte activation and reactive gliosis. Glia 50:427–434.

Pekny M, Wilhelmsson U, Pekna M (2014) The dual role of astrocyte activation and reactive gliosis. Neuroscience Letters 565:30–38.

Pivonkova H, Benesova J, Butenko O, Chvatal A, Anderova M (2010) Impact of global cerebral ischemia on K+ channel expression and membrane properties of glial cells in the rat hippocampus. Neurochemistry International 57:783–794.

Platel J-C, Stamboulian S, Nguyen I, Bordey A (2010) Neurotransmitter signaling in postnatal neurogenesis: The first leg. Brain Research Reviews:1–12.

Platel JC, Dave KA, Bordey A (2008) Control of neuroblast production and migration by converging GABA and glutamate signals in the postnatal forebrain. The

Journal of Physiology 586:3739–3743.

Posmantur R, Kampfl A, Siman R, Liu J, Zhao X, Clifton GL, Hayes RL (1997) A calpain inhibitor attenuates cortical cytoskeletal protein loss after experimental traumatic brain injury in the rat. NSC 77:875–888.

Prajerova I, Honsa P, Chvatal A, Anderova M (2010) Distinc effects of Sonic hedgehog and Wnt-7a on differentiation of neonatal neural stem/progenitor cells in vitro. NSC 171:693–711.

Ransom CB, Liu X, Sontheimer H (2002) BK channels in human glioma cells have enhanced calcium sensitivity. Glia 38:281–291.

Rivers LE, Young KM, Rizzi M, Jamen F, Psachoulia K, Wade A, Kessaris N, Richardson WD (2008) PDGFRA/NG2 glia generate myelinating oligodendrocytes and piriform projection neurons in adult mice. Nature Neuroscience 11:1392–1401.

Robel S, Berninger B, Götz M (2011) The stem cell potential of glia:lessons from reactive gliosis. :1–17.

Rodríguez A, Pérez-Gracia E, Espinosa JC, Pumarola M, Torres JM, Ferrer I (2006) Increased expression of water channel aquaporin 1 and aquaporin 4 in Creutzfeldt-Jakob disease and in bovine spongiform encephalopathy-infected bovine-PrP transgenic mice. Acta Neuropathol 112:573–585.

Roitbak T, Syková E (1999) Diffusion barriers evoked in the rat cortex by reactive astrogliosis. Glia 28:40–48.

Rosell A, Agin V, Rahman M, Morancho A, Ali C, Koistinaho J, Wang X, Vivien D, Schwaninger M, Montaner J (2013) Distal occlusion of the middle cerebral artery in mice: are we ready to assess long-term functional outcome? Transl Stroke Res 4:297–307.

Rusnakova V, Honsa P, Dzamba D, Ståhlberg A, Kubista M, Anderova M (2013) Heterogeneity of astrocytes: from development to injury - single cell gene expression. PLoS ONE 8:e69734.

Saatman KE, Bozyczko-Coyne D, Marcy V, Siman R, McIntosh TK (1996) Prolonged calpain-mediated spectrin breakdown occurs regionally following experimental brain injury in the rat. J Neuropathol Exp Neurol 55:850–860.

Sellers DL, Maris DO, Horner PJ (2009) Postinjury niches induce temporal shifts in progenitor fates to direct lesion repair after spinal cord injury. Journal of Neuroscience 29:6722–6733.

Sicard KM, Fisher M (2009) Animal models of focal brain ischemia. Exp Transl Stroke Med 1:7.

Siesjö BK, Bengtsson F, Grampp W, Theander S (1989) Calcium, excitotoxins, and neuronal death in the brain. Ann N Y Acad Sci 568:234–251.

Simon C, Götz M, Dimou L (2011) Progenitors in the adult cerebral cortex: Cell cycle properties and regulation by physiological stimuli and injury. Glia 59:869–881.

Singer BH, Jutkiewicz EM, Fuller CL, Lichtenwalner RJ, Zhang H, Velander AJ, Li X, Gnegy ME, Burant CF, Parent JM (2009) Conditional ablation and recovery of forebrain neurogenesis in the mouse. J Comp Neurol 514:567–582.

Sirko S et al. (2013) Reactive glia in the injured brain acquire stem cell properties in response to sonic hedgehog. [corrected]. Cell Stem Cell 12:426–439.

Sík A, Smith RL, Freund TF (2000) Distribution of chloride channel-2-immunoreactive neuronal and astrocytic processes in the hippocampus. NSC 101:51–65.

Snider BJ, Gottron FJ, Choi DW (1999) Apoptosis and necrosis in cerebrovascular disease. Ann N Y Acad Sci 893:243–253.

Song H, Stevens CF, Gage FH (2002) Astroglia induce neurogenesis from adult neural stem cells. Nature 417:39–44.

Sozmen EG, Kolekar A, Havton LA, Carmichael ST (2009) A white matter stroke model in the mouse: Axonal damage, progenitor responses and MRI correlates. Journal of Neuroscience Methods 180:261–272.

Spadafora R, Gonzalez FF, Derugin N, Wendland M, Ferriero D, McQuillen P (2010)

Altered fate of subventricular zone progenitor cells and reduced neurogenesis following neonatal stroke. Dev Neurosci 32:101–113.

Stagliano NE, Dietrich WD, Prado R, Green EJ, Busto R (1997) The role of nitric oxide in the pathophysiology of thromboembolic stroke in the rat. Brain Research 759:32–40.

Stahlberg A, Andersson D, Aurelius J, Faiz M, Pekna M, Kubista M, Pekny M (2011) Defining cell populations with single-cell gene expression profiling: correlations and identification of astrocyte subpopulations. Nucleic Acids Research 39:e24–e24.

Strojnik T, Røsland GV, Sakariassen PO, Kavalar R, Lah T (2007) Neural stem cell markers, nestin and musashi proteins, in the progression of human glioma: correlation of nestin with prognosis of patient survival. Surgical Neurology 68:133–143.

Sundelacruz S, Levin M, Kaplan DL (2009) Role of membrane potential in the regulation of cell proliferation and differentiation. Stem Cell Rev and Rep 5:231–246.

Takasawa K-I, Kitagawa K, Yagita Y, Sasaki T, Tanaka S, Matsushita K, Ohstuki T, Miyata T, Okano H, Hori M, Matsumoto M (2002) Increased proliferation of neural progenitor cells but reduced survival of newborn cells in the contralateral hippocampus after focal cerebral ischemia in rats. J Cereb Blood Flow Metab 22:299–307.

Tan X, Shi S-H (2012) Neocortical neurogenesis and neuronal migration. WIREs Dev Biol 2:443–459.

Tatsumi K, Takebayashi H, Manabe T, Tanaka KF, Makinodan M, Yamauchi T, Makinodan E, Matsuyoshi H, Okuda H, Ikenaka K, Wanaka A (2008) Genetic fate mapping of Olig2 progenitors in the injured adult cerebral cortex reveals preferential differentiation into astrocytes. J Neurosci Res 86:3494–3502.

Taupin P (2005) Adult neurogenesis in the mammalian central nervous system: functionality and potential clinical interest. Med Sci Monit 11:RA247–RA252.

Thored P, Arvidsson A, Cacci E, Ahlenius H, Kallur T, Darsalia V, Ekdahl CT, Kokaia Z, Lindvall O (2006) Persistent production of neurons from adult brain stem cells during recovery after stroke. Stem Cells 24:739–747.

Tripathi RB, Rivers LE, Young KM, Jamen F, Richardson WD (2010) NG2 glia generate new oligodendrocytes but few astrocytes in a murine experimental autoimmune Encephalomyelitis model of demyelinating disease. Journal of Neuroscience 30:16383–16390.

Trotter J, Karram K, Nishiyama A (2010) NG2 cells: Properties, progeny and origin. Brain Research Reviews 63:72–82.

Ulas J, Satou T, Ivins KJ, Kesslak JP, Cotman CW, Balázs R (2000) Expression of metabotropic glutamate receptor 5 is increased in astrocytes after kainate-induced epileptic seizures. Glia 30:352–361.

Varela-Nallar L, Inestrosa NC (2013) Wnt signaling in the regulation of adult hippocampal neurogenesis. Front Cell Neurosci 7:100.

Wahl-Schott C, Biel M (2008) HCN channels: Structure, cellular regulation and physiological function. Cell Mol Life Sci 66:470–494.

Wang DD (2003) Biophysical properties and ionic signature of neuronal progenitors of the postnatal subventricular zone in situ. Journal of Neurophysiology 90:2291–2302.

Wang S, Sdrulla AD, diSibio G, Bush G, Nofziger D, Hicks C, Weinmaster G, Barres BA (1998) Notch receptor activation inhibits oligodendrocyte differentiation. Neuron 21:63–75.

Watson BD, Dietrich WD, Busto R, Wachtel MS, Ginsberg MD (1985) Induction of reproducible brain infarction by photochemically initiated thrombosis. Ann Neurol 17:497–504.

Wei B, Nie Y, Li X, Wang C, Ma T, Huang Z, Tian M, Sun C, Cai Y, You Y, Liu F, Yang Z (2011) Emx1-expressing neural stem cells in the subventricular zone give rise to new interneurons in the ischemic injured striatum. European Journal of

Neuroscience 33:819–830.

White BD, Nathe RJ, Maris DO, Nguyen NK, Goodson JM, Moon RT, Horner PJ (2010) Beta-catenin signaling increases in proliferating NG2+ progenitors and astrocytes during post-traumatic gliogenesis in the adult brain. Stem Cells 28:297–307.

Willaime-Morawek S, Seaberg RM, Batista C, Labbe E, Attisano L, Gorski JA, Jones KR, Kam A, Morshead CM, van der Kooy D (2006) Embryonic cortical neural stem cells migrate ventrally and persist as postnatal striatal stem cells. The Journal of Cell Biology 175:159–168.

Wohl SG, Schmeer CW, Friese T, Witte OW, Isenmann S (2011) In Situ dividing and phagocytosing retinal microglia express Nestin, Vimentin, and NG2 in vivo. Linden R, ed. PLoS ONE 6:e22408.

Xie M, Lynch DT, Schools GP, Feustel PJ, Kimelberg HK, Zhou M (2007) Sodium channel currents in rat hippocampal NG2 glia: Characterization and contribution to resting membrane potential. Neuroscience 150:853–862.

Yamamoto S, Nagao M, Sugimori M, Kosako H, Nakatomi H, Yamamoto N, Takebayashi H, Nabeshima Y, Kitamura T, Weinmaster G, Nakamura K, Nakafuku M (2001) Transcription factor expression and Notch-dependent regulation of neural progenitors in the adult rat spinal cord. Journal of Neuroscience 21:9814–9823.

Yamashita T (2006) Subventricular zone-derived neuroblasts migrate and differentiate into mature neurons in the post-stroke adult striatum. Journal of Neuroscience 26:6627–6636.

Yang Q-K, Xiong J-X, Yao Z-X (2013) Neuron-NG2 cell synapses: Novel functions for regulating NG2 cell proliferation and differentiation. BioMed Research International 2013:1–14.

Yoneyama M, Kawada K, Ogita K (2010) Enhanced neurogenesis in the olfactory bulb in adult mice after injury induced by acute treatment with trimethyltin. J Neurosci Res 88:1242–1251.

Young KM, Fogarty M, Kessaris N, Richardson WD (2007) Subventricular zone stem cells are heterogeneous with respect to their embryonic origins and neurogenic fates in the adult olfactory bulb. Journal of Neuroscience 27:8286–8296.

Zabel MK, Kirsch WM (2013) From development to dysfunction: Microglia and the complement cascade in CNS homeostasis. Ageing Research Reviews 12:749–756.

Zamanian JL, Xu L, Foo LC, Nouri N, Zhou L, Giffard RG, Barres BA (2012) Genomic analysis of reactive astrogliosis. Journal of Neuroscience 32:6391–6410.

Zawadzka M, Rivers LE, Fancy SPJ, Zhao C, Tripathi R, Jamen F, Young K, Goncharevich A, Pohl H, Rizzi M, Rowitch DH, Kessaris N, Suter U, Richardson WD, Franklin RJM (2010) CNS-Resident glial progenitor/stem cells produce Schwann cells as well as oligodendrocytes during repair of CNS demyelination. Stem Cell 6:578–590.

Zelenina M (2010) Regulation of brain aquaporins. Neurochemistry International 57:468–488.

Zhang F, Sprague SM, Farrokhi F, Henry MN, Son MG, Vollmer DG (2002) Reversal of attenuation of cerebrovascular reactivity to hypercapnia by a nitric oxide donor after controlled cortical impact in a rat model of traumatic brain injury. J Neurosurg 97:963–969.

Zhao C, Deng W, Gage FH (2008) Mechanisms and functional implications of adult neurogenesis. Cell 132:645–660.

Zhao J-W, Raha-Chowdhury R, Fawcett JW, Watts C (2009) Astrocytes and oligodendrocytes can be generated from NG2 +progenitors after acute brain injury: intracellular localization of oligodendrocyte transcription factor 2 is associated with their fate choice. European Journal of Neuroscience 29:1853–1869.

Zhou M (2005) Development of GLAST(+) Astrocytes and NG2(+) Glia in Rat Hippocampus CA1: Mature astrocytes are electrophysiologically passive. Journal of Neurophysiology 95:134–143.

Zhu X, Bergles DE, Nishiyama A (2007) NG2 cells generate both oligodendrocytes and gray matter astrocytes. Development 135:145–157.

Zhu X, Hill RA, Dietrich D, Komitova M, Suzuki R, Nishiyama A (2011) Age-dependent fate and lineage restriction of single NG2 cells. Development 138:745–753.

Zhu X, Hill RA, Nishiyama A (2008) NG2 cells generate oligodendrocytes and gray matter astrocytes in the spinal cord. NGB 4:19.

ATTACHMENTS

1. **Pavel Honsa**, Helena Pivonkova, David Dzamba, Marcela Filipova, Miroslava Anderova (2012), Polydendrocytes display large lineage plasticity following focal cerebral ischemia, PloS One 7(5), IF 3.730

2. Vendula Rusnakova, **Pavel Honsa**, David Dzamba, Anders Ståhlberg, Mikael Kubista, Miroslava Anderova (2013), Heterogeneity of Astrocytes: From Development to Injury–Single Cell Gene Expression, PloS one 8 (8), IF 3.730

3. **Pavel Honsa**, Helena Pivonkova, Miroslava Anderova (2013), Focal cerebral ischemia induces the neurogenic potential of mouse *Dach1* expressing cells in the dorsal part of the lateral ventricles; Neuroscience, 2013/3/1, IF 3.122

OPEN ACCESS Freely available online

PLoS one

Polydendrocytes Display Large Lineage Plasticity following Focal Cerebral Ischemia

Pavel Honsa[1,2], Helena Pivonkova[1,2], David Dzamba[1,2], Marcela Filipova[1], Miroslava Anderova[1]*

1 Department of Cellular Neurophysiology, Institute of Experimental Medicine, Academy of Sciences of the Czech Republic, Prague, Czech Republic, **2** 2nd Faculty of Medicine, Charles University, Prague, Czech Republic

Abstract

Polydendrocytes (also known as NG2 glial cells) constitute a fourth major glial cell type in the adult mammalian central nervous system (CNS) that is distinct from other cell types. Although much evidence suggests that these cells are multipotent *in vitro*, their differentiation potential *in vivo* under physiological or pathophysiological conditions is still controversial. To follow the fate of polydendrocytes after CNS pathology, permanent middle cerebral artery occlusion (MCAo), a commonly used model of focal cerebral ischemia, was carried out on adult NG2creBAC:ZEG double transgenic mice, in which enhanced green fluorescent protein (EGFP) is expressed in polydendrocytes and their progeny. The phenotype of the $EGFP^+$ cells was analyzed using immunohistochemistry and the patch-clamp technique 3, 7 and 14 days after MCAo. In sham-operated mice (control), $EGFP^+$ cells in the cortex expressed protein markers and displayed electrophysiological properties of polydendrocytes and oligodendrocytes. We did not detect any co-labeling of EGFP with neuronal, microglial or astroglial markers in this region, thus proving polydendrocyte unipotent differentiation potential under physiological conditions. Three days after MCAo the number of $EGFP^+$ cells in the gliotic tissue dramatically increased when compared to control animals, and these cells displayed properties of proliferating cells. However, in later phases after MCAo a large subpopulation of $EGFP^+$ cells expressed protein markers and electrophysiological properties of astrocytes that contribute to the formation of glial scar. Importantly, some $EGFP^+$ cells displayed membrane properties typical for neural precursor cells, and moreover these cells expressed doublecortin (DCX) – a marker of newly-derived neuronal cells. Taken together, our data indicate that polydendrocytes in the dorsal cortex display multipotent differentiation potential after focal ischemia.

Citation: Honsa P, Pivonkova H, Dzamba D, Filipova M, Anderova M (2012) Polydendrocytes Display Large Lineage Plasticity following Focal Cerebral Ischemia. PLoS ONE 7(5): e36816. doi:10.1371/journal.pone.0036816

Editor: Stefan Strack, University of Iowa, United States of America

Received January 11, 2012; **Accepted** April 7, 2012; **Published** May 10, 2012

Funding: This work was supported by the Grant Agency of the Czech Republic – CZ: GA ČR: GA309/09/0717, GA P303/12/0855 and GA 309/08/H079, and by the Grant Agency of Charles University – CZ: GA UK: 383711. The funders had no role in study design, data collection and analysis, decision to publish, or preparation of the manuscript.

Competing Interests: The authors have declared that no competing interests exist.

* E-mail: anderova@biomed.cas.cz

Introduction

In general, the adult central nervous system (CNS) possesses a limited capacity for regeneration after injury, including ischemia. Following ischemic injury, neural tissue recovery is accompanied by the formation of reactive astrogliosis; this process is vital for isolating necrotic tissue from its uninjured surroundings, but concurrently, it markedly impedes regenerative processes. Shortly after ischemia, a series of ionic, neurotransmitter and oxidative radical imbalances occurs that lead to the activation of microglia and subsequently to an increased number of reactive astrocytes. Both cell types release cytokines and other soluble products [1] that play an important role in consecutive processes, including the apoptosis of oligodendrocytes [2] and neurons [3]. Besides the main, well characterized cell types, other cells including polydendrocytes, endothelial cells and pericytes exist in neural tissue; however, our knowledge regarding their functional roles during and after brain ischemia remains limited.

Recently, attention has turned to polydendrocytes and their possible role in regeneration following CNS injuries. Polydendrocytes in the adult brain, known as NG2 glia or oligodendrocyte precursor cells, can be identified by their highly branched morphology and their expression of NG2 proteoglycan (NG2) together with platelet-derived growth factor alpha receptor (PDGFαR) [4]. These cells represent a fourth glial population in the mammalian brain, distinct from mature oligodendrocytes, astrocytes or microglia. Until recently they have been assumed to give rise only to oligodendrocytes in the intact adult CNS, although polydendrocytes are known to be capable of generating neurons and astrocytes *in vitro* in the presence of specific morphogens [5,6] and *in vivo* after transplantation into the hippocampus [7].

Using lineage-specific Cre transgenes, genetic fate-mapping studies in the intact CNS have revealed inconsistent findings. The capability of polydendrocytes to differentiate into oligodendrocytes *in vivo* was clearly confirmed by [8]; however, [9] also described the differentiation of polydendrocytes into grey matter astrocytes. Moreover, several recent studies have described the generation of new neurons in the piriform cortex from polydendrocytes in PDGFαR- or Plp-promoter-driven Cre transgenic mice [8,10]. On the other hand, in NG2- or Olig2- promoter-driven Cre transgenic animals, such neuronal differentiation was not observed [9,11].

In CNS pathologies such as global cerebral ischemia, polydendrocytes upregulate NG2 and significantly increase their

proliferation rate [12,13]. Apparently, the pathophysiological changes at the site of injury may enable polydendrocytes to display larger lineage plasticity and thus contribute to CNS regeneration; nevertheless, the electrophysiological properties of polydendrocytes and their fate after CNS injury have not been determined in detail.

In the present study, we examined the fate of polydendrocytes *in vivo* after focal ischemia using transgenic mice that express Cre under the control of the NG2 promoter. We performed complex immunohistochemical and electrophysiological analyses to determine the differentiation potential of polydendrocytes and the electrophysiological properties of the newly-derived cells after ischemia in adult mice.

Materials and Methods

Transgenic mice

All procedures involving the use of laboratory animals were performed in accordance with the European Communities Council Directive 24 November 1986 (86/609/EEC) and animal care guidelines approved by the Institute of Experimental Medicine ASCR Animal Care Committee. The generation of NG2creBAC transgenic mice, which express constitutively active Cre in NG2 cells, has been described previously [9]. NG2creBAC mice were crossed with the reporter mouse strain Z/EG to generate NG2creBAC:ZEG double transgenic mice. The mice carrying both modifications were selected by PCR. These double transgenic mice express Cre recombinase under the control of the mouse NG2 (Cspg4) promoter/enhancer. In the Cre recombinase-expressing cells, lacZ expression is replaced with EGFP expression, and these cells can be easily visualized and tracked. Since we detected no sex differences, both male and female mice were used in our experiments. All mouse strains were obtained from The Jackson Laboratory, Bar Harbor, USA.

Induction of distal middle cerebral artery occlusion (MCAo) in adult mice

Mice (60–90 days old) were anaesthetized for induction with 1.5% Isoflurane and maintained in 1% Isoflurane using a vaporizer (Tec-3, Cyprane Ltd., Keighley, UK). A skin incision between the orbit and the external auditory meatus was made. A 1–2 mm hole was drilled through the frontal bone 1 mm rostral to the fusion of the zygoma and the squamosal bone and about 3.5 mm ventral to the dorsal surface of the brain. The middle cerebral artery (MCA) was exposed after the dura was opened and removed. The MCA was occluded by short coagulation with bipolar tweezers at a proximal location, followed by transection of the vessel to ensure permanent disruption. The mice received 0.5 ml saline subcutaneously, and the body temperature during the surgery was maintained at $37\pm1^{\circ}C$ using a heating pad. Sham operated animals (controls) were subjected to same surgery procedure, without vessel occlusion. To visualize the ischemic region, unfixed brain slices were stained with 2% 2.3.5-triphenyltetrazolium chloride (TTC) at 37°C for 20 minutes.

Preparation of acute brain slices

The mice were deeply anaesthetized 3, 7 or 14 days after MCAo (3, 7, 14d MCAo) with pentobarbital (PTB) (100 mg/kg, i.p.) and perfused transcardially with cold (4–8°C) isolation solution containing (in mM): 110 NMDG-Cl, 2.5 KCl, 24.5 $NaHCO_3$, 1.25 Na_2HPO_4, 0.5 $CaCl_2$, 7 $MgCl_2$, 20 glucose, osmolality 290 mOsm/kg. The mice were decapitated, the brains were quickly dissected out and transversal 200 μm thick slices were cut using a vibration microtome (HM 650 V, Thermo Scientific Microm, Walldorf, Germany). The slices were incubated for 30 minutes at 34°C in the isolation solution and then held at room temperature in artificial cerebrospinal fluid solution (aCSF) containing (in mM): 122 NaCl, 3 KCl, 28 $NaHCO_3$, 1.25 Na_2HPO_4, 1.5 $CaCl_2$, 1.3 $MgCl_2$, 10 glucose, osmolality 305 mOsm/kg. Solutions were equilibrated with 95% O_2/5% CO_2 to a final pH of 7.4. Osmolality was measured using a vapor pressure osmometer (Vapro 5520, Wescor, Logan, UT, USA).

Electrophysiological recordings

Acute brain slices were transferred to a recording chamber mounted on the stage of an upright microscope (Axioscop, Zeiss, Gottingen, Germany) equipped with a high-resolution digital camera (AxioCam HRc, Zeiss, Germany) and electronic micromanipulators (Luigs & Neumann, Ratingen, Germany). The chamber was continuously perfused with oxygenated aCSF at a rate of 3 ml/min at $25\pm2^{\circ}C$. Electrophysiological recordings were performed using an EPC-10 patch-clamp amplifier in combination with PATCHMASTER software (HEKA Elektronik, Lambrecht/Pfalz, Germany). Recording pipettes with a tip resistance of ~10 MΩ were made from borosilicate capillaries (0.86 ID, Sutter Instruments Company, Novato, CA, USA) using a Brown-Flaming micropipette puller (P-97, Sutter Instruments). Electrodes were filled with an intracellular solution containing (in mM): 130 K-gluconate, 0.5 $CaCl_2$, 5 EGTA, 10 HEPES, 3 Mg-ATP and 0.3 Na-GTP; the final pH was adjusted to 7.2 with KOH. The resting membrane potential (RMP) was measured by switching the EPC-10 amplifier to the current-clamp mode. The membrane resistance (Rm) was calculated from the current elicited by a 10 mV test pulse depolarizing the cell membrane from the holding potential of −70 mV to −60 mV for 50 ms, 40 ms after the onset of the depolarizing pulse. Membrane capacitance (Cm) was determined automatically from the Lock-in protocol by PATCHMASTER. Clamping the cell membrane from the holding potential of −70 mV to values ranging from −160 mV to +40 mV for 50 ms at 10 mV intervals evoked membrane currents. To isolate the voltage-gated delayed outwardly rectifying K^+ (K_{DR}) current component, a voltage step from −70 to −60 mV was used to subtract time- and voltage-independent currents. To activate the K_{DR} currents only, the cells were held at −50 mV, and the amplitude of the K_{DR} currents was measured at +40 mV at the end of the pulse. The fast activating and inactivating outwardly-rectifying K^+ (K_A) current component was isolated by subtracting the current traces clamped at −110 mV from those clamped at −50 mV, and its amplitude was measured at the peak value. Tetrodotoxin- (TTX, Alomone Labs, Jerusalem, Israel) sensitive Na^+ currents were isolated by subtracting the current traces measured in 1 μM TTX-containing solution from those measured under control conditions. Na^+ currents amplitudes were measured at the peak value. Inwardly-rectifying K^+ (K_{IR}) currents were determined at −160 mV at the end of the pulse. Current densities (CD) were calculated by dividing the maximum current amplitudes by the corresponding Cm for each individual cell. The patch-clamp data analyses were performed using FITMASTER software (HEKA Elektronik, Lambrecht/Pfalz, Germany).

Immunohistochemistry and cell identification

The mice were deeply anaesthetized 3, 7, or 14 days after MCAo with PTB (100 mg/kg, i.p.) and perfused transcardially with 20 ml of saline followed by 20 ml of cooled 4% paraformaldehyde (PFA) in 0.1 M phosphate buffer (PB). Brains were dissected out, post-fixed for 2 hours and placed stepwise in solutions with gradually increasing sucrose concentrations (10%, 20%, 30%) for cryoprotection. Coronal, 30 μm thick slices were

prepared using a microtome (HM550, Microm International, Walldorf, Germany). For cell identification after patch-clamp recording, the measured cells were filled with Alexa Fluor 594 hydrazide (0.1 mM; Molecular Probes, Invitrogen, CA, USA) by dialyzing the cytoplasm with the patch pipette solution. Post-recording, the slices were fixed with 4% PFA in 0.1 M PB for 25 minutes and then kept at 4–8°C in phosphate-buffered saline (PBS). The slices were incubated with 5% Chemiblocker (Millipore, MA, USA) and 0.2% Triton in PBS. This blocking solution was also used as the diluent for the antisera. The slices were incubated with the primary antibodies at 4–8°C overnight, and the secondary antibodies were applied for 2 hours. The list of primary and secondary antibodies is summarized in Table 1. To visualize the cell nuclei, the slices were incubated with 300 nM 4, 6-diamidino-2-phenylindole (DAPI) in PBS for 5 minutes at room temperature and mounted using Aqua Poly/Mount (Polysciences Inc., Eppelheim, Germany). All chemicals were purchased from Sigma–Aldrich (St. Louis, MO, USA), unless otherwise stated.

A Zeiss 510DUO LSM confocal microscope equipped with Arg/HeNe lasers and 40× or 63× oil objectives was used for immunohistochemical analysis. Stacks of consecutive confocal images taken at intervals of 3 μm were acquired sequentially with two lasers to avoid cross-talk between fluorescent labels. The background noise of each confocal image was reduced by averaging four image inputs. For each image stack the gain and detector offset were adjusted to minimize saturated pixels, yet still permit the detection of weakly stained cell processes. Colocalization images and their maximum *z* projections were made using a Zeiss LSM Image Browser.

Table 1. Primary and secondary antibodies used for immunohistochemistry.

Antigen	Dilution	Isotype	Manufacturer	Secondary antibody
Aldh1	1:100	Mouse IgG	NeuroMab	GAM 594/660
APC	1:200	Mouse IgG	Calbiochem	GAM 594/660
Caspase-3	1:300	Mouse IgG	Alexis Biochem.	GAM 660
CD11b	1:200	Mouse IgG	Millipore	GAM 594
DCX	1:1000	Rabbit IgG	Abcam	GAR 594/660
GFAP	1:800	Mouse IgG	Sigma-Aldrich	Cy3 conjugated
GFP	1:800	Goat IgG	Abcam	FITC conjugated
GLAST	1:500	Rabbit IgG	Abcam	GAR 594/660
Ki-67	1:1000	Rabbit IgG	Abcam	GAR 594/660
Nestin	1:800	Mouse IgG	Millipore	GAM 594/660
Neun	1:100	Mouse IgG	Millipore	GAM 594
NG2	1:400	Rabbit IgG	Millipore	GAR 594/660
Olig-2	1:1000	Rabbit IgG	Millipore	GAR 660
Pax-6	1:300	Rabbit IgG	Covance	GAR 594
PCNA	1:500	Mouse IgG	Abcam	GAM 594
PDGFαR	1:200	Rabbit IgG	Santa Cruz	GAR 594/660
PDGFβR	1:200	Rabbit IgG	Santa Cruz	GAR 594/660
S100β	1:150	Mouse IgG	Sigma-Aldrich	GAM 660
Vimentin	1:1000	Mouse IgG	Abcam	GAM 594

Aldh1, aldehyde dehydrogenase–1; APC adenomatous polyposis coli; CD11b, integrin alpha M; DCX, doublecortin; GFAP, glial fibrillary acidic protein; GFP, green fluorescent protein; GLAST, glutamate/aspartate transporter; NG2, chondroitin sulfate proteoglycan; PCNA, proliferating cell nuclear antigen; PDGFαR, platelet-derived growth factor receptor alpha; PDGFβR, platelet-derived growth factor receptor beta; S100β, β-subunit of S100 calcium binding protein; GAR 594/660, goat anti-rabbit IgG conjugated with Alexa Fluor 594 or 660; GAM 594/660, goat anti-mouse IgG conjugated with Alexa Fluor 594 or 660 (all secondary antibodies from Invitrogen).
doi:10.1371/journal.pone.0036816.t001

Cell counts

To determine the fate of polydendrocytes in the peri-lesional cortex, confocal images (315 μm×315 μm×20 μm) covering the borders of the ischemic core were taken from brain coronal slices from control mice and from mice 3, 7 and 14 days after MCAo (5–7 animals from each group, 5 regions from one slice, bregma −1.2 mm) and stained for NG2, nestin, glial fibrillary acidic protein (GFAP), Ki-67 and doublecortin (DCX). The total number of EGFP positive ($EGFP^+$) cells and the number of cells that were double positive for EGFP and NG2, nestin, Ki-67, GFAP or DCX were counted in the cortex within the astrogliotic region. Between 1000 and 1500 $EGFP^+$ cells were scored. The number of cells was estimated from superimposed images using a GSA Image Analyzer v3.7.7 (Bansemer & Scheel GbR, Rostock, Germany) and expressed as the percentage of double-positive cells from the total number of $EGFP^+$ cells.

Statistics

The results are expressed as the mean ± SEM. Statistical analyses of the differences between groups were performed using one-way ANOVA for multiple comparisons with Dunnett's post-hoc test. Values of $p<0.05$ were considered significant (*), $p<0.01$ very significant (**) and $p<0.001$ extremely significant (***).

Results

Under physiological conditions EGFP expression is restricted to polydendrocytes and oligodendrocytes in the dorsal cortex of NG2creBAC:ZEG mice

To determine the fate of polydendrocytes *in vivo*, we used a transgenic mouse strain in which Cre recombinase is expressed under the control of the mouse NG2 promoter [9]. After crossing with Z/EG reporter mice, the NG2creBAC:ZEG mice exhibited widespread EGFP expression in a large population of cells in the brain and spinal cord. Polydendrocytes express NG2 and PDGFαR [14]; however, both proteins are downregulated immediately upon differentiation. Therefore, our approach enabled us to follow the fate of differentiating polydendrocytes based on their EGFP labeling.

To determine the phenotype of $EGFP^+$ cells in the adult brain, we performed a complex immunohistochemical analysis of brain coronal sections; first, we counted the total number of $EGFP^+$ cells in the dorsal part of the cortex of the control animals. We found 9892 ± 783 $EGFP^+$ cells per mm^3, which represented $4.1\%\pm0.3\%$ of all $DAPI^+$ cells. $EGFP^+$ cells could be divided into several morphological types. The first, most common morphological phenotype comprised cells with several highly branched processes and small round cell bodies, characteristics typical of polydendrocytes. These cells were predominantly positive for the polydendrocytic markers NG2 and PDGFαR (Fig. 1A, B). NG2 proteoglycan was uniformly expressed on the surface of the cell body and processes; however, staining for PDGFαR revealed its typical polarized expression [8]. EGFP was expressed in $89\%\pm2.3\%$ of $NG2^+$ cells throughout the brain, while $55.4\%\pm1.2\%$ of $EGFP^+$ cells expressed NG2 in the cortex of control mice, which is in agreement with previous studies performed on this mouse strain [9,15]. The lack of EGFP detection in approximately 11% of $NG2^+$ cells may have been caused by the lack of Cre expression or incomplete Cre-mediated

recombination in NG2$^+$ cells, or by the inadequate expression of the reporter driven by the promoter in Z/EG mice. NG2$^+$ cells are known to possess the highest proliferation rate in the adult mammalian brain, which was confirmed by immunostaining for Ki-67 (a nuclear cellular marker of proliferation). In the dorsal cortex, 3.7%±1.3% of EGFP$^+$ cells expressed Ki-67 and 20.6%±2.3% of EGFP$^+$ cells expressed PCNA, which is in agreement with previously published data [13,16]. This discrepancy between the numbers of Ki-67- and PCNA-positive EGFP$^+$ cells is probably caused by the longer-lasting stability of PCNA when compared to Ki-67 [17].

The second group of EGFP$^+$ cells displayed a typical oligodendrocyte morphology, with large, round cell bodies; they expressed the oligodendrocytic marker Adenomatous polyposis coli (APC, Fig. 1C) and represented 27.6±3.5% of the total number of EGFP$^+$ cells. The third group of EGFP$^+$ cells in the dorsal cortex had a morphology resembling that of pericytes and, accordingly, they expressed the marker of pericytes – platelet-derived growth factor beta receptor (PDGFβR) – on their cytoplasmatic membrane (Fig. S1A).

Since it has been shown that in some Cre transgenics a certain subpopulation of astrocytes can be EGFP$^+$ [11,18], we analyzed the dorsal cortex for the expression of several astrocytic markers. Nonetheless, we did not detect EGFP$^+$ cells expressing any astrocytic markers, such as GFAP, glutamate/aspartate transporter (GLAST) or aldehyde dehydrogenase-1 (Aldh1). However, a subpopulation of EGFP$^+$ cells expressed the β-subunit of S100 calcium binding protein (S100β, Fig. 1D). Since S100β is not a specific astrocytic marker and is expressed in astrocytes as well in polydendrocytes [10,19], we cannot describe these cells as astrocytes. Moreover, these EGFP$^+$/S100β$^+$ cells expressed NG2 and had the typical morphology of polydendrocytes (Fig. 1D), thus classifying them as polydendrocytes. Finally, we also tested whether some EGFP$^+$ cells expressed markers of microglia, but we never detected any EGFP$^+$ cells positive for integrin alpha M (CD11b) or Iba-1 (Fig. S1B) – commonly used markers of microglia. Based on our extensive immunohistochemical analysis of the uninjured adult dorsal cortex, we can conclude that the expression of EGFP is restricted only to polydendrocytes, oligodendrocytes and pericytes in adult NG2creBAC:ZEG double transgenic mice.

Increased proliferation of polydendrocytes in response to focal cerebral ischemia

To determine whether polydendrocytes in the dorsal cortex of adult mice display an extended differentiation potential in response to ischemic injury, we took advantage of NG2creBAC:-ZEG double transgenic mice to enable us to follow cells with NG2

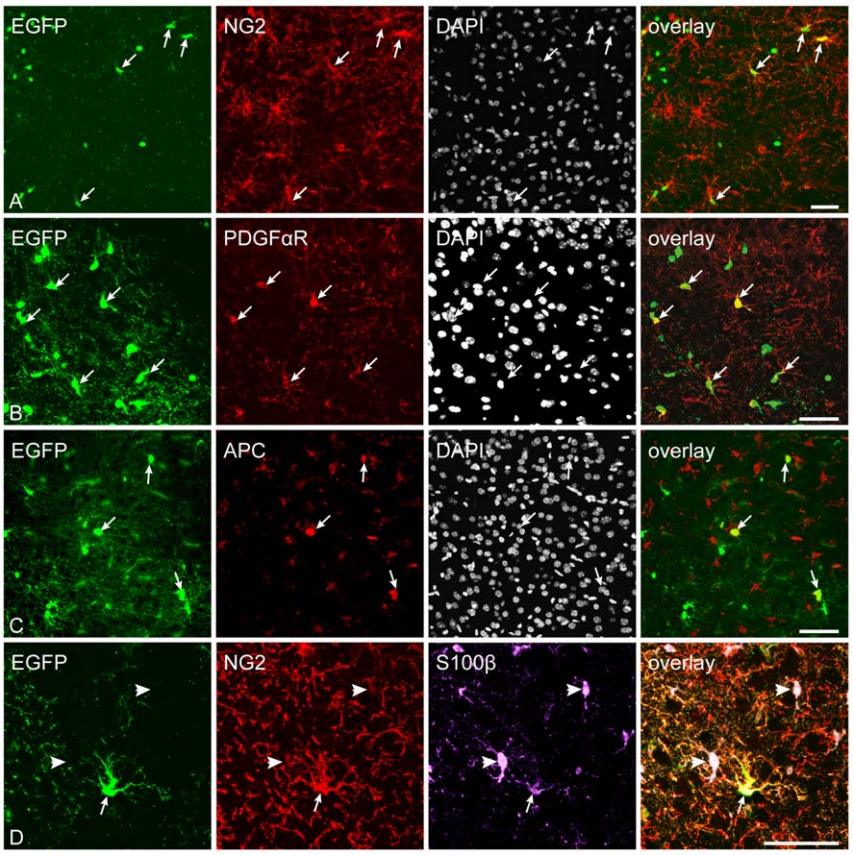

Figure 1. Enhanced green fluorescent protein (EGFP) expression is restricted to polydendrocytes and oligodendrocytes in the control dorsal cortex of NG2creBAC:ZEG mice. *A*, Immunostaining for NG2 proteoglycan in the cortex illustrating the high number of EGFP$^+$/NG2$^+$ cells. White arrows highlight several examples. *B*, The same population of EGFP$^+$ cells expressed platelet-derived growth factor alpha (PDGFαR) in a typical polarized pattern only in part of the processes. *C*, A subpopulation of EGFP$^+$ cells in the dorsal cortex expressed the oligodendrocyte lineage marker adenomatous polyposis coli (APC). *D*, Double immunohistochemistry revealed the co-expression of β-subunit of S100 calcium binding protein (S100β) with NG2 in EGFP$^+$ cells, which excludes S100β as a specific marker of astrocytes. The EGFP$^-$/NG2$^-$ cells are astrocytes (indicated by arrowheads). Scale bars, 50 μm.
doi:10.1371/journal.pone.0036816.g001

expression even after its loss. The same mouse strains were recently used in a study that described the differentiation of polydendrocytes after a stab wound injury [15] and simultaneously, this study confirmed the suitability of this mouse strain for use in these types of experiments. In contrast to this study we used a highly reproducible model of mouse MCAo with a minimal mortality rate and high reproducibility [20]. Three days after MCAo the ischemic lesion developed in the dorsal brain and occupied approximately one-third of the cortex in the left hemisphere (Fig. 2A). The necrotic tissue was surrounded by massive astrogliosis beginning 3 days after MCAo with a maximal intensity of GFAP staining 7 days after MCAo (Fig. 2B). The size of the ischemic lesion and the intensity of GFAP staining gradually decreased starting on the seventh day of ischemia, and 14 days after MCAo the lesion comprised approximately 25% of its original size.

Three days after MCAo the number, distribution and morphology of $EGFP^+$ cells were significantly changed at the lesion border (Fig. 3D–F) when compared to controls (Fig. 3A–C). $EGFP^+$ cells had larger cell bodies with a smaller number of processes, and their numbers significantly increased (24798 ± 1937 $EGFP^+$ cells/mm^3; $p<0.001$). The estimated number represented $9.8\%\pm0.6\%$ of all $DAPI^+$ cells and was approximately 2.5-fold higher than that found in controls (Fig. 4A2, C). At this time point only $36.0\%\pm2.9\%$ of $EGFP^+$ cells expressed NG2 (Fig. 3D, 4D), while in $19.6\%\pm1.5\%$ of $EGFP^+$ cells we detected the expression of nestin, which is an intermediate filament upregulated in immature proliferating glia [21] (Fig. 3E). The number of $EGFP^+$/$nestin^+$ cells was significantly increased when compared to controls (Fig. 4D; $p<0.001$). Furthermore, the number of proliferating cells, which were positive for Ki-67, significantly increased 3 days after MCAo (Fig. 3F), reaching $11.5\%\pm2.7\%$ of all $EGFP^+$ cells (Fig. 4D; $p<0.05$) and PCNA was expressed in $59.8\%\pm2.5\%$ of $EGFP^+$ cells (Fig. S2A). Since recent studies [22] have described the very rapid proliferation of polydendrocytes after injury, we also examined the number of proliferating $EGFP^+$ cells in the very early stage after MCAo. Two days after MCAo, 34.9% of $EGFP^+$ cells expressed Ki-67 and 75.5% of $EGFP^+$ cells expressed PCNA. Only in a few $EGFP^+$ cells (6 from 990 $EGFP^+$ cells) did we detect a very low expression of GFAP in the cell processes 3 days after MCAo.

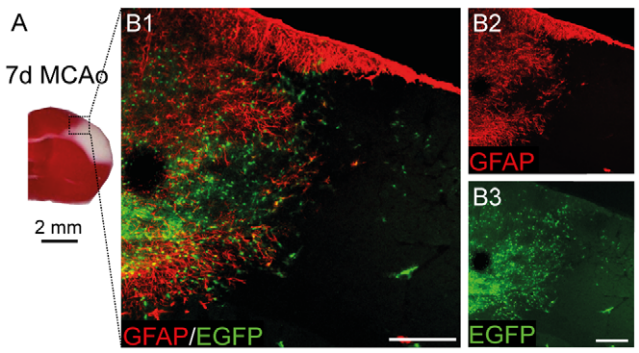

Figure 2. Focal cerebral ischemia leads to a marked increase in the number of $EGFP^+$ cells around the ischemic lesion 7 days after MCAo. ***A***, A coronal brain section stained with triphenyltetrazolium chloride indicates the volume of ischemic tissue (white color) 7 days after MCAo. The boxed area in ***A*** is shown in higher magnification in ***B***. ***B1–B2***, An overview image showing glial fibrillary acidic protein (GFAP) overexpression around the ischemic region. ***B3***, Typical localization and a high number of enhanced green fluorescent protein positive ($EGFP^+$) cells around the ischemic core 7 days after MCAo. Note that few $EGFP^+$ cells were found directly in the ischemic tissue. Scale bars, 50 μm.
doi:10.1371/journal.pone.0036816.g002

Collectively, 3 days after MCAo a large number of polydendrocytes expressed proliferative markers, which accords well with the higher number of $EGFP^+$ cells at the lesion borders. In addition, a large number of $EGFP^+$ cells appeared that did not express polydendrocytic markers, which might already indicate changes in their phenotype in response to ischemia.

Polydendrocytes differentiate into reactive astrocytes and neuronal precursor cells in the later stages after ischemia

To follow the fate of polydendrocytes and their progeny during the later stages of astrogliosis, we analyzed brains 7 days after MCAo. At this time point the number of $EGFP^+$ cells significantly increased when compared to controls. These $EGFP^+$ cells had a more complex morphology with multiple processes, and there was a sharp interface between the ischemic/necrotic and astrogliotic tissue. We counted 30555 ± 1355 $EGFP^+$ cells/mm^3, which represented $12.5\%\pm0.4\%$ of all $DAPI^+$ cells ($p<0.001$). This number was 3-fold higher than in controls (Fig. 4A3, C). However, only $25.4\%\pm1.2\%$ of these $EGFP^+$ cells expressed NG2 (Fig. 3G, 4D). Moreover, a large number of newly derived cells started to express proteins that are typical for cell types other than polydendrocytes or oligodendrocytes. Almost 17% ($16.8\%\pm1.6\%$) of $EGFP^+$ cells expressed high levels of GFAP in their processes (Fig. 3H, 4D, S2B), and these $GFAP^+$/$EGFP^+$ cells were localized in regions very close to the ischemic tissue or had even migrated directly into the ischemic core (Fig. 3H). These cells lacked the typical bushy protoplasmic morphology but resembled the morphology of reactive astrocytes, and some of them were positive for markers of reactive astrocytes, such as vimentin (data not shown). The expression of nestin in $EGFP^+$ cells declined 7 days after MCAo: $nestin^+$/$EGFP^+$ cells comprised $4.3\%\pm1.0\%$ of all $EGFP^+$ cells (Fig. 4D). However, nestin expression did not entirely correlate with GFAP staining in $EGFP^+$ cells and was still present in $EGFP^+$/$NG2^+$ cells. Furthermore, a small subpopulation of $GFAP^+$/$EGFP^+$ cells expressed Ki-67 (Fig. S2C) while in total $8.8\%\pm2.1\%$ of $EGFP^+$ cells were positive for this marker (Fig. 4D).

Since it has been demonstrated previously that polydendrocytes can give rise to neurons *in vitro* and after their transplantation into the hippocampus [7,23], we examined $EGFP^+$ cells for the expression of DCX, a marker of newly derived neurons and neuroblasts. Surprisingly, we found that almost $5.0\%\pm1.9\%$ of $EGFP^+$ cells (Fig. 4D) expressed DCX 7 days after MCAo. The expression of DCX was localized in the cell bodies as well as in the short processes (Fig. 3I, S2D). Additionally, we also found the expression of the transcription factor Pax-6 in several $EGFP^+$ cells 3 and 7 days after MCAo (Fig. S3A). This transcription factor is known to drive glial cells to adopt a neuronal phenotype [24]. To exclude the possibility that DCX^+/$EGFP^+$ cells in the ischemic border might originate from the neurogenic region in the subventricular zone (SVZ), we also analyzed in detail the expression of EGFP in this area. In agreement with previously published studies [10,25], we never observed the co-expression of EGFP with other than polydendrocytic markers in the SVZ and, moreover, the density of $EGFP^+$ cells in the lateral part of the SVZ was lower than in the surrounding nervous tissue (Fig. 3C). Moreover, we also tested if $EGFP^+$ cells expressed some markers of reactive microglia after MCAo; however, we never detected any expression of CD11b (Fig. S3B) or Iba-1 in $EGFP^+$ cells (Fig. S3C).

Further analyses of ischemic brains 14 days after MCAo revealed that the number of $EGFP^+$ cells was still significantly

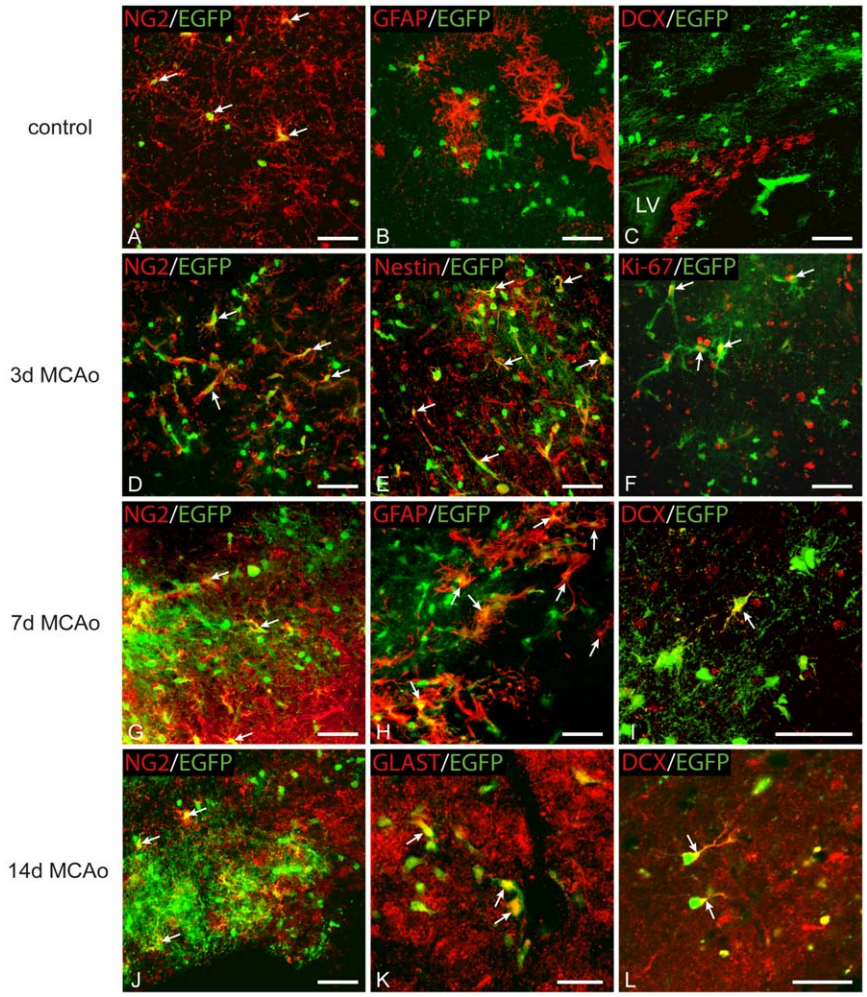

Figure 3. Enhanced green fluorescent protein positive (EGFP$^+$) cells express markers of astrocytes and neuronal precursor cells in the dorsal cortex after ischemia. ***A***, EGFP$^+$ cells in sham-operated mice (control) expressed a high level of NG2 proteoglycan in the majority of processes. White arrows highlight several examples. ***B***, Virtually no EGFP$^+$ cells in the dorsal control cortex were positive for glial fibrillary acidic protein (GFAP). ***C***, Low density of EGFP$^+$ cells in the subventricular zone (SVZ). EGFP$^+$ cells were never labeled for doublecortin (DCX) in the SVZ of control brains or those after ischemia, which indicates the absence of polydendrocytes from the process of adult neurogenesis; LV, lateral ventricle. ***D***, Three days after MCAo the number of EGFP$^+$ cells is significantly increased when compared to controls. Moreover, a large number of EGFP$^+$ cells expressed markers of proliferating cells – nestin (***E***) and Ki-67 (***F***). ***G***, EGFP$^+$ cells were present at high density seven days after MCAo; however, only a small subpopulation of them expressed NG2 proteoglycan. ***H***, Some EGFP$^+$ cells were positive for the astrocytic marker GFAP. ***I***, Starting 7 days after MCAo some scattered cells expressed DCX in their cell bodies and processes. ***J***, Fourteen days after MCAo only a small subpopulation of EGFP$^+$ cells expressed NG2 proteoglycan. ***K***, EGFP$^+$ cells expressing glutamate/aspartate transporter (GLAST), a marker of mature astrocytes. ***L***, A subpopulation of EGFP$^+$ cells displaying polarized and highly developed processes, which were positive for DCX. Scale bars, 50 μm.
doi:10.1371/journal.pone.0036816.g003

enhanced when compared to controls (26199 ± 1763 cells/mm^3) and that they represented $9.3\% \pm 0.4\%$ of all DAPI$^+$ cells (Fig. 4A4, C; $p<0.001$). Immunohistochemical staining for NG2 revealed its high expression at the lesion border, but only $26.5\% \pm 2.8\%$ of EGFP$^+$ cells expressed this proteoglycan (Fig. 3J). The number of GFAP$^+$/EGFP$^+$ cells was slightly decreased compared to 7 days after MCAo, but still $13.7\% \pm 1.2\%$ of EGFP$^+$ cells expressed GFAP (Fig. 4D). Furthermore, these cells seemed to have a more developed phenotype, based on their strong expression of the astrocyte-specific marker GLAST (Fig. 3K). The number of proliferating EGFP$^+$ cells declined and reached the proliferation rate of the controls, and only $1.2\% \pm 0.4\%$ of EGFP$^+$ cells expressed nestin (Fig. 4D). On the other hand, we still detected a large number of DCX$^+$/EGFP$^+$ cells comprising $8.9\% \pm 1.6\%$ of all EGFP$^+$ cells (Fig. 4D). Concurrently, in these cells immunohistochemistry revealed the localization of DCX protein predominantly in the processes, which were more developed than those observed 7 days after MCAo (Fig. 3L).

In brain sections obtained one month after MCAo we detected only rarely the co-expression of EGFP with markers of mature neurons. There were only a few EGFP$^+$/NeuN$^+$ cells in the vicinity of the ischemic lesion (data not shown); however, we also found several DCX$^+$/EGFP$^+$ cells expressing the apoptotic marker caspase-3 (Fig. S3D).

In addition, we examined brain sections from all time points for the oligodendrocytic marker APC; however, the number of APC$^+$/EGFP$^+$ cells was very low in the proximity of the ischemic region, therefore immunohistochemical quantification was not carried out.

In summary, a detailed analysis of the ischemic border between 7 and 30 days after MCAo revealed that polydendrocytes can contribute to the generation of reactive astrocytes and, moreover,

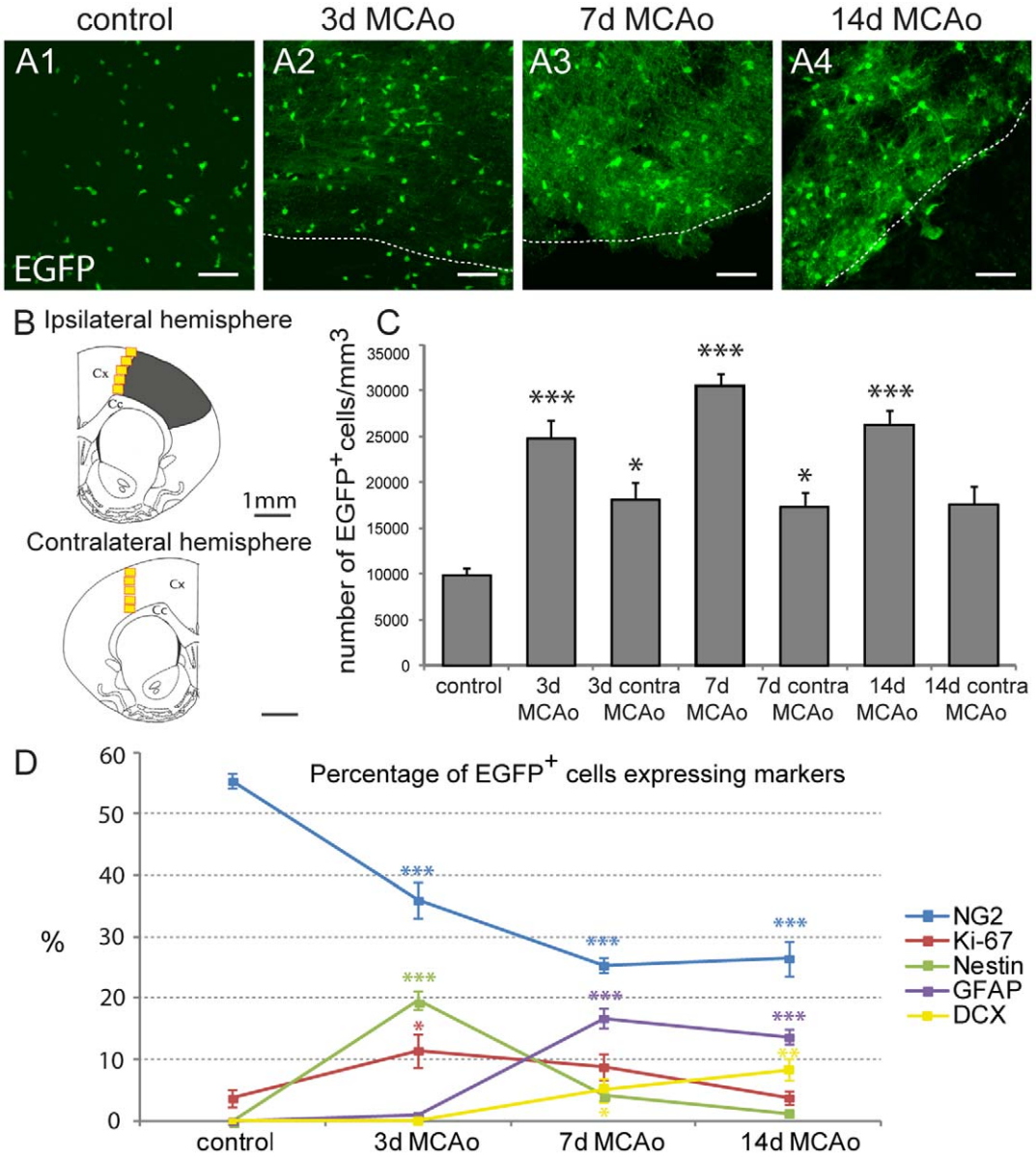

Figure 4. Quantification of the changes in the number of enhanced green fluorescent protein positive (EGFP$^+$) cells and in the expression of markers typical for glia, neurons and proliferating cells evoked by MCAo. ***A***, Brain sections showing the increasing number and different distribution of EGFP$^+$ cells 3, 7 and 14 days after MCAo (***A2, A3, A4***) when compared to controls (***A1***). Borders of the ischemic tissue are highlighted with the dashed lines. Scale bars, 50 μm. ***B***, Schematic figure of coronal slices of the ipsilateral and contralateral hemispheres depicting the size and localization of tissue injury 7 days after MCAo (grey region), together with the highlighted regions used for immunohistochemical quantification (yellow squares) in both hemispheres; Cx, cortex; Cc, corpus callosum. ***C***, Bar graph showing the quantification of EGFP$^+$ cell numbers per 1 mm^3 in the ipsilateral and contralateral hemispheres in control mice and after MCAo. ***D***, Graph showing the percentage of EGFP$^+$ cells expressing markers of polydendrocytes (NG2), proliferating cells (Ki-67, nestin), astrocytes (glial fibrillary acidic protein, GFAP) and neuronal precursor cells (doublecortin, DCX) in controls and after MCAo. Asterisks indicate significant differences between control cortex and post-ischemic cortex; *, $p<0.05$; ***, $p<0.001$.
doi:10.1371/journal.pone.0036816.g004

they can differentiate into a transient population of immature neuronal precursor cells, probably due to the influence of growth factors near the ischemic tissue.

Polydendrocytes do not change phenotype in the contralateral hemisphere of ischemic animals

Concurrently, we examined the contralateral uninjured hemisphere for the number of EGFP$^+$ cells and the expression of the studied markers at all time points after MCAo. Three days after MCAo we found 18066±1951 EGFP$^+$ cells/mm^3, which represented 7.3%±0.8% of all DAPI$^+$ cells in the dorsal contralateral cortex. This number was significantly higher compared to controls, and the increased quantity of EGFP$^+$ cells was maintained 7 days after MCAo as well (Fig. 4C; $p<0.05$). To determine the phenotype of the EGFP$^+$ cells in the contralateral hemisphere, we analyzed the brain sections for all of the studied markers. We found no significant changes in the expression of cell type-specific markers in EGFP$^+$ cells compared to controls with

the exception of proliferation markers (Ki-67, PCNA, nestin). We found that Ki-67 was expressed by 9.2±2.8% of all EGFP$^+$ cells 3 days after MCAo, which was a significantly higher percentage than that found in controls ($p<0.05$). Interestingly another proliferation marker, PCNA, was expressed by 51.9% of EGFP$^+$ cells. Moreover, some EGFP$^+$ cells expressing low levels of nestin were found in the contralateral hemisphere 3 days after MCAo (data not shown).

Polydendrocytes respond to ischemia with significant changes in their electrophysiological properties

Based on immunohistochemical staining, we found that polydendrocytes, besides their self-renewal, give rise to a large population of astrocytes, but also to neuronal precursor cells. Next, we were interested to determine what electrophysiological properties polydendrocytes and their progeny display after MCAo.

Using the patch-clamp technique in the whole cell configuration, we initially determined the electrophysiological phenotype of EGFP$^+$ cells in control brains. Intracellular staining with a fluorescent dye revealed that many EGFP$^+$ cells had several radially oriented primary and secondary processes, resembling the multi-process morphology typical of polydendrocytes, as described previously [26]. Post-recording immunohistochemical analysis confirmed that these EGFP$^+$ cells are positive for PDGFαR and NG2 (Fig. 5a1). In agreement with previous findings [27], we never observed dye-coupling between individual NG2$^+$/EGFP$^+$ cells in controls or after MCAo. As expected, electrophysiological recordings revealed a complex current pattern typical of a polydendrocytic population, i.e., they displayed time- and voltage-independent K^+ conductance together with K_{DR}, K_A and K_{IR} currents in controls [28] (Fig. 5A). Their average RMP was −77.5±1.3 mV (n = 22), Rm was 121.1±10.7 MΩ and Cm was 9.5±0.8 pF. Current densities were 17.5±6.5 pA/pF for K_{IR} currents, 8.1±2.3 pA/pF for K_{DR} currents and 12.4±3.0 pA/pF for K_A currents (Table 2.). Cells displaying a complex current pattern represented 81.5%±9.9% of all measured EGFP$^+$ cells in the control cortex (Fig. 6E).

After MCAo we found EGFP$^+$ cells with a complex current pattern at all studied time points; however, their number, passive membrane properties and current densities were markedly changed when compared to controls. Three days after MCAo EGFP$^+$ cells displaying a complex current pattern had a significantly increased Rm ($p<0.01$), which accords well with the significantly decreased CD of K_{IR} currents and time- and voltage-independent K^+ conductance when compared to controls (Table 2.; $p<0.01$). On the other hand, the CD of K_{DR} currents was significantly increased when compared to controls ($p<0.001$). These changes in the membrane properties have been shown to reflect the high proliferative activity of polydendrocytes soon after ischemia [13,29], which is also in good correlation with the increased expression of Ki-67 and nestin in EGFP$^+$ cells 3 days after ischemia. Interestingly, in this early phase after ischemia we also detected TTX-sensitive Na^+ currents with a low CD of 3.6±1.3 pA/pF in these cells (8 from 35 cells, Fig. 6A); their presence probably contributed to the significantly depolarized RMP when compared to controls ($p<0.05$) [13,27]. Since Na^+ currents in grey matter polydendrocytes are detected predominately in the early postnatal stages [27], we might conclude that polydendrocytes early after ischemia resemble the immature developing stages of polydendrocytes [23]. Post-recording immunohistochemical identification 3 days after MCAo revealed their positivity for NG2 and nestin (Fig. 6a1). Seven days after MCAo the percentage of EGFP$^+$ cells with a complex current pattern had significantly decreased to 23.4%±6.9% ($p<0.001$) (Fig. 6E). These

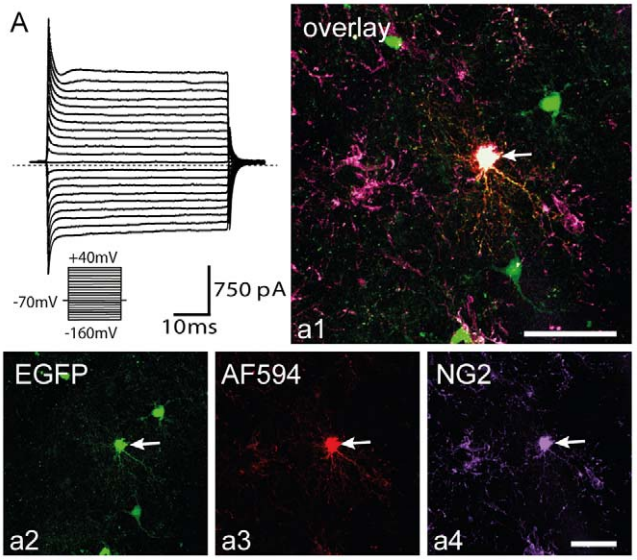

Figure 5. Enhanced green fluorescent protein positive (EGFP$^+$) cells in the cortex of sham-operated mice are NG2$^+$ polydendrocytes displaying a complex current pattern. ***A***, Polydendrocytic current pattern in controls measured after depolarizing the cell membrane from a holding potential of −70 mV to +40 mV and hyperpolarizing to −160 mV (see the inset, bottom). Polydendrocytes showed a complex current pattern, i.e., time- and voltage-independent K^+ currents, K_{DR}, K_A and K_{IR} currents. The dashed line marks zero current. ***a1–a4***, Polydendrocyte expressing EGFP in control cortex (***a2***), loaded with Alexa Fluor 594 hydrazid during patch-clamp measurement (***a3***), subsequently stained with an antibody directed against NG2 proteoglycan (***a4***). Scale bars, 50 µm.
doi:10.1371/journal.pone.0036816.g005

cells were depolarized and, moreover, they had significant increased CD of K_{DR} currents when compared to controls ($p<0.001$). Fourteen days after MCAo we found a further significant decrease in the quantity of the EGFP$^+$ cells with a complex current pattern when compared to controls. Only 20.9%±6.1% ($p<0.001$) of all measured EGFP$^+$ cells revealed a complex current pattern (Fig. 6E). These cells had a significantly depolarized RMP ($p<0.05$), but no other significant differences in their membrane properties were found when compared to controls. These cells always expressed only polydendrocytic markers, such as NG2 and PDGFαR, 7 and 14 days after MCAo.

Taken together, our electrophysiological analyses of polydendrocytes during the post-ischemic period revealed significant changes in their membrane properties 3 days after MCAo that coincided with their increased proliferation and their declining incidence 7 and 14 days after MCAo.

Polydendrocytes differentiate into cells with the functional properties of astrocytes after ischemia

During the post-ischemic period a subpopulation of EGFP$^+$ cells displayed a current profile with predominant high time- and voltage-independent non-decaying K^+ conductance, a so-called passive current pattern (Fig. 6B). These cells were detected in all post-ischemic periods, and their passive membrane properties as well as their current densities did not significantly differ at the studied time points after MCAo (Table 3.). Fourteen days after MCAo these cells had an RMP of −47.5±1.0 mV, Rm was 135.3±8.0 MΩ and Cm reached 7.5±0.6 pF (n = 33). The current density reached 0.5±0.3 pA/pF for K_{IR} and 8.0±3.3 pA/pF for K_{DR} currents, which was completely blocked

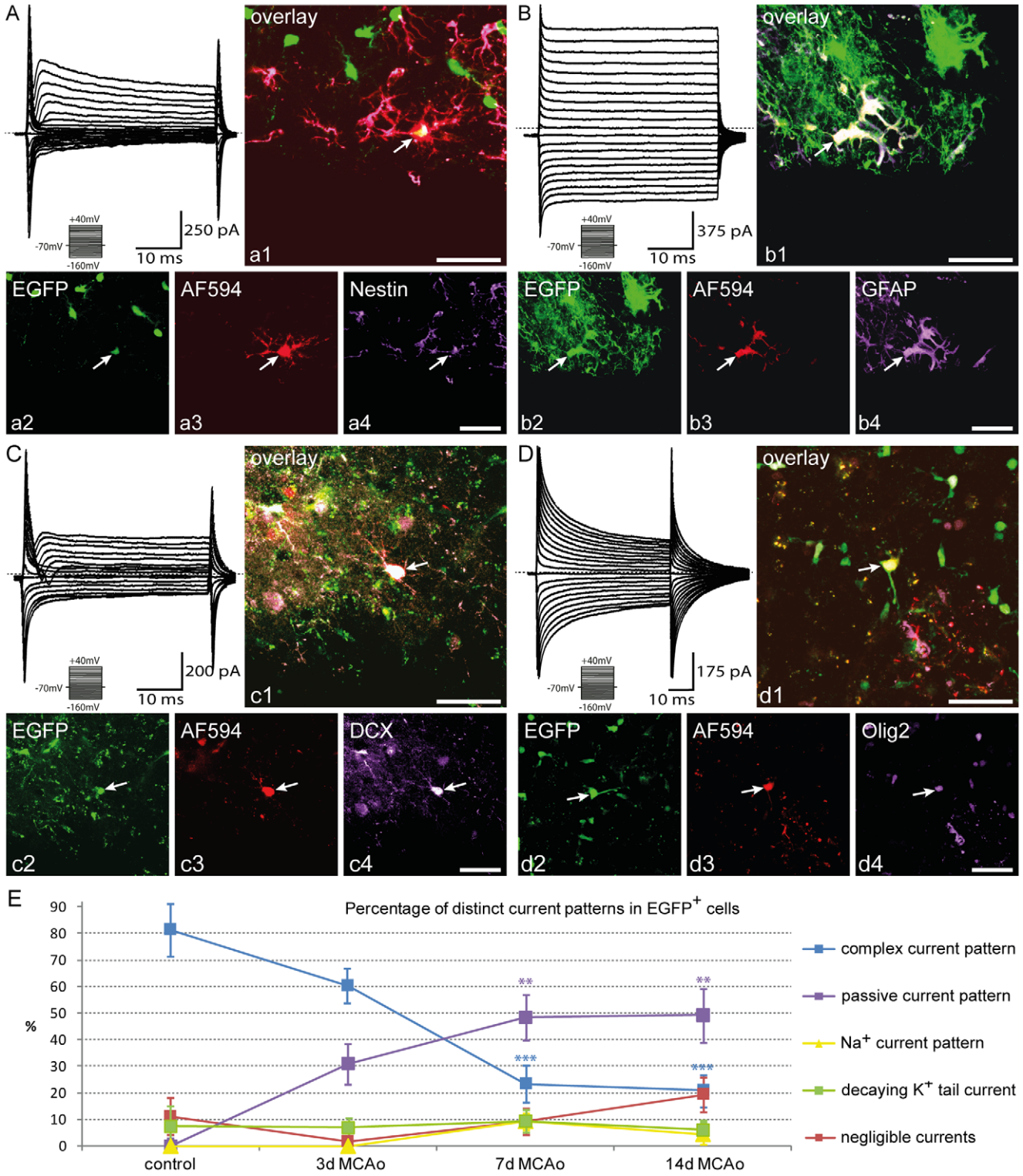

Figure 6. Polydendrocytes differentiate into cells with distinct current patterns after MCAo. ***A***, A typical current pattern of polydendrocytes measured 3 days after MCAo in response to cell membrane depolarization from a holding potential of −70 mV to +40 mV and hyperpolarization to −160 mV (see the inset, bottom). Polydendrocytes showed a current pattern with K_{DR}, K_A, small K_{IR} currents and fast activating Na^+ inward currents in a few cells 3 days after MCAo. Zero current is marked by the dashed line. ***a1–a4***, Polydendrocyte expressing enhanced green fluorescent protein (EGFP) 3 days after MCAo (***a2***) loaded with Alexa Fluor 594 hydrazid during patch-clamp measurement (***a3***) subsequently stained with an antibody directed against nestin (***a4***). White arrow indicates the recorded cell. Scale bars, 50 μm. ***B***, Current pattern of $EGFP^+$ astrocytes 7 days after MCAo recorded using the same protocol as in (***A***). $EGFP^+$ astrocytes showed a passive current pattern, i.e., time- and voltage-independent non-decaying K^+ currents, with only small voltage activated K^+ currents. Zero current is marked by the dashed line. ***b1–b4***, Astrocytes expressing EGFP 7 days after MCAo (***b2***) loaded with Alexa Fluor 594 hydrazid during patch-clamp measurement (***b3***), subsequently stained with an antibody directed against glial fibrillary acidic protein (GFAP, ***b4***), a marker of astrocytes. Note dye coupling (b3) between $EGFP^+$ cells with a passive current pattern

compared to EFGP$^+$ cells with a complex current pattern in A (a3). Scale bars, 50 μm. ***C***, Current pattern of EGFP$^+$ neuronal precursor cells 7 days after MCAo measured with the same protocol as in (***A***). EGFP$^+$ neuronal precursor cells displayed outwardly rectifying K^+ currents (K_{DR}, K_A currents) together with higher Na^+ currents when compared to polydendrocytes. ***c1–c4***, Neuronal precursor cells expressing EGFP 7 days after MCAo (***c2***), loaded with Alexa Fluor 594 hydrazid during patch-clamp measurement (***c3***), subsequently stained with an antibody directed against doublecortin (DCX, ***c4***), a marker of newly-derived neuronal precursor cells. Scale bars, 50 μm. ***D***, Current pattern of EGFP$^+$ oligodendrocytes 7 days after MCAo measured with the same protocol as in (***A***). EGFP$^+$ oligodendrocytes displayed time- and voltage-independent K^+ currents decaying during the duration of the voltage pulse. ***d1–d4***, Oligodendrocytes expressing EGFP 7 days after MCAo (***d2***) loaded with Alexa Fluor 594 hydrazid during patch-clamp measurement (***d3***), subsequently stained with an antibody directed against Olig2 (***d4***). **E**, Graph showing the percentage of EGFP$^+$ cell with distinct current patterns. Asterisks indicate significant differences between control cortex and post-ischemic cortex; **, $p<0.01$; ***, p<0,001.
doi:10.1371/journal.pone.0036816.g006

by 1 mM 4-aminopyridine (4-AP). We found significant differences in the percentage of these cells in the post-ischemic periods. EGFP$^+$ cells with a passive current pattern were never detected in controls, and their distribution increased with time after ischemia. Their number was significantly increased 7 and 14 days after MCAo when compared to controls; they represented 48.4%±8.5% ($p<0.01$) and 49.3%±10.2% ($p<0.01$), respectively, of all measured cells (Fig. 6E). Some of them expressed nestin, Ki-67 or GFAP 3 days after MCAo; however, in the later phases after MCAo only GFAP (Fig. 6b1) or GLAST were detected by immunohistochemical post-recording identification. Starting 7 days after MCAo intracellular staining with a fluorescent dye showed that some EGFP$^+$ cells with a passive current pattern were dye-coupled to other EGFP$^+$ or EGFP$^-$ cells (Fig. 6b3). We can conclude that a certain subpopulation of newly-derived cells of polydendrocyte origin expresses astrocytic markers and these cells also display membrane properties typical of reactive astrocytes.

Polydendrocytes also differentiate into cells with the functional properties of immature neuronal precursor cells after ischemia

In agreement with our immunohistochemical analysis, we also detected a subpopulation of EGFP$^+$ cells that expressed a current profile that resembled that of neuronal precursor cells (Fig. 6c). These cells were detected 7 and 14 days after MCAo, and their passive membrane properties as well as the current densities of their voltage activated channels did not significantly differ between these two time points. Seven days after MCAo these cells had an RMP about −58.2±5.0 mV, their Rm was 840.4±144.9 MΩ and Cm was 5.2±0.9 pF (n = 6). The current densities reached 1.3±1.3 pA/pF for K_{IR} currents, 34.7±6.0 pA/pF for K_{DR} currents and 17.9±2.0 pA/pF for K_A currents. These cells also expressed TTX-sensitive Na^+ currents, but with a significantly higher CD (39.5±10.2 pA/pF, $p<0.01$) (Table 4.) and clearly different kinetics when compared to polydendrocytes with Na^+ currents 3 days after MCAo. The Na^+ currents in neuronal precursor cells displayed significantly faster activation after depolarization steps when compared to Na^+ currents in polydendrocytes and, in addition, these currents were activated at a significantly lower voltage threshold (−18.0±5.8 mV) than in polydendrocytes (2.9±4.2 mV, $p<0.05$). The percentage of neuronal precursor cells reached 9.4%±3.1% of all measured cells 7 days after MCAo and 4.5%±4.0% 14 days after MCAo (Fig. 6E). Post-recording immunohistochemical identification confirmed DCX expression in EGFP$^+$ neuronal precursor cells (Fig. 6c1).

Table 2. Electrophysiological properties of EGFP$^+$ cells with a complex current pattern.

	Control	3 d MCAo	7 d MCAo	14 d MCAo
RMP (mV)	−77.5±1.3	−69.5±2.1 (*)	−59.5±5.2 (***)	−65.2±3.1 (*)
Rm (MΩ)	121.1±10.7	525.3±88.4 (**)	372.7±42.5	309.3±39.7
Cm (pF)	9.5±0.8	8.9±0.8	7.2±0.9	8.8±1.3
K_{IR} (pA/pF)	17.5±6.5	3.3±0.8 (**)	9.6±1.3	7.0±1.3
K_{DR} (pA/pF)	8.1±2.3	29.6±3.4 (***)	31.2±3.6 (***)	8.3±1.9
K_A (pA/pF)	12.4±3.0	14.7±2.1	11.7±3.0	14.6±3.4
Na (pA/pF)	0.0±0.0	3.5±1.3 (*)	0.0±0.0	0.0±0.0
n	22	35	15	14
%	81.0±9.9	60.0±6.6	23.4±6.9 (***)	20.9±6.1 (***)

RMP, resting membrane potential; Rm, membrane resistance; Cm, membrane capacitance; K_{IR}, current density of inwardly-rectifying K^+ currents; K_{DR}, current density of voltage-gated delayed outwardly-rectifying K^+ currents; K_A, current density of the fast activating and inactivating outwardly-rectifying K^+ currents; Na, current density of Na^+ currents; n, number of measured cells; %, percentage of the cell type;
*, $p<0.05$;
**, $p<0.01$;
***, $p<0.001$.
doi:10.1371/journal.pone.0036816.t002

After ischemia only a small population of oligodendrocytes in the cortex arises from polydendrocytes

Furthermore, in some EGFP$^+$ cells we have recorded time- and voltage-independent K^+ currents decaying during the duration of the voltage pulse, a typical current pattern of oligodendrocytes [30] (Fig. 6D). These cells were present at all analyzed time points, and their electrophysiological properties and quantity did not significantly change after MCAo when compared to controls (Fig. 6E). Seven days after MCAo they had an RMP of −54.5±4.9 mV, Rm was 815.8±120.6 MΩ and Cm was 9.8±3.9 pF (n = 6). The current densities reached 4.4±4.4 pA/pF for K_{IR} currents, 11.6±5.2 pA/pF for K_{DR} currents and 6.5±3.6 pA/pF for K_A currents. These cells were positive for APC or Olig2 (Fig. 6d1) as revealed by post-recording immunohistochemical identification.

Certain subpopulation of EGFP$^+$ cells in the ischemic cortex are pericytes

Finally, the last identified subpopulation based on electrophysiological properties comprised cells with negligible voltage activated or time- and voltage-independent K^+ currents and was present in both control and post-ischemic brains. These cells did not significantly differ in their electrophysiological properties or quantity (Fig. 6E) at any studied time points. Post-recording immunohistochemical identification showed that they did not express common neuronal or glial markers; however, we were able to occasionally detect PDGFβR expression on their surface, which classified them as pericytes.

Table 3. Electrophysiological properties of EGFP$^+$ cells with a passive current pattern.

	3 d MCAo	7 d MCAo	14 d MCAo
RMP (mV)	−56.0±4.4	−52.8±2.7	−47.5±1.0
Rm (MΩ)	165.0±13.0	168.4±8.3	135.3±8.0
Cm (pF)	8.4±0.9	9.7±1.6	7.5±0.6
K_{IR} (pA/pF)	2.7±1.3	2.8±1.1	0.5±0.3
K_{DR} (pA/pF)	10.5±3.0	9.0±1.9	8.0±3.3
K_A (pA/pF)	0.0±0.0	0.0±0.0	0.0±0.0
Na (pA/pF)	0.0±0.0	0.0±0.0	0.0±0.0
n	18	31	33
%	31.0±7.6	48.4±8.5	49.3±10.2

RMP, resting membrane potential; Rm, membrane resistance; Cm, membrane capacitance; K_{IR}, current density of inwardly-rectifying K^+ currents; K_{DR}, current density of voltage-gated delayed outwardly-rectifying K^+ currents; K_A, current density of the fast activating and inactivating outwardly-rectifying K^+ currents; Na, current density of Na^+ currents; n, number of measured cells; %, percentage of the cell type.

doi:10.1371/journal.pone.0036816.t003

Discussion

In the present study, we used mice with constitutively active Cre driven by the NG2-promoter that, after breeding with a reporter strain, allow fate mapping of a large population of polydendrocytes. In accordance with previous studies [10], we detected the generation of oligodendrocytes in the uninjured adult brain; however, in contradiction to some earlier reports [9,18], our study did not confirm the generation of astrocytes and therefore excludes polydendrocytes as multipotent cells in the healthy adult brain.

After detailed characterization of the phenotype of EGFP$^+$ cells in the healthy brain, the mice were subjected to focal cerebral ischemia, which triggered dramatic changes in the morphology, number and phenotype of EGFP$^+$ cells. The number of EGFP$^+$ cells after ischemia was significantly increased; the cells displayed heterogeneous morphology and expressed markers of astrocytes and neuronal precursor cells. Moreover, polydendrocyte multipotency was confirmed by detailed electrophysiological analysis, which also proved the generation of astrocytic and neuronal precursor phenotypes from EGFP$^+$ cells after ischemia.

Polydendrocytes are unipotent cells in the healthy adult brain

A number of recent studies have shown the importance of selecting an appropriate polydendrocytic marker as a Cre promoter. In our study we used NG2, as a generally accepted marker of polydendrocytes and, moreover, this proteoglycan is not down-regulated after injury as in the case of PDGFαR [12]. Although NG2 and PDGFαR are strongly co-expressed in control cells, more distinct polydendrocytic subpopulations can arise after ischemia.

We used the NG2creBAC mice strain with constitutively active Cre expression and a high recombination rate, in which a large polydendrocyte population and their progeny express EGFP. This enabled us to analyze a larger sample of EGFP$^+$ cells before and after ischemia than in mice with an inducible form of Cre with low recombination efficiency. Although inducible Cre brings the advantage of labeling a cohort of cells with a currently expressed marker, our analysis proved that we had a well characterized cell population clearly restricted to only polydendrocytes, oligodendrocytes and pericytes before ischemia in the adult cortex. Polydendrocytes expressing NG2 and EGFP displayed immunocytochemical and electrophysiological properties that suggested the absence of any additional subpopulations of polydendrocytes in the adult cortex. This finding is in agreement with study [31], where was detected a uniform population of polydendrocytes in the adult hippocampus.

Polydendrocytes respond to ischemia by increased proliferation

After ischemia we detected a significantly increased number of EGFP$^+$ cells on the ischemic lesion edge at all studied time points, a phenomenon already described after a stab wound [11,15], cryoinjury [32], in experimental autoimmune encephalomyelitis [33] or focal demyelination [34]. Based on the extensive proliferation of polydendrocytes in the early stages after injury (a 3-fold higher number of Ki-67$^+$/EGFP$^+$ cells and a 2.9-fold higher number of PCNA$^+$/EGFP$^+$ cells 3 days after MCAo when compared to controls), we assume that this increased number of EGFP$^+$ cells is caused by the generation of new EGFP$^+$ cells from existing polydendrocytes. However, we cannot entirely exclude polydendrocyte migration from the surrounding tissue to the site of injury. Another eventuality is that other cell types began to transiently express NG2, as was shown, for example, in the case of microglia cells. Although several recent studies have reported the low expression of NG2 in resting microglia, we never detected EGFP in these CD11b$^+$/Iba-1$^+$ cells in the control brain [35]. Moreover, the transiently increased expression of NG2 has been shown in activated microglia cells after several types of injury [35–37]; on the other hand, other studies exclude the possibility of NG2 expression in these cells [31,38,39]. In our study, we never detected EGFP$^+$ cells that displayed any microglial immunohistochemical or electrophysiological properties at any studied time point after MCAo. This phenomenon indicates that microglia cells after injury really do not activate the NG2 promoter or that a weak or short, transient activation of the CSPG4 promotor in the adult brain is not sufficient to trigger the expression of EGFP in other cells types, thus confirming that newly-derived EGFP$^+$ cells originate from pre-ischemic EGFP$^+$ cells.

Table 4. Electrophysiological properties of EGFP$^+$ neuronal precursor cells.

	7 d MCAo	14 d MCAo
RMP (mV)	−58.2±5.0	−62.7±9.3
Rm (MΩ)	840.4±144.9	1189.7±631.9
Cm (pF)	5.2±0.9	6.9±0.9
K_{IR} (pA/pF)	1.3±1.3	0.0±0.0
K_{DR} (pA/pF)	34.70±6.0	46.1±5.8
K_A (pA/pF)	17.9±2.0	15.7±2.5
Na (pA/pF)	39.5±10.2	21.5±12.0
n	6	3
%	9.4±3.1	4.5±4.1

RMP, resting membrane potential; Rm, membrane resistance; Cm, membrane capacitance; K_{IR}, current density of inwardly-rectifying K^+ currents; K_{DR}, current density of voltage-gated delayed outwardly-rectifying K^+ currents; K_A, current density of the fast activating and inactivating outwardly-rectifying K^+ currents; Na, current density of Na^+ currents; n, number of measured cells; %, percentage of the cell type.

doi:10.1371/journal.pone.0036816.t004

Immunohistochemical analysis showed an increased amount of NG2 at the lesion site in the later phases after ischemia, which accords well with previously published results [40]; however, the total number of $EGFP^+$ cells with detectable NG2 expression decreased. This phenomenon can be explained by the increased release of soluble NG2 form from many cell types into the extracellular space [40] and, concurrently, by differentiating of $NG2^+$ polydendrocytes into another cell type.

Genetic fate mapping enabled us to determine the functional properties of polydendrocytes even in the later phases after ischemia, when it is extremely difficult to perform patch-clamp measurements of newly-derived cells in the gliotic scar full of reactive astrocytes and microglia. We found that polydendrocytes responded to ischemia with marked changes in their electrophysiological properties, especially in the early phases after ischemia. However, in the late phases after ischemia their membrane properties were comparable to those of controls, indicating the rapid recovery of polydendrocytic electrophysiological properties to the pre-ischemic state.

Polydendrocytes display multipotent differentiation potential after ischemia

Based on immunohistochemical analysis, ~75% of $EGFP^+$ cells did not express NG2 14 days after MCAo and electrophysiological analysis revealed ~80% of $EGFP^+$ cells with a current pattern distinct from that of polydendrocytes. The expression of GFAP, GLAST or vimentin together with a passive current pattern and dye-coupling in a large subpopulation of $EGFP^+$ cells evidenced that polydendrocytes can give rise to reactive astrocytes after ischemia. The generation of a reactive astrocyte subpopulation from polydendrocytes was already shown in models of cryoinjury [32], stab wound injury, experimental autoimmune encephalomyelitis or focal demyelination. However, in the majority of these injuries the generation of new astrocytes was limited and represented ~8% of $EGFP^+$ cells, and their number declined in the later phases after injury. In our study we detected ~17% of $EGFP^+$ cells with an astrocytic phenotype 7 days after ischemia, and their number only slightly decreased in the later phases after ischemia. This discrepancy is probably caused by using different injury models. In addition, the majority of studies employed rather mild types of cortical injuries or models of demyelination in the spinal cord; in contrast, we used a model of severe ischemic brain injury, in which the stronger involvement of repair processes and higher levels of growth factors could play an important role, resulting in greater differentiation of polydendrocytes into astrocytes. Moreover, we analyzed in detail the electrophysiological properties of newly-derived astrocytes. These cells had a passive current profile with 4-AP sensitive K_{DR} currents, which were further decreased in the later phases after ischemia. Our results are in good agreement with previously published electrophysiological analyses of reactive astrocytes after ischemia in the hippocampus [13] and cortex [41] and show that these newly-derived astrocytes are comparable with other reactive astrocyte populations in the later phases after ischemia.

Importantly, we also identified cells of polydendrocyte origin that displayed the immunohistochemical and electrophysiological properties of neuronal precursor cells and comprised ~9% of $EGFP^+$ cells 7 days after ischemia. Although recent studies described DCX expression and the differentiation of $PDGF\alpha R^+$ or PLP^+ cells into neurons in the healthy adult brain, this phenomenon was always strictly localized only in the piriform cortex [8,10]. Nevertheless, in our study we did not detect any $EGFP^+/DCX^+$ cells in any brain regions including the SVZ of sham-operated mice. After ischemia, some $EGFP^+/DCX^+$ cells displayed Na^+ currents with a significantly higher CD and markedly different kinetics when compared to polydendrocytes, together with high membrane resistance, which is a typical feature of immature neuroblasts [42]. Since it is relatively easy to force polydendrocytes *in vitro* to differentiate into neurons [5–7], a suitable mixture of growth factors and morphogenes released at the lesion site can probably also promote this phenomenon *in vivo*.

However, detailed analysis of these cells in the later phases after ischemia revealed that these cells were probably incapable of surviving and maturing into cells with a more developed neuronal phenotype. This assumption is based on our observation of the strong expression of caspase-3 in several $EGFP^+/DCX^+$ cells, and their inability to survive in the damaged ischemic region was also described previously in the newly-derived SVZ neuroblasts migrating into the site of injury after stroke [43]. We described the generation of neuronal precursor cells in mature, but still very young mice; however, we must assume that multipotency and the ability to differentiate into different cell types is strongly correlated with age. Many studies describing the multipotency of polydendrocytes were performed using postnatal or very young animals [5,6], so the ability to produce cells of the neuronal lineage could be strongly suppressed in older mice. The same scenario probably applies to the ability of polydendrocytes to give rise to astrocytes in the healthy brain. As was shown recently, polydendrocytes in the embryonic brain differentiate into astrocytes, but this capability is not maintained into adulthood [44].

In our study we also detected $EGFP^+$ oligodendrocytes before and after ischemia; however, in comparison to the large number of other newly-derived cell types, newly generated oligodendrocytes did not comprise the major cell population that originated from polydendrocytes after ischemia. The low number of $EGFP^+$ oligodendrocytes in the gray matter of the healthy brain is in agreement with previous studies describing the generation of oligodendrocytes predominantly in the white matter [10,45]. Nonetheless, we also detected a low number of oligodendrocytes after ischemia, which accords well with recent findings [16], but is in contrast to other recently published studies [10,15]. Importantly, we employed a more severe model of injury in which high levels of glutamate are released and which results in extensive neuroinflammation, and this might be an adverse environment for oligodendrocyte survival, which are strongly susceptible to excitotoxic death [46].

The last type of $NG2^+/EGFP^+$ cells found in uninjured and ischemic brains are the often overlooked pericytes. Since these cells express both NG2 and PDGFαR [47], they are probably involved in every fate mapping study that uses these proteins as markers of polydendrocytes. In our study pericytes were identified based on PDGFβR expression and the absence of any voltage activated currents; fourteen days after ischemia, their number almost doubled when compared to controls. Although we did not perform a detailed immunohistochemical analysis, there was an evident increase in the number of $EGFP^+$ cells that displayed a pericytic morphology and lined vessels in the vicinity of the ischemic lesion. Of note, a recent study described a massive proliferation of a distinct subclass of pericytes and their participation in scar tissue formation following spinal cord injury [48]. In contrast to these findings, we did not detect any $EGFP^+$ pericytes inside the ischemic core, which might be caused by our employing a different model of injury in a different CNS region. Moreover, the existence of several types of pericytes was described previously [49,50], therefore the $NG2^+$ pericytes labeled in our study could have a different role following ischemic injury. Recently, the wide differentiation potential of pericytes was

demonstrated *in vitro* [51], so we cannot exclude their contribution to the generation of different cell phenotypes after ischemia.

It is probable that polydendrocytes close to the ischemic region are exposed to factors and signals that indicate that tissue homeostasis and the integrity of the blood–brain barrier has been disrupted. Which components present in the serum, or which signals released from neural and non-neural elements are responsible for their increased proliferation and/or fate decision, remains to be determined. Nevertheless, these factors are likely to activate the Notch-1 pathway, as suggested by its up-regulation in reactive glial cells after injury [52–54]. A similar up-regulation was described for bone morphogenetic factor in the post-injury niche, and this factor was shown to drive the differentiation of polydendrocytes into astrocytes, while simultaneously its antagonist Noggin reverses this process [55]. A very important role in controlling the proliferation and differentiation of polydendrocytes is also played by the β-catenin signaling pathway, which is strongly activated after cortical injury [56]. It seems that information about massive ischemic injury is delivered to polydendrocytes in a large part of the CNS; however, only the directly exposed subpopulation of polydendrocytes responds to this pathology not only by proliferation, but also by differentiation into another cell types.

Supporting Information

Figure S1 Enhanced green fluorescent protein (EGFP) is expressed also in pericytes, but not in microglia in the control dorsal cortex of NG2creBAC:ZEG mice. A, Immunostaining for PDGFβR in the cortex showing several PDGFβR$^+$/EGFP$^+$ cells with morphology of pericytes. White arrows highlight several examples. B, Image showing immunostaining for microglial marker Iba-1; however, EGFP$^+$ cells never express this marker. Scale bars, 50 μm.
(TIF)

Figure S2 Proliferation and multipotency of EGFP$^+$ cells after MCAo. A, Immunostaining for PCNA in the cortex showing almost all EGFP$^+$ cells expressing this proliferation marker 3 days after MCAo. White arrows highlight several examples. B, Image showing all channels from Fig. 3H and orthogonal projection of this EGFP$^+$/GFAP$^+$ cell 7 days after MCAo. C, Several EGFP$^+$/GFAP$^+$ cells proliferate 7 days after MCAo based on Ki-67 expression. D, Image showing in detail EGFP$^+$ cells with strong expression of doublecortin (DCX) 7 days after MCAo. Scale bars, 50 μm.
(TIF)

Figure S3 Immunohistochemical properties of EGFP$^+$ cells after MCAo. A, Immunostaining for Pax-6 in the cortex showing several EGFP$^+$ cells expressing this transcription factor 7 days after MCAo. White arrows highlight several examples. B, Image showing a CD11b staining on EGFP$^+$ cells 7 days after MCAo. The ischemic region is filled with activated microglia cells; however, no microglia expressed EGFP. C, Image showing a Iba-1 staining on EGFP+ cells 7 days after MCAo, also this marker of microglia and macrophages was not co-expressed with EGFP. D, Several EGFP$^+$/DCX$^+$ cells expressed apoptotic marker caspase-3 14 days after MCAo. Scale bars, 50 μm.
(TIF)

Acknowledgments

The authors would like to thank to Helena Pavlikova for excellent technical assistance. We also thank James Dutt for helpful comments and suggestions.

Author Contributions

Conceived and designed the experiments: PH MA. Performed the experiments: PH HP DD MF. Analyzed the data: PH HP. Wrote the paper: PH MA.

References

1. Tian D-S, Dong Q, Pan D-J, He Y, Yu Z-Y, et al. (2007) Attenuation of astrogliosis by suppressing of microglial proliferation with the cell cycle inhibitor olomoucine in rat spinal cord injury model. Brain Res 1154: 206–214.
2. Yang Y, Jalal FY, Thompson JF, Walker EJ, Candelario-Jalil E, et al. (2011) Tissue inhibitor of metalloproteinases-3 mediates the death of immature oligodendrocytes via TNF-α/TACE in focal cerebral ischemia in mice. J Neuroinflammation 8: 108.
3. Pettigrew LC, Kindy MS, Scheff S, Springer JE, Kryscio RJ, et al. (2008) Focal cerebral ischemia in the TNFalpha-transgenic rat. J Neuroinflammation 5: 47.
4. Nishiyama A (2007) Polydendrocytes: NG2 cells with many roles in development and repair of the CNS. Neuroscientist 13: 62–76.
5. Kondo T, Raff M (2000) Oligodendrocyte precursor cells reprogrammed to become multipotential CNS stem cells. Science 289: 1754–1757.
6. Belachew S, Chittajallu R, Aguirre A, Yuan X, Kirby M, et al. (2003) Postnatal NG2 proteoglycan-expressing progenitor cells are intrinsically multipotent and generate functional neurons. J Cell Biol 161: 169–186.
7. Aguirre A, Chittajallu R, Belachew S, Gallo V (2004) NG2-expressing cells in the subventricular zone are type C-like cells and contribute to interneuron generation in the postnatal hippocampus. J Cell Biol 165: 575–589.
8. Guo F, Maeda Y, Ma J, Xu J, Horiuchi M, et al. (2010) Pyramidal Neurons Are Generated from Oligodendroglial Progenitor Cells in Adult Piriform Cortex. J Neurosci 30: 12036–12049.
9. Zhu X, Hill RA, Nishiyama A (2008) NG2 cells generate oligodendrocytes and gray matter astrocytes in the spinal cord. Neuron Glia Biol 4: 19–26.
10. Rivers LE, Young KM, Rizzi M, Jamen F, Psachoulia K, et al. (2008) PDGFRA/NG2 glia generate myelinating oligodendrocytes and piriform projection neurons in adult mice. Nat Neurosci 11: 1392–1401.
11. Dimou L, Simon C, Kirchhoff F, Takebayashi H, Goetz M (2008) Progeny of Olig2-Expressing Progenitors in the Gray and White Matter of the Adult Mouse Cerebral Cortex. J Neurosci 28: 10434–10442.
12. Hampton D, Rhodes K, Zhao C, Franklin R, Fawcett J (2004) The responses of oligodendrocyte precursor cells, astrocytes and microglia to a cortical stab injury, in the brain. Neuroscience 127: 813–820.
13. Pivonkova H, Benesova Jana, Benesova J, Butenko O, Chvatal A, et al. (2010) Impact of global cerebral ischemia on K+ channel expression and membrane properties of glial cells in the rat hippocampus. Neurochem Int 57: 783–794.
14. Trotter J, Karram K, Nishiyama A (2010) NG2 cells: Properties, progeny and origin. Brain Res Rev 63: 72–82.
15. Komitova M, Serwanski DR, Richard Lu Q, Nishiyama A (2011) NG2 cells are not a major source of reactive astrocytes after neocortical stab wound injury. Glia 59: 800–809.
16. Anderova Miroslava, Vorisek I, Pivonkova H, Benesova Jana, Vargova L, et al. (2011) Cell death/proliferation and alterations in glial morphology contribute to changes in diffusivity in the rat hippocampus after hypoxia-ischemia. J Cereb Blood Flow Metab 31: 894–907.
17. Muskhelishvili L, Latendresse JR, Kodell RL, Henderson EB (2003) Evaluation of Cell Proliferation in Rat Tissues with BrdU, PCNA, Ki-67(MIB-5) Immunohistochemistry and In Situ Hybridization for Histone mRNA. Journal of Histochemistry & Cytochemistry 51: 1681–1688.
18. Zhu X, Bergles DE, Nishiyama A (2008) NG2 cells generate both oligodendrocytes and gray matter astrocytes. Development 135: 145–157.
19. Cahoy JD, Emery B, Kaushal A, Foo LC, Zamanian JL, et al. (2008) A transcriptome database for astrocytes, neurons, and oligodendrocytes: a new resource for understanding brain development and function. J Neurosci 28: 264–278.
20. Carmichael ST (2005) Rodent models of focal stroke: size, mechanism, and purpose. NeuroRx: the journal of the American Society for Experimental NeuroTherapeutics 2: 396–409.
21. Michalczyk K, Ziman M (2005) Nestin structure and predicted function in cellular cytoskeletal organisation. Histol Histopathol 20: 665–671.
22. Simon C, Götz M, Dimou L (2011) Progenitors in the adult cerebral cortex: Cell cycle properties and regulation by physiological stimuli and injury. Glia 59: 869–881.
23. Chen P-H, Cai W-Q, Wang L-Y, Deng Q-Y (2008) A morphological and electrophysiological study on the postnatal development of oligodendrocyte precursor cells in the rat brain. Brain Res 1243: 27–37.
24. Heins N, Malatesta P, Cecconi F, Nakafuku M, Tucker KL, et al. (2002) Glial cells generate neurons: the role of the transcription factor Pax6. Nat Neurosci 5: 308–315.
25. Komitova M, Zhu X, Serwanski DR, Nishiyama A (2009) NG2 cells are distinct from neurogenic cells in the postnatal mouse subventricular zone. J Comp Neurol 512: 702–716.

26. Nishiyama A, Komitova M, Suzuki R, Zhu X (2009) Polydendrocytes (NG2 cells): multifunctional cells with lineage plasticity. Nat Rev Neurosci 10: 9–22.
27. Xie M, Lynch DT, Schools GP, Feustel PJ, Kimelberg HK, et al. (2007) Sodium channel currents in rat hippocampal NG2 glia: Characterization and contribution to resting membrane potential. Neuroscience 150: 853–862.
28. Schools GP, Zhou M, Kimelberg HK (2003) Electrophysiologically "complex" glial cells freshly isolated from the hippocampus are immunopositive for the chondroitin sulfate proteoglycan NG2. J Neurosci Res 73: 765–777.
29. Knutson P, Ghiani CA, Zhou JM, Gallo V, McBain CJ (1997) K+ channel expression and cell proliferation are regulated by intracellular sodium and membrane depolarization in oligodendrocyte progenitor cells. J Neurosci 17: 2669–2682.
30. Chvatal A, Anderova Miroslava, Sykova E (2004) Analysis of K+ accumulation reveals privileged extracellular region in the vicinity of glial cells in situ. J Neurosci Res 78: 668–682.
31. Karram K, Goebbels S, Schwab M, Jennissen K, Seifert G, et al. (2008) NG2-expressing cells in the nervous system revealed by the NG2-EYFP-knockin mouse. genesis 46: 743–757.
32. Tatsumi K, Takebayashi H, Manabe T, Tanaka KF, Makinodan M, et al. (2008) Genetic fate mapping of Olig2 progenitors in the injured adult cerebral cortex reveals preferential differentiation into astrocytes. J Neurosci Res 86: 3494–3502.
33. Tripathi RB, Rivers LE, Young KM, Jamen F, Richardson WD (2010) NG2 Glia Generate New Oligodendrocytes But Few Astrocytes in a Murine Experimental Autoimmune Encephalomyelitis Model of Demyelinating Disease. J Neurosci 30: 16383–16390.
34. Zawadzka M, Rivers LE, Fancy SPJ, Zhao C, Tripathi R, et al. (2010) CNS-Resident Glial Progenitor/Stem Cells Produce Schwann Cells as well as Oligodendrocytes during Repair of CNS Demyelination. Stem Cell 6: 578–590.
35. Wohl SG, Schmeer CW, Friese T, Witte OW, Isenmann S (2011) In Situ Dividing and Phagocytosing Retinal Microglia Express Nestin, Vimentin, and NG2 In Vivo. PLoS ONE 6: e22408.
36. Zhu L, Lu J, Tay SSW, Jiang H, He BP (2010) Induced NG2 expressing microglia in the facial motor nucleus after facial nerve axotomy. NSC 166: 842–851.
37. Gao Q, Lu J, Huo Y, Baby N, Ling EA, et al. (2010) NG2, a member of chondroitin sulfate proteoglycans family mediates the inflammatory response of activated microglia. NSC 165: 386–394.
38. Bulloch K, Miller MM, Gal-Toth J, Milner TA, Gottfried-Blackmore A, et al. (2008) CD11c/EYFP transgene illuminates a discrete network of dendritic cells within the embryonic, neonatal, adult, and injured mouse brain. J Comp Neurol 508: 687–710.
39. Nishiyama A, Yu M, Drazba JA, Tuohy VK (1997) Normal and reactive NG2+ glial cells are distinct from resting and activated microglia. J Neurosci Res 48: 299–312.
40. Jones LL, Yamaguchi Y, Stallcup WB, Tuszynski MH (2002) NG2 is a major chondroitin sulfate proteoglycan produced after spinal cord injury and is expressed by macrophages and oligodendrocyte progenitors. J Neurosci 22: 2792–2803.
41. Anderova Miroslava, Antonova T, Petrik D, Neprasova Helena, Chvatal A, et al. (2004) Voltage-dependent potassium currents in hypertrophied rat astrocytes after a cortical stab wound. Glia 48: 311–326.
42. Lacar (2010) Imaging and recording subventricular zone progenitor cells in live tissue of postnatal mice. Front Neurosci.
43. Carlen M, Meletis K, Göritz C, Darsalia V, Evergren E, et al. (2009) Forebrain ependymal cells are Notch-dependent and generate neuroblasts and astrocytes after stroke. Nat Neurosci 12: 259–267.
44. Zhu X, Hill RA, Dietrich D, Komitova M, Suzuki R, et al. (2011) Age-dependent fate and lineage restriction of single NG2 cells. Development 138: 745–753.
45. Kang SH, Fukaya M, Yang JK, Rothstein JD, Bergles DE (2010) NG2+ CNS Glial Progenitors Remain Committed to the Oligodendrocyte Lineage in Postnatal Life and following Neurodegeneration. Proc Natl Acad Sci USA 68: 668–681.
46. Matute C, Alberdi E, Domercq M, Sánchez-Gómez M-V, Pérez-Samartín A, et al. (2007) Excitotoxic damage to white matter. J Anat 210: 693–702.
47. Richardson WD, Young KM, Tripathi RB, McKenzie I (2011) NG2-glia as Multipotent Neural Stem Cells: Fact or Fantasy? Proc Natl Acad Sci USA 70: 661–673.
48. Goritz C, Dias DO, Tomilin N, Barbacid M, Shupliakov O, et al. (2011) A Pericyte Origin of Spinal Cord Scar Tissue. Science 333: 238–242.
49. Hamilton TG, Klinghoffer RA, Corrin PD, Soriano P (2003) Evolutionary Divergence of Platelet-Derived Growth Factor Alpha Receptor Signaling Mechanisms. Molecular and Cellular Biology 23: 4013–4025.
50. Bondjers C, He L, Takemoto M, Norlin J, Asker N, et al. (2006) Microarray analysis of blood microvessels from PDGF-B and PDGF-Rbeta mutant mice identifies novel markers for brain pericytes. FASEB J 20: 1703–1705.
51. Montiel-Eulefi E, Nery AA, Rodrigues LC, Sánchez R, Romero F, et al. (2012) Neural differentiation of rat aorta pericyte cells. Cytometry A 81: 65–71.
52. Wang S, Sdrulla AD, diSibio G, Bush G, Nofziger D, et al. (1998) Notch receptor activation inhibits oligodendrocyte differentiation. Proc Natl Acad Sci USA 21: 63–75.
53. Yamamoto S, Nagao M, Sugimori M, Kosako H, Nakatomi H, et al. (2001) Transcription factor expression and Notch-dependent regulation of neural progenitors in the adult rat spinal cord. J Neurosci 21: 9814–9823.
54. Grandbarbe L, Bouissac J, Rand M, Hrabé de Angelis M, Artavanis-Tsakonas S, et al. (2003) Delta-Notch signaling controls the generation of neurons/glia from neural stem cells in a stepwise process. Development 130: 1391–1402.
55. Sellers DL, Maris DO, Horner PJ (2009) Postinjury Niches Induce Temporal Shifts in Progenitor Fates to Direct Lesion Repair after Spinal Cord Injury. J Neurosci 29: 6722–6733.
56. White BD, Nathe RJ, Maris DO, Nguyen NK, Goodson JM, et al. (2010) Beta-catenin signaling increases in proliferating NG2+ progenitors and astrocytes during post-traumatic gliogenesis in the adult brain. Stem Cells 28: 297–307.

OPEN ACCESS Freely available online

PLOS ONE

Heterogeneity of Astrocytes: From Development to Injury – Single Cell Gene Expression

Vendula Rusnakova[1], Pavel Honsa[2], David Dzamba[2], Anders Ståhlberg[3], Mikael Kubista[1], Miroslava Anderova[2]*

1 Laboratory of Gene Expression, Institute of Biotechnology, Academy of Sciences of the Czech Republic, Prague, Czech Republic, **2** Department of Cellular Neurophysiology, Institute of Experimental Medicine, Academy of Sciences of the Czech Republic, Prague, Czech Republic, **3** Sahlgrenska Cancer Center, Department of Pathology, Sahlgrenska Academy at the University of Gothenburg, Gothenburg, Sweden

Abstract

Astrocytes perform control and regulatory functions in the central nervous system; heterogeneity among them is still a matter of debate due to limited knowledge of their gene expression profiles and functional diversity. To unravel astrocyte heterogeneity during postnatal development and after focal cerebral ischemia, we employed single-cell gene expression profiling in acutely isolated cortical GFAP/EGFP-positive cells. Using a microfluidic qPCR platform, we profiled 47 genes encoding glial markers and ion channels/transporters/receptors participating in maintaining K^+ and glutamate homeostasis per cell. Self-organizing maps and principal component analyses revealed three subpopulations within 10–50 days of postnatal development (P10–P50). The first subpopulation, mainly immature glia from P10, was characterized by high transcriptional activity of all studied genes, including polydendrocytic markers. The second subpopulation (mostly from P20) was characterized by low gene transcript levels, while the third subpopulation encompassed mature astrocytes (mainly from P30, P50). Within 14 days after ischemia (D3, D7, D14), additional astrocytic subpopulations were identified: resting glia (mostly from P50 and D3), transcriptionally active early reactive glia (mainly from D7) and permanent reactive glia (solely from D14). Following focal cerebral ischemia, reactive astrocytes underwent pronounced changes in the expression of aquaporins, nonspecific cationic and potassium channels, glutamate receptors and reactive astrocyte markers.

Citation: Rusnakova V, Honsa P, Dzamba D, Ståhlberg A, Kubista M, et al. (2013) Heterogeneity of Astrocytes: From Development to Injury – Single Cell Gene Expression. PLoS ONE 8(8): e69734. doi:10.1371/journal.pone.0069734

Editor: Michal Hetman, University of Louisville, United States of America

Received April 26, 2013; **Accepted** June 12, 2013; **Published** August 5, 2013

Funding: This work was supported by the Academy of Sciences of the Czech Republic IBT AS CR [AVOZ50520701] and UEM AS CR [AV0Z50390703]; by Grant Agency of the Czech Republic [P303/13/02154S]; by an EMBO Short Term Fellowship [ASTF 110-2011] and an ESF Functional Genomics Short Visit Grant [2426]. The funders had no role in study design, data collection and analysis, decision to publish, or preparation of the manuscript.

Competing Interests: The authors have declared that no competing interests exist.

* E-mail: anderova@biomed.cas.cz

Introduction

Astrocytes comprise a heterogeneous cell type with several subgroups; for review see [1]. Even within the same brain region multiple astrocytic subgroups have been observed [2]. In addition to morphological differences, astrocytes show diversity in Ca^{2+} signalling, gap junction coupling, and the expression of membrane proteins such as K^+ channels, glutamate receptors and transporters; for review see [3]. It was recently shown that astrocyte heterogeneity also rests on the expression of inwardly rectifying (KIR) and two-pore-domain K^+ (K2P) channels [4]. In our recent work we demonstrated the presence of two distinct subpopulations of astrocytes that respond differently to oxygen-glucose deprivation, probably due to their different expression of chloride channels (ClC2), inwardly rectifying K^+ channels (KIR4.1) and K2P channels, such as TREK-1 and TWIK-1 [5]. Astrocytes also change their properties during development. In contrast to neurons, astrocytes are formed at late stages of embryogenesis (from E16 and onward) and during the first postnatal weeks [6], and the mouse cortex is not fully developed until between the 3rd and 4th week after birth [7]. The origin of astrocytes is not fully known; possibly they arise from distinct groups of progenitors [8], and some subpopulations may be generated from NG2 glia cells [9]. NG2 glia are characterized by their expression of NG2 chondroitin sulphate proteoglycan (CSPG4) and platelet-derived growth factor α receptor (PDGFαR). After their discovery, NG2 glia were found to be oligodendrocyte progenitor cells [10]. Later, NG2 glia were also shown to be progenitors of some groups of reactive astrocytes [11,12], which appear after CNS injury. This process, termed astrogliosis, is characterized by the increased expression of glial fibrillary acidic protein (GFAP) and Nestin, followed by the elevated expression of vimentin [13]. Another characteristic of astrogliosis is the high expression of aquaporins, especially of AQP1 and AQP9, which are proteins rarely expressed in healthy tissue [14,15]. Several publications have reported reactive astrocytes expressing proteoglycans [16,17] and glutamate metabotropic receptor 5 (*Grm5*) [18,19]. Traditionally, astrocytes are identified by the expression of GFAP [20]. However GFAP is not always expressed in non-reactive astrocytes, and GFAP is frequently not immunohistochemically detected in astrocytes in healthy tissue [21]. Other complementary markers are therefore used to identify astrocytes, including S100β [22], excitatory amino acid transporter 1 and 2 (EAAT1 and 2) [23], glutamine synthetase (GS) [24] and aldehyde dehydrogenase 1 family member L1 (ALDH1L1) [25]. Since non-glial cells also express some of these markers, detecting a combination of markers is needed for the reliable identification of astrocytes [26].

Altogether, there is evidence of astrocyte heterogeneity between, as well as within, CNS regions. To characterize the different types of astrocytes that appear under various conditions, single-cell studies are necessary. Single cell gene expression profiling is a novel and powerful method to study cell heterogeneity [27]. It has already been used to establish the presence of distinct subpopulations of astrocytes in a seemingly homogenous macroscopic population [5,28]. Single cell expression profiling is challenging because of the limited amount of RNA present in a single cell. Very efficient reverse transcription is needed, and for the analysis of more than some 10 genes preamplification is required. Cells express mRNAs in bursts [29,30], resulting in large natural variation in the number of any transcript among cells, which can be modelled with a lognormal distribution [31]. To obtain biologically relevant and statistically significant conclusions, rather large numbers of cells must be analysed [32]. A particularly powerful approach to distinguish different cells and subtypes of cells is to study the correlation of transcript levels within individual cells [33]. This kind of information is not available when studying classical samples composed of many cells.

Our goal was to characterize astrocytes based on changes in their gene expression profiles throughout development and after focal cerebral ischemia. We used single cell RT-qPCR profiling to analyse EGFP-positive ($EGFP^+$) cells collected by fluorescence-activated cell sorting (FACS) from the cortex of GFAP/EGFP transgenic mice with the objective of identifying and characterizing subpopulations of astrocytes. We focus our profiling effort on glial glutamate transporters and receptors as well as on ion channels, which are critical for the maintenance of the ionic/neurotransmitter homeostasis of neurons and glial cells under physiological conditions as well as in pathological states.

Materials and Methods

Induction of an Ischemic Lesion in Adult GFAP/EGFP Mice

All experiments were performed on cells from acutely isolated brains of GFAP/EGFP transgenic mice [line designation TgN(GFAPEGFP)], in which the expression of EGFP is controlled by the human GFAP promoter [34]. All procedures involving the use of laboratory animals were performed in accordance with the European Communities Council Directive 24 November 1986 (86/609/EEC) and animal care guidelines approved by the Institute of Experimental Medicine, Academy of Sciences of the Czech Republic (Animal Care Committee on April 17, 2009; approval number 85/2009).

Prior to the induction of focal ischemia, 50-day-old (P50) mice were anaesthetized with 1.5% isoflurane (Abbot) and maintained in 1% isoflurane using a vaporizer (Tec-3, Cyprane Ltd., Keighley). A skin incision between the orbit and the external auditory meatus was made, and a 1–2 mm hole was drilled through the frontal bone 1 mm rostral to the fusion of the zygoma and the squamosal bone and about 3.5 mm ventral to the dorsal surface of the brain. The middle cerebral artery (MCA) was exposed after the dura was opened and removed. The MCA was occluded by short coagulation with bipolar tweezers (SMT, Czech Republic) at a proximal location, followed by transection of the vessel to ensure permanent occlusion. The mice received 0.5 ml saline solution subcutaneously, and during the surgery the body temperature was maintained at $37\pm1^{\circ}C$ using a heating pad.

Immunohistochemistry

The mice were deeply anaesthetized with pentobarbital (PTB, 100 mg/kg, i.p.) and perfused transcardially with 20 ml of saline followed by 20 ml of cooled 4% paraformaldehyde in 0.1 M phosphate buffer. Brains were dissected out, fixed with paraformaldehyde overnight, cryoprotected with sucrose and sliced into 30 μm coronal slices using a microtome (HM550, Microm International). The slices were incubated with 5% Chemiblocker (Millipore) and 0.2% Triton in PBS then with the primary antibodies at $4^{\circ}C$ overnight. As primary antibodies, we used anti-GFAP (1:800, Sigma-Aldrich, mouse, conjugated with Cy3), anti-GFAP (1:800, Sigma-Aldrich, mouse), anti-NG2 (1:400, Chemicon, rabbit) and anti-PDGFαR (1:200, Santa Cruz, rabbit). Finally, the secondary antibody was applied for 2 hours, either goat anti-mouse IgG or goat anti-rabbit IgG conjugated with Alexa Fluor 660 (Molecular Probes). A Zeiss 510DUO LSM confocal microscope equipped with Arg/HeNe lasers was used for immunohistochemical analysis. Colocalization images and their maximum z projections were made using a Zeiss LSM Image Browser.

Preparation of Cell Suspensions from the Cortex of GFAP/EGFP Mice

GFAP/EGFP transgenic mice 10, 20, 30 and 50 days old (P10, P20, P30, P50) or 3, 7, and 14 days after middle cerebral artery occlusion (MCAO) (D3, D7, D14) were deeply anesthetized with PTB (100 mg/kg, i.p.) and perfused transcardially with cold (4–$8^{\circ}C$) isolation buffer containing (in mM): NaCl 136.0, KCl 5.4, Hepes 10.0, glucose 5.5, osmolarity 290 ± 3 mOsmol/kg. The forebrain was isolated by the removal of the olfactory lobes, cerebellum, and midbrain/hindbrain structures by dissection. To isolate the cerebral cortex, the brain (+2 mm to −2 mm from bregma) was sliced into 400 μm coronal sections using a vibrating microtome HM650V (MICROM International GmbH), and the dorsal cerebral cortex was carefully dissected out from the ventral white matter tracks. The tissue was incubated with continuous shaking at $37^{\circ}C$ for 90 minutes in 5 ml of a papain solution (20 U/ml) and 0.2 ml DNase (both from Worthington) prepared in isolation buffer. After papain treatment, the tissue was mechanically dissociated by gentle trituration using a 1 ml pipette. Dissociated cells were layered on the top of 5 ml of Ovomucoid inhibitor solution (Worthington) and harvested by centrifugation ($140\times g$ for 6 minutes). This method routinely yielded $\sim2\times10^6$ cells per mouse. Cell aggregates were removed by filtering with a 30 μm cell strainer (Becton Dickinson), and the cells were kept on ice until sorting.

Collection of Single $EGFP^+$ Cells

Single cells were sorted using flow cytometry (BD Influx). The flow cytometer was manually calibrated to deposit a single cell in the centre of each collection tube. Hoechst 33258 (Life Technologies) was added to the suspension of cells to check viability. Initially, cell sorting was performed with a negative control (no fluorescent cells) in order to set the fluorescence threshold for collecting $EGFP^+$ cells and to avoid auto-fluorescent cells. After setting the threshold, all $EGFP^+$ cells that crossed this level of fluorescence were collected. Single cells were collected into 96-well plates (Life Technologies) containing 5 μl nuclease-free water with bovine serum albumin (1 mg/μl, Fermentas) and RNaseOut 20 U (Life Technologies). Plates were placed on a pre-cooled rack. The glial cells collected were positive for EGFP and viable. Collected cells in 96-well plates were immediately placed at $-80^{\circ}C$. For analysing individual developmental or post-ischemic stages, the cells were isolated from 1 mouse (P10), 2 mice (P20), 1 mouse (P30), 1 mouse (P50), 2 mice (D3), 2 mice (D7) and 1 mouse (D14).

cDNA Synthesis

cDNA synthesis was performed with SuperScript III RT (Life Technologies). Lysed single cells in 5 µl water containing 0.5 µM dNTP (Promega), 1.0 µM oligo (dT15) (Invitrogen) and 1.0 µM random hexamers (Eastport) were incubated at 70°C for 5 min. 50 mM Tris–HCl, 75 mM KCl, 3 mM $MgCl_2$, 5 mM dithiothreitol, 20 U RNaseOut and 100 U SuperScript III (all Life Technologies) were added to a final volume of 10 µl. Reverse transcription was performed at 25°C for 5 min, then at 50°C for 60 min, followed by 55°C for 15 min and finally terminated by heating at 70°C for 15 min. Four µl from each sample was diluted 4 times and used for pre-testing. Five µl of cDNA was used for preamplification.

qPCR

Primers were designed using BeaconDesigner (version 7.91, Premier Biosoft International) as previously described [5]. Primer sequences are provided in Table S1. All single cells were pre-tested for the expression of glutamate transporter (*Eaat2*), glutamine synthetase (*Glul*), which are markers of astrocytes, and chondroitin sulphate proteoglycan (*Cspg4*) and platelet-derived growth factor α receptor (*Pdgfra*), which are markers of NG2 glia, to select samples for further gene expression profiling using assays for 47 genes. A CFX384 (Biorad) was used for all qPCR measurements. To each reaction (10 µl) containing iQ SYBR Green Supermix (BioRad) and 400 nM of each primer (EastPort), we added 3 µl of diluted cDNA. The temperature profile was 95°C for 3 min followed by 50 cycles of amplification (95°C for 15 s, 60°C for 15 s and 72°C for 20 s). All samples were subjected to melting curve analysis. The same experimental setup was used to test preamplification.

Preamplification and qPCR

The applied preamplification protocol was verified on samples from three animals. The RNA was extracted and cDNA was prepared to test the preamplification protocol. Each reaction contained 25 µl of iQ Supermix (BioRad), 5 µl of a mix of all primers (final concentration 25 nM each), 5 µl of non-diluted cDNA, and water added to a final volume of 50 µl. The temperature profile was 95°C for 3 min followed by 18 cycles of amplification (95°C for 20 s, 57°C for 4 min and 72°C for 20 s on a Biorad CFX96). The samples were diluted 5 times in water. The expression of all genes was measured in preamplified and non-preamplified samples. The average difference between preamplified and non-preamplified samples and the standard deviations of the differences were calculated. The same setup was then used for the preamplification of single cells.

High Throughput qPCR

The sample reaction mixture had a volume of 5 µl and contained 2.4 µl of diluted preamplified cDNA, 0.25 µl of DNA Binding Dye Sample Loading Reagent (Fluidigm), 2.5 µl SsoFast EvaGreen Supermix (Biorad), and 0.01 µl ROX (Invitrogen). The primer reaction mixture had a final volume of 5 µl and contained 2.5 µl Assay Loading Reagent (Fluidigm) and 2.5 µl of a mix of reverse and forward primers, corresponding to a final concentration of 4 µM. The chip was first primed with an oil solution in the NanoFlex™ 4-IFC Controller (Fluidigm) to fill the control wells of the dynamic array. The reaction mixture (5 µl) was loaded into each sample well, and 5 µl of the primer reaction mixtures was loaded into each assay well of the 48×48 dynamic array. The dynamic array was then placed in the NanoFlex™ 4-IFC Controller for automatic loading and mixing. After 55 min the dynamic array was transformed to the BioMark qPCR platform (Fluidigm). The cycling program was 3 min at 95°C for activation, followed by 40 cycles of denaturation at 95°C for 5 s, annealing at 60°C for 15 s, and elongation at 72°C for 20 s. After PCR, melting curves were collected between 60°C and 95°C with 0.5°C increments.

Data Pre-processing

qPCR data were pre-processed for expression analysis using GenEx (MultiD, version 5.3) as follows: Cq values registered from amplifications that generated melting curves with aberrant Tm were removed, Cq values larger than 26 were replaced with 26, and Cq values with products giving rise to a double peak in melting curves (corresponding to a mixture of expected and aberrant PCR products) were replaced with 26. All missing data, for each gene separately, were then replaced with the highest Cq +2, effectively assigning a concentration of 25% of the lowest measured concentration to the off-scale values. The Cq data were, for each gene separately, converted into relative quantities expressed relative to the sample with the lowest expression (maximum Cq) and finally converted to a logarithmic scale with base 2. The data were not normalized to any reference genes because of the large variation of all transcript levels among individual cells [33]; with this pre-processing, the levels are expressed per cell.

Analysis

Basic statistics were calculated. The non-parametric Mann-Whitney test was used to compare the expression of individual genes between groups of cells. Kohonen self-organizing maps (SOM) of size 3×1, dividing the cells into three groups, were trained using GenEx with the following parameters: 0.10 learning rate, 3 neighbors and 5000 iterations. The SOM analysis was repeated eight times with identical classification of the cells in six of the repeats. This classification of cells into three groups was substantiated with principal component analysis (PCA). The division of cells into three groups by SOM does not imply that there are three distinct subtypes of cells; the cells may also be changing their expression pattern from one state to another, and the SOM then divides the cells into different phases: those just starting to change, those that have undergone substantial change, and finally cells approaching completion. Distinct subtypes, when such are present, appear as separated clusters in PCA. For Kohonen SOM and PCA the data were mean-centered to reduce the effect of variation in the overall expression levels of the different genes. The Spearman correlation coefficients between genes were calculated for each group separately (SAS vers. 9.2) using all data, including the managed off-scale data, and then also for the truly positive expression values only. Only correlation coefficients for genes expressed in at least 50% of cells and having a p-value <0.05 were considered for further analysis. Indirect correlations between genes were established by calculating partial Spearman correlation coefficients (only genes expressed in at least 80% of the cells were considered). An interaction was considered indirect when the correlation coefficient lost significance (at 95% confidence) or was reduced to below 0.4 [28].

Results

$EGFP^+$ cells from GFAP/EGFP transgenic mice are today routinely used by several research groups [4,35] and characterizing their gene expression profile is highly desirable. Because of the possible heterogeneity of astrocytes, single cells were collected by flow cytometry, lysed, and analyzed individually by RT-qPCR. For preamplification and further analysis we selected $EGFP^+$ cells

that were also positive for the astrocytic markers *Glul* and/or *Eaat2* and EGFP$^+$ cells that were also positive for *Cspg4* and/or *Pdgfra*, which are markers of NG2 glia. In these cells the gene expression of the following markers was measured: glial cell markers (*Eaat1, Gfap, Gfapδ, Glul, S100b, Pdgfra, Cspg4*), developmental markers nestin and vimentin (*nes and vim*), aquaporins (*Aqp1, Aqp4, Aqp9*), subunits of glutamate ionotropic AMPA receptors (*Gria1, Gria2, Gria3, Gria4*), glutamate ionotropic NMDA receptors (*Grin1, Grin2a, Grin2b, Grin2c, Grin2d, Grin3a*), glutamate ionotropic kainate receptors (*Grik1, Grik2, Grik3, Grik4, Grik5*), glutamate metabotropic receptors (*Grm1, Grm3, Grm5*), outwardly rectifying K^+ channels (*Kcna3, Kcna4, Kcna5*), inwardly rectifying K^+ channels (*Kcnj2, Kcnj10, Kcnj16*), two pore domain K^+ channels (*Kcnk1, Kcnk2, Kcnk10*) and hyperpolarization-activated cyclic nucleotide-gated channels (*Hcn1, Hcn2, Hcn3, Hcn4*), voltage-gated chloride channels (*Clcn2*), transient receptor potential channels (*Trpv4*), and *Snap25* encoding synaptosomal-associated protein SNAP-25. The markers were selected based on our previous work [5], which revealed significant differences between astrocytic subpopulations in the expression of genes coding for membrane proteins.

For the profiling of a large number of genes on the Biomark platform, it is necessary to preamplify the cDNA; in this regard, we have extensively optimized and validated the preamplification protocol. Our validation scheme is based on three samples that are profiled with and without preamplification and the measured Cq values are compared. Unbiased preamplification should result in the same ΔCq for all of the genes. The reproducibility of the preamplification is reflected by the standard deviation (SD) of the three ΔCq replicates measured for each gene. For our panel and protocol the SD was below 0.5 cycles for almost all genes. Only one gene (*Grin2d*) showed a large standard deviation (SD = 3.7 cycles) (Figure S1) and was omitted in the expression analysis. Inspecting the validation results, we did not find correlation between assay efficiency and ΔCq.

All cells collected from the cortex were analysed for the expression of *Eaat2*, *Glul*, *Cspg4*, and *Pdgfra* to estimate the ratio between cells that express only astrocytic markers (*Eaat2* and *Glul*) and cells that also express at least one of the NG2 glia markers (Figure 1). The number of cells that expressed only astrocytic markers increased, while the number of cells that also expressed NG2 glia markers decreased during postnatal development. After ischemic injury there was a distinct increase in the number of cells expressing NG2 glia markers 3 days after MCAO, but their number decreased again at later post-ischemic stages. In neither system did the expression profile depend on the EGFP intensity of the cells or on their size. Notably, cells expressing NG2 glia markers were distributed across the entire sorter gate (Figure 2, green dots). For single cell qPCR expression profiling 64 cells were collected from P10, 60 cells from P20, 89 cells from P30, 50 cells from P50, 90 cells from D3, 74 cells from D7, and 78 cells from D14. The cDNA produced from these cells was preamplified and measured on the Biomark platform.

Characteristics of EGFP$^+$ Cells Collected from Different Stages of Postnatal Development

The majority of EGFP$^+$ cells isolated from P10 mice expressed *Cspg4* and/or *Pdgfra* (87%) and *S100b* (80%). More than 70% of these cells also expressed *Eaat1*, *Grik1-3*, *5*, *Gria2-4* and *Kcnj16* (Figure 3A). Generally, cells at P10 were transcriptionally very active (Table 1). The expression profile of cells collected at P20 was different. *Cspg4* and/or *Pdgfra* were expressed in only 32% of the cells, and the expressions of *Kcnj16*, *Eaat1*, *Grik1*, *Grik3*, *Grik5*, *Gria2*, and *Gria4* were also reduced. *Gria3* expression remained high and the expression of *Hcn2*, *Grm5* and *Grin2a* increased. Cells at P30 and P50 displayed very similar expression patterns (Figure 3B). The expression of most genes was lower than at the earlier stages; only *Eaat1*, *Glul*, *Grin2a*, *Gria2* and *Aqp4* showed high expression. The fraction of cells positive for *Pdgfra* and/or *Cspg4* decreased to only 22% and 6% at P30 and P50, respectively.

Cells collected between P10 and P50 were divided by SOM into 3 groups based on their expression profiles (Figure 3C). This SOM classification was fully reproducible - repeated independent classifications predicted the same groups. This shows that the collection of cells is not homogeneous. SOM itself cannot tell if there are distinctly different groups or gradual changes, but the cells can be divided reproducibly into three subpopulations. The spatial separation between the clusters in the PCA suggests that the subpopulations are distinct (Figure 3B). Dividing the cells into more than three groups with SOM did not reveal any additional differences and was not supported by the PCA. We compared the average expression of the individual genes in the three subpopulations, which we henceforth refer to as A1, A2 and A3 (Table S2). Subpopulation A1 was characterized by the high expression of *Pdgfra*, *Cspg4*, *Grik1-3*, *Grik5*, *Gria2-4*, *Grin2a*, *Grin3a*, *Kcnj16*, *Eaat1*, *Glul*, *S100b*, *Snap25* and *Kcnj10* (Figure 3C) and was comprised mainly of P10 cells (composition: 64%, 19%, 13% and 2% of P10, P20, P30 and P50, respectively; Figure 3D). Subpopulation A2 was characterized by the low expression of most genes, including *Eaat1*, *Cspg4*, *Pdgfra*, *Grik5*, *Gria2* and *Grin3a*; only *Glul*, *Hcn2*, *Gria3* and *Grin2a* were highly expressed. Subpopulation A2 was comprised mainly of P20 cells (57%); cells from the other stages (P10, P30 and P50) were present at similarly low levels (Figure 3D). In addition to the classical astrocyte markers *Eaat1*, *Glul*, Aqp4, subpopulation A3 also expressed *Grik5*, *Gria2-3*, *Grin2a*, *Grm3* and *Kcnj16* at high levels and was comprised mainly of P30 and P50 cells (46% of each).

The relation between the expressions of different genes among the individual cells can be evaluated by calculating correlation coefficients. The calculation can include all cells, including those that did not express the genes of interest, or only those cells that had measurable expression. When all cells are considered, the dominant effect is whether a cell expresses both genes or not, while when cells with missing data are filtered out, the correlation coefficient is dominated by the expression levels of genes (Table S3, S4 and S5, Figure S2A–C). Although 95% of all cells in subpopulation A1 expressed *Pdgfra* as well as *Cspg4*, the correlation between their expressions was weak (r = 0.44), which means that they are expressed independently of each other in individual cells. We hypothesize that their expression might be regulated by different transcriptional factors and/or that such a weak correlation between *Pdgfra* and *Cspg4* expression might reflect the different stages of astrocyte maturation even within the A1 subpopulation, which comprises EGFP$^+$ cells from P10 and P20. The correlation between the expression of *Gria2* and *Cspg4* was negligible, while *Gria2* expression correlated with *Pdgfra* (r = 0.60) (Table S3). In subpopulation A3, correlated expression was found between *Glul* and *Eaat1* (r = 0.59) when considering only cells with valid expression data (74 cells) and between *Eaat1* and *Gria2* (r = 0.73). Notably, the correlation of *Eaat1* with *Glul* and of *Eaat1* with *Gria2* in subpopulations A1 and A2 was much lower, thus the increasing correlation between *Glul* and *Eaat1* clearly mirrors the maturation process of astrocytes.

Interestingly, gene expression profiling revealed that a large number of EGFP$^+$ cells express *Cspg4* as well as *Pdgfra* at P10, while at P50 we detected only a negligible number of EGFP$^+$ cells that co-expressed these markers (Figure 1). Furthermore, we also detected the co-expression of *Gfap* and *Cspg4*/*Pdgfra* in most of the cells at P10; this co-expression gradually decreased at P20 and

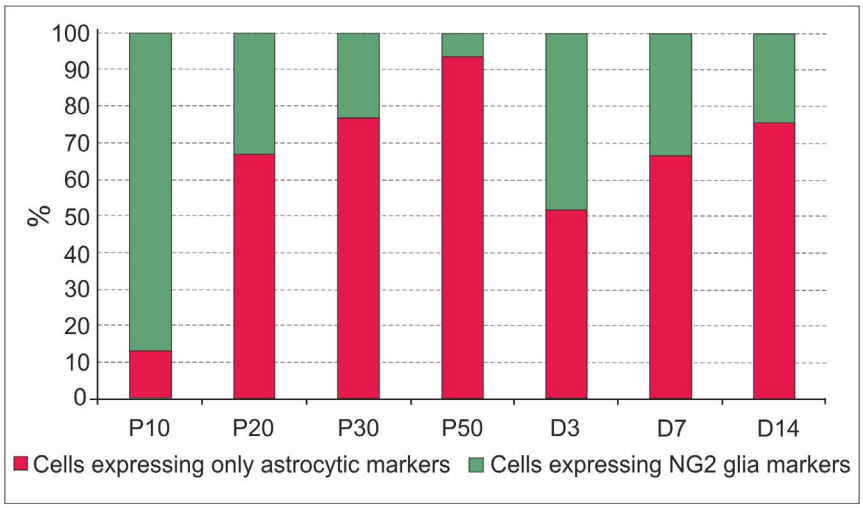

Figure 1. Characteristics of EGFP$^+$ cells in the cortex of GFAP/EGFP mice. (**A**) Percentage of EGFP$^+$ cells expressing either predominantly astrocytic or NG2 glia markers during postnatal development (P10, P20, P30, and P50) and at 3, 7 and 14 days (D3, D7 and D14) following focal cerebral ischemia. Cells expressing *Cspg4* and/or *Pdgfra* receptor are shown in green, while cells expressing only *Eaat2* and/or *Glul* are shown in red. The total numbers of the investigated cells were 137 for P10, 94 for P20, 157 for P30, 50 for P50, 148 for D3, 96 for D7 and 136 for D14.
doi:10.1371/journal.pone.0069734.g001

P30, and at P50 there was no co-expression detected. In order to confirm this observation on the protein level, we carried out immunohistochemical analyses, which revealed the co-expression of GFAP and PDGFαR or of GFAP and NG2 in EGFP$^+$ cells only at P10 and P20, but not at P50 (Figure 4, Figure S3).

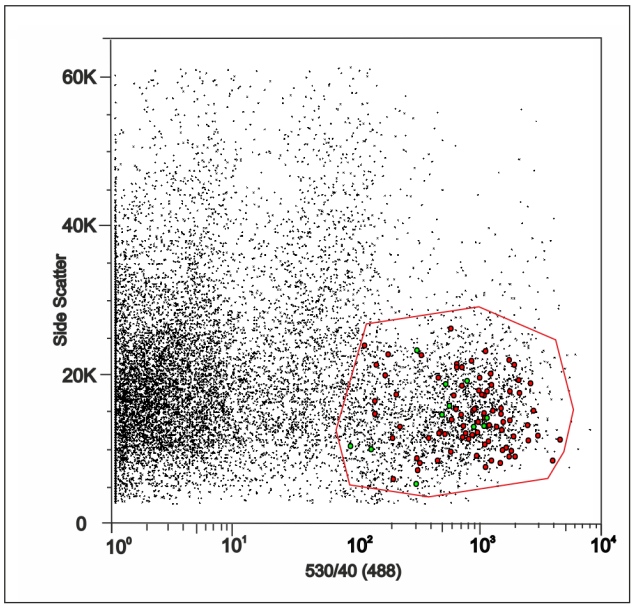

Figure 2. FACS analysis of EGFP$^+$ cells isolated from the cortex of 20-day-old mice. EGFP$^+$ cells sorted based on EGFP intensity (x axis) and side scatter intensity reflecting cell size (y axis). During the selection of cells by FACS, their position is automatically saved in the plot, and thus it is possible to determine the expression profile of each individual cell in the plot after qPCR analysis. The red line indicates the sorter gate and each dot represents one cell. Cells positive for *Cspg4* and/or *Pdgfra* are indicated in green while those positive only for *Eaat1* and/or *Glul* are shown in red. The latter are also drawn larger for better resolution. The small black dots represent all of the cells from which we selected our samples.
doi:10.1371/journal.pone.0069734.g002

Expression Profiling of Reactive Glia Following Focal Cerebral Ischemia

Three days after ischemia the expression profiles of the cells had changed. Approximately 50% of all EGFP$^+$ cells began to express *Pdgfra*, *Vim*, and *Grik5*, while *Aqp4*, *Glul* and *Eaat1* expression was decreased. Seven days after ischemia the cells were transcriptionally more active with particularly high expression of *Pdgfra*, *Vim*, *S100b*, *Eaat1*, *Glul*, *Gria2-4*, *Grin2a*, *Grin2b*, *Grik2*, *Grik5*, potassium channels *Kcna4*, *Kcna5*, *Kcnj10*, *Kcnj16*, *Aqp4* and *Hcn2*. Furthermore, the cells also began to express *Gfap* and *Gfapδ*. At this time, the expression of *Glul* returned to the basal level (P50, Figure 5A). Fourteen days after ischemia, the difference in expression compared to control (P50) was the largest. The expression of *Vim*, *Gfap*, *Gfapδ*, *Aqp4*, *S100b* and *Grm3* had dramatically decreased, while the expression of *Hcn1*, *Hcn2*, *Hcn3*, *Aqp1*, *Aqp9*, *Grm5*, *Gria3*, *Grin2a*, *Grin2d*, *Snap25* and *Kcna3* had markedly increased. At all post-ischemic stages, we found some cells expressing *Cspg4* and *Pdgfra*.

All cells (P50, D3, D7 and D14) were divided by SOM into 3 subpopulations and confirmed by PCA to have different expression profiles (Figure 5B). We will refer to these subpopulations as B1, B2 and B3. To characterize these subpopulations, we compared the expressions of the genes individually in histograms and by conventional univariate statistics. Almost all cells from P50 were assigned to subpopulation B1 (48 out of 50) (Figure 5C), and they comprised 35% of the B1 cells. 47% of B1 cells were from D3, 15% from D7, and only 3 B1 cells were from D14 (Figure 5D). The B1 subpopulation displayed the lowest overall transcriptional activity; high expression was observed only for *Eaat1*, *Glul*, *Aqp4* and *Gria2*. Subpopulation B2 was more transcriptionally active with the high expression of genes encoding glutamate ionotropic receptors, K^+ channels, *Grm3*, *Aqp4*, *Hcn2*, *Gfap*, *Gfapδ*, *Glul*, *Eaat1*, *S100b*, *Vim*, *Cspg4*, and *Pdgfra*. Most B2 cells were from D7 (66%), 31% were from D3 and only 2 cells were from P50. Notably, the two P50 cells also expressed *Pdgfra* and *Cspg4*. Subpopulation B3 was composed of only D14 cells. The very high expression of many genes makes this group unique, and there is no overlap in the PCA between B3 and the other subpopulations. Clearly, the B3 subpopulation is distinct. We also noted that the EGFP

Table 1. Statistics describing gene expression in different postnatal developmental stages or post-ischemic stages.

	Percentage of positive cells							Average relative expression log_2						
Gene	**P10**	**P20**	**P30**	**P50**	**D3**	**D7**	**D14**	**P10**	**P20**	**P30**	**P50**	**D3**	**D7**	**D14**
All cells (count)	64	60	79	50	90	74	78							
Cspg4	77%	32%	46%	4%	49%	35%	38%	3.63	1.45	2.22	0.10	1.99	1.45	1.63
Pdgfra	78%	40%	51%	4%	49%	35%	42%	6.32	2.38	3.37	0.25	3.03	2.36	2.71
Eaat1	83%	65%	92%	90%	88%	80%	87%	4.21	2.35	5.41	6.00	4.48	4.84	5.81
Glul	63%	58%	92%	92%	76%	81%	92%	2.16	2.80	4.50	5.79	3.61	5.91	5.84
Gfap	8%	13%	27%	8%	40%	57%	40%	0.29	0.47	1.15	0.35	1.55	4.14	1.95
Gfap D	19%	20%	44%	32%	47%	64%	40%	0.40	0.55	1.27	0.75	1.66	3.75	1.40
S100b	80%	48%	62%	64%	72%	85%	82%	2.05	1.37	1.87	1.54	2.09	3.81	2.28
nestin	11%	3%	11%	0%	23%	16%	10%	0.24	0.11	0.46	0.00	0.92	0.68	0.45
Vim	31%	23%	30%	18%	60%	82%	55%	0.79	0.69	0.91	0.45	3.33	5.91	1.89
Snap25	61%	25%	35%	26%	27%	26%	77%	1.93	0.82	1.53	1.15	0.82	0.86	4.02
Aqp1	2%	50%	0%	0%	1%	4%	79%	0.03	1.13	0.00	0.00	0.02	0.13	4.89
Aqp4	33%	25%	65%	72%	48%	70%	59%	1.03	0.70	2.96	2.81	1.38	4.15	2.78
Aqp9	9%	40%	5%	2%	0%	8%	91%	0.24	1.26	0.22	0.04	0.00	0.23	6.77
Clcn2	27%	27%	22%	28%	33%	28%	31%	0.76	0.86	0.88	1.27	0.96	1.50	1.30
Hcn1	19%	43%	29%	12%	0%	22%	96%	0.46	2.21	1.24	0.48	0.00	0.94	8.81
Hcn2	59%	95%	0%	24%	43%	55%	95%	1.52	5.05	0.00	0.61	1.38	3.30	8.78
Hcn3	31%	62%	28%	10%	22%	34%	88%	0.65	2.08	0.74	0.26	0.51	0.84	6.55
Hcn4	67%	43%	84%	72%	24%	80%	27%	1.40	1.23	1.88	1.46	0.52	1.69	1.85
Trpv4	38%	17%	34%	28%	39%	34%	35%	1.17	0.40	1.16	0.81	1.13	1.27	1.25
Grik1	67%	30%	44%	14%	40%	47%	63%	2.37	0.91	1.70	0.43	1.28	1.89	2.26
Grik2	75%	58%	38%	30%	42%	61%	47%	2.67	1.65	1.39	0.90	1.31	2.87	1.52
Grik3	70%	32%	48%	8%	44%	31%	33%	2.54	1.11	2.17	0.21	1.62	1.28	1.25
Grik4	45%	15%	22%	4%	19%	30%	14%	1.14	0.42	0.76	0.08	0.53	1.12	0.37
Grik5	86%	47%	54%	72%	77%	68%	69%	3.45	1.42	2.14	2.38	3.26	3.39	3.07
Grin3a	67%	32%	61%	10%	43%	35%	51%	2.27	0.90	2.46	0.25	1.25	1.36	1.58
Gria1	41%	12%	16%	8%	18%	16%	28%	0.87	0.28	0.37	0.22	0.44	0.63	0.72
Gria2	91%	62%	52%	74%	76%	66%	77%	5.22	2.45	2.60	3.54	3.19	3.25	4.08
Gria4	75%	53%	44%	24%	44%	54%	42%	2.67	1.45	1.71	0.83	1.59	2.54	1.54
Grin1	13%	32%	39%	18%	28%	50%	50%	0.27	0.69	1.03	0.47	0.63	1.26	1.30
Grin2a	47%	77%	49%	48%	46%	54%	97%	1.67	3.20	2.45	2.58	1.71	3.11	8.56
Grin2b	61%	33%	33%	30%	44%	57%	59%	1.82	0.90	1.30	1.24	1.37	2.60	2.19
Grin2c	13%	8%	23%	48%	28%	30%	35%	0.29	0.17	0.57	1.55	0.79	0.96	0.94
Grin2d	2%	15%	14%	4%	8%	4%	64%	0.03	0.42	0.55	0.17	0.20	0.11	3.05
Gria3	84%	87%	41%	12%	53%	49%	100%	4.23	4.55	2.21	0.58	2.29	2.46	9.49
Grm1	30%	18%	27%	32%	37%	31%	31%	0.89	0.64	1.01	1.18	1.20	1.24	1.34
Grm3	20%	27%	33%	62%	44%	61%	41%	0.60	1.01	1.35	2.39	1.43	2.80	1.89
Grm5	38%	82%	29%	0%	30%	27%	92%	0.77	2.45	0.77	0.00	0.71	0.64	7.18
Kcna3	25%	67%	18%	14%	23%	27%	91%	0.52	1.47	0.33	0.31	0.52	0.68	6.00
Kcna4	33%	45%	38%	22%	19%	53%	37%	0.99	1.69	1.58	0.73	0.60	2.36	1.48
Kcna5	25%	30%	42%	22%	41%	64%	38%	0.79	0.89	1.58	0.64	1.29	2.83	1.33
Kcnj10	95%	45%	72%	74%	79%	82%	88%	2.05	1.12	1.33	1.48	1.92	3.04	1.96
Kcnj16	66%	30%	54%	52%	60%	55%	58%	2.37	0.96	2.11	2.15	2.25	2.64	2.38
Kcnj2	17%	17%	19%	14%	23%	49%	29%	0.51	0.56	0.73	0.44	0.81	2.12	0.96
Kcnk1	22%	15%	30%	24%	26%	11%	28%	0.53	0.44	1.10	0.65	0.62	0.43	0.94
Kcnk10	67%	25%	33%	20%	44%	50%	32%	1.54	0.55	0.78	0.48	1.02	1.23	0.79
Kcnk2	34%	17%	23%	4%	31%	12%	41%	1.09	0.41	0.80	0.16	0.87	0.42	1.35

doi:10.1371/journal.pone.0069734.t001

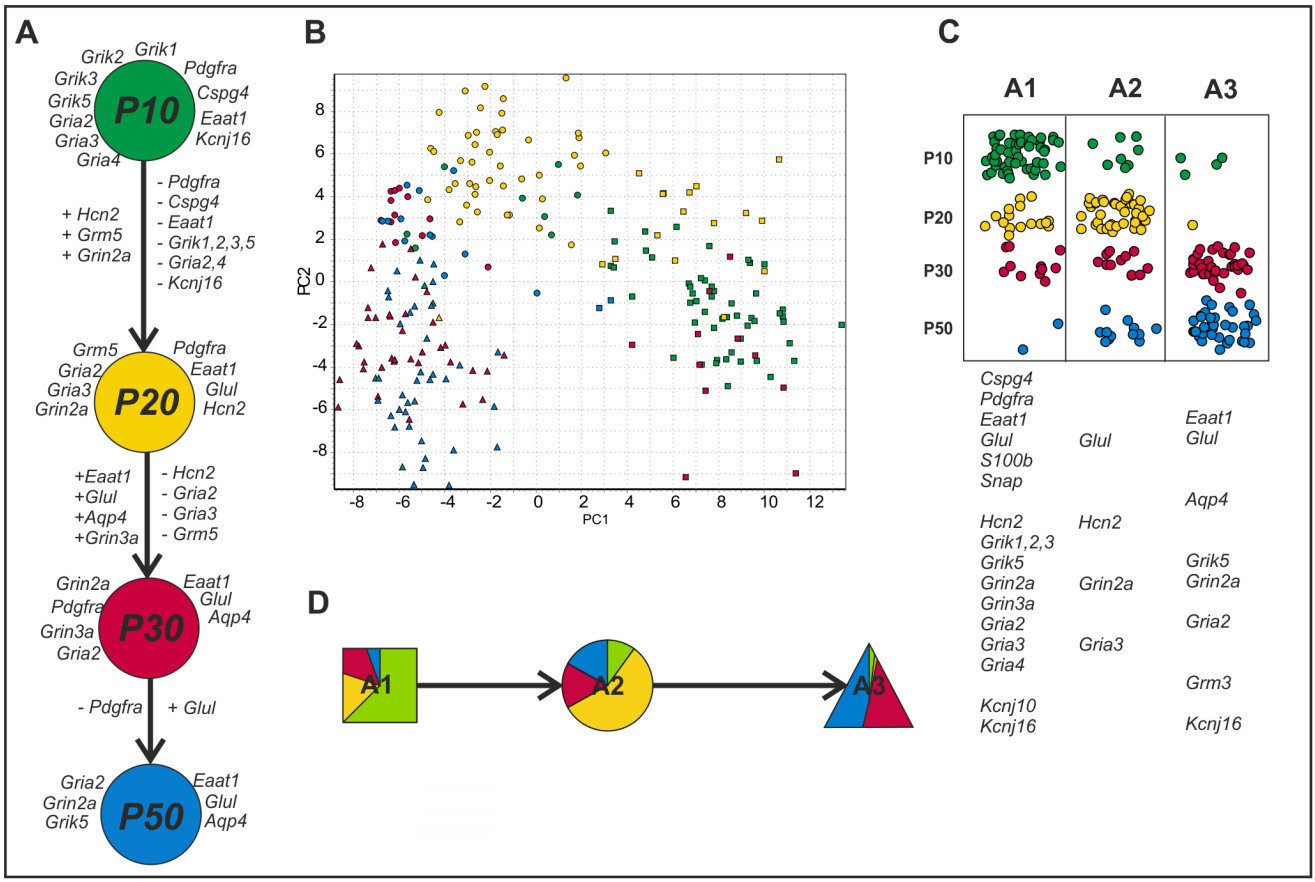

Figure 3. Gene expression profiling of cortical EGFP$^+$ cells during postnatal development. (**A**) Changes in the gene expression of highly expressed (log_2 relative average expression above 2.3 from all data) astrocytic/NG2 glia markers and membrane proteins at P10 (green), P20 (yellow), P30 (red), and P50 (blue). The listed genes show at least 2-fold up (+) or 2-fold down-regulation (−) between sequential developmental stages. (**B**) PCA clustering of cells from all development stages (data mean-centered along genes). The stages are indicated in color (P10 green; P20 yellow; P30 in red, and P50 in blue), and the three groups identified by SOM are indicated by symbols (squares for A1; circles for A2, and triangles for A3). (**C**) The incidence of cells from the three subpopulations at different postnatal developmental stages. The genes under the table indicate highly expressed genes (log2 relative average expression above 1.8 and at least 40% positive cells) in particular subpopulations. (**D**) The distribution of developmental stages in the subpopulations.
doi:10.1371/journal.pone.0069734.g003

fluorescence of these cells was much higher compared to that of cells classified as B1 and B2.

Generally, astrocytes isolated from post-ischemic stages (D3, D7 and D14) showed much higher gene expression than those collected from the postnatal developmental stages. Within each subpopulation B1-B3 we found many significant correlations. The strongest are listed in Tables S6, S7 and S8 and visualized in Figure S2D–F. Interestingly, the expression of *Pdgfra* and of *Cspg4* were strongly correlated when cells with non-measurable expression (r = 0.89, 0.71 and 0.87 in B1, B2 and B3) were included, but the correlation was lost when only cells with measurable expression were considered. The expressions of *Eaat1* and *Glul* in B1 and B3 were correlated (r = 0.66 and 0.79), and a correlation of *Eaat1* and *Aqp4* was found in B1, B2 and B3 (r = 0.43, 0.69, 0.81). A strong correlation was also found between the expressions of *Gfap* and *Gfapδ* in B1 and B2 (r = 0.76 and 0.87) and between the expressions of *Aqp1* and *Aqp9* in B3 (r = 0.78). The expressions of the latter two genes also correlated with those of *Hcn1*, *Hcn2*, *Hcn3*, *Hcn4*, *Grin2a*, *Grin2d*, *Gria3*, *Grm5*, *Kcna3*, *and Kcnk2*. In fact, the expressions of almost all of these genes were strongly correlated on the single cell level in B3 (r close to or larger than 0.7, Figure S4A). Such a strong correlation between the above-listed genes suggests significant alterations in the membrane properties of reactive astrocytes at D14, namely the appearance of *Hcn1-4*, which so far have been described only in neurons [36]. On the other hand, a significant negative correlation was found between the expressions of *Cspg4* or *Pdgfra* and *Glul*, *Aqp9*, *Hcn1*, *Grin2a* and *Gria3* (r<-0.55). This clearly demonstrates that astrocytes from D14 (B3 subpopulation) lose the expression of *Cspg4* and *Pdgfra* while they change into reactive astrocytes comprising a permanent glial scar.

The calculated partial Spearman correlation coefficients surprisingly indicated that there was no direct interaction between *Aqp9* and *Aqp1* (Figure S4B), but the observed correlation can be accounted for as being mediated via *Hcn2* or *Kcna3*. Further, *Aqp9* does not mediate any interaction between *Hcn1*, *Hcn2*, *Hcn3*, *Gria3*, *Grm5* and *Aqp1*. Out of the total 21 possible direct interactions, *Gria3* and *Hcn2* were involved in 10 (Figure S4C and S2D).

Further classification of the reactive glial cells in subpopulation B3 using SOM revealed that it is not a homogenous group; rather there are two subgroups, which we refer to as B3A and B3B. Their existence was clearly confirmed by PCA (Figure 6A). Viewing the data in a 3-dimensional PC1 vs. PC2 vs. PC3 space shows that the B3A/B3B subpopulations separate along PC3 (Figure 6B). Hence, the genes distinguishing B3A from B3B are those with high

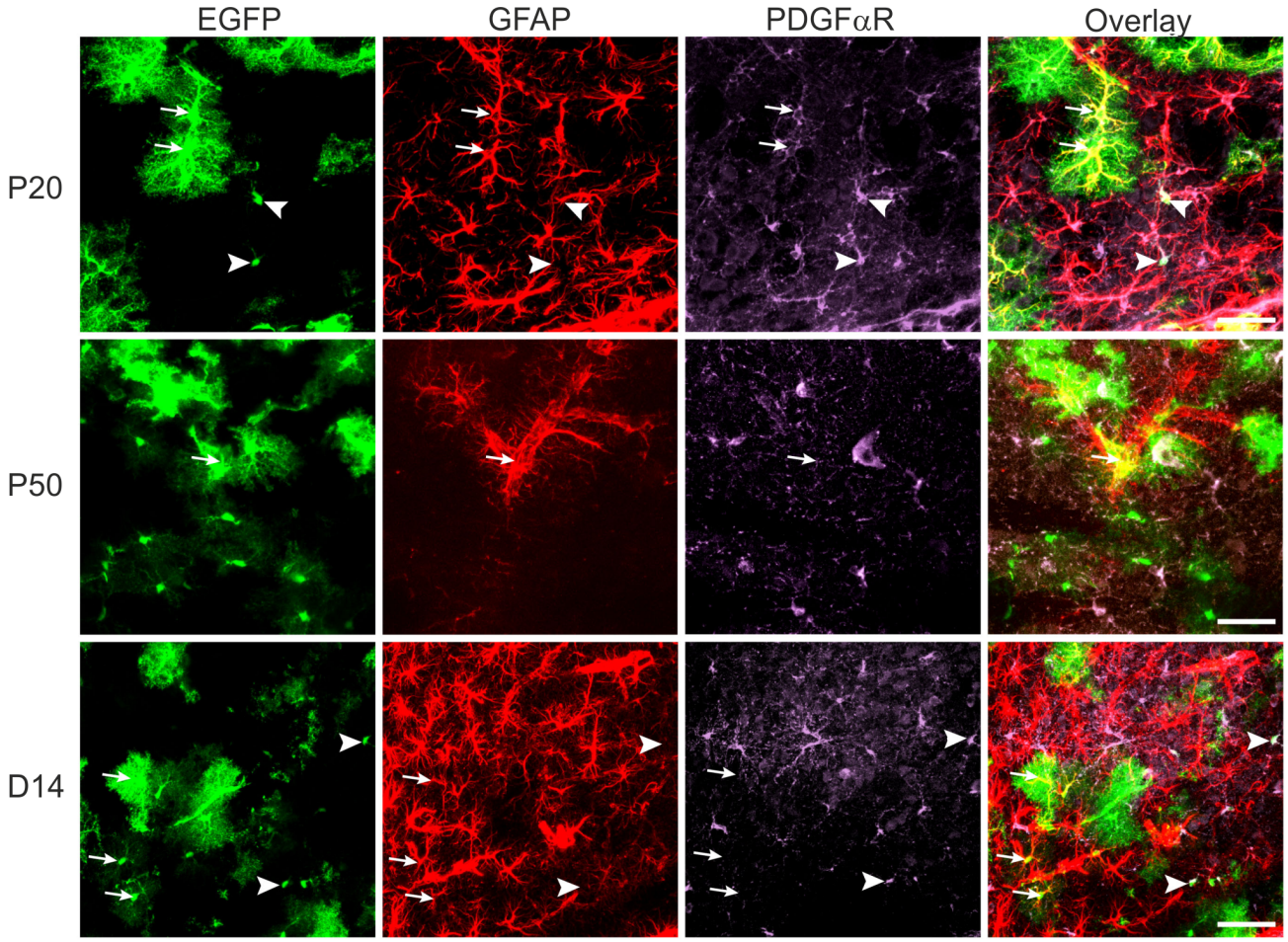

Figure 4. Immunohistochemical analysis of EGFP$^+$ cells. P20, P50, and D14 cells expressing EGFP (green), GFAP (red), and PDGFαR (violet). Arrowheads indicate cells co-expressing EGFP and PDGFαR, and arrows indicate cells positive for EGFP and GFAP. Note, at P20 there are cells positive for all three markers. Scale bars, 50 µm.
doi:10.1371/journal.pone.0069734.g004

weights in PC3, thus being different from the genes distinguishing B3 from B1/B2, which are those with high weights in PC1 and PC2. The expression of genes in the B3A and B3B subgroups were compared using the non-parametric Mann-Whitney test, and those with significant p-values after Bonferroni correction for multiple testing ($p<0.00109$) are shown in Figure 6C. The most important differences between the B3A and B3B subgroups are the down-regulation of *Pdgfra, Cspg4* and *Grik2* and the up-regulation of *Eaat1, Glul, Aqp1, Aqp4, Aqp9, Hcn1, Hcn2, Hcn3, Grin2a, Gria3, Grm3, Grm5* and *Kcna3* (Figure 6C).

Similarly as in the early stages of development, post-ischemic astrocytes also co-expressed *Gfap* and *Cspg4/Pdgfra* (approximately 40%); however, on the protein level we did not detect such co-expression (Figure 4).

Discussion

We show that cortical EGFP$^+$ cells collected during postnatal development as well as cells collected after focal cerebral ischemia are highly heterogeneous with respect to their gene expression profiles. Our findings demonstrate that the issue of astrocyte heterogeneity is complicated, but can be approached with single cell expression profiling, which reveals and distinguishes cell subpopulations. With single cell resolution we can identify rare cells, an approach impossible in classical bulk measurements [37]. Furthermore, single cell profiling avoids the ambiguity of normalization [38].

Astrocyte Heterogeneity during Postnatal Development

We have shown that during postnatal development, the number of EGFP$^+$ cells expressing the astrocytic markers *Glul* and/or *Eaat1* increases towards adulthood, while the number of cells expressing *Cspg4* and/or *Pdgfra* is reduced. Similarly to previous findings, we show that in addition to *Glul*, the expression of *Eaat1*, *Aqp4* and *Grin2a* is induced during development [39]. This is an opposite tendency to that reported by Stanimirovic and colleagues [40], but their experiments were carried out *in vitro*, in a purely astrocytic culture, where glutamate uptake and glutamine synthesis might be compromised. We also found a substantial decrease in *Grik2, Grik3, Gria2, Gria3* and *Gria4* expression during development, which is in agreement with previous data demonstrating the expression of kainate receptors in glial precursor cells, while mature astrocytes show an NMDA-specific responses [41,42]. Similar decline in *Grik1-5* expression during development was described recently by Cahoy and colleagues (Cahoy et al., 2008). In agreement with the findings of Matthias and colleagues [43], we found that EGFP$^+$ cells that express *Cspg4* and/or *Pdgfra* also express *Gria2-4* at high levels, while the low expression of *Gria2-4* is observed in EGFP$^+$

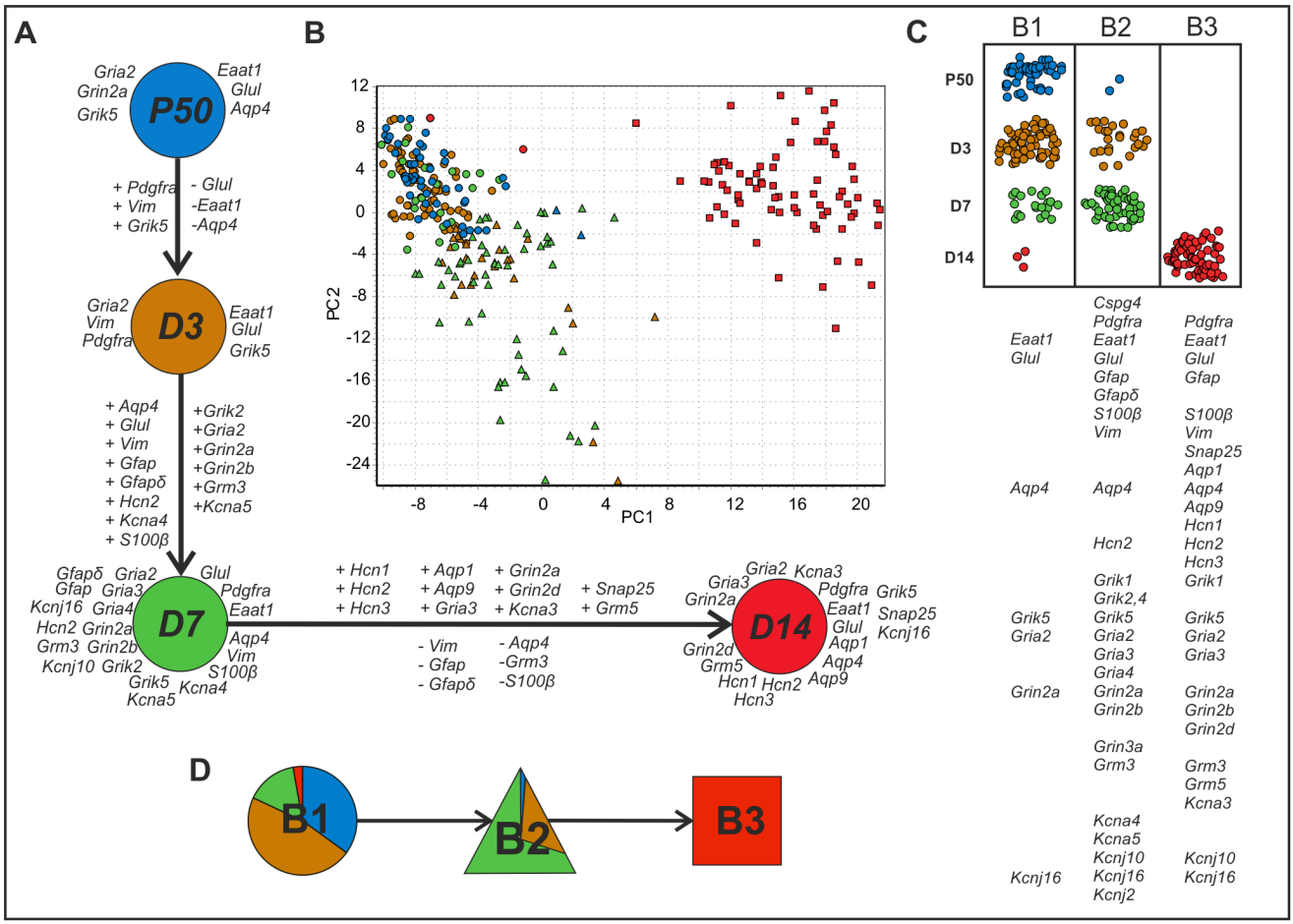

Figure 5. Change in the gene expression of EGFP$^+$ cells after MCAO. (**A**) Changes in the gene expression of highly expressed (log_2 relative average expression above 2.3 from all data) astrocytic/NG2 glia markers and membrane proteins at P50 (blue), D3 (orange), D7 (green), and D14 (red). The listed genes show at least 2-fold up (+) or 2-fold downregulation (−) between sequential stages. (**B**) PCA clustering of cells from all post-ischemic stages and P50 (data mean-centered along genes). The stages are indicated in color (P50 blue, D3 orange, D7 green, and D14 red), and the three groups identified by SOM are indicated by symbols (squares for B3; circles for B1 and triangles for B2). (**C**) The incidence of cells from the three subpopulations at post-ischemic stages and P50. The genes under the table indicate highly expressed genes (log2 relative average expression above 1.8 and at least 40% positive cells) in particular subpopulations. (**D**) The distribution of control and post-ischemic stages in individual subpopulations.
doi:10.1371/journal.pone.0069734.g005

astrocytes that do not express markers of polydendrocytes. These authors also claimed that EGFP$^+$ cells co-express glutamate receptors and transporters, which is supported by our single cell data. As shown in Table 1, we found the co-expression of glutamate receptors and glutamate transporters in individual EGFP$^+$ cells. Among cells collected at the postnatal developmental stages P10-P50, we distinguish 3 subpopulations here referred to as A1, A2 and A3 (Figure 3). A3 cells exhibit features previously described in mature astrocytes with very high expression of *Eaat1*, *Glul* and *Aqp4* [23]. Cells in A1 also express *Eaat1*, but they also have high levels of *Cspg4* and *Pdgfra*, which are traditionally associated with NG2 glia [44]. Nevertheless, *Cspg4* expression in P1-P17 astrocytes was already described elsewhere (Cahoy et al., 2008). Subpopulation A2 is the most unique with high expression of *Glul*, *Hcn2*, *Gria3*, and *Grin2a*, while the transcriptional activity of the other studied genes is rather low. Based primarily on the elevated expression of *Glul* and the low *Gria3* levels, we hypothesize that A2 is an intermediate stage between A1 and A3 (Table S2). This hypothesis is also supported by the prevalence of A2 cells at P20. It is still a matter of debate whether astrocytes can be derived from CSPG4- and/or PDGFαR-positive cells; some recent evidence suggests this possibility following CNS injuries [9,12]. Interestingly, the A1 subpopulation, mostly comprising cells from P10–20, is characterized by the increased expression of subunits of ionotropic AMPA/kainate receptors, such as *Grik1-3*, *Grik5*, *or Gria2-4*, which makes these cells sensitive to AMPA/kainate receptor–mediated glutamate injury. The presence of *Gria2* encoding GluA2 subunits suggests that AMPA receptors in the A1 subpopulation might be impermeable for Ca^{2+}. The subpopulations A3 and B1, which mainly represent mature astrocytes at P30-P50, show besides the expression of classical markers such as *Eaat1*, *Glul* and *Aqp4*, also the dominant expression of *Gria2*, suggesting AMPA receptor impermeability to Ca^{2+}. Moreover, *Kcnj10* and *Kcnj16*, encoding inwardly rectifying Kir4.1 and Kir5.1 channels, are both highly expressed in immature cortical glia, while in mature astrocytes *Kcnj16* prevails. Since heteromeric Kir4.1/5.1 and homomeric Kir4.1 have distinct ion channel properties, such differences in the expression of K^+ channels that participate in K^+ uptake might result in the diverse ability of astrocytes to take up/distribute high extracellular K^+ during increased neuronal activity or in pathological states, such as ischemia or trauma. Notably, even though mature/immature

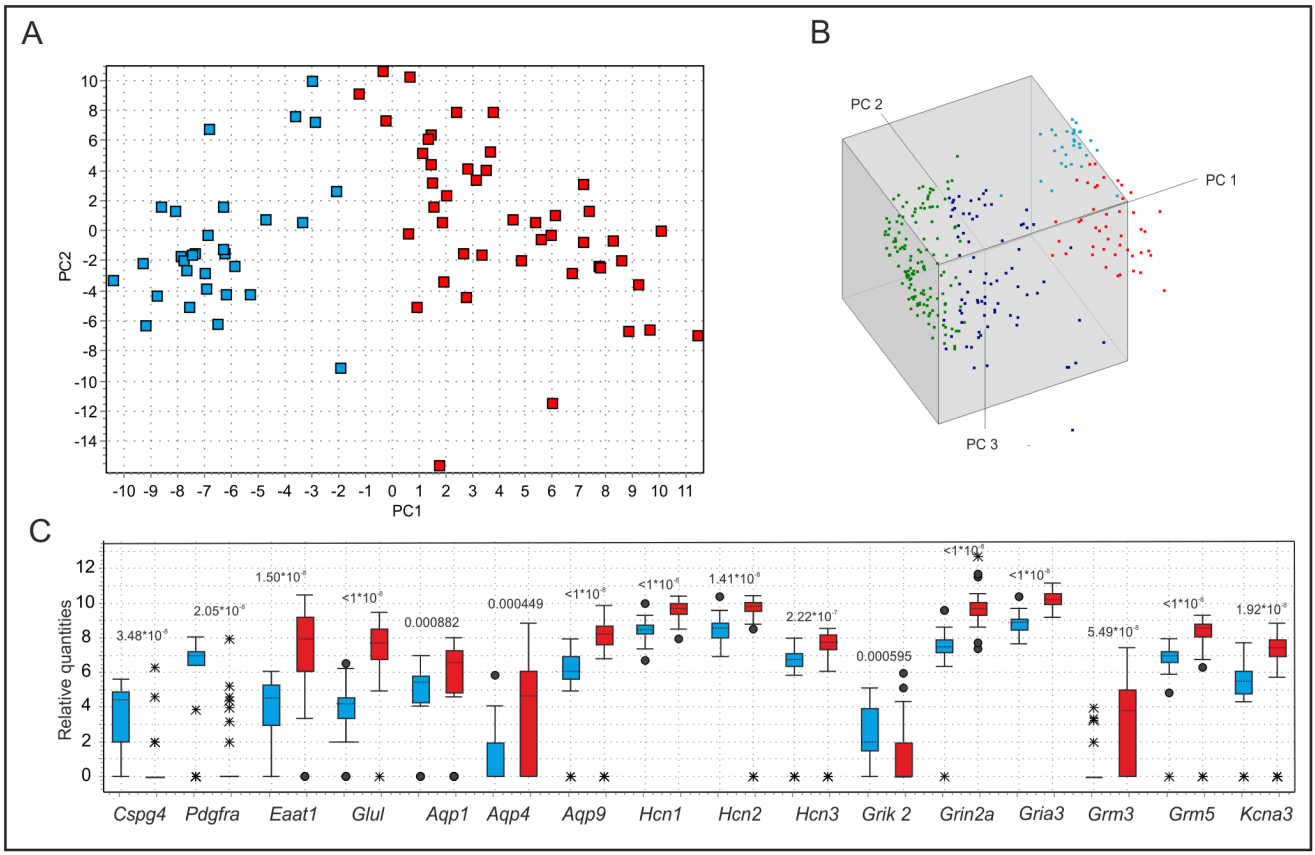

Figure 6. Classification of reactive glia (B3) into two subgroups. (A) PCA scatter plot of the cells in subpopulation B3 (reactive glia). Colors indicate the two groups (B3A red and B3B blue) obtained by decomposing the data by SOM analysis (data are mean-centered). (B) Three-dimensional PCA scatter plot of all post-ischemic cells and P50 reflecting the normal state for comparison - B1 (green), B2 (dark blue), B3A (red) and B3B (light blue). PC3 separates B3A from B3B. The first PC accounts for 32%, the second 14% and the third 8%, of the total variance in the data. (C) Box plots showing genes differentially expressed in B3A (red) and B3B (blue). The box indicates the median value and the 25th and 75th percentiles, the whiskers are 1.5× the distance of the 25th and 75th percentiles, the circles indicate outliers and the crosses extreme outliers. p-values (Mann-Whitney) are indicated for each gene.
doi:10.1371/journal.pone.0069734.g006

astrocytes have been shown to display different K^+ current profiles during development in the rat hippocampal CA1 region [45], such as outward rectifying, variably rectifying and passive current patterns, we found no significant differences in the transcription activities of inwardly and outwardly rectifying K^+ channels or K2P channels between the A1-A3 subpopulations. We found the expression of *Kcnj10* (encoding the Kir4.1 channel) in the $EGFP^+$ cells to be rather constant, while higher levels of *Kcnj16* (encoding Kir5.1) transcripts were found in cells from subpopulations A1 and A3. We did not see any correlation between *Aqp4* and *Kcnj10* expression on the cellular level in any of the subpopulations in agreement with previous data showing the lack of any direct interaction between Kir4.1 and AQP4 [46,47] and their different regulations of expression [48]. In agreement with recent findings [25,49] we showed that $EGFP^+$ mature cortical astrocytes from P30 and P50 (comprising the B3 subpopulation) express low levels of *Grm5*, as a result of a significant decrease in *Grm5* expression towards astrocytic maturation, and a high level of *Grm3*. Nedergaard and colleagues suggested that mGluR5 activity underlies glutamate–induced Ca^{2+} signalling only in immature postnatal astrocytes, while in mature astrocytes other transmitters, such as endocannabinoids, purines, norepinephrine, and acetylcholine, as well as changes in extracellular Ca^{2+}, may trigger astrocytic Ca^{2+} signalling. The activation of mGluR3, a Gi/Go receptor negatively coupled to adenylate cyclase, probably does not participate in glutamate-induced Ca^{2+} signalling as its activation did not trigger a Ca^{2+} increase in adult astrocytes [49]. Since the activation of mGluR3 inhibits cyclic adenosine monophosphate (cAMP) formation, it might participate in the regulation of processes such as astrocyte proliferation, the expression of glutamate receptor GLAST or GFAP expression [50,51].

Gene Expression in Post-ischemic Astrocytes

After CNS injury, such as trauma or ischemia, or in CNS neurodegenerative disorders, the properties of astrocytes change; the cells become reactive [52,53]. This is in line with our finding that the gene expression profile of astrocytes alters following focal ischemia. Particularly affected is the expression of *Gfap, Gfapδ*, *S100b* and *Vim*, which was also observed previously [13,53]. Fourteen days after ischemia, *Aqp1* and *Aqp9* were up-regulated as described earlier [14,15], and similarly to previous reports, we found upregulated *Grm5* [18,19]. Generally, *Aqp1* and/or *Aqp9* are elevated in hypertrophied, GFAP overexpressing astrocytes in a number of pathological states, such as ischemic or traumatic brain injury, Alzheimer's or Creutzfeldt-Jakob diseases [54–56]. In the present study, we detected their increased expression only in the B3 subpopulation, which comprises mostly $EGFP^+$ cells 14 days

after MCAO. Such a delayed increase in their expression suggests that they are probably not implicated in water movements during oedema formation/resolution, but they might play a role as metabolite channels facilitating the diffusion of glycerol and lactate, as suggested previously [57,58]. Moreover, the ischemic brain undergoes marked remodelling, which involves the migration of neighbouring cells to the injury site, thus the increased *Aqp1* expression may reflect a migratory phenotype of reactive astrocytes as AQP1 was shown to promote cell migration in epithelial cells [59] and glial tumors [60,61]. The B2 and B3 subpopulations also highly express AMPA receptor subunits, especially *Gria3*, which suggests that AMPA receptors may significantly contribute to Na^+/Ca^{2+} influx into the reactive astrocytes, and together with the strong expression of metabotropic glutamate receptors (*Grm1, Grm5*) these receptors possibly mediate Ca^{2+} oscillations and glutamate release, as mentioned previously [62]. Furthermore, an increase in *Grm5* expression in reactive astrocytes might lead to the increased activity of mGluR5 and thus contribute to astrocytic apoptosis, as described recently [63]. On the other hand, an anti-apoptotic effect mediated by mGluR3 activation that leads to reduced intracellular levels of cAMP was described in cultured astrocytes after their exposure to nitric oxide [64]. In addition, Aguado and colleagues [65] demonstrated that the activation of ionotropic glutamate receptors is required for the generation of correlated astrocytic network activity, essential for neuronal development and synaptic plasticity. In mature astrocytes under physiological conditions (P50), the Ca^{2+} permeability of AMPA receptors is diminished compared to immature stages (P10) due to the predominant expression of *Gria2*. Interestingly, mRNAs encoding kainate receptor subunits (*Grik1,2,3,5*) are also significantly increased in the B2 and B3 subpopulations; however, their function in reactive astrocytes and those from immature (P10) animals has not yet been elucidated.

Marked changes were also observed in the expression of different types of ion channels, such as outwardly and inwardly rectifying K^+ channels and chloride channels (ClC2), and moreover, Trpv4 expression almost doubled after ischemia, when comparing the B2 and B3 subpopulations to B1. Despite the fact that the expression of *Kcna3-5*, encoding the outwardly rectifying K^+ channels Kv1.3, Kv1.4 and Kv1.5, was comparable in the A1–3 subpopulations during development, it markedly increased in the post-ischemic B2 and B3 subpopulations. Such an increase might point to the fact that astrocytes enter the cell cycle and proliferate following ischemic injury, as shown previously [66]. In addition, an increase in *Clc2* expression could suggest the participation of astrocytes in delivering Cl^- to the site of intensive GABAergic transmission [67], or Cl^- efflux can play a role in astrocyte proliferation/migration as suggested for gliomas [68]. Furthermore, enhanced *Trpv4* expression following MCAO was detected in both the B2 and B3 subpopulations, which is in agreement with our recent data demonstrating an increased expression/function of TRPV4 following hypoxic/ischemic injury of the rat hippocampus [69]. TRPV4 upregulation might originate from its role as an osmosensor as shown in astrocytes [70] or from a possible role of this channel in Ca^{2+} signalling in post-ischemic astrocytes, which may result in astrocytic cell death [71]. A transient increase in *Nes* observed in cells 3 and 7 days after MCAO might support the hypothesis that these subpopulations comprise proliferative/newly derived cells. A striking finding is the high expression of *Hcn1-4*, which encodes hyperpolarization–activated non-specific cationic channels permeable for K^+/Na^+, so far described only in neurons. Despite the fact that their role in astrocytes is unknown, we hypothesize that they might have a role in determining the astrocyte resting membrane potential or they might interact with the glutamate release machinery as described recently for presynaptic terminals [72]. A question that still remains incompletely elucidated is the origin of reactive glia. Certain subpopulations of reactive astrocytes have been shown to arise from NG2 glia [73] or from proliferating astrocytes [74]. Based on our findings, we propose that the B2 subpopulation, which is characterized by an increase in the expression of several astrocytic markers including *Gfap, S100b, Gfapδ* and *Vim*, but also by a marked increase in *Nes, Pdgfra* and *Cspg4*, comprises astrocytes in an ''intermediate stage'' that increase in number as astrogliosis develops (Figure 5). We hypothesize that either NG2 glia give rise to the B2 subpopulation, which eventually develops into fully reactive astrocytes with a distinct expression profile as in subpopulation B3, or they might represent dedifferentiated mature astrocytes with increased proliferative activity. The latter possibility is supported by the fact that they display a relatively similar gene expression profile as $EGFP^+$ cells of the immature cortex (Figure 3). Interestingly, B1 and B2 show some similarity (e.g., the expression of *Pdgfra, Cspg4, Grik1-3, Grik5, Gria2-4, Grin2a* and *Kcnj16*) to the A1 subpopulation observed during early postnatal development (Table S2). Using partial Spearman correlation calculations, we did not identify any master gene in B3 that would account for all of the changes observed upon astrocyte reactivity that follows ischemic injury; however, it is clear that *Gria3* and *Hcn2* are of high importance. In subpopulation B3 we identified several, previously not recognized highly expressed genes: *Hcn1-3, Grin2a, Gria2, Gria3, Grm5* and *Kcna3*. We also found the high expression of *Snap25*, which is expressed only minimally in the other subpopulations and has been suggested to be a marker of cells with exocytotic capabilities under physiological conditions [25]. Similar observations were made in rats [75], where SNAP25 was found upregulated 3 and 12 days after injury. Despite the fact that synaptosomal-associated protein SNAP-25 has not been detected in astrocytes but SNAP-23 [76], our data revealed mRNA levels coding SNAP-25 were significantly increased in cortical astrocytes 14 days post-ischemia (B3 subpopulation). As astrocytes are known to release glutamate and aspartate in response to elevated intracellular calcium levels via a vesicular release mechanism in which SNARE proteins are implicated, high levels of *Snap25* might be a sign of a significant glutamate release from reactive astrocytes. We found a positive correlation between the expressions of *Snap25, Eaat1* and *Glul* and the absence of any correlation with *Cspg4* and *Pdgfra* in B3. We also found a strong correlation between *Eaat1* and *Aqp4* expression, which is in accordance with a recent report suggesting the close relation of excitatory amino acid transporters (*Eaat*) and *Aqp4* under pathological conditions with the massive release of glutamate [14]. Although an association between AQP4 and mGluR5 has been reported [77], we found no correlation on the gene expression level. On the other hand, we did find an extremely strong correlation between *Aqp1/Aqp9* and *Grm5* levels in B3.

Heterogeneity of reactive astrocytes in the vicinity of an ischemic lesion has been described previously [22,78,79]. Even within the B3 subpopulation of reactive astroglia, we found evidence for two subgroups using SOM and PCA: B3A and B3B. B3A is positive for traditional astrocytic markers, while B3B has a substantially higher expression of traditional NG2 glia markers (Figure 6). *Cspg4* has been proposed as a hallmark of reactive astrocytes [16]. Even though the entire B3 population has high overall transcriptional activity, much higher than B1 and B2, there is a difference in the expression levels of many genes between the B3A and B3B subgroups. Since we isolated cells from the vicinity of an ischemic lesion, it is possible that B3 comprises cells permanently converted to reactive glia, which are in different

states or at different distances from the site of the ischemic lesion. Employing Affymetrix GeneChip arrays, the gene expression profiling of reactive astrocytes by Zamanian and colleagues [53] provided transcriptome databases for two subtypes of reactive astrocytes that will be highly useful in generating new and testable hypotheses of their function, as well as for providing new markers to detect different types of reactive astrocytes.

Co-expression of PDGFαR and GFAP in EGFP$^+$ Cells

Our finding that at P10 almost all EGFP$^+$ cells express *Cspg4* and *Pdgfra* and that EGFP$^+$ cells co-express *Gfap* and *Cspg4*/*Pdgfra* was confirmed by immunohistochemistry. (Figure 4, Figure S3); [35]. Similarly, Cahoy and co-authors [25] also detected the high expression of *Cspg4* in immature astrocytes (P7, P17), which declined with astrocyte maturation; however, they never detected *Pdgfra* expression in astrocytes, but rather *Pdgfrb*, which is known to be expressed in pericytes [80]. Although GFAP is a traditional marker of astrocytes and we collected cells where the expression of EGFP is driven by a GFAP promoter, its mRNA level was very low, not at all comparable with the expression of *Cspg4* and *Pdgfra*. The GFAP protein must therefore be stable with slow turnover in the cortex. Nevertheless, *Gfap* and *Gfapδ* increased with astrocyte maturation similarly to the highly expressed *Glul, Eaat1* and *Aqp4*. Interestingly, in subpopulations A1, B2 and B3, *Cspg4* and *Pdgfra* are co-expressed on the mRNA level in 95% of cells, but the correlation between their expressions on the single cell level is not particularly strong ($r = 0.44$, $p = 0.001$ for A1, $r = 0.23$, $p = 0.151$ for B2, $r = 0.27$, $p = 0.159$ for B3). *Cspg4* and *Pdgfra* also show quite different correlations with other genes. This suggests *Cspg4* and *Pdgfra* are expressed independently of each other in individual cells, even in cells from the same subpopulation. The absence of correlation between highly expressed genes in individual cells of the same kind has been observed previously [33] and has been interpreted as the cells having independent transcription regulatory mechanisms, which leads to independent transcriptional bursts.

We do not think that the expression of *Cspg4* or *Pdgfra* in EGFP/GFAP cells isolated from the cortex of P10 animals was detected simply due to sensitivity in which low transcript levels are amplified. PDGFαR and NG2 are expressed in these cells also on the protein level as demonstrated by immunohistochemistry in Figure 4 for PDGFαR and in Figure S3 for NG2. These images show without any doubt that EGFP-positive cells (P10–20 mice) co-express GFAP and PDGFαR or NG2, the expression of which disappears at P50. More interestingly, in post-ischemic tissue the expression of both *Cspg4* and *Pdgfra* reappears; however, their expression on the protein level does not coincide with EGFP/GFAP-positive reactive astrocytes, which might suggest that newly generated reactive astrocytes lose both NG2 or PDGFαR when they reach the stage of fully developed reactive astroglia 14 days post ischemia, while those still expressing NG2 and/or PDGFαR might partially comprise cells in transition into reactive astrocytes or dedifferentiated astrocytes that display the gene expression profile of immature P10-P20 astrocytes (A1 subpopulation). This is also obvious from the division of the B3 subpopulation into two groups: B3A and B3B (Figure 6). Cells in the B3A group express *Cspg4* and *Pdgfra*, while the expression of *Eaat1, Glul* and *Aqp4* is significantly lower than in the B3B group. Therefore, NG2 or PDGFαR-positive cells may reflect astrocytes in a transitional stage similar to that described by Zhu and colleagues [81]. They showed that a subpopulation of GS$^+$ astrocytes is the progeny of NG2 cells, thus confirming the previous finding that NG2 cells give rise to protoplasmic astrocytes. They also showed the co-expression of aldehyde dehydrogenase (*Aldh1L*1, another marker of astrocytes) immunoreactivity in their somata and faint PDGFαR immunoreactivity in their processes, indicative of transitional cells that are losing PDGFαR and acquiring Aldh1L1. Similar data showing the co-expression of GFAP and NG2 in ischemic tissue were described in our recent publication [12].

The Basis of Astrocyte Heterogeneity

The heterogeneity of astrocytes even within an individual brain region, such as the cortex, might already arise during their development. Some astrocytes originate from cells in the ventricular zone via radial glia intermediates, while other astrocytes arise from immature cells that migrate in the perinatal period from the dorso-ventral subventricular zone into the brain [82]. Radial glia, which give rise to distinct subsets of forebrain neurons and later on to glial cells, must be highly heterogeneous themselves with respect to their progenitor function, which strongly depends on the expression of different sets of transcription factors such as Emx1 and Dach1. Progenitors expressing these transcription factors give rise, besides cortical and hippocampal CA1 neurons, to a subset of cortical and hippocampal astrocytes [83–85] and also to a subpopulation of astroglia in the dorsal roof of the subventricular zone [86]. How the developmental heterogeneity of astrocytes relates to their functional heterogeneity still remains unresolved. In addition, astrocytes might also display a spatial heterogeneity as they surround blood vessels and/or different synapses. Nonetheless, a diversity of astrocytic responses to pathological stimuli, such as oxygen-glucose deprivation or hypotonic stress, has been demonstrated in the cortex [5,87]. As reported earlier [88], there also exists a subpopulation of astrocytes that do not express GFAP and that were not considered in this study.

Conclusions

We have used single cell expression profiling and multivariate expression analysis to identify and characterize subpopulations of astrocytes present during postnatal development and after focal cerebral ischemia. We found that transcriptional activity decreases during development and that fully mature astrocytes express mainly *Eaat1, Glul, Aqp4* and *Kcnj10* and *Kcnj16*. After a brain injury the situation rapidly changes - the astrocytes become reactive and express *Eaat1, Glul, Aqp1, Aqp9, Snap25,* hyperpolarization-activated cation channels *Hcn1, Hcn2, Hcn3*, glutamate receptors *Grin2a, Gria2, Gria3, Grm5* and potassium channels *Kcna3* and *Vim*.

Supporting Information

Figure S1 Validation of pre-amplification. Three separate RNA samples were isolated from the cortex of three different mice, transcribed and preamplified. cDNA levels were measured with preamplification (P) and without preamplification (NP). The average difference (ΔCq) and the standard deviation of the difference between P and NP for each gene were calculated for each of the three RNA samples.
(TIF)

Figure S2 Schemas of all correlations higher than 0.6 for subpopulation A1 (A), subpopulation A2 (B), subpopulation A3 (C), subpopulation B1 (D), subpopulation B2 (E), and subpopulation B3 (F). Positive correlations are indicated by green lines, while red lines indicate negative correlations.
(TIF)

Figure S3 Immunohistochemical analysis of EGFP$^+$ cells. The expression of GFAP and NG2 was analyzed in the cortex of 10 days-old EGFP/GFAP mice. Note that at P10 there are EGFP-positive cells co-expressing GFAP and NG2.
(TIF)

Figure S4 Interactions between highly expressed "key" genes in subpopulation B3. (**A**) All significant correlations ($p<0.05$) between the expressions of gene pairs are indicated. (**B**) Partial Spearman correlation coefficients were calculated to separate direct and indirect interactions between genes. The lines indicate a direct correlation that remains significant after the removal of indirect (via a third gene) correlations. (**C**) Correlation that remains significant after removing the effect of Hcn2. (**D**) Correlation that remains significant after removing the effect of Gria3.
(TIF)

Table S1 PCR assay information and primer sequences.
(DOCX)

Table S2 Statistics describing the gene expression for each postnatal developmental subpopulation or post-ischemic subpopulations.
(DOCX)

Table S3 Correlation within development subpopulation A1.
(XLSX)

Table S4 Correlation within development subpopulation A2.
(XLSX)

Table S5 Correlation within development subpopulation A3.
(XLSX)

Table S6 Correlation within development subpopulation B1.
(XLSX)

Table S7 Correlation within development subpopulation B2.
(XLSX)

Table S8 Correlation within development subpopulation B3.
(XLSX)

Author Contributions

Conceived and designed the experiments: VR MK MA. Performed the experiments: VR PH DD. Analyzed the data: VR AS MK MA. Contributed reagents/materials/analysis tools: MK MA. Wrote the paper: VR MA.

References

1. Reichenbach WH (2005) Astrocytes and ependymal cells. In: Kettenmann H, Ransom BR, editor. Neuroglia. 2 ed. New York: Oxford University Press. 19–36.
2. Oberheim NA, Takano T, Han X, He W, Lin JH, et al. (2009) Uniquely hominid features of adult human astrocytes. The Journal of neuroscience : the official journal of the Society for Neuroscience 29: 3276–3287.
3. Matyash V, Kettenmann H (2010) Heterogeneity in astrocyte morphology and physiology. Brain research reviews 63: 2–10.
4. Seifert G, Huttmann K, Binder DK, Hartmann C, Wyczynski A, et al. (2009) Analysis of astroglial K+ channel expression in the developing hippocampus reveals a predominant role of the Kir4.1 subunit. The Journal of neuroscience : the official journal of the Society for Neuroscience 29: 7474–7488.
5. Benesova J, Rusnakova V, Honsa P, Pivonkova H, Dzamba D, et al. (2012) Distinct expression/function of potassium and chloride channels contributes to the diverse volume regulation in cortical astrocytes of GFAP/EGFP mice. PLoS One 7: e29725.
6. Ge WP, Miyawaki A, Gage FH, Jan YN, Jan LY (2012) Local generation of glia is a major astrocyte source in postnatal cortex. Nature 484: 376–380.
7. Freeman MR (2010) Specification and morphogenesis of astrocytes. Science 330: 774–778.
8. Zhang Y, Barres BA (2010) Astrocyte heterogeneity: an underappreciated topic in neurobiology. Current opinion in neurobiology 20: 588–594.
9. Trotter J, Karram K, Nishiyama A (2010) NG2 cells: Properties, progeny and origin. Brain research reviews 63: 72–82.
10. Stallcup WB, Beasley L (1987) Bipotential glial precursor cells of the optic nerve express the NG2 proteoglycan. The Journal of neuroscience : the official journal of the Society for Neuroscience 7: 2737–2744.
11. Alonso G (2005) NG2 proteoglycan-expressing cells of the adult rat brain: possible involvement in the formation of glial scar astrocytes following stab wound. Glia 49: 318–338.
12. Honsa P, Pivonkova H, Dzamba D, Filipova M, Anderova M (2012) Polydendrocytes display large lineage plasticity following focal cerebral ischemia. PLoS One 7: e36816.
13. Robel S, Berninger B, Gotz M (2011) The stem cell potential of glia: lessons from reactive gliosis. Nature reviews Neuroscience 12: 88–104.
14. Zelenina M (2010) Regulation of brain aquaporins. Neurochemistry international 57: 468–488.
15. Hwang IK, Yoo KY, Li H, Lee BH, Suh HW, et al. (2007) Aquaporin 9 changes in pyramidal cells before and is expressed in astrocytes after delayed neuronal death in the ischemic hippocampal CA1 region of the gerbil. Journal of neuroscience research 85: 2470–2479.
16. McKeon RJ, Jurynec MJ, Buck CR (1999) The chondroitin sulfate proteoglycans neurocan and phosphacan are expressed by reactive astrocytes in the chronic CNS glial scar. The Journal of neuroscience : the official journal of the Society for Neuroscience 19: 10778–10788.
17. Komitova M, Perfilieva E, Mattsson B, Eriksson PS, Johansson BB (2002) Effects of cortical ischemia and postischemic environmental enrichment on hippocampal cell genesis and differentiation in the adult rat. Journal of cerebral blood flow and metabolism : official journal of the International Society of Cerebral Blood Flow and Metabolism 22: 852–860.
18. Ferraguti F, Corti C, Valerio E, Mion S, Xuereb J (2001) Activated astrocytes in areas of kainate-induced neuronal injury upregulate the expression of the metabotropic glutamate receptors 2/3 and 5. Experimental brain research Experimentelle Hirnforschung Experimentation cerebrale 137: 1–11.
19. Ulas J, Satou T, Ivins KJ, Kesslak JP, Cotman CW, et al. (2000) Expression of metabotropic glutamate receptor 5 is increased in astrocytes after kainate-induced epileptic seizures. Glia 30: 352–361.
20. Jacque CM, Vinner C, Kujas M, Raoul M, Racadot J, et al. (1978) Determination of glial fibrillary acidic protein (GFAP) in human brain tumors. Journal of the neurological sciences 35: 147–155.
21. Sofroniew MV, Vinters HV (2010) Astrocytes: biology and pathology. Acta neuropathologica 119: 7–35.
22. Walz W (2000) Controversy surrounding the existence of discrete functional classes of astrocytes in adult gray matter. Glia 31: 95–103.
23. Regan MR, Huang YH, Kim YS, Dykes-Hoberg MI, Jin L, et al. (2007) Variations in promoter activity reveal a differential expression and physiology of glutamate transporters by glia in the developing and mature CNS. The Journal of neuroscience : the official journal of the Society for Neuroscience 27: 6607–6619.
24. Mearow KM, Mill JF, Vitkovic L (1989) The ontogeny and localization of glutamine synthetase gene expression in rat brain. Brain research Molecular brain research 6: 223–232.
25. Cahoy JD, Emery B, Kaushal A, Foo LC, Zamanian JL, et al. (2008) A transcriptome database for astrocytes, neurons, and oligodendrocytes: a new resource for understanding brain development and function. The Journal of neuroscience : the official journal of the Society for Neuroscience 28: 264–278.
26. Kimelberg HK (2004) The problem of astrocyte identity. Neurochemistry international 45: 191–202.
27. Klein CA, Zohlnhofer D, Petat-Dutter K, Wendler N (2005) Gene expression analysis of a single or few cells. Current protocols in human genetics/editorial board, Jonathan L Haines [et al] Chapter 11: Unit 11 18.
28. Ståhlberg A, Andersson D, Aurelius J, Faiz M, Pekna M, et al. (2011) Defining cell populations with single-cell gene expression profiling: correlations and identification of astrocyte subpopulations. Nucleic acids research 39: e24.
29. Raj A, Peskin CS, Tranchina D, Vargas DY, Tyagi S (2006) Stochastic mRNA synthesis in mammalian cells. PLoS biology 4: e309.
30. Raj A, van Oudenaarden A (2009) Single-molecule approaches to stochastic gene expression. Annual review of biophysics 38: 255–270.

31. Bengtsson M, Hemberg M, Rorsman P, Stahlberg A (2008) Quantification of mRNA in single cells and modelling of RT-qPCR induced noise. BMC molecular biology 9: 63.
32. Ståhlberg A, Rusnakova V, Forootan A, Anderova M, Kubista M (2013) RT-qPCR work-flow for single-cell data analysis. Methods 59: 80–88.
33. Ståhlberg A, Bengtsson M (2010) Single-cell gene expression profiling using reverse transcription quantitative real-time PCR. Methods 50: 282–288.
34. Nolte C, Matyash M, Pivneva T, Schipke CG, Ohlemeyer C, et al. (2001) GFAP promoter-controlled EGFP-expressing transgenic mice: a tool to visualize astrocytes and astrogliosis in living brain tissue. Glia 33: 72–86.
35. Benesova J, Hock M, Butenko O, Prajerova I, Anderova M, et al. (2009) Quantification of astrocyte volume changes during ischemia in situ reveals two populations of astrocytes in the cortex of GFAP/EGFP mice. Journal of neuroscience research 87: 96–111.
36. Wahl-Schott C, Biel M (2009) HCN channels: structure, cellular regulation and physiological function. Cell Mol Life Sci 66: 470–494.
37. Ståhlberg A, Rusnakova V, Kubista M (2013) The added value of single-cell gene expression profiling. Brief Funct Genomics.
38. Sindelka R, Ferjentsik Z, Jonak J (2006) Developmental expression profiles of Xenopus laevis reference genes. Dev Dyn 235: 754–758.
39. da Cunha A, Aloyo VJ, Vitkovic L (1991) Developmental regulation of GAP-43, glutamine synthetase and beta-actin mRNA in rat cortical astrocytes. Brain research Developmental brain research 64: 212–215.
40. Stanimirovic DB, Ball R, Small DL, Muruganandam A (1999) Developmental regulation of glutamate transporters and glutamine synthetase activity in astrocyte cultures differentiated in vitro. International journal of developmental neuroscience : the official journal of the International Society for Developmental Neuroscience 17: 173–184.
41. Palygin O, Lalo U, Pankratov Y (2011) Distinct pharmacological and functional properties of NMDA receptors in mouse cortical astrocytes. Br J Pharmacol 163: 1755–1766.
42. Ziak D, Chvatal A, Sykova E (1998) Glutamate-, kainate- and NMDA-evoked membrane currents in identified glial cells in rat spinal cord slice. Physiological research/Academia Scientiarum Bohemoslovaca 47: 365–375.
43. Matthias K, Kirchhoff F, Seifert G, Huttmann K, Matyash M, et al. (2003) Segregated expression of AMPA-type glutamate receptors and glutamate transporters defines distinct astrocyte populations in the mouse hippocampus. The Journal of neuroscience : the official journal of the Society for Neuroscience 23: 1750–1758.
44. Butt AM, Hamilton N, Hubbard P, Pugh M, Ibrahim M (2005) Synantocytes: the fifth element. Journal of anatomy 207: 695–706.
45. Zhou M, Schools GP, Kimelberg HK (2006) Development of GLAST(+) astrocytes and NG2(+) glia in rat hippocampus CA1: mature astrocytes are electrophysiologically passive. Journal of neurophysiology 95: 134–143.
46. Nagelhus EA, Horio Y, Inanobe A, Fujita A, Haug FM, et al. (1999) Immunogold evidence suggests that coupling of K+ siphoning and water transport in rat retinal Muller cells is mediated by a coenrichment of Kir4.1 and AQP4 in specific membrane domains. Glia 26: 47–54.
47. Connors NC, Adams ME, Froehner SC, Kofuji P (2004) The potassium channel Kir4.1 associates with the dystrophin-glycoprotein complex via alpha-syntrophin in glia. The Journal of biological chemistry 279: 28387–28392.
48. Liu H, Yang M, Qiu GP, Zhuo F, Yu WH, et al. (2012) Aquaporin 9 in rat brain after severe traumatic brain injury. Arquivos de neuro-psiquiatria 70: 214–220.
49. Sun W, McConnell E, Pare JF, Xu Q, Chen M, et al. (2013) Glutamate-dependent neuroglial calcium signaling differs between young and adult brain. Science 339: 197–200.
50. Lyon L, Kew JN, Corti C, Harrison PJ, Burnet PW (2008) Altered hippocampal expression of glutamate receptors and transporters in GRM2 and GRM3 knockout mice. Synapse 62: 842–850.
51. Masood K, Besnard F, Su Y, Brenner M (1993) Analysis of a segment of the human glial fibrillary acidic protein gene that directs astrocyte-specific transcription. J Neurochem 61: 160–166.
52. Pekny M, Nilsson M (2005) Astrocyte activation and reactive gliosis. Glia 50: 427–434.
53. Zamanian JL, Xu L, Foo LC, Nouri N, Zhou L, et al. (2012) Genomic analysis of reactive astrogliosis. The Journal of neuroscience : the official journal of the Society for Neuroscience 32: 6391–6410.
54. Hoshi A, Yamamoto T, Shimizu K, Ugawa Y, Nishizawa M, et al. (2012) Characteristics of aquaporin expression surrounding senile plaques and cerebral amyloid angiopathy in Alzheimer disease. J Neuropathol Exp Neurol 71: 750–759.
55. McCoy E, Sontheimer H (2010) MAPK induces AQP1 expression in astrocytes following injury. Glia 58: 209–217.
56. Rodriguez A, Perez-Gracia E, Espinosa JC, Pumarola M, Torres JM, et al. (2006) Increased expression of water channel aquaporin 1 and aquaporin 4 in Creutzfeldt-Jakob disease and in bovine spongiform encephalopathy-infected bovine-PrP transgenic mice. Acta Neuropathol 112: 573–585.
57. Badaut J, Petit JM, Brunet JF, Magistretti PJ, Charriaut-Marlangue C, et al. (2004) Distribution of Aquaporin 9 in the adult rat brain: preferential expression in catecholaminergic neurons and in glial cells. Neuroscience 128: 27–38.
58. Badaut J, Regli L (2004) Distribution and possible roles of aquaporin 9 in the brain. Neuroscience 129: 971–981.
59. Hara-Chikuma M, Verkman AS (2006) Aquaporin-1 facilitates epithelial cell migration in kidney proximal tubule. J Am Soc Nephrol 17: 39–45.
60. McCoy E, Sontheimer H (2007) Expression and function of water channels (aquaporins) in migrating malignant astrocytes. Glia 55: 1034–1043.
61. Papadopoulos MC, Verkman AS (2008) Potential utility of aquaporin modulators for therapy of brain disorders. Prog Brain Res 170: 589–601.
62. Bezzi P, Carmignoto G, Pasti L, Vesce S, Rossi D, et al. (1998) Prostaglandins stimulate calcium-dependent glutamate release in astrocytes. Nature 391: 281–285.
63. Paquet M, Ribeiro FM, Guadagno J, Esseltine JL, Ferguson SS, et al. (2013) Role of metabotropic glutamate receptor 5 signaling and homer in oxygen glucose deprivation-mediated astrocyte apoptosis. Mol Brain 6: 9.
64. Durand D, Carniglia L, Caruso C, Lasaga M (2011) Reduced cAMP, Akt activation and p65-c-Rel dimerization: mechanisms involved in the protective effects of mGluR3 agonists in cultured astrocytes. PLoS One 6: e22235.
65. Aguado F, Espinosa-Parrilla JF, Carmona MA, Soriano E (2002) Neuronal activity regulates correlated network properties of spontaneous calcium transients in astrocytes in situ. J Neurosci 22: 9430–9444.
66. Anderova M, Vorisek I, Pivonkova H, Benesova J, Vargova L, et al. (2011) Cell death/proliferation and alterations in glial morphology contribute to changes in diffusivity in the rat hippocampus after hypoxia-ischemia. J Cereb Blood Flow Metab 31: 894–907.
67. Sik A, Smith RL, Freund TF (2000) Distribution of chloride channel-2-immunoreactive neuronal and astrocytic processes in the hippocampus. Neuroscience 101: 51–65.
68. Ransom CB, O'Neal JT, Sontheimer H (2001) Volume-activated chloride currents contribute to the resting conductance and invasive migration of human glioma cells. J Neurosci 21: 7674–7683.
69. Butenko O, Dzamba D, Benesova J, Honsa P, Benfenati V, et al. (2012) The increased activity of TRPV4 channel in the astrocytes of the adult rat hippocampus after cerebral hypoxia/ischemia. PLoS One 7: e39959.
70. Benfenati V, Amiry-Moghaddam M, Caprini M, Mylonakou MN, Rapisarda C, et al. (2007) Expression and functional characterization of transient receptor potential vanilloid-related channel 4 (TRPV4) in rat cortical astrocytes. Neuroscience 148: 876–892.
71. Pamenter ME, Perkins GA, McGinness AK, Gu XQ, Ellisman MH, et al. (2012) Autophagy and apoptosis are differentially induced in neurons and astrocytes treated with an in vitro mimic of the ischemic penumbra. PLoS One 7: e51469.
72. Neitz A, Mergia E, Eysel UT, Koesling D, Mittmann T (2011) Presynaptic nitric oxide/cGMP facilitates glutamate release via hyperpolarization-activated cyclic nucleotide-gated channels in the hippocampus. Eur J Neurosci 33: 1611–1621.
73. Zhao JW, Raha-Chowdhury R, Fawcett JW, Watts C (2009) Astrocytes and oligodendrocytes can be generated from NG2+ progenitors after acute brain injury: intracellular localization of oligodendrocyte transcription factor 2 is associated with their fate choice. The European journal of neuroscience 29: 1853–1869.
74. Komitova M, Serwanski DR, Lu QR, Nishiyama A (2011) NG2 cells are not a major source of reactive astrocytes after neocortical stab wound injury. Glia 59: 800–809.
75. Patanow CM, Day JR, Billingsley ML (1997) Alterations in hippocampal expression of SNAP-25, GAP-43, stannin and glial fibrillary acidic protein following mechanical and trimethyltin-induced injury in the rat. Neuroscience 76: 187–202.
76. Hepp R, Perraut M, Chasserot-Golaz S, Galli T, Aunis D, et al. (1999) Cultured glial cells express the SNAP-25 analogue SNAP-23. Glia 27: 181–187.
77. Illarionova NB, Gunnarson E, Li Y, Brismar H, Bondar A, et al. (2010) Functional and molecular interactions between aquaporins and Na,K-ATPase. Neuroscience 168: 915–925.
78. Anderova M, Antonova T, Petrik D, Neprasova H, Chvatal A, et al. (2004) Voltage-dependent potassium currents in hypertrophied rat astrocytes after a cortical stab wound. Glia 48: 311–326.
79. Bordey A, Lyons SA, Hablitz JJ, Sontheimer H (2001) Electrophysiological characteristics of reactive astrocytes in experimental cortical dysplasia. Journal of neurophysiology 85: 1719–1731.
80. Arimura K, Ago T, Kamouchi M, Nakamura K, Ishitsuka K, et al. (2012) PDGF receptor beta signaling in pericytes following ischemic brain injury. Curr Neurovasc Res 9: 1–9.
81. Zhu X, Zuo H, Maher BJ, Serwanski DR, LoTurco JJ, et al. (2012) Olig2-dependent developmental fate switch of NG2 cells. Development 139: 2299–2307.
82. Marshall CA, Suzuki SO, Goldman JE (2003) Gliogenic and neurogenic progenitors of the subventricular zone: who are they, where did they come from, and where are they going? Glia 43: 52–61.
83. Gorski JA, Talley T, Qiu M, Puelles L, Rubenstein JL, et al. (2002) Cortical excitatory neurons and glia, but not GABAergic neurons, are produced in the Emx1-expressing lineage. J Neurosci 22: 6309–6314.
84. Machon O, van den Bout CJ, Backman M, Rosok O, Caubit X, et al. (2002) Forebrain-specific promoter/enhancer D6 derived from the mouse Dach1 gene controls expression in neural stem cells. Neuroscience 112: 951–966.
85. Prajerova I, Honsa P, Chvatal A, Anderova M (2010) Neural stem/progenitor cells derived from the embryonic dorsal telencephalon of D6/GFP mice differentiate primarily into neurons after transplantation into a cortical lesion. Cell Mol Neurobiol 30: 199–218.
86. Honsa P, Pivonkova H, Anderova M (2013) Focal cerebral ischemia induces the neurogenic potential of mouse Dach1-expressing cells in the dorsal part of the lateral ventricles. Neuroscience.

87. Benesova J, Hock M, Butenko O, Prajerova I, Anderova M, et al. (2009) Quantification of astrocyte volume changes during ischemia in situ reveals two populations of astrocytes in the cortex of GFAP/EGFP mice. J Neurosci Res 87: 96–111.

88. Walz W, Lang MK (1998) Immunocytochemical evidence for a distinct GFAP-negative subpopulation of astrocytes in the adult rat hippocampus. Neurosci Lett. 257(3): 127–30.

Neuroscience 240 (2013) 39–53

FOCAL CEREBRAL ISCHEMIA INDUCES THE NEUROGENIC POTENTIAL OF MOUSE *DACH1*-EXPRESSING CELLS IN THE DORSAL PART OF THE LATERAL VENTRICLES

P. HONSA, H. PIVONKOVA AND M. ANDEROVA *

Department of Cellular Neurophysiology, Institute of Experimental Medicine, Academy of Sciences of the Czech Republic, Videnska 1083, Prague, Czech Republic

Abstract—The mouse *Dach1* gene, involved in the development of the neocortex and the hippocampus, is expressed by neural stem cells (NSCs) during early neurogenesis, and its expression also continues in a subpopulation of cells in the dorsal part of the lateral ventricles (LV) of the adult mouse brain. In this study we aimed to elucidate the role of *Dach1*-expressing cells in adult neurogenesis/gliogenesis under physiological as well as post-ischemic conditions, employing transgenic mice in which the expression of green fluorescent protein (GFP) is controlled by the D6 promotor of the mouse *Dach1* gene. A neurosphere-forming assay of GFP$^+$ cells isolated from the dorsal part of the LV was carried out with subsequent differentiation *in vitro*. To elucidate the neurogenic/gliogenic potential of GFP$^+$ cells in the dorsal part of the LV, *in situ* immunohistochemical/electrophysiological analyses of GFP$^+$ cells in adult sham-operated brains (controls) and those after middle cerebral artery occlusion (MCAo) were performed. The GFP$^+$ cells isolated from the dorsal part of the LV of controls formed neurospheres and differentiated solely into a glial phenotype, while those isolated after MCAo also gave rise to cells with the properties of neuronal precursors. *In situ* analyses revealed that GFP$^+$ cells express the phenotype of adult NSCs or neuroblasts in controls as well as following ischemia. Following MCAo we found a significantly increased number of GFP$^+$ cells expressing doublecortin as well as a number of GFP$^+$ cells migrating through the rostral migratory stream into the olfactory bulb, where they probably differentiated into calretinin$^+$ interneurons. Collectively, our results suggest the involvement of the mouse *Dach1* gene in adult neurogenesis; cells expressing this gene exhibit the properties of adult NSCs or neuroblasts and respond to MCAo by enhanced neurogenesis.

Key words: mouse *Dach1* gene, adult neurogenesis/gliogenesis, MCAo, patch-clamp, interneurons, rostral migratory stream.

INTRODUCTION

Adult neurogenesis is a spatially restricted process that takes place under normal conditions in two specific neurogenic brain regions: the subgranular zone (SGZ) in the dentate gyrus of the hippocampus, where new dentate granule cells are generated, and the subventricular zone (SVZ) of the lateral ventricles (LV), where new neurons are generated and then migrate through the rostral migratory stream (RMS) to the olfactory bulb to become interneurons (Gage, 2002). Adult neurogenesis responds to external or internal stimuli by changing the rate of new cell production, accompanied by an expansion of the neurogenic regions. Ischemic brain injury is one of the most important triggers of such neurogenic region expansion, resulting in increased neurogenesis and the promotion of neuroblast migration to the ischemic boundary in the cortex and striatum (Jin et al., 2001; Arvidsson et al., 2002; Parent et al., 2002). Here, the newborn neuroblasts differentiate into GABAergic neurons or interneurons (Arvidsson et al., 2002; Hou et al., 2008; Liu et al., 2009), and the latter are integrated into neuronal networks receiving synaptic input and firing action potentials (Yamashita, 2006; Hou et al., 2008).

The location of SVZ neurogenesis is predominantly situated in the lateral walls of the LV (Ming and Song, 2011); however, a subpopulation of newly derived cells may, under certain circumstances, arise in the dorsal part of the LV (Kohwi et al., 2007). Based on fate-mapping studies, the cells in the dorsal part of the LV originate in the embryonic cortex and can be found only in the dorsal part of the LV. The well described homeobox protein Emx-1, a member of the Emx family of transcription factors, plays an important role in controlling the embryonic development of the dorsal cortex and subsequently, it determines the phenotype of the cells in the dorsal part of the LV (Young et al., 2007). A similar role is played by the mouse *Dach1* gene, a recently

*Corresponding author. Address: Department of Cellular Neurophysiology, Institute of Experimental Medicine (ASCR), Videnska 1083, 142 20 Prague 4, Czech Republic. Tel: +420-241062050; fax: +420-241062783.

E-mail address: anderova@biomed.cas.cz (M. Anderova).

Abbreviations: aCSF, artificial cerebrospinal fluid; aNSCs, adult neural stem cells; bFGF, basic fibroblast growth factor; BLBP, brain lipid-binding protein; CD, current densities; DAPI, 4,6-diamidino-2-phenylindole; DCX, doublecortin; EDTA, ethylenediaminetetraacetic acid; EGTA, ethylene glycol tetraacetic acid; GCL, granular cell layer; GFAP, glial fibrillary acidic protein; GFP, green fluorescent protein; GL, glomerular layer; HEPES, 4-(2-hydroxyethyl)-1-piperazineethanesulfonic acid; LV, lateral ventricles; MCA, middle cerebral artery; MCAo, middle cerebral artery occlusion; OB, olfactory bulb; PB, phosphate buffer; PBS, phosphate-buffered saline; PLL, poly-L-lysine; PTB, pentobarbital; RMS, rostral migratory stream; SVZ, subventricular zone; TH, tyrosine hydroxylase; TTC, triphenyltetrazolium chloride; TTX, tetrodotoxin.

0306-4522/13 $36.00
http://dx.doi.org/10.1016/j.neuroscience.2013.02.048

identified mouse homolog of Drosophila dachshund that is expressed in various embryonic tissues, including the developing neocortex (Machon et al., 2002). A forebrain-specific 2.5-kb enhancer element termed D6 from the mouse *Dach1* gene was isolated by Machon et al. (2002), and a D6-green fluorescent protein (GFP) reporter gene mouse line was created. In these mice, D6 enhancer activity is first detected at embryonic day 10.5 in scattered cells of the arising cortical vesicles, while by embryonic day 12.5, D6 activity expands throughout the developing neocortex and the hippocampus. Cultured D6/GFP cells, which were derived from the embryonic and early postnatal neocortex, show characteristics of neural stem cells (Prajerova et al., 2009). In the adult mouse brain, D6 enhancer activity is persistent in some subpopulations of neurons and astrocytes of the cortical plate, in the CA1 layer of the hippocampus and in certain cell subpopulations in the dorsal part of the LV.

In this study we aimed to elucidate the role of the GFP-positive cell subpopulation that persists in the dorsal part of the LV and displays a sustained *D6* promoter/enhancer activity (further termed GFP^+ cells) in adult neurogenesis or gliogenesis under physiological as well as ischemic conditions. We were interested whether the neural stem/progenitor phenotype of GFP^+ cells that was described previously in the embryonic and early postnatal phases is also maintained in adult mice; therefore, we used a neurosphere-forming assay with isolated GFP^+ cells and their subsequent *in vitro* differentiation, followed by immunocytochemical and electrophysiological analyses. We also aimed to define the immunohistochemical and electrophysiological properties of GFP^+ cells in the dorsal part of the LV *in situ*. Since many types of CNS injuries lead to a significant expansion of regions where SVZ neurogenesis takes place (Gotts and Chesselet, 2005), we employed a model of cortical focal cerebral ischemia to determine whether GFP^+ cells in the dorsal part of the SVZ could respond to this pathological condition by increased proliferation or differentiation. Moreover, we aimed to elucidate whether GFP^+ cells in the dorsal wall of the LV can play a significant role in the process of post-ischemic neuroregeneration in the adult cortex.

EXPERIMENTAL PROCEDURES

Transgenic mice

All procedures involving the use of laboratory animals were performed in accordance with the European Communities Council Directive 24 November 1986 (86/609/EEC) and animal care guidelines approved by the Institute of Experimental Medicine ASCR Animal Care Committee.

For all experiments we used D6/GFP mice, kindly provided by Dr. Machon and Dr. Kozmik (Machon et al., 2002).

Induction of distal middle cerebral artery occlusion (MCAo) in adult mice

Mice (60–90 days old) were anaesthetized for induction with 1.5% isoflurane and maintained in 1% isoflurane using a vaporizer (Tec-3, Cyprane Ltd., Keighley, UK). A skin incision between the orbit and the external auditory meatus was made, and a 1–2 mm hole was drilled through the frontal bone 1 mm rostral to the fusion of the zygoma and the squamosal bone and ~3.5 mm ventral to the dorsal surface of the brain. The middle cerebral artery (MCA) was exposed after the dura was opened and removed. The MCA was occluded by short coagulation with bipolar tweezers at a proximal location, followed by transection of the vessel to ensure permanent disruption. The mice received 0.5-ml saline subcutaneously, and their body temperature during the surgery was maintained at 37 ± 1 °C using a heating pad. Sham-operated animals (controls) were subjected to the same surgery procedure, without dura opening and vessel occlusion. To visualize the ischemic region, unfixed brain slices were stained with 2% 2.3.5-triphenyltetrazolium chloride (TTC) at 37 °C for 20 min. This MCAo model yielded smaller infarcts localized only in the cortical region; however, benefits from minimal mortality when compared to an intraluminal approach (Xi et al., 2004).

Isolation of NSCs from the dorsal part of the lateral ventricles

Control animals or mice 4 days after MCAo were deeply anesthetized with sodium pentobarbital (PTB, 100 mg/kg, i.p.), and perfused transcardially with cold (4–8 °C) isolation solution containing (in mM): 110 NMDG-Cl, 2.5 KCl, 24.5 $NaHCO_3$, 1.25 Na_2HPO_4, 0.5 $CaCl_2$, 7 $MgCl_2$, 20 glucose, osmolality 290 ± 3 mOsmol/kg. The forebrain was isolated by the removal of the olfactory lobes, cerebellum, and midbrain/hindbrain structures by dissection. To isolate the dorsal part of the LV, the brain was sliced in 0.45-mm coronal sections using a vibrating microtome HM650V (MICROM International GmbH, Walldorf, Germany), and the dorsal part of the LV was carefully dissected away from the dorsal white matter tracks and from the lateral walls of the ventricular zone. The tissue was incubated with continuous shaking at 37 °C for 60 min in 5 ml of a papain solution (20 U/ml) and 0.2-ml DNAase (both from Worthington, Lakewood, NJ). After papain treatment the tissue was mechanically dissociated by gentle trituration using a 1-ml pipette. Dissociated cells were layered on top of 5 ml of Ovomucoid inhibitor solution (Worthington) and harvested by centrifugation (140*g* for 6 min). The resulting single-cell suspension was cultured as floating neurospheres in a humidified atmosphere with 5% CO_2 at 37 °C and maintained in Neurobasal-A medium supplemented with B27-supplement, penicillin/streptomycin (all from Invitrogen, Carlsbad, CA, USA), 4 mM glutamine (Sigma–Aldrich, St. Louis, MO, USA; further referred to as basal medium), 10 ng/ml basic fibroblast growth factor (bFGF) and 30 ng/ml EGF (both from Peprotech, USA). Several isolations were used for single cell assays; the cells were diluted and cultivated in 96-well plates. After 1 week the formed neurospheres were analyzed or used for further analyses of their differentiation potential. They were moved onto poly-L-lysine-coated cover slips (PLL, Sigma–Aldrich) and cultivated in basal medium supplemented with 20 ng/ml bFGF, then analyzed after 4 days of differentiation. In another set of experiments the cells were cultivated in Petri dishes, and after 1 week of cultivation, the formed neurospheres were trypsinized (0.05% trypsin + 0.02% EDTA; Sigma–Aldrich) and used for *in vitro* experiments.

Cell differentiation *in vitro*

Cells were trypsinized and plated on PLL-coated cover slips (PLL, Sigma–Aldrich) at a cell density of $6 \times 10^4/cm^2$ and cultured in basal medium supplemented with 20 ng/ml bFGF. Four days after the onset of differentiation, the cells were analyzed for the expression of K^+ and Na^+ currents using the patch-clamp technique, and after fixation, the cells were analyzed for the expression of neuronal/glial cell markers.

Preparation of acute brain slices

Control animals (n = 7 animals) or mice 4 days after MCAo (n = 7 animals) were deeply anaesthetized with PTB (100 mg/kg, i.p.) and perfused transcardially with cold (4–8 °C) isolation solution. The mice were decapitated, the brains were quickly dissected out and transversal 200-μm thick slices were cut using a vibrating microtome (HM 650 V, Thermo Scientific Microm, Walldorf, Germany). The slices were incubated for 30 min at 34 °C in isolation solution and then held at room temperature in artificial cerebrospinal fluid (aCSF) containing (in mM): 122 NaCl, 3 KCl, 28 $NaHCO_3$, 1.25 Na_2HPO_4, 1.5 $CaCl_2$, 1.3 $MgCl_2$, 10 glucose, osmolality 305 ± 3 mOsmol/kg. Solutions were equilibrated with 95% O_2/5% CO_2 to a final pH of 7.4. Osmolality was measured using a vapor pressure osmometer (Vapro 5520, Wescor, Logan, UT, USA).

Electrophysiological recordings

Acute brain slices or cover slips with differentiated cells were transferred to a recording chamber mounted on the stage of an upright microscope (Axioscop, Zeiss, Gottingen, Germany) equipped with a high-resolution digital camera (AxioCam HRc, Zeiss, Germany) and electronic micromanipulators (Luigs & Neumann, Ratingen, Germany). The chamber was continuously perfused with oxygenated aCSF at a rate of 3 ml/min at 25 ± 2 °C. Electrophysiological recordings were performed using an EPC-10 patch-clamp amplifier in combination with PATCHMASTER software (HEKA Elektronik, Lambrecht/Pfalz, Germany). Recording pipettes with a tip resistance of ~10 MΩ were made from borosilicate capillaries (0.86 ID, Sutter Instruments Company, Novato, CA, USA) using a Brown–Flaming micropipette puller (P-97, Sutter Instruments). Electrodes were filled with an intracellular solution containing (in mM): 130 K-gluconate, 0.5 $CaCl_2$, 5 EGTA, 10 HEPES, 3 Mg-ATP and 0.3 Na-GTP; the final pH was adjusted to 7.2 with KOH. V_m was measured by switching the EPC-10 amplifier to the current-clamp mode. R_m was calculated from the current elicited by a 10 mV test pulse (50 ms duration) depolarizing the cell membrane from the holding potential of −70 to −60 mV and 40 ms after the onset of the depolarizing pulse. C_m was determined automatically from the Lock-in protocol by PATCHMASTER. To obtain the current pattern of each cell, the cell membrane was clamped from the holding potential of −70 mV to values ranging from −160 to +40 mV for 50 ms at 10-mV intervals. To isolate the delayed outwardly rectifying K^+ (K_{DR}) current component, a voltage step from −70 to −60 mV was used to subtract time- and voltage-independent currents. To activate the K_{DR} currents only, the cells were held at −50 mV, and the amplitude of the K_{DR} currents was measured at +40 mV at the end of the pulse. The fast activating and inactivating outwardly rectifying K^+ (K_A) current component was isolated by subtracting the current traces clamped at −110 mV from those clamped at −50 mV, and its amplitude was measured at the peak value. Tetraethylammonium chloride (TEA, 10 mM) and 4-aminopyridine (4-AP; 5 mM, both Sigma–Aldrich) were used to identify the K_A and K_{DR} current components. Tetrodotoxin- (TTX, Alomone Labs, Jerusalem, Israel) sensitive Na^+ currents were isolated by subtracting the current traces measured in 1 μM TTX-containing solution from those measured under control conditions. Na^+ current amplitudes were measured at the peak value. Inwardly rectifying K^+ (K_{IR}) currents were determined at −160 mV at the end of the pulse, and a voltage step from −70 to −60 mV was used to subtract time- and voltage-independent currents. Current densities (CD) were calculated by dividing the maximum current amplitudes by the corresponding C_m for each individual cell. The patch-clamp data analyses were performed using FITMASTER software (HEKA Elektronik, Lambrecht/Pfalz, Germany).

Immunohistochemistry and cell identification

The mice were deeply anaesthetized 4 days after MCAo with PTB (100 mg/kg, i.p.) and perfused transcardially with 20 ml of saline followed by 20 ml of cooled 4% paraformaldehyde (PFA) in 0.1 M phosphate buffer (PB). Brains were dissected out, post-fixed for 2 h and placed stepwise in solutions with gradually increasing sucrose concentrations (10%, 20%, 30%) for cryoprotection. Coronal, 30-μm thick slices were prepared using a microtome (HM550, Microm International, Walldorf, Germany). For cell identification after patch-clamp recording, the measured cells were filled with Alexa Fluor 594 hydrazide (0.1 mM; Molecular Probes, Invitrogen, CA, USA) by dialyzing the cytoplasm with the patch pipette solution. Post-recording, the slices were fixed with 4% PFA in 0.1 M PB for 25 min and then kept at 4–8 °C in phosphate-buffered saline (PBS). The slices were incubated with 5% Chemiblocker (Millipore, MA, USA) and 0.2% Triton in PBS, a blocking solution that was also used as the diluent for the antisera. The slices were incubated with the primary antibodies at 4–8 °C overnight, and the secondary antibodies were applied for 2 h. The list of primary and secondary antibodies is summarized in Table 1. To visualize the cell nuclei, the slices were incubated with 300 nM 4,6-diamidino-2-phenylindole (DAPI) in PBS for 5 min at room temperature and mounted using Aqua Poly/Mount (Polysciences Inc., Eppelheim, Germany). All chemicals were purchased from Sigma–Aldrich (St. Louis, MO, USA), unless otherwise stated.

A Zeiss 510DUO LSM confocal microscope equipped with Arg/HeNe lasers was used for immunohistochemical analysis. Stacks of consecutive confocal images taken at intervals of 3 μm were acquired sequentially with two or three lasers to avoid cross-talk between fluorescent labels. The background noise of each confocal image was reduced by averaging four image inputs. For each image stack the gain and detector offset were adjusted to minimize saturated pixels, yet still permitting the detection of weakly stained cell processes. Colocalization images and their maximum z projections were made using a Zeiss LSM Image Browser.

Cell counts

To determine the number of DCX^+/GFP^+ cells in the dorsal part of the LV or the number of GFP^+ neurons in the glomerular or granular cell layer in the olfactory bulb (OB), confocal images (315 × 315 × 20 μm) covering the studied regions were taken of brain coronal slices from controls and from mice 4 days or 4 weeks after MCAo (5–9 animals from each group, three regions from one slice, bregma −0.5 mm). Between 1000 and 1500 GFP^+ cells were scored. The number of cells was estimated from superimposed images using a GSA Image Analyzer v3.7.7 (Bansemer & Scheel GbR, Rostock, Germany) and expressed as the percentage of DCX^+ cells from the total number of GFP^+ cells or as the number of GFP^+ cells per mm^3.

Statistics

The results are expressed as the mean ± standard error of the mean (SEM). Statistical analyses of the differences between controls and MCAo animals were performed using an unpaired t test. Values of $p < 0.05$ were considered significant (*), $p < 0.01$ very significant (**) and $p < 0.001$ extremely significant (***).

RESULTS

The subventricular zone of the LV is one of the most important regions of adult neurogenesis in the

Table 1. Primary and secondary antibodies used for immunohistochemistry

Antigen	Dilution	Isotype	Manufacturer	Secondary antibody
BLBP	1:200	Rabbit IgG	Abcam	GAM 594
DCX	1:1000	Rabbit IgG	Abcam	GAR 594/660
Calbindin	1:200	Mouse IgG	Millipore	GAR 594
Calretinin	1:400	Mouse IgG	Millipore	GAM 594
GFAP	1:800	Mouse IgG	Sigma–Aldrich	Cy3 conjugated
Ki-67	1:1000	Rabbit IgG	Abcam	GAR 594/660
Nestin	1:800	Mouse IgG	Millipore	GAM 594/660
NeuN	1:100	Mouse IgG	Millipore	GAM 594
Parvalbumin	1:200	Mouse IgG	Millipore	GAM 594
TH	1:400	Mouse IgG	Millipore	GAM 594

BLBP, brain lipid-binding protein; DCX, doublecortin; GFAP, glial fibrillary acidic protein; TH, tyrosine hydroxylase; GAR 594/660, goat anti-rabbit IgG conjugated with Alexa Fluor 594 or 660; GAM 594/660, goat anti-mouse IgG conjugated with Alexa Fluor 594 or 660 (all secondary antibodies from Invitrogen).

mammalian brain. Neurogenesis predominantly occurs in the lateral wall of the LV; however, several studies have described the existence of cell populations with neurosphere- forming ability also in the dorsal part of the LV (Willaime-Morawek et al., 2006; Young et al., 2007). The D6/GFP mice were developed primarily for studying the role of the mouse *Dach1* gene in the embryonic development of the neocortex; however, persisting activity of this gene was also detected in the adult mouse brain. Besides a subpopulation of neurons and astrocytes in the dorsal cortex and CA1 area in the hippocampus, the mouse *Dach1* gene is also active in a narrow region in the dorsal part of the LV (Fig. 1).

Initially, we performed immunohistochemical analyses to identify the phenotype of GFP^+ cells in this region. GFP^+ cells could be found along the entire area of the dorsal part, and they formed several rows of cells in the subependymal zone; moreover, a large number of GFP^+ cells was found at the beginning of the RMS in the anterior horn of the SVZ. The majority of GFP^+ cells expressed glial fibrillary acidic protein (GFAP), a marker of astrocytes (Fig. 1A–G), but also markers of adult neural stem cells (aNSCs). The assumption that GFP^+ cells in this region expressed the phenotype of aNSCs was confirmed by the immunohistochemical detection of nestin (Fig. 1H–N) and brain lipid-binding protein (BLBP; data not shown). All three markers were expressed mainly by GFP^+ cells with many well-developed processes; however, we also detected GFP^+ cells without or with a few short processes, scattered throughout the entire dorsal area. Nevertheless, their density was higher in the proximity of the lateral RMS, and they predominantly expressed doublecortin (DCX), a marker of migrating neuroblasts (Fig. 2A–G). We were also interested in the proliferative activity of GFP^+ cells in this region. Immunostaining for Ki-67 revealed that the majority of proliferating cells were present in the lateral wall of the LV (the most common site of adult neurogenesis); however, several GFP^+ cells in the dorsal part of the LV also expressed this marker of proliferation (Fig. 2H–N). In contrast to previous studies (Machon et al., 2002), we did not detect the expression of ependymal cell markers in GFP^+ cells (S100β, CD133) in the dorsal part of the LV in the adult brain (data not shown).

To determine whether the GFP^+ cells possess the properties of neural stem/progenitor cells also in the adult brain, we used a single cell neurosphere-forming assay. We carefully dissected the dorsal wall of the LV from the brain of controls and prepared a single cell suspension that was diluted and cultured under proliferating conditions in 96-well plates. After 1 week these cells formed neurospheres, and 26.1 ± 2.5% ($n = 5$ animals) of them expressed GFP and were GFAP- or nestin-positive (Fig. 3A, B). The same neurosphere-forming assay was performed with GFP^+ cells isolated from mice 4 days after middle cerebral artery occlusion (MCAo). These cells also formed GFP^+ neurospheres, and their number was significantly ($p < 0.01$) increased to 43.2 ± 4.3% ($n = 5$ animals) when compared to controls (Fig. 3I); some of them comprised, besides $GFAP^+$ or $nestin^+$, also DCX^+/GFP^+ cells (Fig. 3C). The neurospheres were further cultured under differentiating conditions. The cells attached to the PLL-coated cover slips and expressed predominantly glial markers, such as nestin, BLBP or GFAP (Fig. 3D, G, H); however, the expression of the neuronal progenitor marker DCX was found only in cells originating from the ischemic brains and never from the control brains (Fig. 3E, F). Although control as well as ischemic neurospheres could be passaged, the number of GFP^+ cells dramatically decreased with an increasing number of passages; therefore, only neurospheres cultured for 1 week without further passages were used for all experiments.

Differentiated GFP^+ cells display a passive or neuronal current pattern

To determine the electrophysiological properties of differentiated GFP^+ cells isolated from control brains or those 4 days after MCAo, we performed patch-clamp recordings in the whole-cell configuration. We recorded around 35 cells from both groups, and two cell populations with distinct membrane properties and current patterns were detected, correlating with the morphological and immunohistochemical features described above. GFP^+ cells isolated from control brains had only a large flat morphology and expressed time- and voltage-independent non-decaying K^+ currents (Fig. 4J),

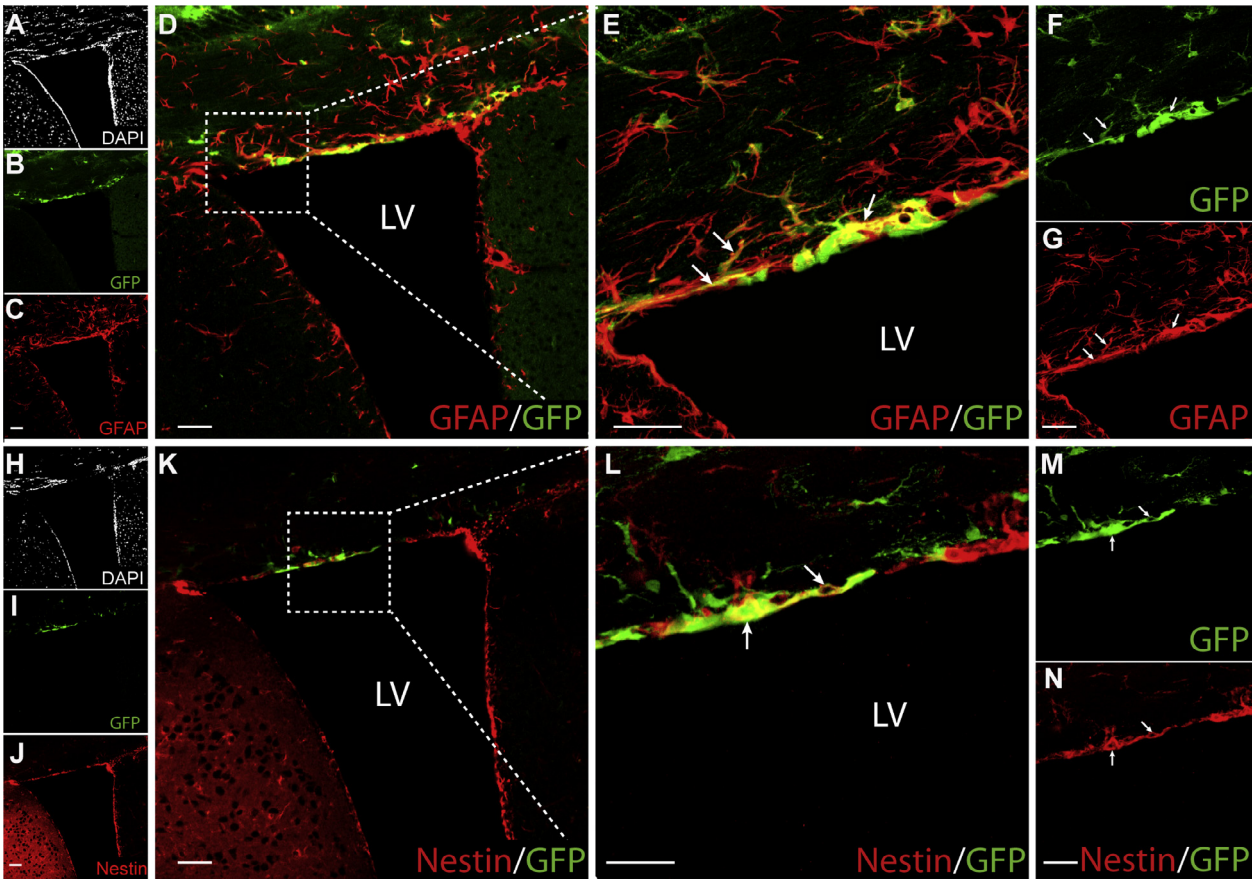

Fig. 1. Characterization of GFP$^+$ cells in the dorsal part of the lateral ventricles (LV) in controls. (A–D) Images illustrating the localization of GFP$^+$ (B) and GFAP$^+$ cells (C) around the LV. (E–G) A detailed image of GFP$^+$ cells in the dorsal part of the LV shows the expression of GFAP in many GFP$^+$ cells. (H–K) Overview of the LV showing the localization of GFP$^+$ (I) and nestin$^+$ cells (J) around the LV. (L–N) A detailed image of GFP$^+$ cells in the dorsal part of the LV shows the expression of nestin in many GFP$^+$ cells. White arrows indicate GFP$^+$/GFAP$^+$ or GFP$^+$/nestin$^+$ cells. DAPI was used to visualize the cell nuclei and the borders of the LV. Scale bars = 50 μm. (For interpretation of the references to color in this figure legend, the reader is referred to the web version of this article.)

membrane potential (V_m) of −78.1 ± 2.0 mV (n = 43 cells), membrane resistance (R_m) of 63.8 ± 8.5 MOhms (n = 43 cells) and membrane capacitance (C_m) of 65.0 ± 9.7 pF (n = 43 cells). These cells displayed a previously described passive current pattern (Zhou, 2005), with no expression of voltage-activated currents (Table 2). All these cells were identified post-recording as GFAP$^+$ (Fig. 4A–D) or nestin$^+$ (data not shown). On the other hand, in the cell culture obtained from ischemic brains we found two electrophysiological phenotypes in the GFP$^+$ cells. We detected a subpopulation of GFP$^+$ cells with a passive current pattern and moreover, some cells displayed electrophysiological properties resembling those of neuronal precursors (a neuronal-like current pattern; Bellardita et al., 2011). The passive cells isolated from ischemic brains had a significantly depolarized V_m (p < 0.001, n = 24 cells), an increased R_m (p < 0.001, n = 24 cells) and a decreased C_m (p < 0.001, n = 24 cells) when compared to passive cells from controls (Table 2). GFP$^+$ cells with a neuronal current pattern comprised 27.0 ± 10.2% of all measured GFP$^+$ cells isolated from ischemic brains (Fig. 4I). They differed significantly in their V_m, R_m and C_m when compared to passive cells and moreover, these cells expressed large amplitudes of outwardly rectifying K$^+$ currents, specifically the delayed outwardly rectifying K$^+$ (K_{DR}) current and inactivating outwardly rectifying K$^+$ (K_A) current (Table 2), which were almost completely blocked by 4-AP together with TEA (Fig. 4K, L). Post-recording identification revealed the predominant expression of DCX in these GFP$^+$ cells (Fig. 4E–H). In summary, these data indicate that GFP$^+$ cells isolated from the dorsal part of the LV of control brains have the ability to form neurospheres *in vitro* and their differentiation potential is mainly gliogenic. On the other hand, GFP$^+$ cells isolated from the dorsal part of the LV of ischemic brains also form neurospheres; however, their potential is also neurogenic.

GFP$^+$ cells express two distinct electrophysiological phenotypes *in situ*

We also performed *in situ* patch-clamp recordings to determine the phenotype of GFP$^+$ cells in the dorsal part of the LV in control brains and brains 4 days after MCAo. Based on this analysis we divided the GFP$^+$ cells into two distinct electrophysiological phenotypes. The first group comprised cells with many long processes and a large elongated cell body. These cells displayed time-

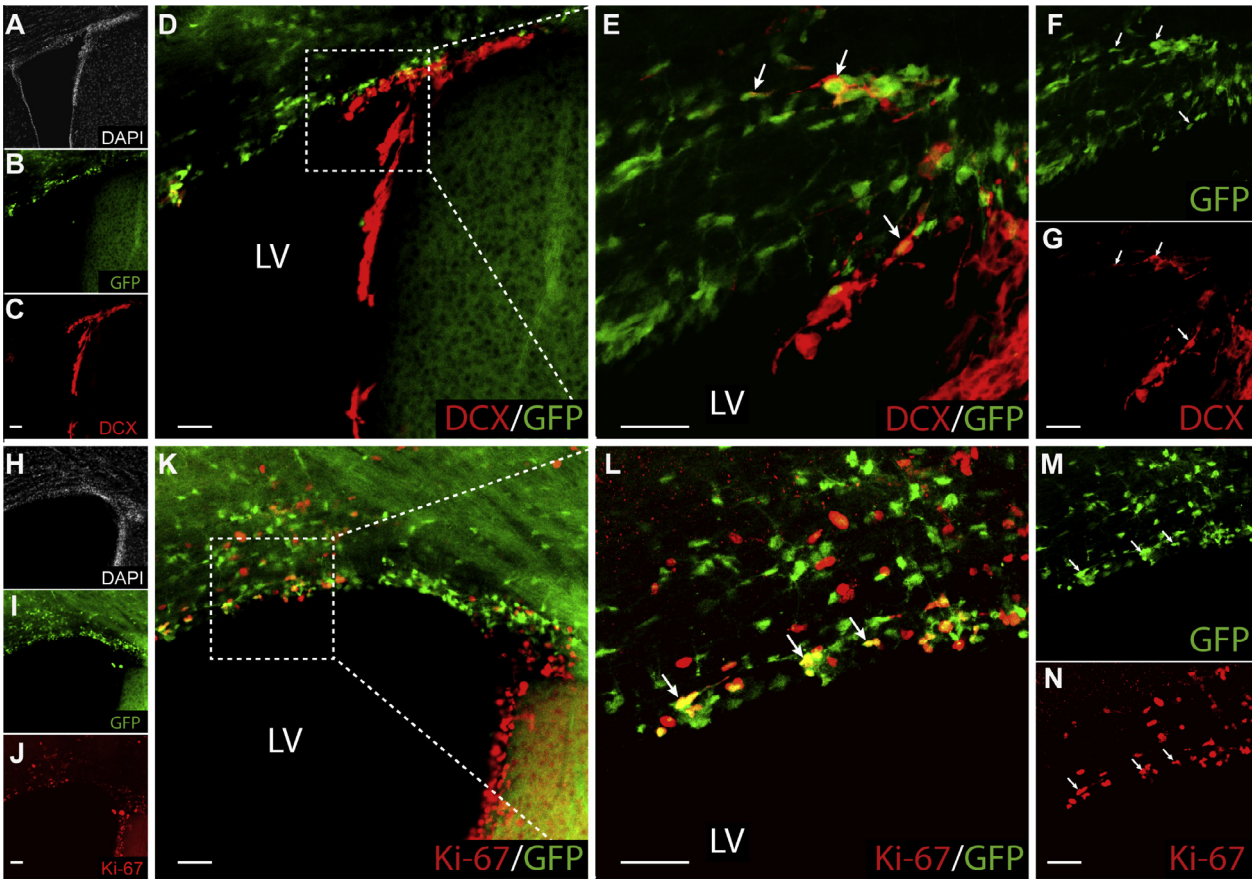

Fig. 2. Characterization of GFP^+ cells in the dorsal part of the lateral ventricles (LV) in controls. (A–D) overview of the LV showing the localization of GFP^+ (B) and DCX^+ cells (C) around the LV. (E–G) A detailed image of GFP^+ cells in the dorsal part of the LV shows the expression of DCX in several GFP^+ cells. (H–K) overview of the LV showing the localization of GFP^+ (I) and Ki-67^+ cells (J) around the LV. (L–N) A detailed image of GFP^+ cells in the dorsal part of the LV shows the expression of the proliferation marker Ki-67 in several GFP^+ cells. White arrows indicate GFP^+/Ki-67^+ or GFP^+/DCX^+ cells. DAPI was used to visualize the cell nuclei and the borders of the LV. Scale bars = 50 μm. (For interpretation of the references to color in this figure legend, the reader is referred to the web version of this article.)

and voltage-independent non-decaying K^+ conductance (Fig. 5A), and they had a hyperpolarized V_m and a low R_m (Table 3). Post-recording identification revealed the predominant expression of GFAP (Fig. 5B–E), nestin or olig2 in these cells (data not shown). Their membrane properties were similar to those described previously in aNSCs in the SVZ (Liu et al., 2006; Lacar et al., 2010) and thus, we may classify them as aNSCs. They were found in control brains as well as in brains 4 days after MCAo; however, their electrophysiological properties significantly differed. Passive cells recorded in ischemic brains displayed a significantly depolarized V_m ($p < 0.05$, $n = 25$ cells) and an increased R_m ($p < 0.05$, $n = 25$ cells) when compared to passive cells in control brains.

The second group comprised cells with a small round cell body with no or only a few short processes. They displayed significantly different membrane properties when compared to cells with a passive current pattern; further, these cells expressed large amplitudes of outwardly rectifying K^+ currents, especially K_{DR} currents (Fig. 5F, Table 3). A subpopulation of these cells expressed TTX-sensitive Na^+ currents; however, their CD was insufficient to produce action potentials. Post-recording identification revealed the predominant expression of DCX in these GFP^+ cells (Fig. 5G–J). Their membrane properties were similar to those described previously in neuroblasts in the SVZ (Lacar et al., 2010), thus we may classify them as neuroblasts. They were found in control brains as well as in brains 4 days after MCAo, and their passive membrane properties did not significantly differ between these two time points; nevertheless, the CDs of the K_A current were significantly increased in neuroblasts recorded 4 days after MCAo when compared to controls ($p < 0.001$, $n = 14$ cells; Table 3.).

Taken together, the results of our patch-clamp analysis of GFP^+ cells *in situ* revealed that the mouse *Dach1* gene is active in a certain subpopulations of cells with electrophysiological properties similar to aNSCs or neuroblasts, and focal cerebral ischemia has an important impact on the membrane properties of these cells.

MCAo induces an increase in the production of GFP^+/DCX^+ neuroblasts

To determine the influence of focal cerebral ischemia on adult neurogenesis in the dorsal part of the LV, we

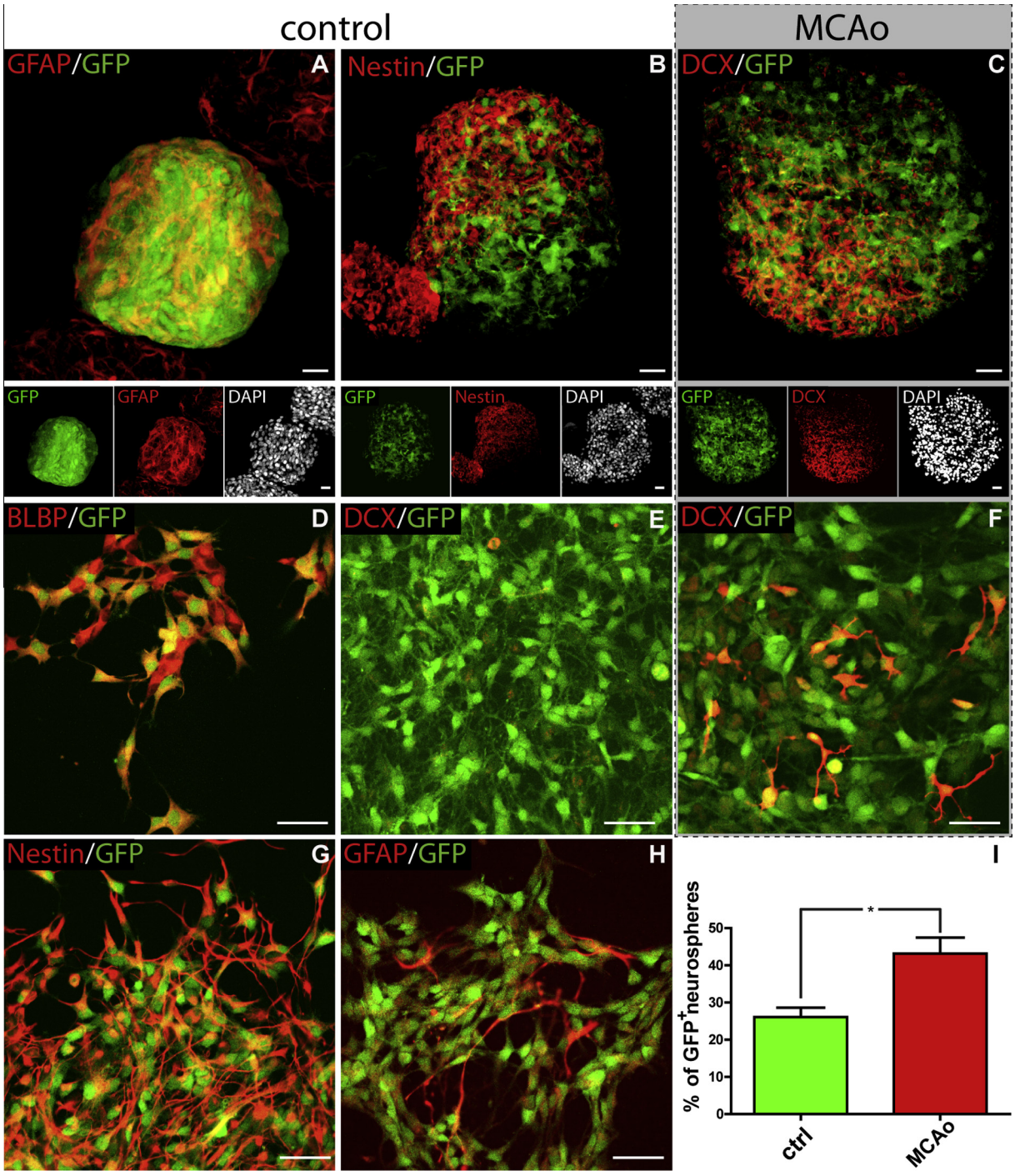

Fig. 3. GFP^+ cells form neurospheres *in vitro*. (A) An image showing neurospheres formed from GFP^+ cells isolated from the dorsal part of the lateral ventricles (LV) in controls. Many GFP^+ cells expressed GFAP. (B) An image showing neurospheres formed from GFP^+ cells isolated from the dorsal part of the LV in controls. Many GFP^+ cells expressed nestin. (C) An image showing neurospheres formed from GFP^+ cells isolated from the dorsal part of the LV in mice 4 days after MCAo. Several neurospheres consisted of GFP^+/DCX^+ cells. (E) Four days after differentiation, almost all GFP^+ cells from control neurospheres express BLBP. (F) Four days after differentiation, virtually no GFP^+ cells from control neurospheres express DCX, which is in contrast to the frequent expression of DCX in GFP+ cells originating from neurospheres cultivated from ischemic brains (F). Panels G and H depict the strong expression of neural stem cell markers (Nestin and GFAP) in differentiated GFP^+ cells. (I) Graph shows the increased number of neurospheres formed from GFP^+ cells isolated from the dorsal part of the LV from an ischemic mouse brain. Scale bars = 50 μm.

estimated the number of GFP^+/DCX^+ neuroblasts in control brains and brains 4 days after MCAo. In controls 9.4 ± 1.0% (n = 6 animals) of all GFP^+ cells in the dorsal part of the LV expressed DCX (Fig. 6A, B). In the brains 4 days after MCAo we determined the number of GFP^+/DCX^+ cells in the dorsal part of the ipsilateral as well as contralateral LV to reveal whether the ischemic injury had an impact on neurogenesis in the dorsal part of

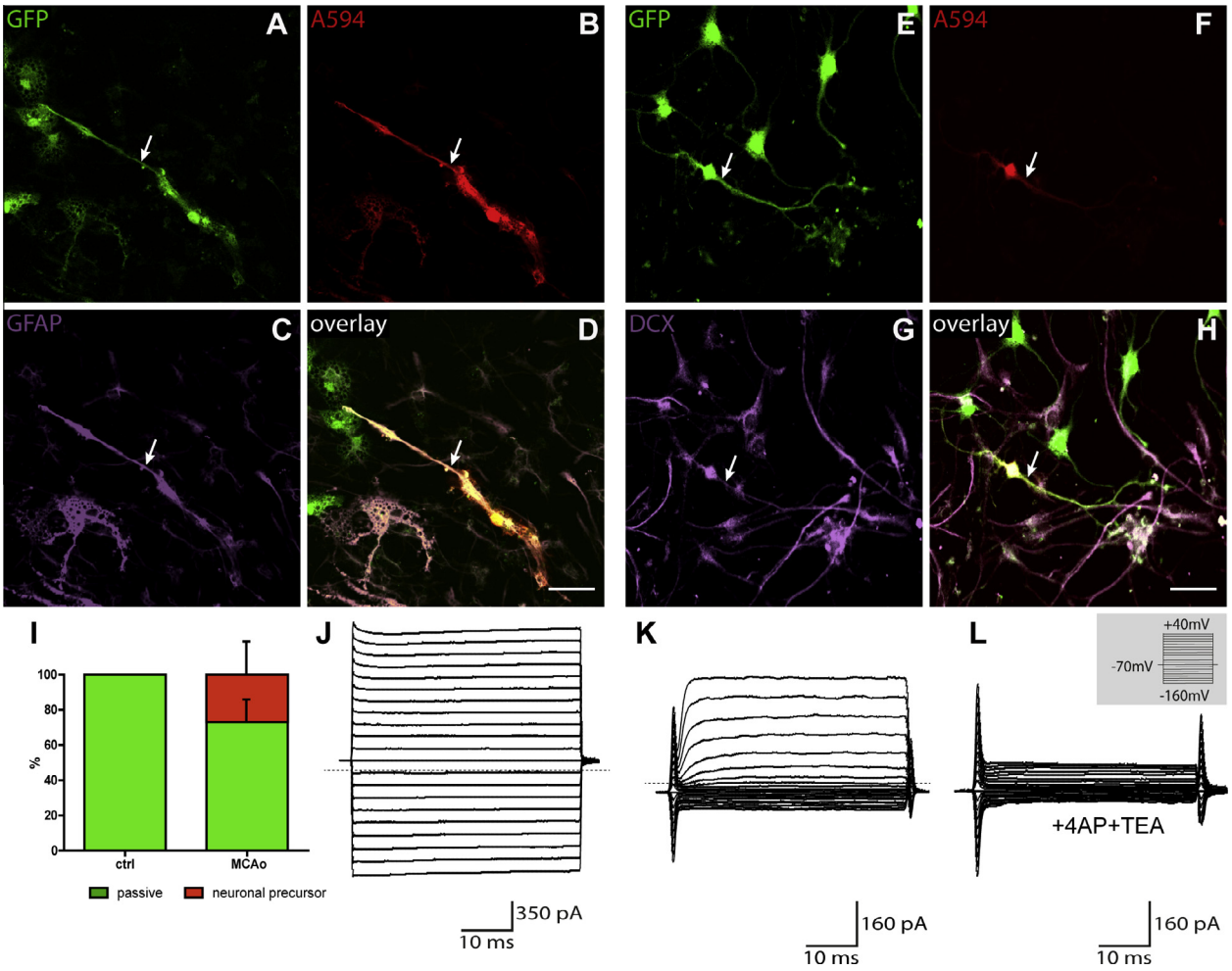

Fig. 4. The *in vitro* differentiation potential of GFP+ cells is altered following MCAo. (A) GFP^+ cell isolated from a control brain and differentiated for 4 days, then loaded with Alexa Fluor 594 hydrazid during patch-clamp measurement (B) and subsequently stained with an antibody directed against GFAP (C). An overlayed image is shown in (D). (E) GFP^+ cell isolated from an ischemic brain loaded with Alexa Fluor 594 hydrazid during patch-clamp measurement (F), subsequently stained with an antibody directed against DCX (G). An overlayed image is shown in (H). The white arrows indicate the recorded cells. (I) Graph demonstrating the differences in the incidence of passive and neuronal precursor cells between GFP^+ cells isolated from control animals and from ischemic brains 4 days after MCAo. (J) All GFP^+ cells isolated from controls differentiated into cells with a passive current pattern, i.e., time- and voltage-independent non-decaying K^+ currents, with only small voltage-activated K^+ currents. Zero current is marked by the dashed line. The current pattern was obtained after depolarizing/hyperpolarizing the cell membrane from a holding potential of −70 mV; for the voltage protocol see the inset in (L). (K) A subpopulation of GFP^+ cells isolated from ischemic brains differentiated into cells with a neuronal current pattern, i.e., outwardly rectifying K^+ currents (K_{DR}, K_A currents). Zero current is marked by the dashed line. The current pattern was obtained with the same protocol as in (J). (L) Outwardly rectifying K^+ currents were almost completely blocked by 4-AP and TEA. Scale bars = 50 μm. (For interpretation of the references to color in this figure legend, the reader is referred to the web version of this article.)

the LV in both hemispheres. We found that MCAo resulted in an increased number of GFP^+ cells ipsilaterally (Fig. 6C) and also that the number of GFP^+/DCX^+ cells significantly increased to 15.4 ± 1.9% of all GFP^+ cells ($p < 0.05$, $n = 6$ animals, Fig. 6A, C) when compared to control brains. Moreover, the number of GFP^+/DCX^+ in the dorsal part of the contralateral LV was also significantly increased and reached 18.7 ± 1.6% ($p < 0.001$, $n = 6$ animals, Fig. 6A, D) when compared to control brains. These results indicate that GFP^+ cells with an active *mouse Dach1* gene in the dorsal part of the LV play an important role in the increased production of neuroblasts after injury and that this process is also enhanced in the contralateral hemisphere.

GFP^+ cells in other brain regions

Additionally we were interested in the localization and properties of GFP^+ cells in other brain regions with respect to subventricular zone neurogenesis and GFP^+ cell migration. The first region where we found GFP^+ cells was the RMS. As shown in a sagittal section from adult D6/GFP mouse (Fig. 7B–E), the GFP^+ cells were found in and around the stream of migrating neuroblasts and probably participated in the formation of the glial tunnel, based on the expression of GFAP in their processes. The RMS navigates neuroblasts into the olfactory bulb (OB), where they differentiate into olfactory neurons and interneurons (Singer et al., 2009).

Table 2. Electrophysiological properties of GFP^+ cells *in vitro*

	Control	MCAo	
	Passive	Passive	Neuronal
V_m (mV)	−78.1 ± 2.0	−60.7 ± 3.5***	−43.6 ± 3.8
R_m (MOhms)	63.8 ± 8.5	137.2 ± 21.3***	716.5 ± 160.2
C_m (pF)	65.0 ± 9.7	20.7 ± 3.1***	8.4 ± 0.5
K_{IR} (pA/pF)	0.5 ± 0.2	2.6 ± 0.7***	0.3 ± 0.2
K_{DR} (pA/pF)	4.2 ± 0.9	5.2 ± 1.6	24.6 ± 9.3
K_A (pA/pF)	0.6 ± 0.4	1.5 ± 0.6	9.8 ± 6.1
I_{Na} (pA/pF)	0.0 ± 0.0	0.0 ± 0.0	0.0 ± 0.0
n	43	24	9
%	100.0 ± 0.0	73.0 ± 10.2	27.0 ± 10.2

V_m, resting membrane potential; R_m, membrane resistance; C_m, membrane capacitance; K_{IR}, current density of inwardly-rectifying K^+ currents; K_{DR}, current density of voltage-gated delayed outwardly-rectifying K^+ currents; K_A, current density of the fast activating and inactivating outwardly-rectifying K^+ currents; I_{Na}, current density of Na^+ currents; *n*, number of measured cells; %, percentage of the cell type.

*** $p < 0.001$ (control vs. MCAo).

Therefore, we examined coronal sections through the OB and found GFP^+ cells scattered in the granular cell layer (GCL) (15,711 ± 3243 GFP^+cell/mm^3, $n = 6$ animals) and glomerular layer (GL) (13,261 ± 3433 GFP^+cell/mm^3, $n = 6$ animals). These cells had large round cell bodies and mostly one long process; immunohistochemistry revealed the expression of a marker of mature neurons – NeuN (Fig. 7F–I). Detailed immunohistochemical analyses revealed the expression of the interneuronal marker calretinin in GFP^+ cells in the GL and GCL (Fig. 7O–R), and some GFP^+ cells in the GL also expressed tyrosine hydroxylase (TH) (Fig. 7S–V).

We also analyzed the distribution and phenotype of GFP^+ cells in the RMS and the OB after MCAo. As mentioned before, the number of DCX^+/GFP^+ cells was significantly increased in the dorsal part of the LV 4 days after MCAo, while 1 week after MCAo GFP^+ cells were also present inside the RMS between the migrating neuroblasts and expressed DCX (Fig. 7B–E). We were interested whether DCX^+/GFP^+ cells could leave the RMS and migrate into the site of the ischemic lesion; however, we did not find any GFP^+ cells around the cortical ischemic lesion expressing DCX or other neuronal markers at any studied point after MCAo. On the other hand, 4 weeks after MCAo we found a significantly increased number of GFP^+ neurons in the ipsilateral GCL (35,637 ± 6801 GFP^+cell/mm^3, $n = 8$ animals, $p < 0.05$) as well as in the ipsilateral GL (26,486 ± 2827) GFP^+cell/mm^3, $n = 8$ animals, $p < 0.05$); (Fig. 7J–N) when compared to controls. Interestingly, we also found an increased number of GFP^+ neurons in the contralateral OB in quantities almost identical to those in the ipsilateral part (data not shown). Thus, we can conclude that OB GFP^+ neurons express calretinin and TH and that there is a significantly increased number of GFP^+ neurons following ischemic injury, probably due to/resulting from enhanced adult neurogenesis after injury. On the other hand, we found no signs of GFP^+ cells contributing to neuroregeneration at the site of the ischemic lesion.

DISCUSSION

In the present study, we used transgenic mice with GFP expression driven by the D6 promoter of the mouse *Dach1* gene, which allows visualizing cells with active mouse *Dach1* gene expression in the dorsal part of the LV. We have shown that GFP^+ cells isolated from this region are able to subsequently proliferate and differentiate *in vitro*; GFP^+ cells isolated from controls displayed only gliogenic potential; however, GFP^+ cells from ischemic brains also possess neurogenic potential, based on immunohistochemical and electrophysiological analyses. Similar analyses carried out *in situ* revealed two populations of GFP^+ cells in the dorsal part of the LV. The first population expressed properties comparable to adult neural stem cells, while the second resembled neuroblasts. Focal cerebral ischemia influenced the phenotype of these cells and moreover, ischemic injury significantly increased the number of GFP^+/DCX^+ cells in the dorsal part of the LV in both hemispheres. We also detected GFP^+ cells in two brain regions connected with the process of SVZ adult neurogenesis – the rostral migratory stream and the OB. In controls GFP^+ cells expressed predominantly GFAP and possibly participated in forming a glial tunnel in the RMS, while GFP^+ cells in the OB adopted the phenotype of $calretinin^+$ interneurons in the GCL and GL and also TH^+ interneurons in the GL. Ischemic injury led to occurrence of GFP^+/DCX^+ cells in the stream of migrating neuroblasts in the RMS and to a significantly increased number of GFP^+ interneurons in both the GCL and GL in the OB without changes to their phenotype.

The presence of multipotent *Dach1*-expressing cells was described previously in the embryonic and early postnatal mouse brain using *in vitro* differentiation (Machon et al., 2002). In our study we used adult mouse brains, where mouse *Dach1* expression is localized predominantly in the cortex and the hippocampal CA1 region in differentiated cells (neurons and astrocytes) (Machon et al., 2002); however, we also found a narrow region in the dorsal part of the LV where *Dach1*-expressing cells showed the properties of aNSCs. Interestingly, these cells displayed a unipotent differentiation potential *in vitro* when isolated from healthy control brains; nevertheless, they revealed an expanded differentiation potential when isolated 4 days after focal cerebral ischemia. However, ischemic injury did not change the differentiation potential of *Dach1*-expressing cells *in vivo*, which is in agreement with previous results (Liu et al., 2007, 2009). The discrepancy between the *in vivo* and *in vitro* results could be explained by the different responses of isolated cells to MCAo, as was shown previously in regard to changes in mRNA expression after injury between cells *in vivo* and *in vitro* (Liu et al., 2007). Electrophysiological analysis performed *in vitro* revealed that passive cells originating from ischemic brains expressed significantly altered membrane properties when compared to those from controls. Their membrane potential was significantly depolarized, their membrane resistance was

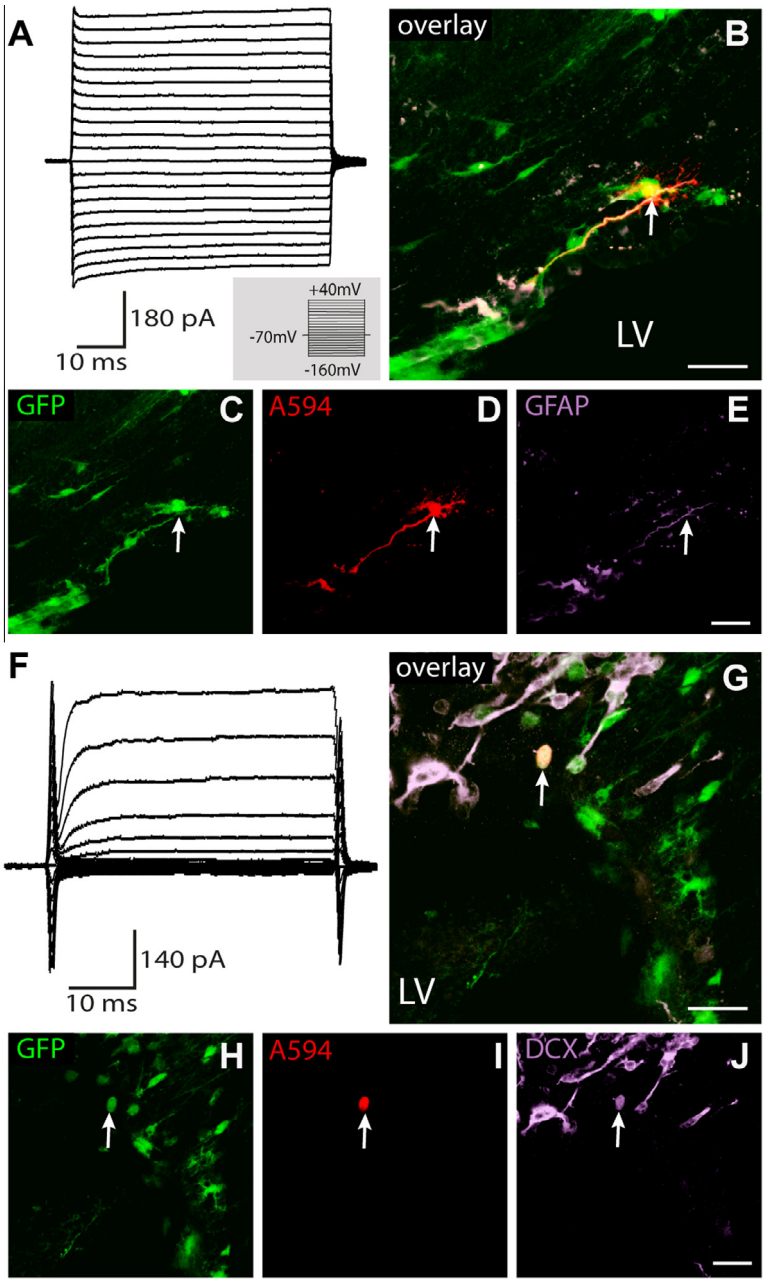

Fig. 5. GFP$^+$ cells *in situ* displayed two electrophysiologically and immunohistochemically distinct phenotypes. (A) A portion of GFP$^+$ cells expressed a passive current pattern, i.e., time- and voltage-independent non-decaying K^+ currents, with only small voltage-activated K^+ currents. The current pattern was obtained after depolarizing/hyperpolarizing the cell membrane from a holding potential of −70 mV, for the voltage protocol see the inset. Zero current is marked by the dashed line. (B–E) GFP$^+$ cell with a passive current pattern (C), labeled with Alexa Fluor 594 hydrazid during patch-clamp measurement (D), subsequently stained with an antibody directed against glial fibrillary acidic protein (GFAP, E), a marker of astrocytes. An overlayed image is shown in (B). (F) Many GFP$^+$ cells expressed a neuronal current, i.e., outwardly rectifying K^+ currents (K_{DR}, K_A currents) together with higher Na^+ currents. The current pattern was obtained with the same protocol as in (A). Zero current is marked by the dashed line. (G–J) GFP$^+$ cell with a neuronal current pattern (H), labeled with Alexa Fluor 594 hydrazid during patch-clamp measurement (I), subsequently stained with an antibody directed against doublecortin (DCX, J), a marker of neuronal precursors. An overlayed image is shown in (B). LV, lateral ventricle. Scale bars = 50 μm.

increased and additionally, their membrane capacitance was significantly lower when compared to passive cells isolated from control brains. These membrane properties are in agreement with previously published results that showed increasing membrane resistance with the progression of *in vitro* differentiation (Jelitai et al., 2007); furthermore, the same study described a decreasing number of gap-junction coupled cells with the progression of *in vitro* differentiation, which clarifies our finding of decreased membrane capacitance. Taken together, based on electrophysiological data, *Dach1*-expressing cells isolated from ischemic brains exhibit faster and more pronounced *in vitro* differentiation when compared to those isolated from controls.

On the basis of the electrophysiological data and post-recording identification, we can classify the GFP$^+$ cells in

Table 3. Electrophysiological properties of GFP^+ cells *in situ*

	Control		MCAo	
	Passive	Neuronal	Passive	Neuronal
V_m (mV)	−56.2 ± 1.6	−39.0 ± 4.4	−50.2 ± 1.9*	−46.6 ± 4.1
R_m (MOhms)	213.0 ± 21.7	3193.3 ± 407.6	320.4 ± 40.9*	2690.1 ± 374.2
C_m (pF)	6.3 ± 1.0	3.8 ± 0.2	6.2 ± 1.5	4.2 ± 0.9
K_{IR} (pA/pF)	0.5 ± 0.5	0.4 ± 0.4	3.7 ± 2.2	0.5 ± 0.4
K_{DR} (pA/pF)	16.6 ± 3.6	49.2 ± 5.2	17.3 ± 4.6	38.9 ± 4.6
K_A (pA/pF)	0.0 ± 0.0	0.4 ± 0.4	0.0 ± 0.0	4.8 ± 2.2 (*)
I_{Na} (pA/pF)	0.0 ± 0.0	5.2 ± 2.4	0.0 ± 0.0	1.5 ± 1.0
n	26	22	28	14
%	54.1 ± 9.9	45.9 ± 6.6	66.6 ± 6.9	33.3 ± 6.1

V_m, resting membrane potential; R_m, membrane resistance; C_m, membrane capacitance; K_{IR}, current density of inwardly-rectifying K^+ currents; K_{DR}, current density of voltage-gated delayed outwardly-rectifying K^+ currents; K_A, current density of the fast activating and inactivating outwardly-rectifying K^+ currents; I_{Na}, current density of Na^+ currents; *n*, number of measured cells; %, percentage of the cell type.

* $p < 0.05$ (control vs. MCAo).

the dorsal part of the LV as aNSCs and neuroblasts. One subpopulation of GFP^+ cells displayed large membrane resistance reaching several gigaohms, a depolarized membrane potential and small membrane capacitance. These membrane properties together with the presence of outwardly rectifying K^+ currents clearly classify these cells as neuroblasts (Wang, 2003; Bolteus, 2004; Lacar et al., 2010). Following ischemic injury their membrane properties were not changed; however, the current densities of the K_A currents were significantly increased. Since the increased activity of outwardly rectifying currents is linked to increased cell proliferation, the enhancement of the K_A currents could be related to this process (Knutson et al., 1997). The second GFP^+ cell subpopulation expressed low membrane resistance; a more hyperpolarized membrane potential and higher cell capacitance. Such membrane properties together with the presence of time- and voltage-independent non-decaying K^+ currents classified these cells as aNSCs (Liu et al., 2006; Lacar et al., 2010). In response to ischemic injury, GFP^+ aNSCs expressed a significantly depolarized membrane potential and increased membrane resistance. It was previously shown that these changes in membrane properties accompany increased cell proliferation, and thus we conclude that ischemia could lead to the enhanced proliferation of these GFP^+ aNSCs (Sundelacruz et al., 2009).

Interesting results were obtained by quantifying DCX^+/GFP^+ cell numbers in the dorsal part of the LV in the ipsilateral and contralateral hemispheres. Several previous studies showed that the number of DCX^+ cells after injury is predominantly increased in the SVZ of the ipsilateral hemisphere (Taupin, 2005; Thored et al., 2006; Yamashita, 2006; Liu et al., 2010). However, in our study we also detected an increased number of DCX^+/GFP^+ cells in the dorsal part of the LV in the contralateral hemisphere. These bilateral changes after injury were described previously in the hippocampus (Takasawa et al., 2002), in the cortex (Krüger et al., 2006) and also in the SVZ (Masuda et al., 2007; Li et al., 2010). It seems that *Dach1*-expressing cells in the dorsal part of the LV also respond to a contralateral ischemic injury. Although the exact mechanism underlying this reaction was not clarified, three possibilities were suggested by Masuda et al., 2007: factors from the lesion site might diffuse and affect a wide area of the brain; commissural fibers and the release of neurotransmitters might participate in this reaction (Platel et al., 2008); and hormonal (Li et al., 2010) or growth factors from other brain regions (Kokaia et al., 1998) as well as cytokines from the immune system might be involved (Ma et al., 2008).

Since the SVZ comprises a heterogeneous collection of NSCs that originate in different parts of the embryonic brain and generate different neuronal progeny, we examined the migration and differentiation of GFP^+ cells in the RMS and OB. Previously, the transcriptional factor Emx-1 was shown to control embryonic cortical progenitor proliferation, migration and differentiation, and these cells later comprise a population of aNSCs in the dorsolateral wall of the LV (Young et al., 2007). Based on previous reports, the mouse *Dach1* gene might perform a very similar function during development and therefore, we assume that the GFP^+ cells in the dorsal part of the LV also originate in the embryonic cortex. GFP^+ cells were found around the RMS as well as in the GCL and GL in the OB. We did not find any differences in the distribution of GFP^+ cells between the GL and GCL as was previously shown for Emx-1-expressing cells (Young et al., 2007). Moreover, the majority of these GFP^+ cells were $NeuN^+$, indicating their neuronal phenotype. Therefore, we used a number of neuronal markers (calretinin, calbindin, TH, parvalbumin) to identify their phenotype. We did not find GFP^+ cells expressing parvalbumin or calbindin in any layer of the OB, which correlates well with previously published results showing that $parvalbumin^+$ neurons are not generated from aNSCs in adulthood and that $calbindin^+$ neurons are generated only from aNSCs originating in the lateral wall in the LV and not from aNSCs of cortical origin (Young et al., 2007). Nevertheless, a large population of GFP^+ cells expressed calretinin in the GL as well as in the GCL, which is in agreement with data showing that cortical-derived Emx-1 aNSCs also generate the majority of $calretinin^+$ neurons (Young et al., 2007). In addition,

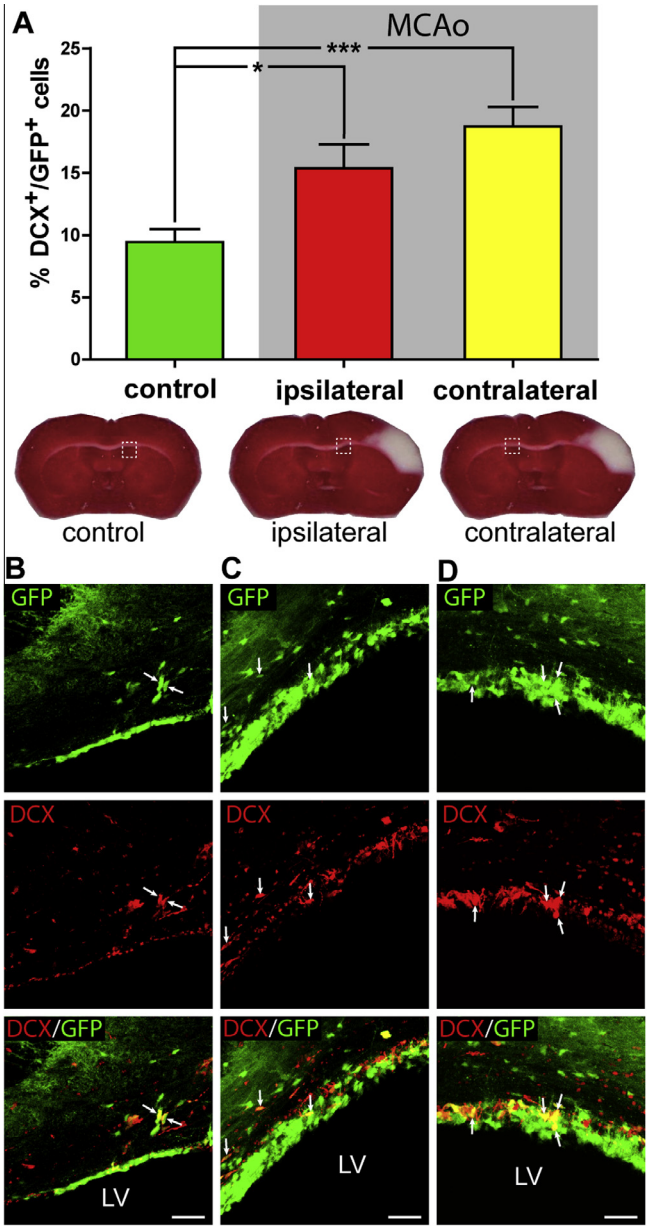

Fig. 6. Ischemia increased the percentage of DCX^+/GFP^+ cells in the dorsal part of the lateral ventricles. (A) Graph showing the percentage of DCX^+ cells from all GFP^+ cells in the dorsal part of the LV. Asterisks indicate significant differences between control ($n = 7$ animals) and post-ischemic (ipsilateral: $n = 7$ animals; contralateral: $n = 7$ animals) dorsal parts of the LV (TTC staining in the lower part of the image); $^*p < 0.05$; $^{***}p < 0{,}001$. (B) An image showing DCX^+ and GFP^+ cells in the dorsal part of the LV in a control brain. Note the localization of GFP^+ cells only in a narrow band in the dorsal part of the LV. (C) Image showing DCX^+ and GFP^+ cells in the dorsal part of the LV on the ipsilateral side of an ischemic brain. Note the increased number of GFP^+ cells in the dorsal part of the LV and the greater incidence of DCX^+ cells around the ipsilateral LV. (D) Image showing DCX^+ and GFP^+ cells in the dorsal part of the LV on the contralateral side of an ischemic brain. Note the significantly increased number of GFP^+ cells in the dorsal part of the LV and the greater incidence of DCX^+ cells around the contralateral LV. Arrows indicate GFP^+/DCX^+ cells. Scale bars = 50 μm.

several GFP^+ cells expressing TH were found in the GL. The fact that we failed to find any calbindin$^+$ neurons in the OB confirmed an earlier theory that aNSCs remain functionally distinct throughout life, generating different subsets of olfactory neurons (Lledo et al., 2008). Taken together, it appears that GFP^+ neurons in the OB are generated in the SVZ and migrate through the RMS to their final location; however, we cannot exclude the possibility that some GFP^+ cells might also originate in the neurogenic zone in the RMS or directly in the OB.

Additionally, we used a model of focal cerebral ischemia to elicit the involvement of *Dach1*-expressing cells from the dorsal part of the LV in brain regeneration after ischemia. In agreement with several previous studies we did not detect GFP^+ cells participating in glial scar formation or the production of new neurons in the cortex in or around the site of ischemic injury at any

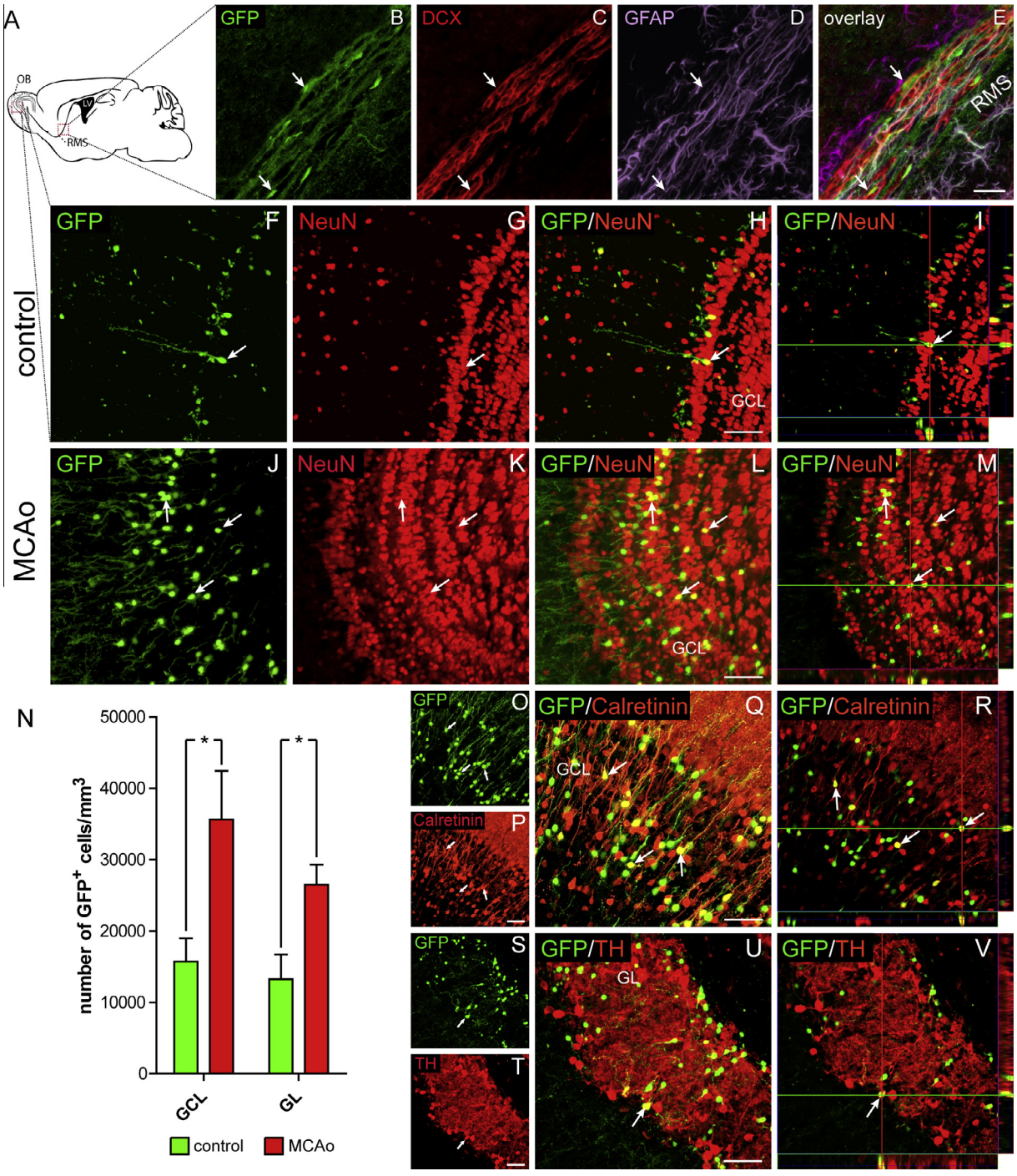

Fig. 7. GFP$^+$ cells from the dorsal part of the LV give rise to OB interneurons. (A) Schematic figure of a sagittal section through an adult mouse brain indicating the regions (red squares) where we analyzed the number of GFP$^+$ cells and their phenotype. (B–E) A detailed image of the rostral migratory stream (RMS) after MCAo showing DCX$^+$/GFP$^+$ cells in the RMS, which is delimited by GFAP$^+$ fibers. The white arrows highlight several DCX$^+$/GFP$^+$ cells. (F–I) Several GFP$^+$ cells were scattered in the granular cell layer (GCL) and expressed a marker of adult neurons (NeuN, G). A detailed orthogonal image confirmed the colocalization of NeuN and GFP in GFP$^+$ cells (I). (J–M) The number of GFP$^+$/NeuN$^+$ cells was significantly increased in the OB 4 weeks after MCAo. (N) Graph showing the number of GFP$^+$ cells in the GCL and GL before and 4 weeks after MCAo. (O–R) Images demonstrating the expression of calretinin in the GFP$^+$ cells in the GCL. (S–V) Images depicting the expression of tyrosine hydroxylase (TH) in the GFP$^+$ cells in the GL. Scale bars = 50 μm. (For interpretation of the references to color in this figure legend, the reader is referred to the web version of this article.)

analyzed time point after injury (4, 28 or 60 days) (Spadafora et al., 2010); on the other hand, some recent reports have described the potential of very similar Emx1-expressing aNSCs to produce new neurons after striatal ischemic injury in neonatal rats (Wei et al., 2011). These contradictory results document

the great variability in the responses of SVZ cells to injury, which could depend on the type or severity of injury, the age of the animals or the species used. Immunohistochemical analyses in the OB revealed a significantly higher number of GFP^+ neuronal cells in the GCL as well as in the GL 28 days after ischemia, which is in perfect correlation with the majority of recent studies describing increased SVZ neurogenesis and a consequently increased number of newly derived neurons in the OB in response to ischemic injury (Koketsu et al., 2006; Ohira, 2010; Yoneyama et al., 2010). On the other hand, these data are in contrast to some recently published results showing a negative influence of ischemia on the number of newly derived cells and their increased apoptotic rate (Spadafora et al., 2010). The use of a slightly different model of MCAo performed in neonatal animals, i.e., during the time period when the formation of the SVZ is still an ongoing process, could explain this discrepancy.

Taken together, our data suggest that the mouse *Dach1* gene does not play an important role only during embryonic or postnatal neural development, but that it is also an important factor in determining the phenotype of aNSCs and progenitors localized in the dorsal part of the LV in the mature brain. After ischemia, the expansion of SVZ neurogenesis significantly increased the proliferation of *Dach1*-expressing cells in the dorsal part of the SVZ; however, this did not change or affect their differentiation or the target of their migration, indicating their low therapeutic potential after cortical injury.

CONCLUSION

In conclusion, *Dach1*-expressing cells possess the ability to contribute to the process of adult neurogenesis and could therefore be used for genetic labeling of the aNSC subpopulation, genetic fate mapping studies or the manipulation of adult neurogenesis.

Acknowledgements—The authors would like to thank Helena Pavlikova for excellent technical assistance. We also thank James Dutt for helpful comments and suggestions. This work was supported by the Grant Agency of the Czech Republic – CZ: GA ČR: P303/12/0855, P304/12/G069 and by the Grant UEM AV CR – AV0Z50390703 from the Academy of Sciences of the Czech Republic.

REFERENCES

Arvidsson A, Collin T, Kirik D, Kokaia Z, Lindvall O (2002) Neuronal replacement from endogenous precursors in the adult brain after stroke. Nat Med 8:963–970.

Bellardita C, Bolzoni F, Sorosina M, Marfia G, Carelli S, Gorio A, Formenti A (2011) Voltage-dependent ionic channels in differentiating neural precursor cells collected from adult mouse brains six hours post-mortem. J Neurosci Res 90:751–758.

Bolteus AJ (2004) GABA release and uptake regulate neuronal precursor migration in the postnatal subventricular zone. J Neurosci 24:7623–7631.

Gage FH (2002) Neurogenesis in the adult brain. J Neurosci 22:612–613.

Gotts JE, Chesselet M-F (2005) Mechanisms of subventricular zone expansion after focal cortical ischemic injury. J Comp Neurol 488:201–214.

Hou S-W, Wang Y-Q, Xu M, Shen D-H, Wang J-J, Huang F, Yu Z, Sun F-Y (2008) Functional integration of newly generated neurons into striatum after cerebral ischemia in the adult rat brain. Proc Natl Acad Sci U S A 39:2837–2844.

Jelitai M, Anderova M, Chvatal A, Madarász E (2007) Electrophysiological characterization of neural stem/progenitor cells during in vitro differentiation: study with an immortalized neuroectodermal cell line. J Neurosci Res 85:1606–1617.

Jin K, Minami M, Lan JQ, Mao XO, Batteur S, Simon RP, Greenberg DA (2001) Neurogenesis in dentate subgranular zone and rostral subventricular zone after focal cerebral ischemia in the rat. Proc Natl Acad Sci U S A 98:4710–4715.

Knutson P, Ghiani CA, Zhou JM, Gallo V, McBain CJ (1997) K+ channel expression and cell proliferation are regulated by intracellular sodium and membrane depolarization in oligodendrocyte progenitor cells. J Neurosci 17:2669–2682.

Kohwi M, Petryniak MA, Long JE, Ekker M, Obata K, Yanagawa Y, Rubenstein JLR, Alvarez-Buylla A (2007) A subpopulation of olfactory bulb GABAergic interneurons is derived from Emx1- and Dlx5/6-expressing progenitors. J Neurosci 27:6878–6891.

Kokaia Z, Andsberg G, Yan Q, Lindvall O (1998) Rapid alterations of BDNF protein levels in the rat brain after focal ischemia: evidence for increased synthesis and anterograde axonal transport. Exp Neurol 154:289–301.

Koketsu D, Furuichi Y, Maeda M, Matsuoka N, Miyamoto Y, Hisatsune T (2006) Increased number of new neurons in the olfactory bulb and hippocampus of adult non-human primates after focal ischemia. Exp Neurol 199:92–102.

Krüger C, Cira D, Sommer C, Fischer A, Schäbitz W-R, Schneider A (2006) Long-term gene expression changes in the cortex following cortical ischemia revealed by transcriptional profiling. Exp Neurol 200:135–152.

Lacar B, Young SZ, Platel JC, Bordey A (2010) Imaging and recording subventricular zone progenitor cells in live tissue of postnatal mice. Front Neurosci 4.

Li J, Siegel M, Yuan M, Zeng Z, Finnucan L, Persky R, Hurn PD, McCullough LD (2010) Estrogen enhances neurogenesis and behavioral recovery after stroke. J Cereb Blood Flow Metab 31:413–425.

Liu F, You Y, Li X, Ma T, Nie Y, Wei B, Li T, Lin H, Yang Z (2009) Brain injury does not alter the intrinsic differentiation potential of adult neuroblasts. J Neurosci 29:5075–5087.

Liu X, Bolteus AJ, Balkin DM, Henschel O, Bordey A (2006) GFAP-expressing cells in the postnatal subventricular zone display a unique glial phenotype intermediate between radial glia and astrocytes. Glia 54:394–410.

Liu XS, Zhang ZG, Zhang RL, Gregg SR, Meng H, Chopp M (2007) Comparison of in vivo and in vitro gene expression profiles in subventricular zone neural progenitor cells from the adult mouse after middle cerebral artery occlusion. Neuroscience 146:1053–1061.

Liu Y, Wang Y, Cheng C, Chen Y, Shi S, Qin J, Xiao F, Zhou D, Lu M, Lu Q, Shen A (2010) A relationship between p27(kip1) and Skp2 after adult brain injury: implications for glial proliferation. J Neurotrauma 27:361–371.

Lledo P-M, Merkle FT, Alvarez-Buylla A (2008) Origin and function of olfactory bulb interneuron diversity. Trends Neurosci 31:392–400.

Ma Y-H, Mentlein R, Knerlich F, Kruse M-L, Mehdorn HM, Held-Feindt J (2008) Expression of stem cell markers in human astrocytomas of different WHO grades. J Neurooncol 86:31–45.

Machon O, van den Bout CJ, Backman M, Røsok Ø, Caubit X, Fromm SH, Geronimo B, Krauss S (2002) Forebrain-specific promoter/enhancer D6 derived from the mouse Dach1 gene controls expression in neural stem cells. Neuroscience 112:951–966.

Masuda T, Isobe Y, Aihara N, Furuyama F, Misumi S, Kim T-S, Nishino H, Hida H (2007) Increase in neurogenesis and

neuroblast migration after a small intracerebral hemorrhage in rats. Neurosci Lett 425:114–119.
Ming G-L, Song H (2011) Adult neurogenesis in the mammalian brain: significant answers and significant questions. Proc Natl Acad Sci U S A 70:687–702.
Ohira K (2010) Injury-induced neurogenesis in the mammalian forebrain. Cell Mol Life Sci 68:1645–1656.
Parent JM, Vexler ZS, Gong C, Derugin N, Ferriero DM (2002) Rat forebrain neurogenesis and striatal neuron replacement after focal stroke. Ann Neurol 52:802–813.
Platel JC, Dave KA, Bordey A (2008) Control of neuroblast production and migration by converging GABA and glutamate signals in the postnatal forebrain. J Physiol (Lond) 586:3739–3743.
Prajerova I, Honsa P, Chvatal A, Anderova M (2009) Neural stem/progenitor cells derived from the embryonic dorsal telencephalon of D6/GFP mice differentiate primarily into neurons after transplantation into a cortical lesion. Cell Mol Neurobiol 30:199–218.
Singer BH, Jutkiewicz EM, Fuller CL, Lichtenwalner RJ, Zhang H, Velander AJ, Li X, Gnegy ME, Burant CF, Parent JM (2009) Conditional ablation and recovery of forebrain neurogenesis in the mouse. J Comp Neurol 514:567–582.
Spadafora R, Gonzalez FF, Derugin N, Wendland M, Ferriero D, McQuillen P (2010) Altered fate of subventricular zone progenitor cells and reduced neurogenesis following neonatal stroke. Dev Neurosci 32:101–113.
Sundelacruz S, Levin M, Kaplan DL (2009) Role of membrane potential in the regulation of cell proliferation and differentiation. Stem Cell Rev Rep 5:231–246.
Takasawa K-I, Kitagawa K, Yagita Y, Sasaki T, Tanaka S, Matsushita K, Ohstuki T, Miyata T, Okano H, Hori M, Matsumoto M (2002) Increased proliferation of neural progenitor cells but reduced survival of newborn cells in the contralateral hippocampus after focal cerebral ischemia in rats. J Cereb Blood Flow Metab 22:299–307.
Taupin P (2005) Adult neurogenesis in the mammalian central nervous system: functionality and potential clinical interest. Med Sci Monit 11:RA247–RA252.
Thored P, Arvidsson A, Cacci E, Ahlenius H, Kallur T, Darsalia V, Ekdahl CT, Kokaia Z, Lindvall O (2006) Persistent production of neurons from adult brain stem cells during recovery after stroke. Stem Cells 24:739–747.
Wang DD (2003) Biophysical properties and ionic signature of neuronal progenitors of the postnatal subventricular zone in situ. J Neurophysiol 90:2291–2302.
Wei B, Nie Y, Li X, Wang C, Ma T, Huang Z, Tian M, Sun C, Cai Y, You Y, Liu F, Yang Z (2011) Emx1-expressing neural stem cells in the subventricular zone give rise to new interneurons in the ischemic injured striatum. Eur J Neurosci 33:819–830.
Willaime-Morawek S, Seaberg RM, Batista C, Labbe E, Attisano L, Gorski JA, Jones KR, Kam A, Morshead CM, van der Kooy D (2006) Embryonic cortical neural stem cells migrate ventrally and persist as postnatal striatal stem cells. J Cell Biol 175:159–168.
Xi G-M, Wang H-Q, He G-H, Huang C-F, Wei G-Y (2004) Evaluation of murine models of permanent focal cerebral ischemia. Chin Med J 117:389–394.
Yamashita T (2006) Subventricular zone-derived neuroblasts migrate and differentiate into mature neurons in the post-stroke adult striatum. J Neurosci 26:6627–6636.
Yoneyama M, Kawada K, Ogita K (2010) Enhanced neurogenesis in the olfactory bulb in adult mice after injury induced by acute treatment with trimethyltin. J Neurosci Res 88:1242–1251.
Young KM, Fogarty M, Kessaris N, Richardson WD (2007) Subventricular zone stem cells are heterogeneous with respect to their embryonic origins and neurogenic fates in the adult olfactory bulb. J Neurosci 27:8286–8296.
Zhou M (2005) Development of GLAST(+) astrocytes and NG2(+) glia in rat hippocampus CA1: mature astrocytes are electrophysiologically passive. J Neurophysiol 95:134–143.

(Accepted 22 February 2013)
(Available online 1 March 2013)